2018

MIXED MATRIX FLAT SHEET AND HOLLOW FIBER MEMBRANES FOR GAS SEPARATION APPLICATIONS

Nicholas W. Linck
University of Kentucky, nwli222@uky.edu
Digital Object Identifier: https://doi.org/10.13023/etd.2018.425

STUDENT AGREEMENT:

I represent that my thesis or dissertation and abstract are my original work. Proper attribution has been given to all outside sources. I understand that I am solely responsible for obtaining any needed copyright permissions. I have obtained needed written permission statement(s) from the owner(s) of each third-party copyrighted matter to be included in my work, allowing electronic distribution (if such use is not permitted by the fair use doctrine) which will be submitted to UKnowledge as Additional File.

I hereby grant to The University of Kentucky and its agents the irrevocable, non-exclusive, and royalty-free license to archive and make accessible my work in whole or in part in all forms of media, now or hereafter known. I agree that the document mentioned above may be made available immediately for worldwide access unless an embargo applies.

I retain all other ownership rights to the copyright of my work. I also retain the right to use in future works (such as articles or books) all or part of my work. I understand that I am free to register the copyright to my work.

REVIEW, APPROVAL AND ACCEPTANCE

The document mentioned above has been reviewed and accepted by the student's advisor, on behalf of the advisory committee, and by the Director of Graduate Studies (DGS), on behalf of the program; we verify that this is the final, approved version of the student's thesis including all changes required by the advisory committee. The undersigned agree to abide by the statements above.

Nicholas W. Linck, Student

Dr. Douglass S. Kalika, Major Professor

Dr. Matthew Beck, Director of Graduate Studies

MIXED MATRIX FLAT SHEET AND HOLLOW FIBER MEMBRANES FOR GAS SEPARATION APPLICATIONS

Dissertation

A dissertation submitted in partial fulfillment of the requirements for the degree of Doctor of Philosophy in the College of Engineering at the University of Kentucky

By

Nicholas W. Linck

Lexington, KY

Directors: Dr. Douglass S. Kalika, Professor of Chemical Engineering Dr. Matthew Weisenberger, Associate Director, Materials Technologies, Center for Applied Energy Research

Lexington, KY

2018

ABSTRACT OF DISSERTATION

MIXED MATRIX FLAT SHEET AND HOLLOW FIBER MEMBRANES FOR GAS SEPARATION APPLICATIONS

Mixed matrix membranes (MMM) offer one potential path toward exceeding the Robeson upper bound of selectivity versus permeability for gas separation performance while maintaining the benefits of solution processing. Many inorganic materials, such as zeolites, metal-organic frameworks, or carbon nanotubes, can function as molecular sieves, but as stand-alone membranes are brittle and difficult to manufacture. Incorporating them into a more robust polymeric membrane matrix has the potential to mitigate this issue.

In this work, phase inversion polymer solution processing for the fabrication and testing of asymmetric flat sheet mixed matrix membranes was employed with CVD-derived multiwall carbon nanotubes (MWCNTs) dispersed in a polyethersulfone (PES) matrix. The effect of MWCNT loading on membrane separation performance was examined. Notably, a distinct enhancement in selectivity was measured for several gas pairs (including O_2/N_2) at relatively low MWCNT loading, with a peak in selectivity observed at 0.1 wt% loading relative to PES. In addition, no post-treatment (e.g. PDMS caulking) was required to achieve selectivity in these membranes. In contrast, neat PES membranes and those containing greater than 0.5 wt.% MWCNT showed gas selectivity characteristic of Knudsen diffusion through pinhole defects. These results suggested

that at low loading, the presence of MWCNTs suppressed the formation of surface defects in the selective layer in flat sheet mixed matrix membranes.

Additionally, a bench-scale, single-filament hollow fiber membrane spinning line was designed and purpose-built at the University of Kentucky Center for Applied Energy Research (CAER). Hollow fiber membrane spinning capability was developed using polyethersulfone (PES) solution dopes, and the process was expanded to include polysulfone (PSf) as well as mixed matrix membranes. The effects of key processing parameters, including the ratio of bore to dope velocities, the spinning air gap length, and the draw-down ratio, were systematically investigated. Finally, direct hollow fiber analogues to flat sheet mixed matrix membranes were characterized. Consistent with the flat sheet experiments, the mixed matrix hollow fiber membranes showed a local maximum in selectivity at a nominal loading of 0.1 wt.% MWCNT relative to the polymer, suggesting that the pinhole suppression effect introduced by MWCNTs was not limited to flat sheet membrane casting.

The development of asymmetric hollow fiber mixed matrix membrane processing and testing capability at the UK Center for Applied Energy Research provides a platform for the further development of gas separation membranes. Using the tools developed through this work, it is possible to further push the frontiers of mixed matrix gas separation by expanding the capability to include more polymers, inorganic fillers, and post treatment processes which previously have been focused primarily on the flat sheet membrane geometry.

KEYWORDS: Hollow fiber membranes, mixed matrix membranes, gas separation, carbon nanotubes, polyethersulfone

Nicholas W. Linck

22 October 2018

MIXED MATRIX FLAT SHEET AND HOLLOW FIBER MEMBRANES FOR GAS SEPARATION APPLICATIONS

By

Nicholas W. Linck

Dr. Douglass S. Kalika
Co-Director of Dissertation

Dr. Matthew Weisenberger
Co-Director of Dissertation

Dr. Matthew Beck
Director of Graduate Studies

22 October 2018

Acknowledgements

I would like to acknowledge my advisors, Dr. Matthew Weisenberger and Dr. Douglass Kalika for the kindness, support, and guidance throughout this entire process. It was thoroughly enjoyable to have them both guiding my research, with Dr. Weisenberger providing most of the day to day advice, assistance, and instruction, while Dr. Kalika provided the project with more big picture guidance and direction. Both of them provided me with the excellent advice and encouragement that I needed to complete this process. I also would like to thank my committee members, Dr. Isabel Escobar, Dr. Mark Meier, and Dr. John Balk, for providing insight and interesting questions to consider during the process.

I would also like to thank my past and present labmates, Dr. David Eaton, Ashley Morris, Jordan Burgess, Sarah Edrington, Nik Hochstrasser, Ruben Sarabia Riquelme, and Aaron Owen for all of their assistance and contributions to my research work. Additionally, I would like to thank Roger Perrone and Steve Summers for their assistance with the construction of the hollow fiber membrane spinning line.

Finally, I would like to acknowledge my wife Rachel as well as my parents, John and Jill Linck. Without their love and support I do not believe that I would have ever finished this work.

This material is based upon work supported by the National Science Foundation under Cooperative Agreement No. 1355438.

Table of Contents

List of Tables……x

List of Figures……xi

Chapter 1: Introduction ……1

1.1 Polymeric Membrane Separations ……1
1.1.1 Homogeneous Dense Film Membranes …… 4
1.1.2 Asymmetric Membranes ……5
1.1.2.1 Flat Sheet Membranes ……10
1.1.2.2 Hollow Fiber Membranes ……12
1.1.2.3 Pinhole Defects and Caulking ……15
1.2 Gas Separation ……17
1.2.1 Equations and Terminology for Gas Separations ……19
1.2.1.1 Permeability Coefficient and Permeance ……19
1.2.1.2 Selectivity ……20
1.2.2 The Robeson Upper Bound ……21
1.2.3 Air Separation ……23
1.2.3.1 Nitrogen Enriched Air (NEA) ……24
1.2.3.2 Oxygen Enriched Air (OEA) ……25
1.2.4 Natural Gas Purification ……27
1.3 Relevant Membrane Polymers of Interest ……29
1.3.1 Cellulose Acetate (CA) ……29
1.3.2 Poly(aryl ether sulfones) ……30
1.3.3 Polyimides ……33
1.3.4 Polymers of Intrinsic Microporosity (PIMs) ……34
1.3.5 Mixed Matrix Membranes (MMM) ……36
1.3.5.1 Zeolite MMM ……37
1.3.5.2 Metal Organic Framework (MOF) MMM ……38
1.3.5.3 Carbon Nanotube (CNT) MMM ……40
1.4 Research Objectives ……42
1.5 References ……46

Chapter 2: Materials and Methods ……53

2.1 Introduction……53
2.2 Materials……53
2.2.1 Polymers……53

2.2.1.1 Polyethersulfone (PES) ……53
2.2.1.2 Polysulfone (PSf) ……54
2.2.1.3 Polydimethylsiloxane (PDMS) ……55
2.2.2 Solvents ……55
2.2.2.1 N,N-dimethylacetimide (DMAc) ……55
2.2.2.2 N-methylpyrrolidone (NMP) ……56
2.2.3 Inorganic Fillers ……56
2.2.3.1 Carbon Nanotubes (CNTs) ……57
2.2.3.2 Carbon Black ……59
2.3 Membrane Fabrication Methods ……59
2.3.1 Flat Sheet Membranes ……59
2.3.1.1 Dope Preparation ……59
2.3.1.1.1 Standard Polymer Dope ……59
2.3.1.1.2 Mixed Matrix Membrane Dope ……60
2.3.1.2 Thin Film Casting/Solvent Exchange and Drying ……62
2.3.2 Hollow Fiber ……63
2.3.2.1 Dope Preparation ……63
2.3.2.2 Hollow Fiber Membrane Spinning Procedure ……64
2.4 Membrane Gas Permeation Testing Methods ……68
2.4.1 Permeation Testing Apparatus ……68
2.4.2 Flat Sheet Membrane Testing Procedure ……69
2.4.3 PDMS Caulking ……71
2.4.4 Hollow Fiber Membrane Testing ……74
2.4.4.1 Hollow Fiber Membrane Module Module Construction ……74
2.4.4.2 Hollow Fiber Membrane Module Testing ……76
2.5 Characterization Methods ……76
2.5.1 Parallel Plate Rheometry ……76
2.5.2 Scanning Electron Microscopy (SEM) ……77
2.5.3 Porometer ……77
2.6 References ……79

Chapter 3: Development of PES-MWCNT Flat Sheet Membranes ……80

3.1 Introduction ……80
3.1.1 Asymmetric Flat Sheet Membranes ……80
3.1.2 Material Systems of Interest ……83
3.1.2.1 Membrane Polymer ……83
3.1.2.2 Mixed Matrix Membranes ……84
3.2 Results and Discussion……87

3.2.1 Rheology of Membrane Casting Dopes ……87
3.2.1.1 Polyethersulfone Viscosity Measurements ……87
3.2.1.2 Mixed Matrix Dope Viscosity Measurements ……89
3.2.2 Flat Sheet Membrane Morphology ……90
3.2.2.1 Effect of Coagulation Bath Composition on Membrane Morphology……..90
3.2.2.2 Effect of Polymer Concentration on Membrane Morphology ……97
3.2.2.3 Effect of Solvent on Membrane Morphology ……103
3.2.2.4 Effect of MWCNT Loading on PES Membrane Morphology ……..109
3.2.3 Gas Permeance and Selectivity for Flat Sheet Membranes ……..114
3.2.3.1 Permeance and Selectivity of PES and PSf Membranes ……..114
3.2.3.2 Effect of MWCNT Loading on PES Membrane Permselectivity ……..114
3.2.3.3 Effect of Carbon Black Loading on PES Membrane Permselectivity ……..123
3.2.3.4 Effect of MWCNT Loading on PES-PDMS Membrane Permselectivity ……127
3.2.3.5 Effect of Carbon Black Loading on PES-PDMS Membrane Permselectivity ……131
3.3 Conclusions ……134
3.4 References ……137

Chapter 4: Hollow Fiber Membrane Spinning and PES-MWCNT Hollow Fiber Membranes……141

4.1 Introduction……142
4.2 Materials and Methods ……143
4.3 Results and Discussion ……143
4.3.1 Effects of Varying Processing Parameters on HFM Characteristics ……143
4.3.1.1 Ratio of Bore Velocity to Dope Velocity (V_b/V_d) ……146
4.3.1.2 Air Gap Distance ……151
4.3.1.3 Ratio of Take-up Velocity to Dope Velocity (Draw Down Ratio) ……155
4.3.2 Gas Separation Properties of Hollow Fiber Membranes ……159
4.3.3 Effect of Multiwall Carbon Nanotubes (MWCNT) Addition ……165
4.3.3.1 Effect of Loading on PES-MWCNT Mixed Matrix HFM Permselectivity ……168
4.3.3.2 Effect of Loading on PES-Carbon Black Mixed Matrix HFM Permselectivity …176
4.4 Conclusions……179
4.5 References ……183

Chapter 5: Conclusions and Future Work ……185

5.1 Conclusions ……185

5.1.1 Flat Sheet Membranes ……185
5.1.2 Hollow Fiber Membranes ……188
5.2 Future Work ……190
Bibliography ……194
Vita ……201

List of Tables

Table 3.1: Membrane casting parameters and test conditions for single gas permeance studies ……..……..114

Table 3.2: Permeance and ideal selectivity of N_2 and O_2 for unfilled PES and PSf membranes in the as-cast and PDMS-caulked state ……..……116

Table 3.3: Summary of the permeance of N_2 and O_2 as well as the O_2/N_2 ideal selectivity for selected mixed matrix flat sheet membranes……123

Table 4.1: Summary of hollow fiber membrane spinning conditions used in flowrate, air gap, and draw down ratio studies……..……..…144

Table 4.2: Processing parameters for V_b/V_d, air gap, and draw down ratio experiments ……..……147

Table 4.3: Processing parameters used for the production of hollow fiber membranes for gas separation testing……..160

Table 4.4: Summary of the permeance of N_2 and O_2 as well as the selectivity of O_2/N_2 for the unfilled hollow fiber and flat sheet membranes ……..161

Table 4.5: O_2/N_2 transport properties for MWCNT-loading hollow fiber membranes as compared to unfilled caulked membranes……171

Table 4.6: O_2/N_2 transport properties for MWCNT-loading flat sheet and hollow fiber membranes with and without PDMS caulking……175

Table 4.7: Comparison of the permeance of N_2 and O_2 and O_2/N_2 selectivity for PES filled with carbon black versus the unfilled PES membrane……..177

Table 4.8: Comparison of the permeance of N_2 and O_2 and O_2/N_2 selectivity of caulked PES hollow fibers filled with 0.1wt.% carbon black to that of the unfilled membrane……..178

List of Figures

Figure 1.1: A schematic representation of the three primary diffusion mechanisms that occur within polymeric gas separation membranes ……..……..……2

Figure 1.2: Schematic representation of an asymmetric flat sheet membrane. (A) ~0.1-1 µm thick dense layer, where gas separation occurs via solution diffusion (B) ~100-200 µm thick porous layer, which provides mechanical support……7

Figure 1.3: Generic ternary phase diagram between polymer, solvent, and non-solvent. (A) Binodal line, (B) Spinodal line, (C) Critical point, where binodal and spinodal are equal, (D) Meta-stable region, (E) Phase separation paths ……..……..8

Figure 1.4: Schematic diagram of a spiral wound membrane module……..11

Figure 1.5: Schematic diagram of hollow fiber membrane spinning line (A) Dope extrusion pump, (B) Bore injection pump, (C) Filtration manifold, (D) Extrusion die (spinneret), (E) Coagulation bath, (F) Take-up godet rollers, and (G) Wash winder. Dashed line represents pathway of the nascent hollow fiber membrane……13

Figure 1.6: Schematic diagram of a porous asymmetric composite membrane (left), along with the electrical resistance analog (right)……17

Figure 1.7: Schematic plot of the Robeson upper bound relationship between membrane efficiency (selectivity) and throughput (permeability) ……..22

Figure 1.8: Polymer repeat unit for (A) polyethersulfone (PES), (B) polysulfone (PSf), and (C) polydimethylsiloxane (PDMS)……31

Figure 1.9: General reaction taking place during the thermal rearrangement process…34

Figure 1.10: Preparation of PIM-1 polymer of intrinsic microporosity……..……35

Figure 1.11: Schematic representation of an asymmetric flat sheet mixed matrix membrane. (A) Dense separating layer, (B) Porous support layer, (C) Dispersed inorganic filler material, which adds a component of molecular sieving to the solution diffusion mechanism……37

Figure 2.1: Chemical structures for solvents used in membrane casting: (A) N,N-dimethylacetimide and (B) N-methylpyrrolidone……..……56

Figure 2.2a: (Top) Schematic diagram of hollow fiber membrane spinning line (A) Dope inlet, (B) Bore fluid inlet, (C) Extrusion die (spinneret), (D) Coagulation bath, (E) Take-up godet rollers, and (F) Wash winder. (Bottom) Photograph of hollow fiber spinning line……65

Figure 2.2b: Schematic diagram of the bore fluid and dope in the air gap between the spinneret and the coagulation bath (left), and a close-up photograph of the air gap with PES dope (right) ……65

Figure 2.3: (Top) schematic diagram of hollow fiber extrusion die. (Bottom) diagram of dope annulus and bore needle……66

Figure 2.4: Diagram of the hollow fiber membrane separation testing apparatus. (A) Gas source, which can flow nitrogen (N_2), helium (He), carbon dioxide (CO2), or oxygen (O_2), (B) Gas flow regulator, (C) Gas pressure gauge, (D) Membrane module, which can be either flat sheet membrane holder or hollow fiber membrane module, and (E) Soap film flowmeter……68

Figure 2.5: Schematic diagram of Millipore Microsyringe Stainless Steel Filter Holder (Cat# xx3002514) that was used for flat sheet membrane testing. (A) Outlet of the filter holder, (B) Flat Teflon O-ring, (C) Stainless steel screen, (D) Flat sheet asymmetric membrane sample, (E) Rounded Teflon O-ring, (F) Top of filter holder with NPT inlet…..70

Figure 2.6: Schematic diagram of HFM PDMS caulking soak (left) and photograph of HFM PDMS caulking soak (right)……..72

Figure 2.7: Hollow fiber membrane module (A) Schematic diagram of HFM module, (B) Empty module shell, (C) HFM bundle, (D) Module prepared for epoxy injection, (E) End view of potted, open fibers, (F) Completed module……..75

Figure 3.1: Schematic diagram demonstrating the mechanism by which selectivity is improved in a mixed matrix membrane. (A) Smaller gas molecules flow freely due to the porous nature of the filler material; (B) larger gas molecules (rejected from the filler via size discrimination are forced to take a more tortuous path through the dense separating layer of the membrane, decreasing their permeability……85

Figure 3.2: Relationship between the polymer dope viscosity and polymer concentration for PES in NMP and DMAc, as well as PSf in NMP ……88

Figure 3.3: Complex viscosity vs. angular frequency for PES-MWCNT and PES-Carbon black dopes with varying filler loadings at 25°C. PES-XXMWCNT corresponds to dope composed of 30 wt.% PES in NMP with XX wt.% MWCNT (or CB) relative to the polymer……..89

Figure 3.4a-b: SEM micrographs of PES thin films coagulated from 38.5 wt.% PES-DMAc dope in bath composed of (A) 0 wt.%, (B) 50 wt.% DMAc/water mixture. Arrows indicate surface that was exposed to coagulation bath. Inset: top surface of thin films at 800x magnification……92

Figure 3.4c-d: SEM micrographs of PES thin films coagulated from 38.5 wt.% PES-DMAc dope in bath composed of (C) 60 wt.%, (D) 70 wt.% DMAc/water mixture. Arrow indicates exposure face. Inset: top surface of thin films at 800x magnification .93

Figure 3.5a-b: SEM micrographs of PSf thin films coagulated from 35 wt.% PES-NMP dope in bath composed of (A) 0 wt.%, (B) 50 wt.% NMP/water mixture. Arrow indicates exposure face……95

Figure 3.5c-d: SEM micrographs of PSf thin films coagulated from 35 wt.% PSf-NMP dope in bath composed of (A) 60 wt.%, (B) 70 wt.% NMP/water mixture. Arrow indicates exposure face ……96

Figure 3.6a-b: SEM micrographs of PES thin films cast using dope composed of (A) 15 wt.% and (B) 20 wt.% PES in DMAc with deionized water as the coagulation medium. Arrow indicates exposure face ……98

Figure 3.6c-d: SEM micrographs of PES thin films cast using dope composed of (C) 25 wt.% and (D) 30 wt.% PES in DMAc with deionized water as the coagulation medium. Arrow indicates exposure face ……99

Figure 3.6e: SEM micrographs of PES thin films cast using dope composed of (E) 35 wt. % PES in DMAc with deionized water as the coagulation medium. Arrow indicates exposure face ……100

Figure 3.7a-b: SEM micrographs of PSf thin films cast using dope composed of (A) 25 wt.% and (B) 27.5 wt.% PSf in NMP with deionized water as the coagulation medium. Arrow indicates exposure face……101

Figure 3.7c-d: SEM micrographs of PSf thin films cast using dope composed of (C) 30 wt.% and (D) 32.5 wt.% PSf in NMP with deionized water as the coagulation medium. Arrow indicates exposure face ……102

Figure 3.7e: SEM micrographs of PSf thin films cast using dope composed of 35 wt.% PSf in NMP with deionized water as the coagulation medium. Arrow indicates exposure face ……..……..103

Figure 3.8a-b: SEM micrographs of PES thin films coagulated from 30 wt.% PES-NMP dope in bath composed of (A) 0 wt.%, (B) 50 wt.% NMP/water mixture. Arrow indicates exposure face ……..104

Figure 3.8c-d: SEM micrographs of PES thin films coagulated from 30 wt.% PES-NMP dope in bath composed of (C) 60 wt.%, (D) 70 wt.% NMP/water mixture. Arrow indicates exposure face ……..105

Figure 3.9a-b: Comparison of SEM micrographs of 30 wt.% PES thin films cast from (A) DMAc and (B) NMP using deionized water as the coagulation medium. Arrow indicates surface that was exposed to coagulation bath……107

Figure 3.9c-d: Comparison of SEM micrographs of 30 wt.% PES thin films cast from (C) DMAc and (D) NMP using 70 wt.% solvent in water as the coagulation medium. Arrow indicates surface that was exposed to coagulation bath ……..108

Figure 3.10: Optical microscope images of 30 wt.% PES in NMP dopes with (A) 0.05, (B) 0.1, and (C) 0.5 wt.% MWCNT dispersions (Arrow indicates MWCNT agglomerate that was not removed during centrifugation). Nominal magnification is 50x ……..110

Figure 3.11: Comparison of SEM micrographs of (A) unfilled PES flat sheet membrane and (B) PES flat sheet membrane loaded with 0.1 wt.% MWCNT. Dopes contain 30 wt.% PES in NMP and deionized water was used as the coagulation medium. Arrow indicates exposure face……..111

Figure 3.12: Comparison of SEM micrographs of (A) unfilled 30 wt.% PES-NMP flat sheet membrane and (B) 30 wt.% PES-NMP flat sheet membrane loaded with 0.1 wt.% MWCNT. 70 wt.% NMP/water was used as the coagulation medium. Arrow indicates exposure face. Inset: Membrane surface that was exposed to coagulation bath……112

Figure 3.13: (Left) SEM image of PES-0.1MWCNT dense film cross-section. Arrows indicate MWCNTs. (Right) photograph of PES and PES-0.1MWCNT membrane coupons, showing macroscopic color change that accompanies MWCNT dispersion…113

Figure 3.14a: Average He, CO_2, O_2, and N_2 permeance (GPU) of PES-MWCNT mixed matrix membranes, plotted against MWCNT loading. Each data point was measured in triplicate and error bars represent standard deviation of the three measurements……118

Figure 3.14b: Average He/N_2, CO_2/N_2, and O_2/N_2 ideal selectivity of PES-MWCNT mixed matrix membranes, plotted against MWCNT loading. Each data point was measured in triplicate and error bars represent standard deviation of the three measurements 119

Figure 3.15a: Average He, CO_2, O_2, and N_2 permeance (GPU) of PES-carbon black mixed matrix membranes, plotted against carbon black loading. Each data point was measured in triplicate and error bars represent standard deviation of the three measurements..125

Figure 3.15b: Average He/N_2, CO_2/N_2, and O_2/N_2 ideal selectivity of PES-carbon black mixed matrix membranes, plotted against carbon black loading. Each data point was measured in triplicate and error bars represent standard deviation of three points……126

Figure 3.16a: Average He, CO_2, O_2, and N_2 permeance (GPU) of PDMS-caulked PES-MWCNT mixed matrix membranes, plotted against MWCNT loading. Each data point was measured in triplicate and error bars represent standard deviation of the three measurements……129

Figure 3.16b: Average He/N_2, CO_2/N_2, and O_2/N_2 ideal selectivity of PDMS-caulked PES-MWCNT mixed matrix membranes, plotted against MWCNT loading. Each data point was measured in triplicate and error bars represent standard deviation of the three measurements……130

Figure 3.17a: Average He, CO_2, O_2, and N_2 permeance (GPU) of PDMS-caulked PES-carbon black mixed matrix membranes, plotted against carbon black loading. Each data point was measured in triplicate and error bars represent standard deviation of three points……132

Figure 3.17b: Average He/N_2, CO_2/N_2, and O_2/N_2 ideal selectivity of PDMS-caulked PES-carbon black mixed matrix membranes, plotted against carbon black loading. Each data point was measured in triplicate and error bars represent standard deviation of three points……133

Figure 4.1a: SEM micrograph showing typical hollow fiber membrane wall morphology, with the dense separating layer, porous support layer, and macrovoids indicated ..145

Figure 4.1b: SEM micrograph showing typical hollow fiber membrane cross section, with outer diameter (OD), inner diameter (ID), and wall thickness (WT) indicated ……146

Figure 4.2: SEM micrographs of PES hollow fiber membranes spun from 30 wt % PES/DMAc dope with V_b/V_d = (A) 0.5, (B) 2.5, and (C) 4.0 ……..149

Figure 4.3: Relationship between fiber dimensions and V_b/V_d for hollow fibers spun from 30 wt% PES/DMAc dope using a 70 wt% DMAc/water bore fluid and a pure water coagulation bath (n = 10 for each fiber sample)……..……151

Figure 4.4: Relationship between fiber dimensions and air gap distance for hollow fibers spun from 30 wt% PES/DMAc dope using a 70 wt% DMAc/water bore fluid and a pure water coagulation bath (n = 10 for each fiber sample) ……..……152

Figure 4.5: SEM micrographs of the porous support layer of hollow fiber membranes spun from 30 wt% PES/DMAc dope with (A) 3 cm air gap distance and (B) 7 cm air gap distance……154

Figure 4.6: SEM micrographs of PES hollow fiber membranes spun from 30 wt % PES/DMAc dope with DDR = (A) 1.0, (B) 1.5, (C) 2.0, and (D) 2.5 ……156

Figure 4.7: Relationship between fiber dimensions and the square root of draw down ratio for hollow fiber membranes spun from 30 wt% PES/DMAc dope, with 70 wt% DMAc/water bore fluid and deionized water coagulation bath (n = 10 for each fiber sample)……157

Figure 4.8: SEM micrographs of substructure of PES hollow fiber membranes spun from 30 wt% PES/DMAc dope with DDR = (A) 1.0, (B) 1.5, (C) 2.0, and (D) 2.5 158

Figure 4.9a: SEM micrographs of hollow fiber membranes spun from dope composed of 30 wt.% PES in NMP (left) and dope composed of 30 wt.% PES in NMP with a MWCNT loading of 0.1 wt.% (right)……..……166

Figure 4.9b: Macroscopic comparison between neat PES HFM (top) and PES HFM loaded with 0.1 wt.% MWCNT (bottom)……..……166

Figure 4.10a: Plot of He, CO_2, O_2, and N_2 permeance against MWCNT loading for PES-MWCNT mixed matrix hollow fiber membranes. Connecting lines provided as a guide for the eye (n = 3 for each composition)……..169

Figure 4.10b: Plot of ideal selectivity for He/N_2, CO_2/N_2, and O_2/N_2 against MWCNT loading of PES-MWCNT mixed matrix hollow fiber membranes. Connecting lines provided as a guide for the eye (n = 3 for each composition)……170

Figure 4.11a: Plot of He, CO_2, O_2, and N_2 permeance against MWCNT loading for PDMS caulked PES-MWCNT mixed matrix hollow fiber membranes. Connecting lines provided as a guide for the eye (n = 3 for each composition)……..173

Figure 4.11b: Plot of He/N_2, CO_2/N_2, and O_2/N_2 ideal selectivity against MWCNT loading for PDMS caulked PES-MWCNT mixed matrix hollow fiber membranes. Connecting lines provided as a guide for the eye (n = 3 for each composition) ……174

Chapter 1: Introduction and Background

1.1 Polymeric Membrane Separations

The first experimental instance of a nonporous polymeric material demonstrating gas permeability was in 1831, when John K. Mitchell filled several balloons, composed of cis-poly(isoprene), with hydrogen gas and left them on the ceiling of his lecture room [1]. When he observed the balloons slowly drop to the floor of the room, Mitchell hypothesized that the hydrogen must be somehow passing through the walls of the balloons. He then repeated the experiment with several other gases, noting that the gases permeated through the walls of the balloon at differing rates, but also that the rates of permeation were not necessarily correlated solely with the size of the permeating molecule. These two fundamental observations are the foundation upon which the commercial development of polymeric gas separation membranes would eventually be built over a century later.

In an ideal scenario, a gas separation membrane would be made of a material that takes a feed mixture of gases A and B and produces a permeate stream of pure gas A and a retentate stream of pure gas B. However, the classes of materials that have the ability to provide a perfect separations, such as palladium based membranes for hydrogen purification [2], are typically very delicate and/or cannot be economically produced at the scale that is necessary for practical processing volumes. The main challenge in the development of gas separation membranes, which polymeric membranes can address, is the industrial-scale production of membrane modules that

offer the highest possible permeability and selectivity, and that are sufficiently robust to withstand high operating pressures and potentially aggressive process environments.

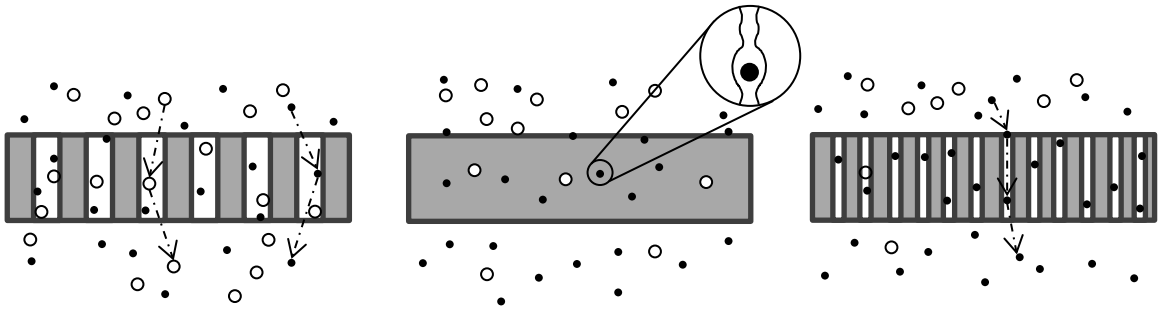

Knudsen Diffusion
Selectivity is proportional to the inverse square root of the ratio of the molecular weights of the two gases, and results in little practical separation.

Solution Diffusion
Selectivity is due to a combination of solubility and diffusivity of the gases within the polymer, resulting in higher gas selectivity.

Molecular Sieving
Selectivity is driven primarily driven by the difference in diffusion rates of smaller molecules relative to the larger molecules across the narrowly defined pores of the membrane.

Figure 1.1: A schematic representation of the three primary diffusion mechanisms that occur within polymeric gas separation membranes.

There are three primary transport mechanisms that can occur within a gas separation membrane: Knudsen diffusion, solution diffusion, and molecular sieving (see Figure 1.1). The first mechanism, Knudsen diffusion, involves pores in the membrane material that are smaller in diameter than the distance a molecule travels before colliding with another molecule (i.e. mean free path). This mechanism results in relative permeation rates for gas pairs that are equal to the inverse of the square root of the ratio of the gas molecular weights [3]. For most applications, Knudsen diffusion results in membrane selectivity that is not sufficient for practical utility. The second diffusion mechanism, molecular sieving, involves separation based on the more rapid diffusion of

the smaller molecules in a feed mixture, with simultaneous rejection, (i.e. filtering) of larger molecules. Membranes based on molecular sieving have received a fair amount of research attention in the last few decades due to their high selectivity and permeability compared to solution diffusion membranes. Zeolites and metal-organic frameworks (MOFs) are examples of the classes of membrane materials that offer high selectivity based on this principle, as their structure encompasses a narrow distribution of pore sizes [4, 5]. The primary drawback of these membranes is that they tend to be very delicate and often are susceptible to fouling. Additionally, they are difficult to scale-up and incorporate into practical membrane modules.

By far the most common transport mechanism for gas separation membranes is solution diffusion [6]. In this type of transport, a gas molecule first dissolves into the membrane material (typically a polymer), then diffuses across the thickness of the membrane due to a concentration gradient, before finally desorbing at the opposite face of the membrane. The solution-diffusion mechanism separates gases based on both their solubility in the membrane material and their mobility once they are dissolved in the membrane. Hence, the overall selectivity of a membrane material for a gas mixture can be described as having a solubility selectivity component and a diffusivity selectivity component. The former differentiates molecules primarily by their condensability, while the latter differentiates molecules primarily by their size. A membrane that uses solution-diffusion as its primary separation mechanism has no continuous pore structure through which the gases can flow, but rather relies on motion of the chain segments of the polymer for the formation of transient gaps in the matrix,

allowing for diffusion to take place from the feed side to the permeate side of the membrane.

Polymeric membranes for gas separations can be classified in two broad categories: they can either be homogeneous (dense) film membranes or they can be asymmetric membranes. Dense film membranes refer to polymeric membranes with a uniform, dense structure across the entire thickness of the membrane, while asymmetric membranes, which can be prepared in either a flat sheet or hollow fiber geometry, consist essentially of a thin, dense layer resting on top of a porous support of the same material. In recent decades, most research and industrial application of membrane-based gas separation has been directed towards asymmetric membranes, but both will be discussed here.

1.1.1 Homogeneous Dense Film Membranes

Homogeneous membranes are the simplest form of a polymeric membrane. They consist of a uniform thin, dense film across which the penetrating molecules diffuse in response to a pressure or concentration gradient. Like any membrane that employs a solution-diffusion separation mechanism, homogeneous membranes separate gas mixtures based on differences in each component's solubility and diffusivity within the membrane material.

Homogeneous membranes are commonly prepared in one of two ways. The first approach is solution-based casting followed by solvent evaporation. In this technique, a thin uniform film of polymer solution is cast on a support and placed under heat and

vacuum until the solvent is removed and all that remains is a solid thin film of polymer material. The second method is by extrusion of molten polymer as a solid thin film. Dense film membranes can be a useful tool for determining the inherent permeability of a particular gas in the polymer and by extension, the inherent selectivity for various potential gas pairs. However, due to their relative thickness, dense film membranes produce gas fluxes that are too low for practical purposes. Therefore, dense film membranes can only be useful if they (a) are composed of a highly permeable polymeric material, such as silicone, or (b) are cast at a very low thickness. Free-standing, dense membranes are often impractical, owing to durability issues [7].

1.1.2 Asymmetric Membranes

Asymmetric membranes have been a staple of the membrane-based separation industry since the invention of cellulose acetate phase-inversion membranes in the early 1960's by Loeb and Souririjan [8]. They are currently used for many different types of separations, such as reverse osmosis, micro-, ultra-, and nanofiltration, as well as dialysis and gas separation. Each of these applications brings into play its own set of challenges and operating requirements. For example, the separation capability of an ultrafiltration membrane is determined by the size and distribution of the pores on the surface of the membrane, while in gas separation, it is necessary to not have any surface pores at all. As discussed above, the separation efficiency of a polymer gas separation membrane is related to the differences in solubility and diffusivity of different gas molecules in the membrane material [9]. An asymmetric gas separation membrane is composed of a thin, dense layer of polymer (approximately 0.1 – 1 μm) on top of an

open, porous sublayer (100 - 200 µm) of the same material, as shown in Figure 1.2. The dense layer is the component of the membrane where all of the separation takes place, as it acts as an ultrathin, homogeneous dense film membrane in its own right, while the underlying porous layer acts solely as mechanical support. The asymmetric membrane morphology provides an enormous advantage over dense homogeneous membranes, as it allows for the dense component of the membrane to be much thinner without sacrificing structural integrity or selectivity. As a result, much higher gas flux can be achieved, thereby increasing the membrane capacity. This dramatic improvement in performance is what allowed membrane technology to begin to compete with other established separation technologies, such as cryogenic distillation, absorption, and adsorption in the 1980's [10].

Figure 1.2: Schematic representation of an asymmetric flat sheet membrane. (A) ~0.1-1 µm thick dense layer, where gas separation occurs via solution diffusion (B) ~100-200 µm thick porous layer, which provides mechanical support.

The primary method of fabrication of asymmetric membranes is by phase inversion of a polymer solution. There are four common techniques for the fabrication of membranes via phase inversion. The first is thermally-induced phase separation (TIPS) [11, 12]. This method relies on the fact that polymers typically become less soluble in solvents as temperature decreases. Demixing is induced by lowering the temperature of the solution until precipitation occurs. After demixing, the solvent can

be removed by either solvent extraction, evaporation, or freeze-drying. The second method for inducing phase inversion is air-casting. This process involves dissolving the polymer in a mixture of a more volatile solvent and a less volatile solvent [13, 14]. The volatile solvent is then allowed to evaporate, which lowers the solubility of the polymer in the solution, causing phase separation. The final two methods both involve exposing a polymer solution (dope) to a substance (non-solvent) in which the solvent is miscible but the polymer is immiscible. The third method for inducing phase separation, vapor phase precipitation, involves phase separation caused by non-solvent vapor penetrating into the solution and lowering the polymer solubility. The fourth method for inducing phase separation, and the method that will receive the most in-depth discussion here, is immersion precipitation.

In the immersion precipitation method, a polymer solution is cast into a thin film or extruded as a hollow fiber and is subject to phase inversion by immersion into a liquid non-solvent bath. This method of phase separation is more complex than methods such as TIPS or air-casting as it takes place in a ternary system with multiple simultaneous diffusion and convection processes operative during membrane formation. The interactions between the three components of the casting system (polymer, solvent, nonsolvent) are generally represented using a ternary phase diagram; a generalized version of a ternary phase diagram for membrane casting is shown in Figure 1.3.

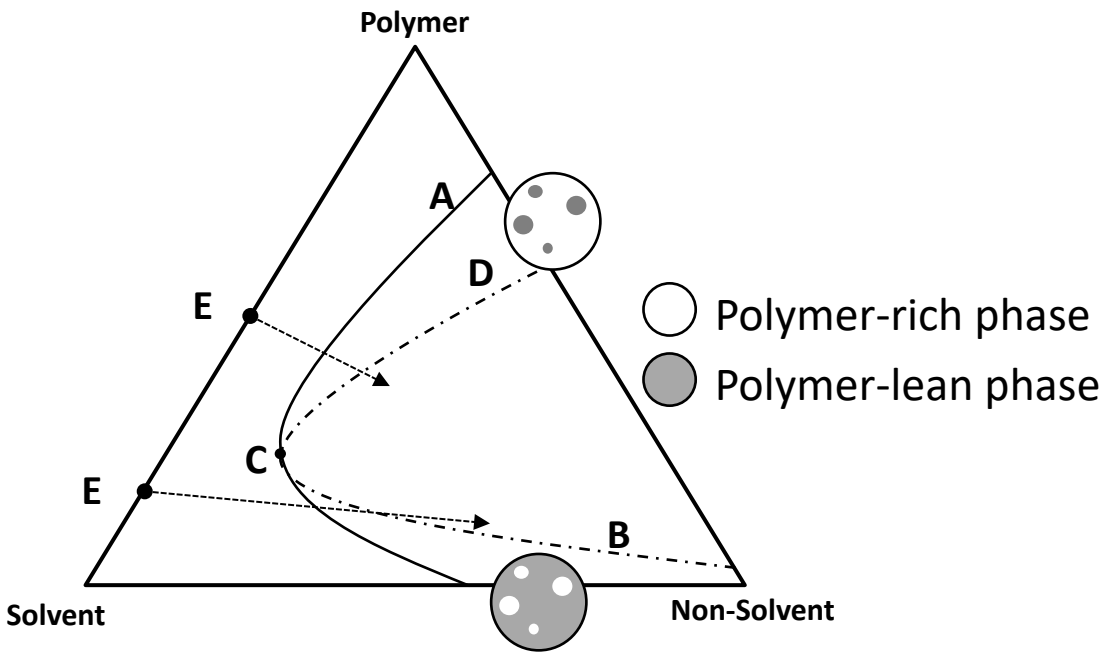

Figure 1.3: Generic ternary phase diagram between polymer, solvent, and non-solvent. (A) Binodal line, (B) Spinodal line, (C) Critical point, where binodal and spinodal are equal, (D) Meta-stable region, (E) Phase separation paths.

When a polymer dope is immersed in a non-solvent bath, the solution separates into two phases, one polymer-rich and one polymer-lean. There are three general possibilities for the morphologies that can evolve during phase separation. Two of these phase separation mechanisms involve the nucleation and growth of one phase within a matrix of another. Nucleation and growth occurs when the composition of the polymer solution (dope) moves from a thermodynamically stable region into a meta-stable region. As shown in Figure 1.3, if the path that the composition of the mixture takes passes below the critical point (where the binodal and spinodal coincide), the formation of a nodular structure, consisting of a polymer-rich phase nucleating within a matrix of polymer-lean phase, is observed. This structure is not conducive to membrane formation. If the path passes through the critical point, only spinodal decomposition

will occur and the morphology will consist solely of an open, porous substructure. This morphology is also not conducive to the formation of viable gas separation membranes. Only if the pathway passes above the critical point through the meta-stable region is the desired asymmetric membrane morphology formed, with a cellular structure emerging from a continuous matrix of polymer-rich phase containing small droplets of polymer-lean phase, which are responsible for pore formation. Additionally, the rate of precipitation of the nascent membrane has a strong effect on the morphology that is obtained. Generally speaking, if the coagulation rate is slow, in a process commonly referred to as delayed demixing, a relatively thick but porous dense separating layer is formed. A rapid rate of coagulation (known as instantaneous demixing) is required in order to form a sufficiently thin, dense and defect free separating layer.

One of the most common issues that arises during the fabrication of polymeric membranes by phase inversion is the formation of structural defects known as macrovoids. In most cases, macrovoids appear as elongated teardrop-shaped pores that extend from the dense separating layer into the porous support layer. The cause of macrovoid formation is one of the more extensively discussed topics in membrane research. The most widely accepted mechanisms at this time are (i) instantaneous liquid-liquid demixing and the nucleation of droplets of polymer-lean phase in a diffusion-driven mechanism, and (ii) local surface instability at the dope/coagulation bath interface, which leads to surface rupture and nonsolvent intrusion into the incipient membrane structure [13, 15, 16].

1.1.2.1 Flat Sheet Membranes

Asymmetric membranes can be formed in two main geometries; flat sheet or hollow fiber. Flat sheet membranes are produced by first casting a polymer dope solution as a thin film onto a substrate. This thin film is then immersed into a bath of nonsolvent (usually water) or a mixture of solvent and nonsolvent. Both the dope composition and the composition of the immersion bath are critical in determining the final morphology of the membrane.

One of the major breakthroughs from the research of Loeb and Sourirajan was the development of a drying procedure that prevented the pore structure of phase-inversion cellulose acetate membranes from collapsing due to internal capillary forces when the membranes were dried [8]. This process was later improved by researchers at DuPont in the late 1970's, who added a solvent exchange step to the drying process [17]. The process that was developed involved removing the residual solvent from the membrane gradually by first soaking it in deionized water long enough to extract the solvent. This step was followed by removal of the water using a water miscible, low boiling point solvent, such as methanol or ethanol [18-21]. The second liquid was then removed using a more volatile solvent that was miscible with the methanol, but was immiscible with water. After the methanol was removed from the film with this more volatile solvent (commonly a hydrocarbon such as pentane or hexane), the solvent was allowed to evaporate away, resulting in a dry flat sheet membrane with an intact pore structure.

For most practical, large-scale processes, flat sheet membranes are incorporated into a spiral wound module, wherein the membrane is wrapped around a central perforated tube and mounted into a module housing. The feed gas mixture is then used to pressurize the module, with the more permeable gas transported preferentially across the membrane and out through the tube at the center, while the less permeable gas exits as retentate. An example of the spiral wound membrane module configuration is shown in Figure 1.4.

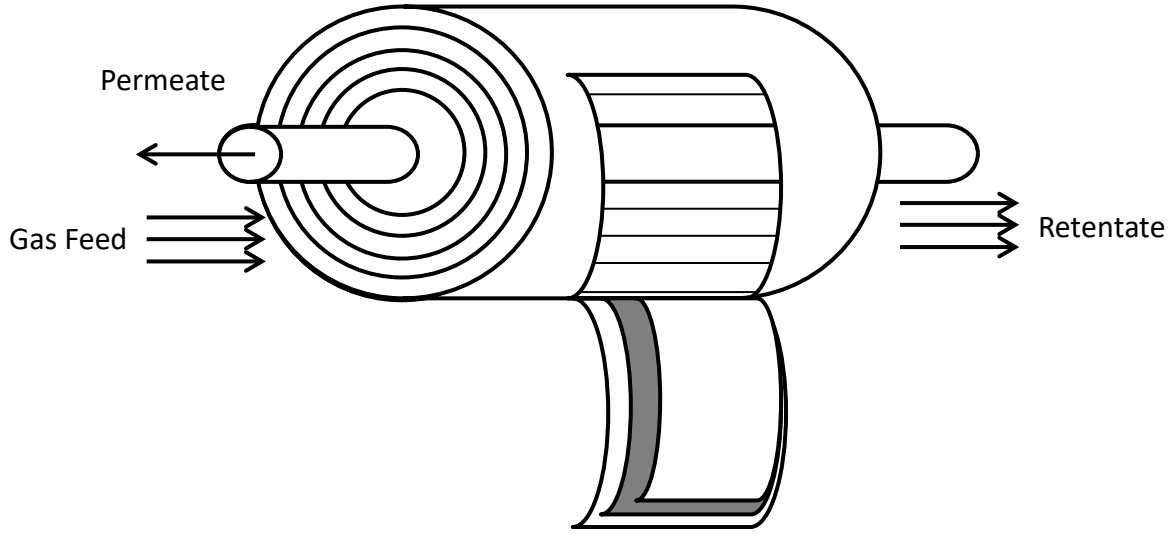

Figure 1.4: Schematic diagram of a spiral wound membrane module.

Flat sheet asymmetric membranes were a large leap forward in the field of membrane technology, as they made it possible for much higher fluxes to be achieved as compared to traditional dense film membranes, without the drawback of low structural integrity.

1.1.2.2 Hollow Fiber Membranes

Asymmetric hollow fiber membranes (HFM) made from polymeric materials were first patented by Mahon in 1966 [22]. Hollow fiber membranes possess multiple features that make them preferable to flat sheet membranes. The hollow fiber membrane geometry gives a higher surface area to volume ratio, meaning that a higher effective membrane area can be achieved for a given size membrane module. This leads to more productive and efficient membrane modules. Hollow fiber membranes also benefit from a self-supporting structure, rendering them much easier to handle during membrane formation and module fabrication.

Hollow fiber membranes are fabricated using a method similar to that of solution spun solid fibers; a generalized schematic of the dry-jet wet spinning process is shown in Figure 1.5. During HFM spinning, the polymer dope solution is metered through an annular spinneret using precise syringe pumps, with a suitable bore fluid metered down the center of the dope through a concentric needle. The nascent fiber then passes through an air gap, where solvent evaporation begins at the dope/air interface and phase inversion begins at the dope/bore interface. Finally, the fiber is immersed in the main coagulation bath (usually composed of water), where phase inversion on the outer wall of the fiber takes place. Once phase inversion is completed, the fiber is taken up out of the bath and wound onto a spool with a water wash. Upon completion of fiber spinning, the residual solvent is removed from the fiber using the

same process of solvent exchange and drying that was described earlier for flat sheet membranes.

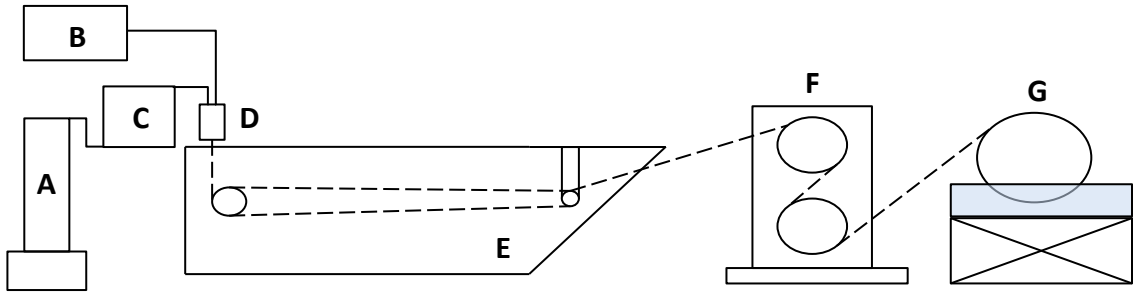

Figure 1.5: Schematic diagram of hollow fiber membrane spinning line (A) Dope extrusion pump, (B) Bore injection pump, (C) Filtration manifold, (D) Extrusion die (spinneret), (E) Coagulation bath, (F) Take-up godet rollers, and (G) Wash winder. Dashed line represents pathway of the nascent hollow fiber membrane.

A key facet of the fiber spinning process is the air gap, as this is where internal phase inversion from the bore fluid begins to form the porous substructure, while the outer dense skin layer emerges simultaneously from a combination of the moisture in the surrounding air and solvent evaporation.

In the half century since they were first invented, a rich literature on the formation and processing of hollow fiber membranes has developed. This literature focuses on two broad areas of study. The first of these is the exploration of various spinning conditions and their effect on the morphology and permselectivity of the resulting membranes [15, 23-33]. In these publications, processing conditions such as shear rate [23], air-gap distance [24, 26], and the dimensions and geometry of the spinneret [27, 32] are found to have profound effects on the final membrane performance. The second broad area of HFM research is concerned with tailoring the

dope formulation in such a way as to (a) minimize the thickness of the dense separating layer while maintaining its integrity, and/or (b) alter the physicochemical properties of the final membrane to improve its overall performance [34, 35]. Some of these methods include (but are not limited to) (i) adding nonsolvent additives to the dope in order to tailor the starting point on the ternary phase diagram, (ii) adding volatile solvent additives, which will be further discussed in the next section, and (iii) the dispersion of inorganic additives into the polymer matrix of the membrane to form a mixed matrix membrane (MMM), which will be discussed in Section 1.3.5.

In many respects, hollow fiber membrane development focuses on identifying casting conditions and dope formulations that produce high-quality flat sheet membranes and applying these to the fabrication of hollow fiber membranes [36]. This provides additional challenges, as the formation mechanism is more complex for HFMs than for flat sheet membranes, and the process conditions that control structure and performance are quite different for HFMs than for flat sheet. One of the primary differences is the presence of two simultaneous coagulation fronts in HFM spinning. When casting a flat sheet membrane, phase-inversion begins at the top surface of the cast film when it is immersed in the coagulation bath, making it fairly easy to control the morphology of the membrane. Hollow fiber fabrication, on the other hand, involves both an internal and external coagulant, each of which controls different parts of the emerging membrane structure. The internal (bore) coagulant controls the morphology of the inner skin of the membrane and much of the porous substructure, while the outer coagulant (along with the air gap) controls the dense separating layer.

Additionally, flat sheet membranes allow much greater control of solvent evaporation prior to phase inversion, as the nature of air-gap spinning allows for only very short times between dope extrusion and contact with the coagulation bath. Further, in HFM spinning, the polymer solution is typically flowing extensionally in the gap as it is accelerated towards the coagulation bath. Cast flat sheet polymer solutions are largely quiescent during phase inversion.

1.1.2.3 Pinhole Defects and Caulking

One of the main issues that arises during the production of asymmetric membranes is the formation of pinhole defects in the dense skin separating layer during phase inversion. These defects are caused by imperfect packing of the polymer chains during phase separation and dramatically reduce the overall performance of the membrane by changing the gas transport mechanism from solution diffusion across the dense skin to Knudsen diffusion through the pinhole channels. This change in diffusion mechanism causes a dramatic loss in selectivity, since Knudsen diffusion only provides a selectivity value that is approximately equal to the inverse of the square root of the ratio of the molecular weights of the constituent gases. With the constant effort to make thinner dense selective layers, the mitigation of pinhole defects becomes ever more important [36].

There are multiple ways to address the question of how to best mitigate the effect of pinhole defects in the dense skin layer of an asymmetric membrane. The simplest answer to the question, but the most difficult to actually achieve in practice, is to

prevent pinhole defects from forming in the first place. Much research has gone into trying to cast (or spin) membrane materials with a defect-free, ultrathin dense selective layer [21, 37-41]. One of the primary methods involves the use of a mixture of solvents, one volatile and one non-volatile, during dope formulation. The addition of a more volatile solvent to the dope causes a more rapid formation of the dense layer in the air gap for hollow fiber membranes (or prior to immersion, in the case of flat sheet membranes) [42]. This method has been fairly well developed, but it is far from perfect, and defects often can still form in the membrane dense layer.

When a membrane is found to have pinhole defects, usually indicated by the exhibition of Knudsen selectivity between gas pairs, the primary method for mitigating these defects is by coating the membrane with a high permeability/low selectivity material, essentially “caulking” the membrane. The resulting membrane is commonly referred to as a composite membrane [43-46]. The most common polymer that is used in this process is polydimethylsiloxane (PDMS), due to it being one of the most permeable polymers in existence. This process mitigates the effect of pinhole defects by changing the diffusion mechanism within the channels from Knudsen diffusion to solution diffusion. The theory describing transport across composite membranes was first proposed in 1981 by Henis and Tripodi [47]. They introduced the idea of quantifying the transport properties of these membranes using a resistance model.

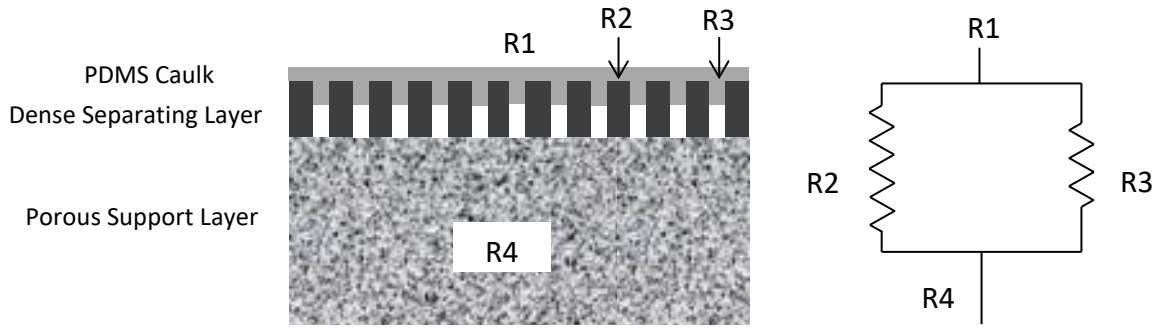

Figure 1.6: Schematic diagram of a porous asymmetric composite membrane (left), along with the electrical resistance analog (right)

As shown in Figure 1.6, the model explains the behavior of a composite gas separation membrane using an analogy with electrical current flow through four resistors. Resistors with resistances R1 and R4 are connected in series with two resistors, R2 and R3, which are connected in parallel to each other. R1 is the diffusion resistance offered by the composite coating of the membrane, R2 is the resistance of the polymer dense layer, R3 the resistance in the defects or pinholes, and R4 is the resistance of the porous substructure of the membrane. This model allows for the ability to predict the separation properties of a composite membrane and has been demonstrated to work in practice to a reasonable degree of accuracy.

1.2 Gas Separation

While the first instance of a polymeric membrane material showing selective permeation of one gas over another dates as far back as the 1830's, commercially viable gas separation membranes did not really emerge until the 1960's. Prior to the pioneering efforts of Loeb and Sourirajan, the field faced serious issues with achieving useful process volumes on a commercial scale. Most attempts to tackle these issues

were primarily aimed at reducing the thickness of a dense film membrane, which led to greater challenges with both an increase in pinhole formation as well as a decrease in the durability of the membrane. In 1970, the asymmetric membrane that Loeb and Sourirajan pioneered for reverse osmosis was finally found to have a gas separation application. The key innovation that came at this time was the ability to transform the membrane from a wet state, as is required for reverse osmosis, to a dry state, as is needed for gas separation, without collapsing the porous support structure [48]. This was achieved using a surfactant-aided solvent exchange and drying procedure. Early gas separation applications relied primarily on flat sheet membranes, but these became less and less common as the technology for asymmetric hollow fiber membranes was established. One of the most well-known of these HFM separators was the Prism® system, based on a polysulfone HFM coated with poly(dimethylsiloxane) (PDMS, or silicone rubber), which was developed by Monsanto (later Air Products) in the late 1970's. These membranes were an additional step forward for the industry, as the solvent exchange and drying procedure for a hydrophobic polymer such as polysulfone was not nearly as tedious and time-consuming as that of the more hydrophilic cellulose acetate membrane. Additionally, polysulfone was chosen for its commercial availability, adequate permselectivity, and easy processability. The strong performance that was exhibited by the Prism® system and other Monsanto products boosted confidence in membrane based gas separators and paved the way for extensive development of the technology from companies such as Dow, DuPont, and Air Products in the 1980's and continuing into the present day.

1.2.1 Equations and Terminology for Gas Separations

Before proceeding too far into the details of specific gas separations, it is necessary to discuss the important terms and basic equations that are used to characterize membrane transport performance. The specifics of the derivation of these equations can be found elsewhere [49]. In most cases, membranes are characterized primarily by two factors, (a) how readily desired gases flow through the membrane (i.e. permeability) and (b) how effective the membrane is at rejecting specific components from the permeate stream (i.e. selectivity).

1.2.1.1 Permeability Coefficient and Permeance

The permeability coefficient (P_A) for a particular gas A describes how quickly gas A can flow through a particular membrane material, normalized by the thickness of the membrane and the applied pressure drop across the membrane. It is expressed by the equation:

$$\mathrm{P}_A = \frac{J_A l}{\Delta P} \qquad [1.1]$$

Where J_A is the steady-state flux of gas component A across the membrane, *l* is the membrane thickness, and ΔP is the trans-membrane pressure difference. P_A is generally viewed as a material property that is not dependent on membrane thickness or pressure drop and is normally expressed in units of Barrer, where:

$$1\ Barrer = \frac{10^{-10} cm^3 (STP) cm}{cm^2 s\ cmHg}$$

Different polymers display different permeability coefficients for different gases, so this material property is very useful in determining the applicability of a membrane polymer for a specific gas. When considering the solution-diffusion model, the permeability coefficient can be expressed with the following equation, where D_A is the effective gas diffusion coefficient and the S_A is the gas solubility coefficient:

$$P_A = D_A S_A \qquad [1.2]$$

The diffusion coefficient is primarily determined by the size of the gas molecule, with larger molecules usually having smaller diffusion coefficients, while the solubility coefficient is mostly dependent on the condensability of the gas molecule as well as interactions between the gas and the polymer matrix.

The gas permeability coefficient can be a very useful property for dense film membranes, where the membrane thickness is easy to measure, or for asymmetric membranes that are comprised of a material for which P_A is known, as it can be used to estimate the thickness of the dense separating layer. For asymmetric membranes where the thickness of the separating layer is not easily measureable, the gas transport performance is best described by gas permeance. The permeance is defined as the pressure normalized flux through the membrane, which is equal to the permeability coefficient divided by the thickness of the membrane:

$$Permeance = \frac{P_A}{l} = \frac{J_A}{\Delta P} \qquad [1.3]$$

Permeance is measured in gas permeation units (GPU), defined as follows:

$$1\ GPU = 10^{-6}\frac{cm^3(STP)}{cm^2\ s\ cm\ Hg}$$

1.2.1.2 Selectivity

The other property that defines the performance of a gas separation membrane is the ideal selectivity between gas pairs. Selectivity characterizes the ability of a polymer to separate two different gases (A and B). The ideal selectivity is defined as

$$\alpha_{A/B} = \frac{(P_A/l)}{(P_B/l)} \qquad [1.4]$$

Ideal selectivity can be defined as the ratio of either the pure gas permeability coefficients or the permeance (provided the measurements are taken on identical membranes). Like the gas permeability, the ideal selectivity is usually treated as a material property of the polymer for a particular gas pair. Ideal selectivity is not a perfect measure of a membrane's ability to separate gases, since it does not take into account potential interactions between the two gases or their influence on the properties of the membrane polymer, but it is still one of the most useful properties for the characterization of gas separation membranes.

1.2.2 The Robeson Upper Bound

In 1991, Lloyd Robeson characterized an empirical upper bound for gas separation membranes, which described the trade-off between permeability (or permeance) and selectivity [50]. Robeson later would revisit the upper bound with nearly two additional decades worth of data in 2008 [51]. In these papers, Robeson

analyzed literature results encompassing a wide range of polymeric membranes in order to fully characterize the inverse relationship between the permeability and selectivity for various gas pairs that involve the common gases of H_2, O_2, N_2, CH_4, and CO_2. This analysis revealed an upper bound to the relationship, which can be represented on a log-log plot of selectivity (α_{ij})versus permeability (P_i) of the faster gas, as shown in Figure 1.7. As demonstrated by Robeson's analysis of the existing literature, virtually no values (i.e. membrane materials) could be found to exist above the upper bound. The upper bound was determined to be a straight line, following the relationship:

$$P_i = k\alpha_{ij}^n \qquad [1.5]$$

where the slope (*n*) of the line is related to the ratio of the Lennard-Jones kinetic diameters of the gases to be separated.

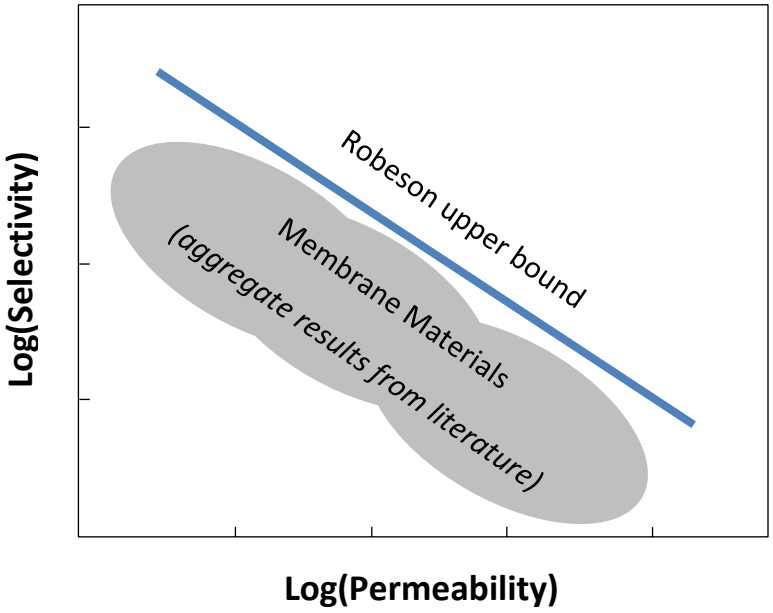

Figure 1.7: Schematic plot of the Robeson upper bound relationship between membrane efficiency (selectivity) and throughput (permeability) [50].

From these results, Robeson concluded that the diffusion coefficient was the primary characteristic that governed the membrane separation capability for the gases in question, but also acknowledged that for more condensable gases at higher pressure, the solubility coefficient also plays a role in gas selectivity and permeability. This review was revolutionary in the sense that it gave a quantitative characterization to a well-known trade-off relationship between the permeability and selectivity of gases and set a goal for future gas separation membrane researchers to exceed the Robeson upper bound.

1.2.3 Air Separation

Membrane-based gas separators can be applied to separate many different feed streams, and two specific examples will be discussed here, as they are two of the most commercially relevant separations. The first of these is the separation of air into a nitrogen enriched component and an oxygen enriched component. The relative permeabilities of the gas constituents of air (namely O_2, N_2, and Ar) in rubber were first characterized by Lord Rayleigh [52]. Since the 1980's, the field has shown rapid expansion, led by companies such as Permea and Dow in the United States, as well as Linde in Germany and Air Products in Norway.

Traditional methods for producing N_2 and O_2 from air include cryogenic distillation and pressure-swing adsorption. Cryogenic distillation works in a similar manner to traditional distillation, but using much lower temperatures. This process involves lowering the temperature of air until it liquefies, then separating the

components based on their boiling points [53]. This process can be used to produce ultrapure N_2 and O_2, but is highly energy intensive and requires large amounts of capital to install and operate. Pressure swing adsorption (PSA) is a process that, unlike cryogenic distillation, can be operated at ambient temperatures. In this process, air is pressurized and gases are separated based on their affinity for an adsorbent material, such as a zeolite. Since it operates at ambient temperatures, PSA provides a significant reduction in both energy and capital costs over cryogenic distillation.

The similar physical properties of N_2 and O_2 lead to fairly low membrane selectivity, compared with other gas separations, such as H_2/CO_2. However, membrane based air separation is now generally seen as favorable over conventional methods for air separation, such as cryogenic distillation and pressure swing adsorption, primarily because of its lower energy consumption and operating costs. Membrane processes can be used to produce nitrogen enriched streams of over 95% N_2 and oxygen enriched streams of 60-80% O_2, which are both adequate for most commercial uses of those gases, as discussed further, below.

1.2.3.1 Nitrogen Enriched Air (NEA)

Since O_2 is the gas that permeates faster through most polymeric membranes, oxygen enriched air (OEA) is usually collected at low recovery in the permeate stream, while nitrogen enriched air (NEA) is collected at higher recovery in the retentate stream. In order to maximize N_2 product recovery and product purity while also reducing capital costs, air is generally separated using a multistage membrane system with a recycle

step. In this system, the retentate from the first membrane unit is fed into a second membrane unit, with the permeate stream from the second unit being compressed and recycled back into the original feed stream. This type of system can produce very high concentrations of N_2 (>99%) at very low recovery using membranes with selectivity as low as 2. In order to recover enough NEA at high concentrations for most practical purposes however, an O_2/N_2 selectivity of approximately 6 or greater is needed.

Nitrogen enriched air produced by membrane-based air separation is used for a variety of purposes in the fields of oil and gas, chemicals and electronics, among others. It is very commonly used as an inerting agent in aircraft fuel tanks in order to reduce exposure to flammable vapors. NEA is also widely used in food storage in order to extend the shelf life of food and reduce spoilage by preventing bacterial growth and eliminating moisture. Additionally, tires filled with NEA rather than air tend to lose pressure at a slower rate, due to the slower transport of nitrogen through the tire walls.

1.2.3.2 Oxygen Enriched Air (OEA)

The ability to produce O_2 from air using membrane based methods has been studied for decades. Initial attempts to produce oxygen enriched air (OEA) were aimed at using PDMS membranes, because of their high O_2 permeability in combination with modest O_2/N_2 selectivity. It wasn't until higher selectivity was achieved (while maintaining high permeability) that the technology began to replace pressure-swing adsorption as the dominant method for OEA production. Currently, the top-of-the-line commercial O_2/N_2 membranes have an ideal selectivity in the range of 8-10 with a

permeability coefficient on the order of 1 Barrer [51]. While this selectivity is reasonably high, the scope of the industry could be considerably expanded if membrane materials with selectivity in the range of 15-20, which is beyond the 2008 Robeson upper bound [51], could be developed at scale. This would allow for the production OEA with above 90% purity, positioning it to rival PSA for more applications.

Oxygen enriched air is most commonly used in combustion-based processes as a way to increase the O_2 content of a reacting fuel-oxidizer mixture, which leads to large improvements in both burn rates and fuel efficiency. For example, when OEA is used as the feed in a power plant, it reduces the amount of N_2 in the flue gas, thereby eliminating a difficult (and expensive) CO_2/N_2 separation that is necessary for CO_2 capture and sequestration. OEA also has the effect of increasing the heating rate and reducing the fuel consumption. Other advantages to using OEA for combustion include a reduction in smoke volume, ignition point of the fuel, and burnout times as well as an increase in heat utilization and radiation heat transfer.

On a smaller scale, OEA has other uses, such as treatment for hypoxia and altitude sickness that are commonly suffered by people who travel to higher altitude areas. A membrane-based OEA production system has the advantage of providing oxygen to someone suffering from altitude sickness, or chronic pulmonary conditions, without the use of a cumbersome and potentially dangerous pressurized oxygen tank. Oxygen enrichment technology can also be used in sleeping tents to improve exercise

performance, provide OEA to aircraft passengers to combat hypoxia, and in some cases, purely for recreational use [52].

1.2.4 Natural Gas Purification

Natural gas contains mostly methane (CH_4), but it also contains several impurities, such as carbon dioxide (CO_2), nitrogen (N_2), hydrogen sulfide (H_2S), water (H_2O), and various heavy hydrocarbons. Each of these impurity concentrations must be reduced in the gas stream in order to meet pipeline specifications by the Federal Energy Regulatory Commission (FERC) [54]. The removal of CO_2 in particular is very important, as it corrodes pipelines, lowers the heating value of the natural gas, and increases the costs associated with compression of the gas. The most commonly used method for removal of natural gas pollutants is amine gas treatment (also called amine scrubbing, gas sweetening, and acid gas removal) [55]. In this process, raw natural gas is passed through an amine solution, usually monoethanol amine (MEA) or diethanol amine (DEA), which absorbs acid gases (H_2S and CO_2). This method works very well, but has the disadvantages of high operating costs as well as the necessity of special materials for equipment construction in order to mitigate corrosion. The primary advantage that amine scrubbing has traditionally held over membrane-based separation is the ability to handle higher volumes and gas streams with extraordinarily high CO_2 content. Amine scrubbing also has the ability to meet standards for CO_2 removal to the ppm level, whereas membrane-based separators struggle to produce gas streams with below 2% CO_2 [56]. Advances in membrane technology over the past two decades have begun to

make membranes competitive with amine absorption [57]. As with air separation, the primary advantage to using membrane-based separation is cost. Membrane-based separator systems tend to have very low installation, operating, and maintenance cost, as well as lower energy consumption during operation. These improvements are generally attributed to the fact that membrane separations do not require a change of phase.

The first demonstrations of acid gas removal from natural gas feed streams using membranes date back to the late 1960's, with the asymmetric cellulose acetate membrane that was developed by Loeb and Sourirajan. These early membranes showed actual selectivities that were much lower than the ideal pure gas selectivity of the gases due to the effects of plasticization caused primarily by CO_2. Plasticization occurs when the concentration of CO_2 is high enough to increase the free volume and mobility of the polymer molecules, which causes the polymer matrix to swell with an accompanying loss of selectivity. This effect can be characterized by a decrease in the glass transition temperature (T_g) of the polymer. Various strategies have been explored to mitigate plasticization in hollow fiber membranes, for example through the use of crosslinked CO_2-resistant polyimides [58] or polyamides [59].

Another contaminant of natural gas streams that must be removed is nitrogen. Nitrogen lowers the BTU value of natural gas and must be below a certain level for sale to a pipeline. N_2 can be separated from natural gas using membranes to produce both pipeline-quality gas and a nitrogen-rich retentate stream. Traditional methods for

removing nitrogen from natural gas feeds include cryogenic distillation and pressure-swing adsorption, similar to air separation. As with air separation, membrane-based separation methods offer both a lower capital cost as well as a lower energy cost. This is an area of active research.

1.3 Relevant Membrane Polymers of Interest

1.3.1 Cellulose Acetate (CA)

Cellulose acetate (CA) was one of the first polymeric membrane materials to be used for natural gas separation applications [48]. It was originally developed for water desalination [60-62], but with the invention of asymmetric phase inversion membranes by Loeb and Sourirajan, as discussed earlier [8], CA became a viable membrane for gas separations as well. Since then, it has been used commercially for multiple gas separations, but it is most effectively used for the removal of acid gases from natural gas and the separation of CO_2 from hydrocarbons. The main advantage that CA membranes have over other commercial membranes is their low cost. They can be made cheaply, mostly because raw cellulose is both abundant and renewable. Additionally, since CA membranes have been around so long, the kinetics and thermodynamics governing their formation are very well understood [13, 14], ensuring that they can be easily fabricated.

There are two main drawbacks to the use of cellulose acetate for gas separations. The first is that it is far from the most efficient polymer for most applications, with gas performance characteristics (i.e. selectivity; permeability) that lie

well below the Robeson upper bound. The other main drawback to the use of CA is that it is very susceptible to CO_2-induced plasticization. This effect causes the CA membrane to lose selectivity in mixed gas environments at high partial pressures of CO_2. Because of these issues, the separation capability of CA is heavily dependent on feed pressure and composition, and thus most research, both commercial and academic, has been focused on other material platforms for gas separations, such as the ones that will be discussed in the following sections.

1.3.2 Poly(aryl ether sulfones)

The poly(aryl ether sulfones) are a class of thermoplastic polymers characterized as having a diphenylene sulfone backbone (-Ar-SO_2-Ar), and they include some of the most commonly used commercial membrane polymers for a wide range of applications [63-67]; see the repeat structures in Figure 1.8. Polysulfones have emerged as an important class of membrane polymers primarily due to their outstanding mechanical strength, dimensiona l stability, and exceptional thermal and chemical resistance.

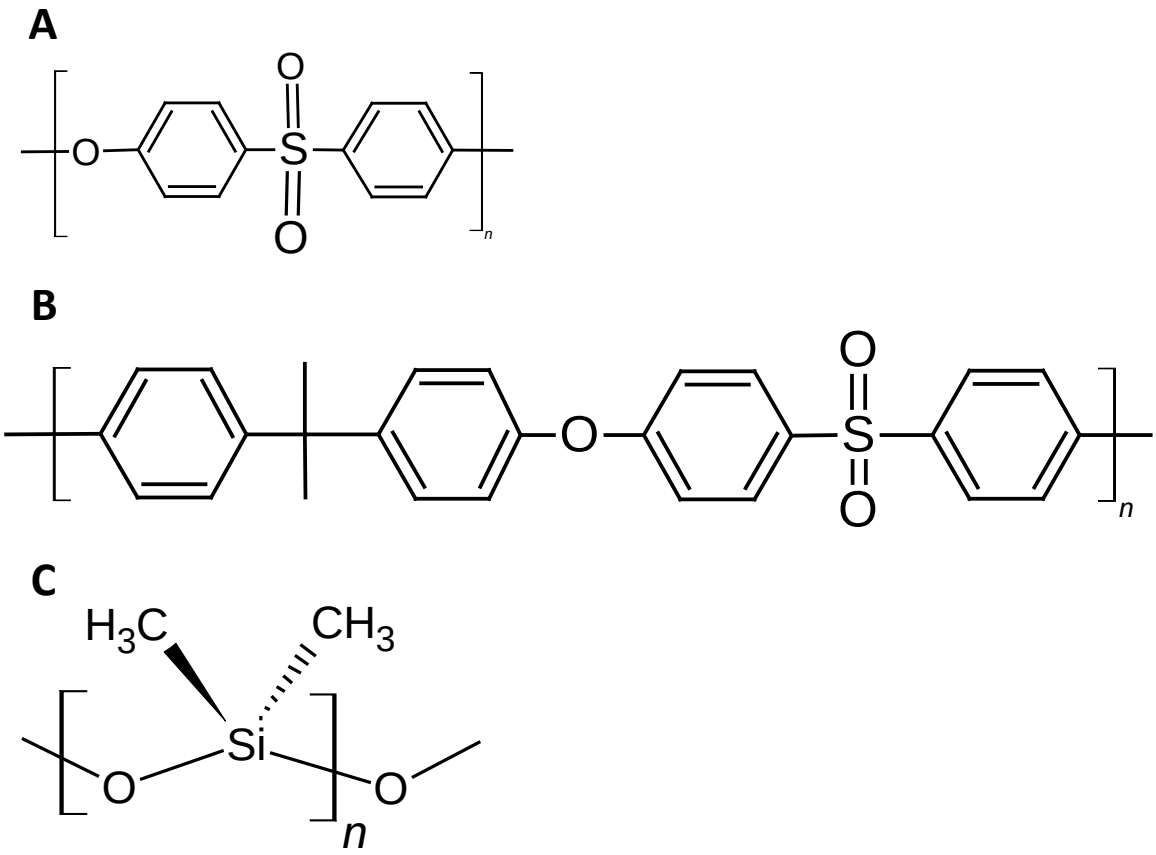

Figure 1.8: Polymer repeat unit for (A) polyethersulfone (PES), (B) polysulfone (PSf), and (C) polydimethylsiloxane (PDMS).

Polyethersulfone (PES) has been used in ultrafiltration and gas separations for decades and readily forms asymmetric membranes via phase inversion, either as a flat sheet or a hollow fiber [68]. PES is a very commonly used polymer in membrane fabrication due to its relatively low cost as compared to other membrane polymers. However, PES is also susceptible to fouling during water filtration due to its high hydrophobicity. Because of this, there has been an emphasis on modification of PES membranes via polymer blending, surface modification [69, 70], and addition of inorganic fillers to form mixed matrix membranes (MMM) [71-73].

Numerous studies have been conducted by Chung et al., exploring the influence of various spinning parameters on the morphology and separation performance of PES hollow fiber membranes [23, 24, 28-30, 32, 65, 74]. These studies include investigations into the effects of air gap distance, spinning temperature, and dope shear rate within the spinneret on the membrane morphology and performance. Much of this research focuses on the formation of macrovoids in PES membranes [15]. Macrovoids are large defects that form during phase inversion. While they do not completely ruin the performance of a membrane, it is often beneficial to avoid the formation of macrovoids, as they are structural defects that can result in mechanical failure of the membrane in high pressure applications.

Polysulfone (PSf) is one of the most commonly used commercial gas separation membranes, and it is the basis for the Air Products PRISM® membrane system discussed earlier. Polysulfone has a similar structure to polyethersulfone, but with an additional bisphenol unit connected by an ether group, as shown in Figure 1.8. This structural difference in the polysulfone repeat, as compared to polyethersulfone, results in less efficient packing, leading to a higher fractional free volume in polysulfone and a higher permeability, while only slightly lowering the selectivity. Polysulfone is widely used for hydrogen and air separations and has similar proximity to the Robeson upper bound as other commercial gas separation polymers, such as Matrimid® polyimide.

1.3.3 Polyimides

Aromatic polyimides are generally useful as gas separation membranes, as they tend to have high permeability and high intrinsic selectivity, and also have good physical properties. In industry, polyimide membranes are used by gas companies Praxair and Air Liquide for natural gas purification, due to an industry-best combination of CO_2 permeability of about 10 Barrer and CO_2/CH_4 selectivity of 36. Matrimid® is the most commonly used commercial polyimide, originally developed for use in the electronics industry, but later found to have gas separation applications as well. Matrimid® is not only used for its good permselectivity, but it also has exceptional mechanical strength and high T_g, which make it a preferred choice for high temperature environments. It also has the advantage of being soluble in common organic solvents, allowing it to be processed in solution, which is necessary for asymmetric membrane fabrication. The main drawback of Matrimid® is that, like cellulose acetate, it is susceptible to CO_2-induced plasticization at high pressures.

One of the most effective strategies to improve the gas permeability (particularly CO_2) in aromatic polyimide materials and combat CO_2-induced plasticization is thermal rearrangement (TR) [75-79]. Thermal rearrangement changes the backbone structure of the membrane from an aromatic polyimide containing hydroxyl groups *ortho* to the imide ring into a thermally-resistant polybenzoxazole (PBO) by heating the polymer to a high temperature (> 400°C) in an inert atmosphere, as shown in Figure 1.9.

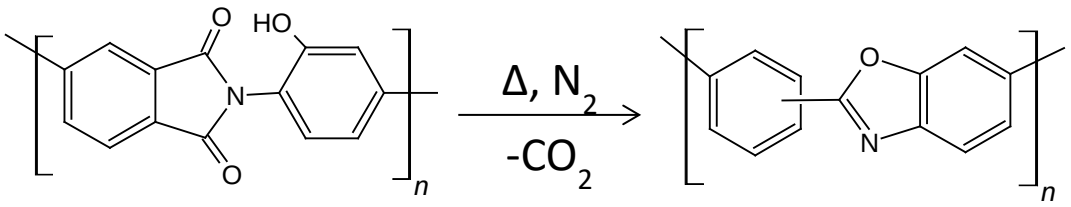

Figure 1.9: General reaction taking place during thermal rearrangement process.

An advantage to the thermal rearrangement process is that it makes it possible to fabricate PBO membranes, which have superior gas separation performance but tend to be insoluble, by solution spinning the polyimide precursor. This allows fabrication of these membranes using readily available industrial processing methods [80]. TR polymeric membranes show much promise, as they have in the past exhibited permselectivities that exceed the empirical Robeson upper bound [75]. There are two major drawbacks to TR polymers, however. The first is the high cost of both the polymer precursors and the processing that is required to fabricate TR membranes. The other issue is that, since high temperatures are required to convert aromatic polyimides to PBOs, some thermal degradation is expected to overlap with the TR process, thereby reducing the mechanical properties of the resulting membranes [77]. Overall, as research into TR polymers improves the technology, their role within the CO_2 removal industry will continue to grow.

1.3.4 Polymers of Intrinsic Microporosity (PIMs)

Another emerging class of polymeric gas separation membrane materials is polymers of intrinsic microporosity (PIMs) [81]. These materials are non-network polymers that mimic the structure of zeolites, due to their rigid molecular structure,

which prevents efficient packing of the polymer chains in the solid state. They were first developed by Budd et al. in the early 2000's [82-84]. The microporosity of these polymers is described as intrinsic, because it is derived solely from their molecular structure and not from any processing history of the material. An example of the molecular synthesis and structure of PIM-1, one of the most commonly used PIMs, is shown in Figure 1.10.

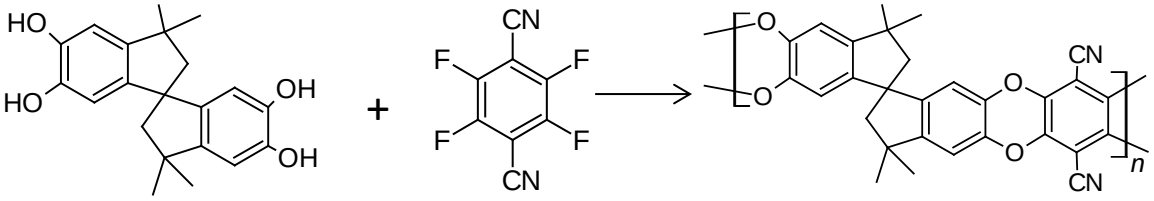

Figure 1.10: Preparation of PIM-1 polymer of intrinsic microporosity.

The two main reactants that are required for this synthesis are an aromatic tetrol and a halogen containing monomer. As the figure shows, the spirocyclic feature of the precursor molecule leads to a contorted confirmation and the formation of a dibenzodioxane ladder structure, which then results in a rigid backbone in the final polymer, which has no rotational freedom but also has a randomly assorted molecular structure.

There are two main drawbacks to PIMs. The first is that, while the aromatic tetrol precursor is readily available at the commercial level, the required aromatic halides tend to be very expensive and limited in their commercial availability [80]. Additionally, it is often difficult to synthesize PIMs in adequate molecular weights and yields, which results in difficulty in the formation of thin film membranes and also

contributes to inadequate mechanical properties. Although the permselectivity of PIMs has been shown to exceed the 1991 Robeson upper bound and approach the 2008 revisited upper bound, when compared with TR polymers for processes like natural gas purification (CO_2/CH_4), PIMs often show similar permeabilities but lower selectivities. The biggest advantage that PIMs have over TR polymers is the lack of a high temperature heat treatment step during fabrication. The removal of this step means that PIMs can be cast directly in their final form, lowering the production cost as well as the energy cost.

1.3.5 Mixed Matrix Membranes (MMM)

In order to overcome the limitations of the solution diffusion gas transport mechanism model (i.e. the Robeson upper bound), while maintaining the processability of polymers, an emerging development in the field of gas separation membrane research is the addition of inorganic additive materials to an asymmetric polymer matrix to form composite membrane materials known as mixed-matrix membranes (MMM). A general schematic of a MMM is shown in Figure 1.11. These materials can improve the permselectivity of a polymeric membrane by adding a component of molecular sieving to the transport mechanism, since inorganic materials often have narrow distributions of pore sizes and geometries. Additionally, these materials often possess chemical functionalities that are not present in polymeric materials, which can increase the solubility selectivity of the membrane by acting as selective adsorbents.

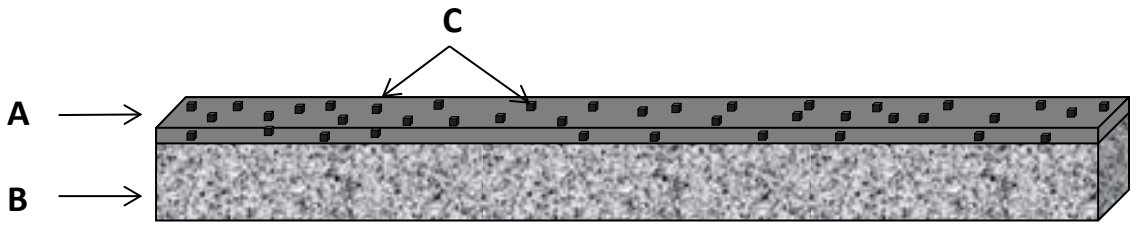

Figure 1.11: Schematic representation of an asymmetric flat sheet mixed matrix membrane. (A) Dense separating layer (B) Porous support layer, (C) Dispersed inorganic filler material, which adds a component of molecular sieving to the solution diffusion mechanism.

The first known application of a MMM for gas separation in the literature involved the dispersion of 5A zeolite into polydimethylsiloxane (PDMS), conducted by Paul and Kemp in the early 1970's [85, 86]. In these studies, the researchers discovered that adding the zeolite to the polymeric matrix caused a large increase in the diffusion time lag, but they did not observe a significant effect on the steady-state diffusion properties. The first to report an increase in selectivity due to the addition of an inorganic filler material were researchers with Honeywell, who observed an increase in O_2/N_2 selectivity in cellulose acetate with the addition of silicalite [87]. Since then, a broad range of filler materials have been observed to improve membrane performance, including zeolites, metal-organic frameworks (MOFs), and carbon materials, such as carbon molecular sieves or carbon nanotubes [88].

1.3.5.1 Zeolite MMM

Zeolites were the first material to be incorporated as the inorganic filler in a mixed-matrix membrane and have shown much promise in the field due to their unique molecular sieving properties. An example of this type of material is described in the

work by Kulprathipanja et al [72]. In this work, microporous and nanoporous zeolite 4A was dispersed in a matrix of polyethersulfone (PES). The research showed an increase in selectivity for several gas pairs, including He/N_2, O_2/N_2, and CO_2/CH_4 for both the micro- and nanoporous zeolite 4A, but also resulted in a decrease in the permeability coefficient for all of the gases studied.

Despite their promise, zeolite MMMs still have not gained much commercial relevance. There are several reasons for this. The first is that zeolites and polymers often suffer from a lack of interfacial compatibility, which leads to an increase in non-selective defects at the interface of the zeolite particles and the polymeric matrix. The other issue that plagues zeolite MMMs is poor mechanical properties, particularly when dealing with thin films. Other challenges include polymer rigidification, pore blocking, and the fact that zeolites often adsorb gases to binding sites, which can result in reduced diffusion for vapors. Because of all of these issues, recent MMM research has moved away from zeolites and toward metal-organic frameworks and inorganic carbon based filler materials.

1.3.5.2 Metal Organic Framework (MOF) MMM

While most of the early work in mixed-matrix membranes was focused on zeolite molecular sieves dispersed in a polymeric matrix, more recent studies of MMMs have been directed toward a relatively new class of microporous materials with metal organic frameworks (MOFs) as the inorganic filler material [5, 89-94]. MOFs are comprised of transition metals or transition metal oxides connected by organic linkages to create

microporous structures. These microporous structures can result in extremely high surface areas, with some reported as high as 10,000 m^2/g. Like zeolites, MOFs can be synthesized quickly, cheaply, and easily. Additionally, MOFs have an enormous range of variability in composition and structure, with the organic linkages providing a platform for chemistries that can improve polymer adhesion [5], thereby reducing nonselective defects that often plague zeolites at the filler-matrix interface. The range of material variables available in MOF-based mixed matrix membranes can be exploited to produce a tunable pore structure, mechanical and chemical stability, as well as CO_2 plasticization resistance in some cases.

The most common sub-class of MOFs to be featured in mixed matrix membranes are zeolitic imidazolate frameworks (ZIFs). ZIFS are usually formed from zinc or cobalt ions tetrahedrally coordinated to imidazolate linkers. They get their name (zeolitic) due to the bond angle similarities with zeolites [88]. Within this sub-class, the most extensively studied for gas separation membrane applications is ZIF-8. In a crystallographic sense, ZIF-8 has a 3.4 Å pore aperture and 11.6 Å cages [88]. The small pore aperture gives this material the properties of a molecular sieve with length scales appropriate for gas separations. Additionally, part of the organic linker of this MOF can rotate within the pores, creating a flexible gate opening mechanism in the pores that can allow larger molecules to diffuse through the pore system. For pure gas measurements, Song, et al. found that ZIF-8/Matrimid® MMMs enhanced the permeability of H_2, CO_2, O_2, N_2, and CH_4 without showing any decrease in selectivity, at loadings as high as 30 wt.% [94]. They have also been applied to hollow fiber

membranes for CO_2/N_2 separations, as demonstrated by Koros et al. [95]. In this work, 17 vol% ZIF-8 was incorporated into a matrix of polyetherimide (Ultem® 1000), which resulted in an increase in CO_2/N_2 selectivity from 30 to 36 while also increasing the permeance of the membrane from 14 GPU to 26 GPU over a neat Ultem hollow fiber membrane.

Overall, MMMs composed of a polymeric matrix with a metal-organic framework are an important emerging class of membrane materials for gas separations. This is due to their relatively low cost, ease of synthesis, accessible range of material variants and strong adhesion to the polymeric matrix.

1.3.5.3 Carbon Nanotube (CNT) MMM

Since they were first described in detail by Ijima in 1991 [96], carbon nanotubes (CNT) have been extensively studied for their thermal, electrical and mechanical properties, as well as their potential utility in membrane applications. For example, in one early approach, polymeric membranes were configured with aligned carbon nanotube arrays and used as nanoporous water filtration membranes, as described by Hinds et al. [97-100]. In more recent years, they have been incorporated as an inorganic filler material in mixed matrix membranes [71, 90, 92, 101-103]. Although it is sometimes difficult to get an even dispersion of carbon nanotubes with good adherence to the polymeric matrix, carbon nanotubes have been found to improve the selectivity of polysulfone [104], and polyethersulfone [102, 105] membranes for gas separation. For example, studies by Ismail, et al., explored potential ways to improve the adhesion

of carbon nanotubes to the polymeric matrix by functionalizing the nanotube surface. Using this approach, they were able to increase the O_2/N_2 ideal selectivity of neat polyethersulfone from 5.6 to 10.65 at a nanotube loading of 0.5 wt.%. A decrease in selectivity was observed as the nanotube content was increased further, which the researchers attributed to an increased presence of interfacial voids. The flat sheet MMM study by Ismail was extended by Zeinali, et al., who further examined carbon nanotube pretreatments as well as the effects of the solvent on the morphology and gas separation properties of the membranes [102]. This study determined that N-methylpyrrolidone (NMP) was the most effective solvent for the fabrication of flat sheet mixed matrix membranes, citing improvements in MWCNT distribution and a reduction in agglomeration as compared to N,N-dimethylacetimide (DMAc). In the hollow fiber geometry, the addition of multi-wall carbon nanotubes that had been pretreated with dry air oxidation, (which removed amorphous carbon and catalyst particles), and were aided in dispersion by the use of Triton X100 surfactant were shown to improve the permeability of polyetherimide (PEI) without any reduction in selectivity for O_2/N_2 [106]. Overall, carbon nanotubes represent a promising but relatively unexplored inorganic filler material for use in mixed matrix membranes, and are of particular interest for incorporation into hollow fiber membrane systems.

1.4 Research Objectives

The research presented in this dissertation was conducted in pursuit of four broad objectives related to the controlled formulation, processing and characterization of flat sheet and asymmetric hollow fiber membranes. These objectives were:

1.) To design, fabricate, and commission a fully-functional hollow fiber membrane spinning line.
2.) To study the phase inversion characteristics of flat sheet membranes to determine the effects of dope composition (including solvent) and coagulation medium on membrane morphology.
3.) To investigate hollow fiber processing conditions as they relate to the resulting dimensions and morphology of hollow fiber membranes.
4.) To examine the effects associated with the inclusion of low levels of nanoscale inorganic filler materials on the gas transport properties of membranes in both the flat sheet and hollow fiber membrane geometries.

Prior to this research work, the capacity to produce hollow fiber membranes did not exist at the University of Kentucky. Accordingly, the first objective pursued was the design, construction and commissioning of a hollow fiber membrane spinning line for the controlled production of polymer hollow fiber membranes. This effort was informed by review of literature and current industrial practice, and drew on extensive in-house expertise available at the UK Center for Applied Energy Research. The resulting spin line was designed to provide all necessary control and versatility to accommodate a wide range of processing rates, formulations and membrane quench conditions.

In order to establish appropriate membrane formulations and quench conditions, the phase inversion characteristics of selected membrane casting systems were studied in the flat sheet geometry. Specifically, the influence of polymer dope composition and coagulation medium on membrane morphology was investigated. These experiments were conducted in order to fully elucidate the morphological features of the resulting polyethersulfone and polysulfone asymmetric membranes across a range of casting conditions. While these studies provided foundational knowledge in the context of the flat sheet geometry, they also informed the determination of dope composition, bore fluid, and external coagulant for hollow fiber membrane spinning. When spinning hollow fiber membranes, it is important that the resulting membrane morphology display a thin, integral dense outer separating layer, minimal macrovoids, a sponge-like porous support layer, and a porous wall on the lumen (interior) side of the membrane. This structure results in a gas separation membrane that exhibits the highest possible permeance without sacrificing selectivity. The compositions of the dope and the bore fluid play a critical role in achieving the desired morphology in hollow fiber membranes.

Three key membrane processing parameters were identified that have the potential to strongly influence the dimensions, morphology and resulting gas separation characteristics of the hollow fiber membranes prepared in this work. These are: (i) the ratio of the bore fluid velocity (i.e. flowrate) to the dope velocity at the exit of the spinneret; (ii) the vertical air gap distance between the spinneret and the coagulation bath; and (iii) the ratio of the take-up velocity of the solid fiber as compared to the

velocity of the dope as it is extruded from the spinneret (i.e. draw down ratio). These parameters were systematically varied in order to determine their influence on the dimensions and morphology of the hollow fiber membranes, relative to the desired morphological features articulated above. Additionally, the experiments were used to establish a standard set of operating conditions for the hollow fiber spinning of mixed matrix membrane formulations.

The final objective of this research was to investigate the inclusion of low levels of nanoscale inorganic filler materials and to assess their influence on the gas transport properties of polyethersulfone and polysulfone membranes. Of particular interest was the inclusion of multiwall carbon nanotubes for the creation of mixed matrix membranes in both the flat sheet and hollow fiber geometries. Utilizing a well-characterized supply of multi-wall carbon nanotubes synthesized in-house, formulation strategies were implemented for the production of casting dopes with uniform nanotube dispersion. The resulting membranes were studied both in terms of their morphology and corresponding permeation properties. The latter studies required the development of gas permeation testing equipment, and the establishment of protocols for the assembly of hollow fiber membrane permeation mini-modules. In addition, post-processing coating methods were used to remediate the surface defects typically encountered with as-cast asymmetric membrane structures.

The chapters that follow describe in detail how the objectives were accomplished. The design and assembly of the hollow fiber membrane spin line, and all experimental details related to membrane formulation, casting and permeation testing

are described in Chapter 2. Chapter 3 presents the results for the flat sheet membrane experiments, including studies on phase inversion morphology and gas transport for unfilled polyethersulfone and polysulfone membranes, as well as mixed matrix membranes based on inclusion of carbon nanotubes and carbon black. Chapter 4 describes hollow fiber membrane processing, including the influence of variations in feed flowrate, vertical gap distance prior to quench, and take-up rate on fiber characteristics. In addition, the permeation properties of the hollow fiber membranes are reported. Finally, Chapter 5 provides a summary of all important conclusions and a discussion of potential future work.

1.5 References

1. Mitchell, J.K., *On the penetrativeness of fluids.* The Journal of the Royal Institution of Great Britain, 1831. **4**: p. 101.
2. Ward, T.L., Dao, T., *Model of hydrogen permeation behavior in palladium membranes.* Journal of Membrane Science, 1999. **153**(2): p. 211-231.
3. Uhlhorn, R.J.R., Keizer, K., Burggraaf, A. J., *Gas and surface-diffusion in modified gamma-alumina systems.* Journal of Membrane Science, 1989. **46**(2-3): p. 225-241.
4. Caro, J., Noack, M., *Zeolite membranes - Recent developments and progress.* Microporous and Mesoporous Materials, 2008. **115**(3): p. 215-233.
5. Keskin, S., Liu, J., Rankin, R. B., *Progress, opportunities, and challenges for applying atomically detailed modeling to molecular adsorption and transport in metal-organic framework materials.* Industrial & Engineering Chemistry Research, 2009. **48**: p. 2355-2371.
6. Wijmans, J.G. and R.W. Baker, *The solution-diffusion model - a review.* Journal of Membrane Science, 1995. **107**(1-2): p. 1-21.
7. B., L. and A.-S. M.N.Z., *Fundamentals of Membrane Processes. In: Fundamentals of Membrane Bioreactors.* Springer Transactions in Civil and Environmental Engineering, 2017.
8. Loeb, S., Sourirajan, S., *Sea water demineralization by means of a semipermeable membrane.* Advances in Chemistry, 1962. **38**: p. 117-132.
9. VandeWitte, P., Dijkstra, P. J., VandenBerg, J. W. A., Feijen, J., *Phase separation processes in polymer solutions in relation to membrane formation.* Journal of Membrane Science, 1996. **117**(1-2): p. 1-31.
10. Koros, W.J., Fleming, G. K., *Membrane-based gas separation.* Journal of Membrane Science, 1993. **83**(1): p. 1-80.
11. Strathmann, H., *Production of microporous media by phase inversion processes.* ACS Symposium Series, 1985. **269**: p. 165.
12. Strathmann, H., Koch, K., *The formation mechanism of phase inversion membranes.* Desalination, 1977. **21**: p. 241.
13. Zeman, L., Fraser, T., *Formation of air-cast cellulose acetate membranes. Part I: Study of macrovoid formation.* Journal of Membrane Science, 1993. **84**: p. 93.
14. Zeman, L., Fraser, T., *Formation of air-cast cellulose acetate membranes. Part II: Kinetics of demixing and microvoid growth.* Journal of Membrane Science, 1994. **87**: p. 267.
15. Peng, N., Chung, T. S., Wang, K. Y., *Macrovoid evolution and critical factors to form macrovoid-free hollow fiber membranes.* Journal of Membrane Science, 2008. **318**(1-2): p. 363-372.
16. Widjojo, N., Chung, T., *Thickness and air gap dependence of macrovoid evolution in phase-inversion asymmetric hollow fiber membranes.* Industrial & Engineering Chemistry Product Research and Development, 2006. **45**: p. 7618-7626.
17. Manos, P., *Solvent drying of cellulose ester membranes*, 1978, DuPont: USA, US4068387.
18. Bindal, R.C., Hanra, M. S., Misra, B. M., *Novel solvent exchange cum immersion precipitation technique for the preparation of asymmetric polymeric membrane.* Journal of Membrane Science, 1996. **118**(1): p. 23-29.

19. Bindal, R.C., M.S. Hanra, and B.M. Misra, *Novel solvent exchange cum immersion precipitation technique for the preparation of asymmetric polymeric membrane.* Journal of Membrane Science, 1996. **118**(1): p. 23-29.
20. Jawad, Z.A., Ahmad, A. L., Low, S. C., Chew, T. L., Zein, S. H. S., *Influence of solvent exchange time on mixed matrix membrane separation performance for CO_2/N_2 and a kinetic sorption study.* Journal of Membrane Science, 2015. **476**: p. 590-601.
21. Kurdi, J., Tremblay, A. Y., *Preparation of defect-free asymmetric membranes for gas separations.* Journal of Applied Polymer Science, 1999. **73**(8): p. 1471-1482.
22. Mahon, H., *Permeability separatory apparatus, permeability separatory membrane element, method of making the same and process utilizing the same*. 1966, Dow Chemical Co, USA ,US3228876.
23. Cao, C., Chung, Tai-Shung, Chen, Shing Bor, Dong, ZhengJun, *The study of elongation and shear rates in spinning process and its effect on gas separation performance of Poly(ether sulfone) (PES) hollow fiber membranes.* Chemical Engineering Science, 2004. **59**(5): p. 1053-1062.
24. Chung, T.S., Hu, X. D., *Effect of air-gap distance on the morphology and thermal properties of polyethersulfone hollow fibers.* Journal of Applied Polymer Science, 1997. **66**(6): p. 1067-1077.
25. Chung, T.S., Kafchinski, E. R., *The effects of spinning conditions on asymmetric 6FDA/6FDAM polyimide hollow fibers for air separation.* Journal of Applied Polymer Science, 1997. **65**(8): p. 1555-1569.
26. Chung, T.S., Z.L. Xu, and W.H. Lin, *Fundamental understanding of the effect of air-gap distance on the fabrication of hollow fiber membranes.* Journal of Applied Polymer Science, 1999. **72**(3): p. 379-395.
27. Peng, N., Chung, T. S., *The effects of spinneret dimension and hollow fiber dimension on gas separation performance of ultra-thin defect-free Torlon® hollow fiber membranes.* Journal of Membrane Science, 2008. **310**(1-2): p. 455-465.
28. Qin, J.J., Gu, J., Chung, T. S., *Effect of wet and dry-jet wet spinning on the sheer-induced orientation during the formation of ultrafiltration hollow fiber membranes.* Journal of Membrane Science, 2001. **182**(1-2): p. 57-75.
29. Qin, J.J., R. Wang, and T.S. Chung, *Investigation of shear stress effect within a spinneret on flux, separation and thermomechanical properties of hollow fiber ultrafiltration membranes.* Journal of Membrane Science, 2000. **175**(2): p. 197-213.
30. Wang, K.Y., Matsuura, T., Chung, T. S., Guo, W. F., *The effects of flow angle and shear rate within the spinneret on the separation performance of poly (ethersulfone) (PES) ultrafiltration hollow fiber membranes.* Journal of Membrane Science, 2004. **240**(1-2): p. 67-79.
31. Wang, R. and T.S. Chung, *Determination of pore sizes and surface porosity and the effect of shear stress within a spinneret on asymmetric hollow fiber membranes.* Journal of Membrane Science, 2001. **188**(1): p. 29-37.
32. Widjojo, N., Chung, T. S., Arifin, D. Y., Weber, M., Warzelhan, V., *Elimination of die swell and instability in hollow fiber spinning process of hyperbranched polyethersulfone (HPES) via novel spinneret designs and precise spinning conditions.* Chemical Engineering Journal, 2010. **163**(1-2): p. 143-153.
33. Yang, Q., Chung, T. S., Chen, S. B., Weber, M., *Pioneering explorations of rooting causes for morphology and performance differences in hollow fiber kidney dialysis membranes spun from linear and hyperbranched polyethersulfone.* Journal of Membrane Science, 2008. **313**(1-2): p. 190-198.

34. Chung, T.S., *A review of microporous composite polymeric membrane technology for air-separation.* Polymers & Polymer Composites, 1996. **4**(4): p. 269-283.
35. Wienk, I.M., Boom, R. M., Beerlage, M. A. M., Bulte, A. M. W., Smolders, C. A., Strathmann, H., *Recent advances in the formation of phase inversion membranes made from amorphous or semi-crystalline polymers.* Journal of Membrane Science, 1996. **113**(2): p. 361-371.
36. Peng, N., Widjojo, N., Sukitpaneenit, P., Teoh, M. M., Lipscomb, G. G., Chung, T. S., Lai, J. Y., *Evolution of polymeric hollow fibers as sustainable technologies: Past, present, and future.* Progress in Polymer Science, 2012. **37**(10): p. 1401-1424.
37. Chung, T., Kafchinski, E. R., Vora, R., *Development of a defect-free 6FDA-durene asymmetric hollow fiber and its composite hollow fibers.* journal of Membrane Science, 1994. **88**: p. 21-36.
38. Clausi, D.T., Koros, W. J., *Formation of defect-free polyimide hollow fiber membranes for gas separations.* Journal of Membrane Science, 2000. **167**(1): p. 79-89.
39. Li, F.Y., et al., *Development and positron annihilation spectroscopy (PAS) characterization of polyamide imide (PAI)–polyethersulfone (PES) based defect-free dual-layer hollow fiber membranes with an ultrathin dense-selective layer for gas separation.* Journal of Membrane Science, 2011. **378**(1-2): p. 541-550.
40. Peng, N., Chung, T. S., Lai, J. Y., *The rheology of Torlon® solutions and its role in the formation of ultra-thin defect-free Torlon® hollow fiber membranes for gas separation.* Journal of Membrane Science, 2009. **326**(2): p. 608-617.
41. Xu, L.R., Zhang, C., Rungta, M., Qiu, W. L., Liu, J. Q., Koros, W. J., *Formation of defect-free 6FDA-DAM asymmetric hollow fiber membranes for gas separations.* Journal of Membrane Science, 2014. **459**: p. 223-232.
42. Pesek, S.C. and W.J. Koros, *Aqueous quenched asymmetric polysulfone hollow fibers prepared by dry/wet phase separation.* Journal of Membrane Science, 1993. **81**(1-2): p. 71-83.
43. Jomekian, A., Mansoori, S. A. A., Monirimanesh, N., Shafiee, A., *Gas transport behavior of DMDCS modified MCM-48/polysulfone mixed matrix membrane coated by PDMS.* Korean Journal of Chemical Engineering, 2011. **28**(10): p. 2069-2075.
44. Li, P., H.Z. Chen, and T.S. Chung, *The effects of substrate characteristics and pre-wetting agents on PAN-PDMS composite hollow fiber membranes for CO_2/N_2 and O_2/N_2 separation.* Journal of Membrane Science, 2013. **434**: p. 18-25.
45. Singh, A., Freeman, B. D., Pinnau, I., *Pure and mixed gas acetone/nitrogen permeation properties of polydimethylsiloxane PDMS.* Journal of Polymer Science Part B-Polymer Physics, 1998. **36**(2): p. 289-301.
46. Zhou, H., Su, Y., Chen, X. R., Luo, J. Q., Tan, S., Wan, Y. H., *Plasma modification of substrate with poly(methylhydrosiloxane) for enhancing the interfacial stability of PDMS/PAN composite membrane.* Journal of Membrane Science, 2016. **520**: p. 779-789.
47. Henis, J.M.S., Tripodi, M. K., *Composite hollow fiber membranes for gas separation - the resistance model approach.* Journal of Membrane Science, 1981. **8**(3): p. 233-246.
48. Gantzel, P.K., Merten, U., *Gas Separations with High-Flux Cellulose Acetate Membranes.* Industrial & Engineering Chemistry Process Design and Development, 1970. **9**(2): p. 331-336.
49. Baker, R.W., Beckman, I. N., Cussler, E. L., Doshi, K, Henis, J. M. S., Koros, W. J., Nakagawa, T., Paul, D. R., Petropoulos, J. H., Pinnau, I., Pixton, M. R., Plate, N, Prasad, R., Shaner, R. L., Wijmans, J. G., Yampolskii, Y. P., *Polymeric Gas Separation Membranes*. 1994: CRC Press Inc.

50. Robeson, L.M., *Correlation of separation factor versus permeability for polymeric membranes.* Journal of Membrane Science, 1991. **62**(2): p. 165-185.
51. Robeson, L.M., *The upper bound revisited.* Journal of Membrane Science, 2008. **320**(1-2): p. 390-400.
52. R. Surya Murali, T.S., and S. Sridhar, *Air Separation by Polymer-based Membrane Technology.* Separation and Purification Reviews, 2013(42): p. 130-186.
53. Latimer, R.E., *Distillation of air.* Chemical Engineering Progress, 1967. **63**(2): p. 35-37.
54. *Federal Energy Regulatory Commission Natural Gas.* . Available from: http://www.ferc.gov/industries/gas.asp., Accessed March 2015
55. Kohl, A. and R. Nielson, *Gas Purification*. 5th ed. 1997: Gulf Publishing.
56. Echt, W., *Hybrid systems combining technologies leads to more efficient gas conditioning*, in *Laurance Reid Gas Conditioning Conference*. 2002: Norman, OK.
57. Sridhar, S., Smitha, B., Aminabhavi, T. M., *Separation of carbon dioxide from natural gas mixtures through polymeric membranes - A review.* Separation and Purification Reviews, 2007. **36**(2): p. 113-174.
58. Chung, T.S., Teoh, S.K., *Development of asymmetric 6FDA-2,6DAT hollow fiber membranes forCO(2)/CH4 separation Part 2. Suppression of plasticization.* Journal of Membrane Science, 2003. **214**(1): p. 57-69.
59. Smith, Z.P., Hernandez, G., Gleason, K. L., Anand, A., Doherty, C. M., Konstas, K., Alvarez, C., Hill, A. J., Lozano, A. E., Paul, D. R., Freeman, B. D., *Effect of polymer structure on gas transport properties of selected aromatic polyimides, polyamides and TR polymers.* Journal of Membrane Science, 2015. **493**: p. 766-781.
60. Su, J.C., Yang, Q., Teo, J. F., Chung, T. S., *Cellulose acetate nanofiltration hollow fiber membranes for forward osmosis processes.* Journal of Membrane Science, 2010. **355**(1-2): p. 36-44.
61. Shieh, J.J., Chung, T. S., *Effect of liquid-liquid demixing on the membrane morphology, gas permeation, thermal and mechanical properties of cellulose acetate hollow fibers.* Journal of Membrane Science, 1998. **140**(1): p. 67-79.
62. Loeb, S., McCutcha J. W, *Electrolytic additives in casting solution for cellulose acetate desalination membranes.* Industrial & Engineering Chemistry Product Research and Development, 1965. **4**(2): p. 114-118.
63. Wang, K., *The effects of flow angle and shear rate within the spinneret on the separation performance of poly(ethersulfone) (PES) ultrafiltration hollow fiber membranes.* Journal of Membrane Science, 2004. **240**(1-2): p. 67-79.
64. Li, Y., et al., *Fabrication of dual-layer polyethersulfone (PES) hollow fiber membranes with an ultrathin dense-selective layer for gas separation.* Journal of Membrane Science, 2004. **245**(1-2): p. 53-60.
65. Chung, T.S., S.K. Teoh, and X.D. Hu, *Formation of ultrathin high-performance polyethersulfone hollow-fiber membranes.* Journal of Membrane Science, 1997. **133**(2): p. 161-175.
66. Kim, H.W., Park, H. B., *Gas diffusivity, solubility and permeability in polysulfone-poly(ethylene oxide) random copolymer membranes.* Journal of Membrane Science, 2011. **372**(1-2): p. 116-124.
67. Ettouney, H., Majeed, U., *Permeability functions for pure and mixture gases in silicone rubber and polysulfone membranes: Dependence on pressure and composition.* Journal of Membrane Science, 1997. **135**(2): p. 251-261.

68. Mosqueda-Jimenez, D.B., Narbaitz, R. M., Matsuura, T., Chowdhury, G., Pleizier, G., Santerre, J. P., *Influence of processing conditions on the properties of ultrafiltration membranes.* Journal of Membrane Science, 2004. **231**(1-2): p. 209-224.
69. Khulbe, K.C., Feng, C., Matsuura, T., *The Art of Surface Modification of Synthetic Polymeric Membranes.* Journal of Applied Polymer Science, 2010. **115**(2): p. 855-895.
70. Won, J., Kim, M. H., Kang, Y. S., Park, H. C., Kim, U. Y., Choi, S. C., Koh, S. K., *Surface modification of polyimide and polysulfone membranes by ion beam for gas separation.* Journal of Applied Polymer Science, 2000. **75**(12): p. 1554-1560.
71. Ismail, A.F., Rahim N.H., Mustafa, A, Matsuura, T, Ng, B.C., Abdullah, S., Hashemifard, S.A., *Gas Separation Performance of Polyethersulfone/Multi-Walled Carbon Nanotubes Mixed Matrix Membranes.* Separation and Purification Reviews, 2011. **80**: p. 20-31.
72. Huang, Z., et al., *Enhanced gas separation properties by using nanostructured PES-zeolite 4A mixed matrix membranes.* Journal of Applied Polymer Science, 2006. **101**(6): p. 3800-3805.
73. Li, Y., Chung, T. S., Cao, C., Kulprathipanja, S., *The effects of polymer chain rigidification, zeolite pore size and pore blockage on polyethersulfone (PES)-zeolite A mixed matrix membranes.* Journal of Membrane Science, 2005. **260**(1-2): p. 45-55.
74. Chung, T.S. and S.K. Teoh, *The ageing phenomenon of polyethersulphone hollow fibre membranes for gas separation and their characteristics.* Journal of Membrane Science, 1999. **152**(2): p. 175-188.
75. Calle, M., Lee, Y. M., *Thermally Rearranged (TR) Poly(ether-benzoxazole) Membranes for Gas Separation.* Macromolecules, 2011. **44**(5): p. 1156-1165.
76. Chen, C.C., Qiu, W. L., Miller, S. J., Koros, W. J., *Plasticization-resistant hollow fiber membranes for CO_2/CH_4 separation based on a thermally crosslinkable polyimide.* Journal of Membrane Science, 2011. **382**(1-2): p. 212-221.
77. Sanders, D.F., Smith, Z. P., Ribeiro, C. P., Guo, R., McGrath, J. E., Paul, D. R., Freeman, B. D., *Gas permeability, diffusivity, and free volume of thermally rearranged polymers based on 3,3'-dihydroxy-4,4'-diamino-biphenyl (HAB) and 2,2'-bis-(3,4-dicarboxyphenyl) hexafluoropropane dianhydride (6FDA).* Journal of Membrane Science, 2012. **409-410**: p. 232-241.
78. Woo, K.T., Dong, G., Lee, J., Kim, J. S., Do, Y. S., Lee, W. H., Lee, H. S., Lee, Y. M., *Ternary mixed-gas separation for flue gas CO_2 capture using high performance thermally rearranged (TR) hollow fiber membranes.* Journal of Membrane Science, 2016. **510**: p. 472-480.
79. Woo, K.T., et al., *Thermally rearranged poly(benzoxazole-co-imide) hollow fiber membranes for CO_2 capture.* Journal of Membrane Science, 2016. **498**: p. 125-134.
80. Sanders, D.E., Smith, Z. P., Guo, R. Robeson, L. M., McGrath, J. E., Paul, D. R., Freeman, B. D., *Energy-efficient polymeric gas separation membranes for a sustainable future: A review.* Polymer, 2013. **54**(18): p. 4729-4761.
81. Budd, P.M., Msayib, K. J., Tattershall, C. E., Ghanem, B. S., Reynolds, K. J., McKeown, N. B., Fritsch, D., *Gas separation membranes from polymers of intrinsic microporosity.* Journal of Membrane Science, 2005. **251**(1-2): p. 263-269.
82. Budd, P.M., Elabas, E. S., Ghanem, B. S., Makhseed, S., McKeown, N. B., Msayib, K. J., Tattershall, C. E., Wang, D., *Solution-processed, organophilic membrane derived from a polymer of intrinsic microporosity.* Advanced Materials, 2004. **16**(5): p. 456-465.
83. Budd, P.M., et al., *Polymers of intrinsic microporosity (PIMs): robust, solution-processable, organic nanoporous materials.* Chemical Communications, 2004(2): p. 230-231.

84. McKeown, N.B., Budd, P. M., *Polymers of intrinsic microporosity (PIMs): organic materials for membrane separations, heterogeneous catalysis and hydrogen storage.* Chemical Society Reviews, 2006. **35**(8): p. 675-683.
85. Kemp, D.R., Paul, D. R., *Gas sorption in polymer membranes containing adsorptive fillers.* Journal of Polymer Science Part B-Polymer Physics, 1974. **12**(3): p. 485-500.
86. Paul, D.R., Kemp, D. R., *Diffusion time lag in polymer membranes containing adsorptive fillers.* Journal of Polymer Science Part C-Polymer Symposium, 1973(41): p. 79-93.
87. Kulprathipanja, S., Neuzil, R.W., Norman, N. L., *Separation of fluids by means of mixed matrix membranes*. 1989, Honeywell International Inc: USA, US5127925A.
88. Galizia, M., Chi, W. S., Smith, Z. P., Merkel, T. C., Baker, R. W., Freeman, B. D., *50th Anniversary Perspective: Polymers and Mixed Matrix Membranes for Gas and Vapor Separation: A Review and Prospective Opportunities.* Macromolecules, 2017. **50**(20): p. 7809-7843.
89. Adams, R., Carson, Cantwell, Ward, Jason, Tannenbaum, Rina, Koros, William, *Metal organic framework mixed matrix membranes for gas separations.* Microporous and Mesoporous Materials, 2010. **131**(1-3): p. 13-20.
90. Aroon, M.A., Ismail, A. F., Matsuura, T., Montazer-Rahmati, M. M., *Performance studies of mixed matrix membranes for gas separation: A review.* Separation and Purification Technology, 2010. **75**(3): p. 229-242.
91. Chung, T.S., Jiang, L. Y., Li, Y., Kulprathipanja, S., *Mixed matrix membranes (MMMs) comprising organic polymers with dispersed inorganic fillers for gas separation.* Progress in Polymer Science, 2007. **32**(4): p. 483-507.
92. Goh, P.S., Ismail, A. F., Sanip, S. M., Ng, B. C., Aziz, M., *Recent advances of inorganic fillers in mixed matrix membrane for gas separation.* Separation and Purification Technology, 2011. **81**(3): p. 243-264.
93. Perez, E.V., Balkus, K. J., Ferraris, J. P., Musselman, I. H., *Mixed-matrix membranes containing MOF-5 for gas separations.* Journal of Membrane Science, 2009. **328**(1-2): p. 165-173.
94. Song, Q.L., Nataraj, S. K., Roussenova, M. V., Tan, J. C., Hughes, D. J., Li, W., Bourgoin, P., Alam, M. A., Cheetham, A. K., Al-Muhtaseb, S. A., Sivaniah, E., *Zeolitic imidazolate framework (ZIF-8) based polymer nanocomposite membranes for gas separation.* Energy & Environmental Science, 2012. **5**(8): p. 8359-8369.
95. Dai, Y., Johnson, J. R., Karvan, O., Sholl, D. S., Koros, W. J., *Ultem®/ZIF-8 mixed matrix hollow fiber membranes for CO_2/N_2 separations.* Journal of Membrane Science, 2012. **401-402**: p. 76-82.
96. Iijima, S., *Helical microtubules of graphitic carbon.* Nature, 1991. **354**(6348): p. 56-58.
97. Hinds, B.J., Chopra, N., Rantell, T., Andrews, R., Gavalas, V., Bachas, L. G., *Aligned multiwalled carbon nanotube membranes.* Science, 2004. **303**(5654): p. 62-65.
98. Majumder, M., Chopra, N., Andrews, R., Hinds, B. J., *Nanoscale hydrodynamics - Enhanced flow in carbon nanotubes.* Nature, 2005. **438**(7064): p. 44-44.
99. Majumder, M., Chopra, N., Hinds, B. J., *Effect of tip functionalization on transport through vertically oriented carbon nanotube membranes.* Journal of the American Chemical Society, 2005. **127**(25): p. 9062-9070.
100. Majumder, M., Chopra, N., Hinds, B. J., *Mass Transport through Carbon Nanotube Membranes in Three Different Regimes: Ionic Diffusion and Gas and Liquid Flow.* ACS Nano, 2011. **5**(5): p. 3867-3877.

101. Goh, P.S., Ng, B. C., Ismail, A. F., Sanip, S. M., Aziz, M., Kassim, M. A., *Effect of Dispersed Multi-Walled Carbon Nanotubes on Mixed Matrix Membrane for O_2/N_2 Separation.* Separation Science and Technology, 2011. **46**(8): p. 1250-1261.
102. S. Zeinali, M.A., *Improving O_2/N_2 Selective Filtration Using Carbon Nanotube-Modified Mixed-Matrix Membranes.* Chemical Engineering and Technology, 2015. **38**(11): p. 2079-2086.
103. Ismail, A.F., Goh, P. S., Sanip, S. M., Aziz, M., *Transport and separation properties of carbon nanotube-mixed matrix membrane.* Separation and Purification Technology, 2009. **70**(1): p. 12-26.
104. Kim, S., Chen, L., Johnson, J. K., Marand, E., *Polysulfone and functionalized carbon nanotube mixed matrix membranes for gas separation: Theory and experiment.* Journal of Membrane Science, 2007. **294**(1-2): p. 147-158.
105. Ismail, A.F., Rahim, N. H., Mustafa, A., Matsuura, T., Ng, B. C., Abdullah, S., Hashemifard, S. A., *Gas separation performance of polyethersulfone/multi-walled carbon nanotubes mixed matrix membranes.* Separation and Purification Technology, 2011. **80**(1): p. 20-31.
106. Goh, P.S., Ng, B. C., Ismail, A. F., Aziz, M., Hayashi, Y., *Pre-treatment of multi-walled carbon nanotubes for polyetherimide mixed matrix hollow fiber membranes.* Journal of Colloid and Interface Science, 2012. **386**: p. 80-87.

Chapter 2: Materials and Methods

2.1 Introduction

The second chapter of this work is dedicated to a detailed discussion of the various materials and experimental methods that were employed. It is divided into two broad sections. The first is focused on the polymers, solvents and inorganic filler materials that were used to prepare the polymer dopes and subsequent membranes. The second section of the chapter is focused on the membrane fabrication procedures and analytical methods that were employed in this work. This includes the casting and post-treatment of flat sheet and hollow fiber membranes, as well as the characterization techniques that were used to examine membrane structure and measure transport properties.

2.2 Materials

2.2.1 Polymers

2.2.1.1 Polyethersulfone (PES)

Polyethersulfone (PES) has been one of the most commonly used polymers in the field of membrane-based separation for several decades. The rigid structure of the repeat unit, as shown in Figure 1.8, imparts good thermal, chemical, and mechanical properties. It also readily forms viable asymmetric membranes via phase-inversion due to its strong hydrophobicity. PES is commercially available and is fairly low cost compared to other polymeric membrane materials. As a result, it has been the focus of extensive membrane development research for use in liquid phase separations (i.e., reverse osmosis, micro/ultra/nanofiltration) as well as gas separations.

The PES resin that was used in this work was Ultrason® polyethersulfone 6020p flakes with approximate molecular weight (M_w) of 55,000 acquired from BASF. The PES was fully amorphous (i.e., non-crystalline) with a glass transition temperature (T_g) of 225°C [1].

2.2.1.2 Polysulfone (PSf)

Polyarylethersulfone (colloquially known as polysulfone (PSf)), as well as other PSf-based polymers, has been used for commercial membrane-based separations since the 1960's. PSf is the basis for the Air Products PRISM membrane system, which is one of the most commonly used gas separation membrane systems in the industry. The polymer repeat unit, shown in Figure 1.8, is similar to that of PES, but with the addition of a second bisphenol moiety. This additional group causes a less efficient packing structure in the bulk polymer, which leads to the membrane having a higher fractional free volume and higher permeability. This inefficient packing structure also tends to decrease the selectivity of the PSf membrane as compared to PES. Like PES, PSf has excellent chemical resistance, mechanical strength and thermal stability.

The polysulfone that was used in these experiments was purchased from Scientific Polymer Products and had a molecular weight (M_w) of approximately 60,000. As with PES, the PSf was fully amorphous, with glass transition temperature (T_g) of 186°C [1].

2.2.1.3 Polydimethylsiloxane (PDMS)

Polydimethylsiloxane (PDMS), or silicone rubber, is a silicon-based polymer that is commonly used in contact lenses and medical devices. Its purpose relevant to this work is to repair pinhole surface defects in polymeric membranes. PDMS is well known as the most permeable of the commercial rubbery polymers [1]. The structure of the polymer repeat unit is shown in Figure 1.8. The large amount of free volume and corresponding high permeability which are characteristic of PDMS lead to low light gas selectivity for the polymer. The high permeability and low selectivity of PDMS make it ideal for use in repairing pinhole defects in membrane materials, because it does not strongly affect the separation characteristics of the membrane polymer itself, but merely changes the diffusion mechanism within the pinholes from high-rate Knudsen diffusion to solution diffusion, thus mitigating the negative effects of the pinholes and allowing the membrane to approach the selectivity of the dense bulk polymer.

The PDMS used in this work was Sylgard-184, a two-part mixture that contained the silicone elastomer as well as a hardening agent. Sylgard-184 was produced by Dow Corning and purchased from Galco Industrial Electronics.

2.2.2 Solvents

2.2.2.1 N,N-Dimethylacetimide (DMAc)

N,N-dimethylacetimide (DMAc) is a polar organic solvent used in organic synthesis and polymer solution processing. It has a high boiling point and is miscible in water; its structure is shown in Figure 2.1a. The most common applications for DMAc are the solution processing of polymer fibers, such as polyacrylonitrile (PAN), and as a

solvent in various adhesives. DMAc has a fairly high potency as a reproductive toxin and is known to damage fertility, as well as being very harmful when brought into contact with skin, ingested, or inhaled. Due to its toxicity, it has become heavily regulated in recent years, and thus has been less commonly used. Some early membrane preparations reported in this work were performed using DMAc, but after a comparison of the morphologies of membranes cast using N-methylpyrrolidone (NMP) showed little to no difference in morphology, NMP was chosen for all subsequent experiments due to its comparatively lower toxicity.

Reagent grade N,N-dimethylacetimide (DMAc) was purchased from Fisher Scientific and was used as received without any further purification.

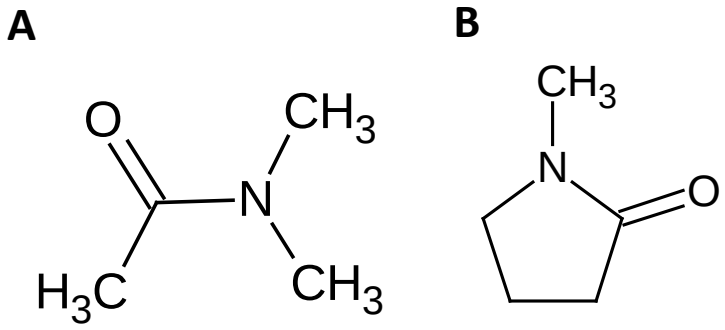

Figure 2.1: Chemical structures for solvents used in membrane casting: (A) N,N-dimethylacetimide, and (B) N-methylpyrrolidone.

2.2.2.2 N-Methylpyrrolidone (NMP)

N-methylpyrrolidone (NMP) is an organic solvent which consists of a 5-membered, nitrogen substituted ring with a methyl group attached to the nitrogen and an adjacent carbonyl, as shown in Figure 2.1b. NMP is similar in application to other

dipolar, aprotic solvents, such as dimethylformamide (DMF) and dimethylsulfoxide (DMSO), and is most commonly applied for solution processing of polymeric materials, due to its miscibility with water, non-volatility, and strong ability to dissolve most common polymers. While it is still relatively hazardous and can cause skin and eye irritation, it is often used as a replacement for DMAc due to its lack of potency as a reproductive toxicant and its relatively rapid clearing from the body. For this reason, most of the experiments reported in this work were performed with NMP rather than DMAc.

ACS grade 1-methyl-2-pyrrolidinone (NMP) was purchased from Alfa Aesar and was used as received without further purification.

2.2.3 Inorganic Fillers

2.2.3.1 Carbon Nanotubes (CNTs)

Carbon nanotubes (CNTs) have been studied extensively since their discovery in the early 1990's owing to their exceptional thermal, electrical and mechanical properties. Because of these extraordinary properties, they have been examined for a large number of applications. One of these applications is as a structural reinforcement in composite materials, due to their unrivaled elastic modulus and extremely high aspect ratio. These attributes make carbon nanotubes a promising replacement for glass or carbon fibers, which comprise the bulk of the filler material in traditional composites. Additionally, their nanoscale size and ability to be produced as either metallic or semiconducting makes them highly desirable as the conducting elements in molecular scale conducting devices. CNTs can be prepared in a variety of allotropes, but the most

common are single wall (SWCNT) and multiwall (MWCNT). SWCNTs are comprised of a single layer graphene sheet rolled into a seamless cylinder, while MWCNTs consist of several layers of graphene that have been rolled into concentric tubes.

Recently, carbon nanotubes have been used for membrane applications. For example, carbon nanotube membranes have been created with carefully aligned carbon nanotubes, which act as nanoporous channels for water filtration membranes [2-4]. MWCNTs have also found application as the inorganic filler for mixed matrix gas separation membranes [5-11]. Though pristine CNTs present challenges with respect to dispersion and adhesion to the polymeric matrix, multiple researchers have found that the introduction of CNTs can enhance membrane selectivity, citing molecular sieving via the inter-layer spacing of the MWCNTs as a contributing mechanism [5, 11].

Multiwall carbon nanotubes (MWCNTs) were acquired from the Center for Applied Energy Research (CAER) Carbon Materials group at the University of Kentucky. The MWCNTs were synthesized via chemical vapor deposition (CVD), using the procedure described by Andrews et al [12]. The CVD synthesis procedure involved passing a solution of xylene and ferrocene into an inert gas stream. This mixture was decomposed at a temperature of 775°C and atmospheric pressure. Under these conditions, iron nanoparticles nucleate and become saturated with carbon. Subsequently, carbon precipitates from the iron nanoparticles into well-aligned arrays of MWCNTs. The MWCNTs that were produced were approximately 50 nm in diameter and approximately 100 μm long. This process has many advantages over other

techniques for producing MWCNTs, such as arc or laser ablation methods, and enables MWCNT production at much larger volumes. However, the MWCNTs that are produced tend to not have as well-defined a graphene structure as the other methods.

2.2.3.2 Carbon Black

Carbon black is a nanoscale porous carbon material with a high surface area to volume ratio. It is typically formed from the incomplete combustion of heavy hydrocarbon products such as various tars. As a result of the electrical conductivity and stable resistance that carbon black provides, it is commonly used as a conductive filler material for plastics, adhesives and films. Additionally, it is used as a filler material in tire rubber, as it works as a mechanical reinforcement and thermal conductor, which reduces tire wear. Carbon black also contributes a small enhancement to the gas barrier properties of the tire rubber, reducing gas diffusion through the tire wall.

99.99% carbon black with a density of 1.8 g/cm^3 and an average particle size of approximately 42 nm was purchased from Alfa Aesar and was used as received.

2.3 Membrane Fabrication Methods

2.3.1 Flat Sheet Membranes

2.3.1.1 Dope Preparation

2.3.1.1.1 Standard Polymer Dope

Polymer solution (dope) was prepared by first drying the polymer flakes for 2 hours at 100°C under vacuum. Appropriate quantities of polymer and solvent (i.e. DMAc or NMP), based on desired dope composition, were weighed using an electronic balance. Polymer flakes were then placed into the solvent with mechanical mixing until all of the flakes dissolved and the dope was homogeneous. The dope was then placed

under vacuum at room temperature overnight for degassing. After vacuum degas, the dope was transferred to a 25 mL glass syringe. The syringe was then placed with the plunger down on the workbench and the excess air was pushed out. When all of the air was removed, the syringe was capped until membrane casting.

2.3.1.1.2 Mixed Matrix Membrane Dope

Previous experience in the CAER Materials Technologies research group led to the development of specific formulation strategies for the dispersion of MWCNTs in polyacrylonitrile (PAN)/DMAc solution dopes. This experience was leveraged to develop a procedure for the preparation of PES-NMP-MWCNT dopes for mixed matrix membrane casting. One of the primary issues that this procedure addresses is agglomeration of filler material. Since any amount of MWCNT agglomeration would be detrimental to membrane performance, it was necessary to use supernatant dispersions of PES-MWCNT produced by ultrasonication and subsequent centrifugation in order to ensure as few agglomerates as possible were present in the final membrane casting dope.

The dope preparation was as follows. The necessary quantities of polyethersulfone, N-methylpyrrolidone (NMP), and multiwall carbon nanotubes (MWCNT) were weighed out, and initially 5 g of PES was added to the NMP and allowed to completely dissolve under magnetic stirring at ambient temperature. This first step was performed in order to increase the viscosity of the solvent and to create a “pre-dope” solution, which aided in the MWCNT dispersion. Once the pre-dope solution was completely homogenized, all of the MWCNTs were added and stirred for a few minutes.

The mixture was then ultrasonicated using a Fisher Scientific 550 sonic dismemberator at 20% power, programmed to operate for 20 min total, with bursts of 30 s of sonication followed by 10 s of rest time to mitigate heat buildup, under constant magnetic stirring. The resulting solution was then split into two equal lots (for centrifuge balance) and centrifuged in an International Equipment Company (IEC) centrifuge at 1550 rpm for 1 h. After centrifuging, the supernatant fluid was decanted and the two lots were recombined in a large beaker and the total residual mass was recorded. The remaining PES flakes were then slowly added to the supernatant solution under constant stirring until the solution became fully homogenized into a viscous, inky, black dope of the desired composition. The solution container was then placed in a vacuum oven at room temperature and allowed to degas overnight. After the vacuum degas, the PES-MWCNT dope was transferred to a 25 mL glass syringe. The syringe was then placed with the plunger side down and the excess gas was pushed out. After the gas was removed, the glass syringe was capped until membrane casting. The sediment portion of the centrifuged mixture was collected and placed in a vacuum oven at 100°C overnight to fully dry the sample and remove all solvent. The mass of the resulting dry sediment was then recorded.

The centrifuge step removed the inorganic filler agglomerates as well as some small portion of the polymer from the dope solution. As such, in order to establish the composition of the final dope, it was necessary to quantify the amounts of the filler and residual polymer that were removed during the centrifugation. First, the total (initial) masses of the solvent ($m_{s,i}$), polymer ($m_{p,i}$), and inorganic filler ($m_{f,i}$) that went into the

dope were recorded. After sonication, centrifugation, and subsequent decantation, the total mass of the supernatant fluid ($m_{t,f}$) was measured. In addition, after they had been dried in a vacuum oven overnight at 100°C, the total mass of the dry sedimented agglomerates was measured ($m_{t,a}$). The dried sediment mixture was then analyzed using thermogravimetric analysis (TGA). The TGA curve was used to deconvolute the weight fraction of the dried sediment that was due to the polymer (X_p) from that of the filler agglomerates (X_f). The masses of the polymer ($m_{p,f}$) and inorganic filler ($m_{f,f}$), in the final dope were calculated using the following equations:

$$m_{p,f} = m_{p,i} - X_p(m_{t,a}) \quad [2.1a]$$

$$m_{f,f} = m_{f,i} - (X_f)(m_{t,a}) \quad [2.1b]$$

The weight fraction of polymer in the casting solution and the weight fraction of inorganic filler (relative to the polymer) in the final membrane can be calculated as:

$$Wt.\%\ Polymer = \left(\frac{m_{p,f}}{mt,f}\right) * 100\% \quad [2.2a]$$

$$Wt.\%\ MWCNT\ = \left(\frac{m_{f,f}}{m_{p.f}+m_{f,f}}\right) * 100\% \quad [2.2b]$$

2.3.1.2 Thin Film Casting/Solvent Exchange and Drying

To cast thin film membranes, dope was first extruded out of the glass syringe onto a piece of borosilicate glass. Casting was performed with a Gardco Microm II adjustable micrometer film applicator with stainless steel blade. The blade height was set at 250 µm to approximate the annular gap between the outer diameter and inner diameter of the hollow fiber spinneret (re: below). The cast film was then immediately

immersed in the coagulation bath and allowed to coagulate for 2 minutes. During this time period, the homogeneous polymer solution inverted into two distinct phases; a polymer-rich phase that formed the bulk of the solid membrane and a polymer-lean phase that formed the pores. This process simultaneously involved mass transport of water into the incipient polymeric membrane, causing the formation of teardrop macrovoids, as well as flux of solvent out of the nascent membrane.

Solvent exchange and drying of the membranes were then performed. Initially, each film was transferred to a deionized water bath and allowed to soak overnight to remove any residual solvent. The films were then transferred to a methanol bath and soaked for three hours to remove the water and finally transferred to a hexanes bath and held for an additional three hours to remove the residual methanol. After the hexanes bath, each membrane was allowed to dry in air at room temperature. The solvent-exchange process, which is instrumental in developing asymmetric thin film membranes for gas separations, was developed by Loeb and Sourirajan in the 1960's [13]. The protocol allows for the membrane to be converted from the wet state, while fully preserving the porous substructure.

2.3.2 Hollow Fiber

2.3.2.1 Dope Preparation

The procedure for preparing hollow fiber membrane spinning dopes was the same as the procedure for preparing flat sheet spinning dopes, as described above (see Section 2.3.1.1). The only difference between the two procedures was the final container of the dope. For flat sheet membranes, the dope was contained in a 25 mL

glass syringe. For hollow fiber membrane spinning, after the dope was homogenized, it was extracted from the mechanical mixer directly into a model 500D syringe pump (Teledyne ISCO, Lincoln, NE), where it was fitted with a vacuum chamber and degassed. After degas, the syringe pump was capped and the excess air was pushed out.

2.3.2.2 Hollow Fiber Membrane Spinning Procedure

A bench-scale hollow fiber membrane spinning line was designed and constructed based on previous spin line designs developed by the Carbon Materials Group at the UK Center for Applied Energy Research. The spin line consists of two syringe pumps, filter manifold, extrusion die, coagulation bath, take up godet, and a wash winder as shown in Figure 2.2.

Dope was extruded from a model 500D syringe pump (Teledyne ISCO, Lincoln, NE) with temperature and flowrate control, capable of sustaining flowrates as low as 0.06 mL/h (0.001 mL/min) and pressures up to 3,750 psi. The bore fluid was metered into the system using a KDS 100 L syringe pump with 50 mL stainless steel syringe (KDS, Holliston, MA) capable of stable flow as low as 20 mL/h (0.33 mL/min) and as high as 425 mL/h (7.08 mL /min).

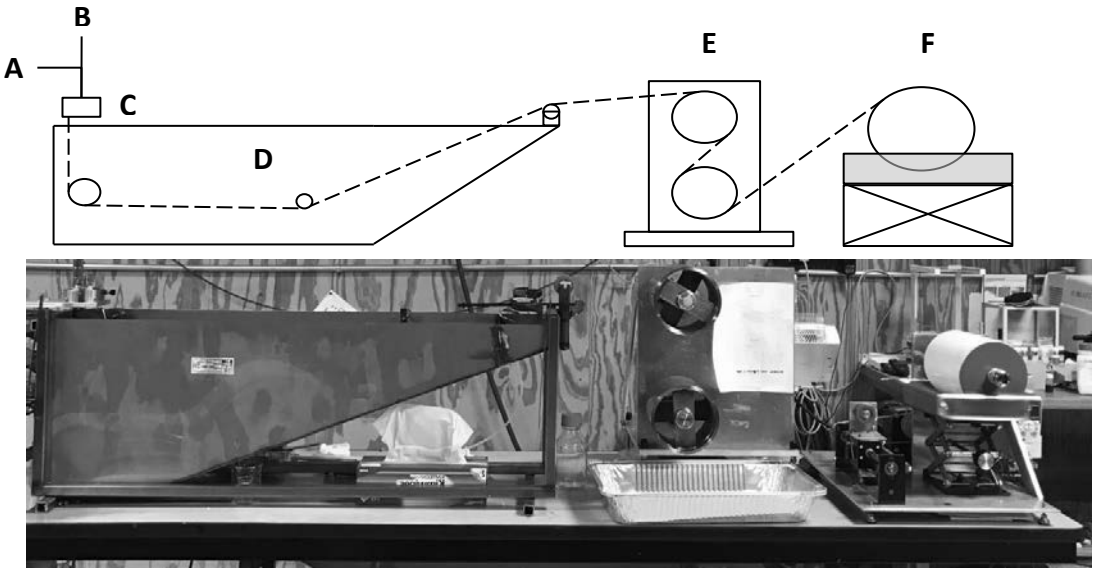

Figure 2.2a: (Top) Schematic diagram of hollow fiber membrane spinning line. (A) Dope inlet, (B) Bore fluid inlet, (C) Extrusion die (spinneret), (D) Coagulation bath, (E) Take-up godet rollers, and (F) Wash winder. (Bottom) Photograph of hollow fiber spinning line.

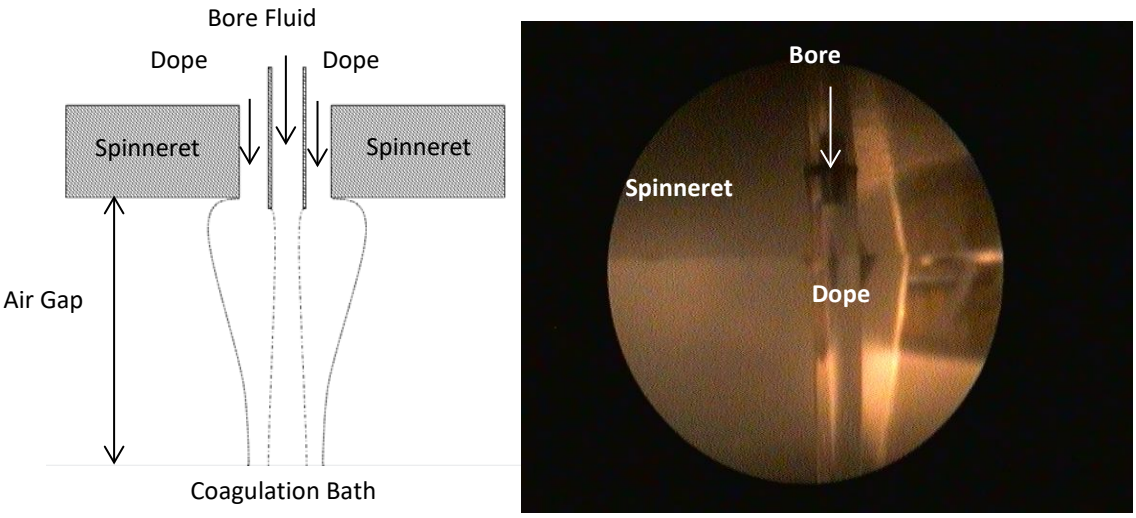

Figure 2.2b: Schematic diagram of the bore fluid and dope in the air gap between the spinneret and the coagulation bath (left), and a close-up photograph of the air gap with PES dope (right).

A schematic diagram of the in-house built extrusion die is shown in Figure 2.3. The die consists of 1/8” NPT inlets with Swagelok fittings for dope and bore fluid as well as a 1/8” NPT air vent to ensure that dope fills the entire conical die cavity. Bore fluid was extruded through an extruder core with gauge 25RW (OD = 0.508 mm; ID = 0.254 mm) hypodermic tubing (Microgroup, Medway, MA). Dope solution was flowed through a 1 mm capillary forming an annulus around the outer diameter of the bore needle. As concentricity of the bore flow wass critical to spinning the hollow fiber, 25 µm/revolution fine adjustment screws (Thor Labs, Newton, NJ) were aligned perpendicular to one another to allow for two-dimensional (x-y) concentric alignment of the needle within the dope annulus. Additionally, the threaded extruder core allowed for a z-dimension needle adjustment.

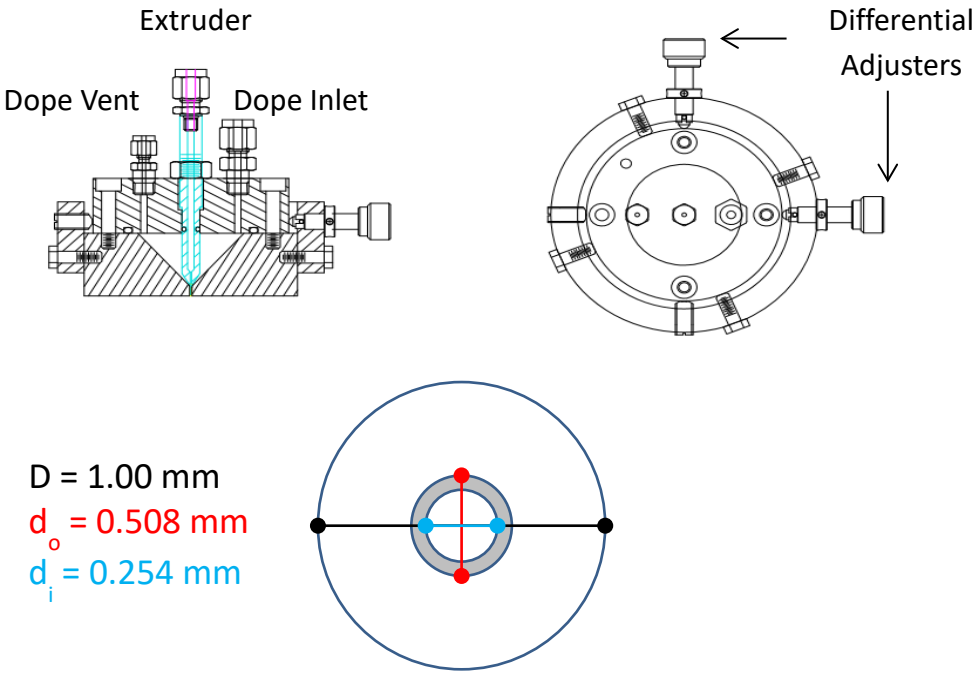

Figure 2.3: (Top) Schematic diagram of hollow fiber extrusion die. (Bottom) diagram of dope annulus and bore needle.

304 stainless steel sheeting was used to build the coagulation bath, which was welded to a frame of 304 stainless steel square tubing. Nascent fiber was drawn downward 4.5 inches (11.4 cm) and turned on a cylindrical Teflon™ guide. The total length of the bath was 48 inches (121.9 cm) and the fiber traveled approximately 28.5 inches (72.4 cm) before turning and completing a second pass prior to leaving the bath and being taken up on the godet rollers, making the total distance traveled within the bath approximately 85.5 inches (217.2 cm). Polished schedule 80 stainless steel rollers (ϕ=6.5”) were powered using a DC gear motor with a DC motor speed control (Bodine Electric Company, Northfield, IL) and a range of take-up speeds between 2.7m/min and 8.5 m/min. The spool winding system consisted of a linear bi-directional gearbox traverser (Cemanco, Pompano Beach, FL) and a schedule 40 PVC spool (ϕ=6.5”), partially submerged in a pan of DI water, which provided continuous washing of the wound fiber. The winder was powered by an identical DC gear motor and motor controller as the take-up godet.

Solvent exchange and drying of hollow fiber membranes were performed using virtually the same method as with flat sheet membranes. First, the hollow fiber membranes were cut off of the spool using a razor blade. The ends of the fibers were then taped to the bottom of a large stainless steel pan to prevent the fibers from curling. The pan was then filled with enough DI water to submerge the fibers and the fibers were left submerged in DI water overnight to remove any residual solvent. The next day, the water was discarded and the fibers were submerged in methanol in order to remove the DI water. After a three hour soak, the methanol was removed from the

pan and discarded. The fibers were then submerged in hexanes for an additional three hours to remove any residual methanol. Finally, the hexanes were removed from the pan, leaving the fibers to dry in air.

2.4 Membrane Gas Permeation Testing Methods

2.4.1 Permeation Testing Apparatus

A schematic representation of the gas permeation testing apparatus is shown in Figure 2.4. The apparatus was composed of a single gas feed (which can flow N_2, He, CO_2, or O_2). The pressure was controlled using a pressure regulator and measured using a digital pressure gauge (Cecomp Electronics, USA). The flowrate of the permeating gas was measured using a soap film flowmeter. The permeation flux of gas A (J_A) was calculated using the equation:

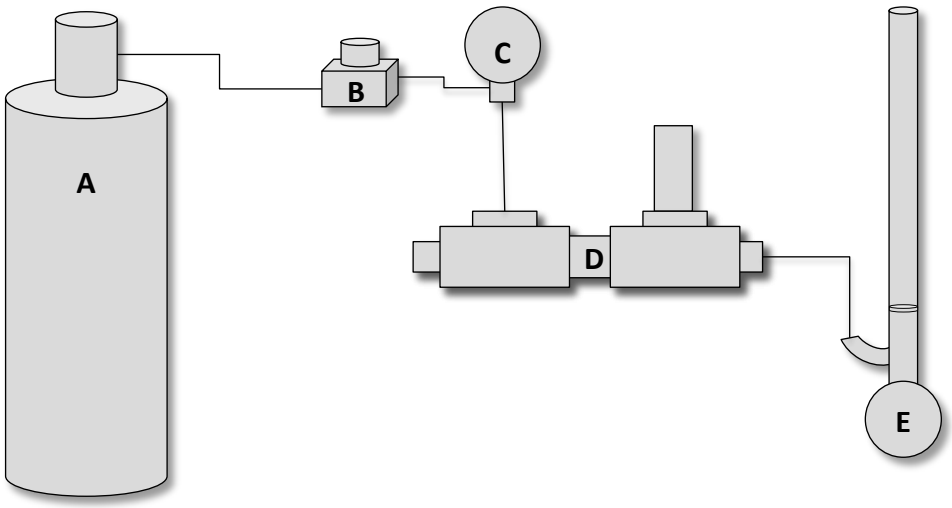

Figure 2.4: Schematic diagram of the hollow fiber membrane gas separation testing apparatus. (A) Gas source, which can flow nitrogen (N_2), helium (He) carbon dioxide (CO_2), or oxygen (O_2), (B) Gas flow regulator, (C) Gas pressure gauge, (D) Membrane module, which can be either flat sheet membrane holder or hollow fiber membrane module, and (E) Soap film flowmeter.

$$J_A = \frac{Q_A}{A} \quad [2.3]$$

Where Q_A is the volumetric flowrate of gas A, measured with the soap film flowmeter, and A is the total surface area of the circular flat sheet membrane or the hollow fiber membrane bundle that is exposed to the gas. The permeance of gas A in the membrane (P_A/l) was then calculated using the following equation:

$$\frac{P_A}{l} = \frac{J_A}{\Delta P} \quad [2.4]$$

where P_A is the permeability coefficient of gas A in the polymer, *l* is the thickness of the dense separating layer of the membrane, and ΔP is the pressure difference across the membrane in cmHg. The permeance is expressed in gas permeance units (GPU), where

$$1\ GPU = 1x10^{-6}\frac{cm^3(STP)}{cm^2\ s\ cmHg}$$

The ideal selectivity between gas A and gas B is then simply defined as the ratio of the pure gas permeance of gas A to the permeance of gas B ($\alpha_{A/B}$), as shown in the following equation:

$$\alpha_{A/B} = \frac{(P_A/l)}{(P_B/l)} \quad [2.5]$$

2.4.2 Flat Sheet Membrane Testing Procedure

The testing procedure for flat sheet membranes was relatively straightforward. After the flat sheet was cast and subsequently subjected to solvent exchange and drying, the membrane was cut into circular coupons of 1 inch diameter using a hole

punch. The circular membrane coupon was then loaded into a Millipore Microsyringe Stainless Steel Filter Holder (Cat# xx3002514). A schematic diagram of the filter holder is shown in Figure 2.5. The cell was assembled with the outlet of the filter holder on the bottom, the NPT inlet to the filter holder on the top, and a flat Teflon O-ring, stainless steel screen, membrane and rounded Teflon O-ring on the inside.

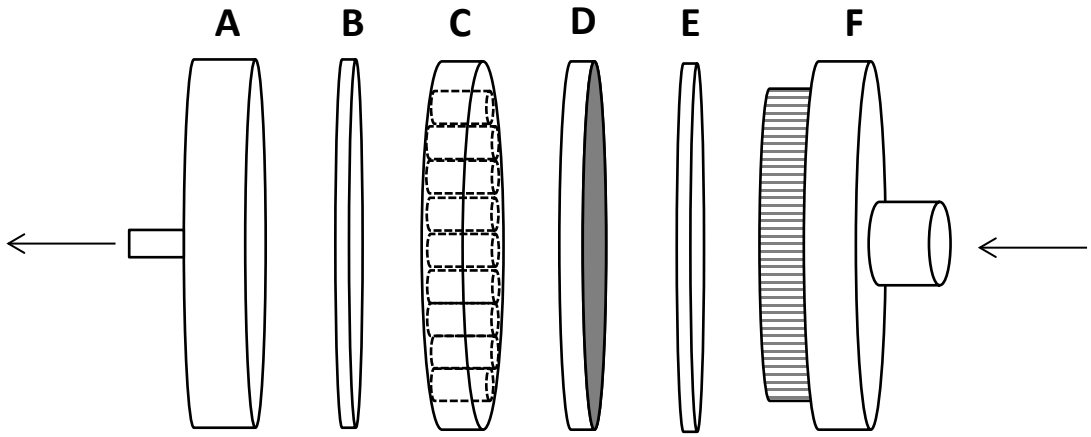

Figure 2.5: Schematic diagram of Millipore Microsyringe Stainless Steel Filter Holder (Cat# xx3002514) that was used for flat sheet membrane testing. (A) Outlet of the filter holder, (B) Flat Teflon O-ring, (C) Stainless steel screen, (D) Flat sheet asymmetric membrane sample, (E) Rounded Teflon O-ring, (F) Top of filter holder with NPT inlet.

After the membrane cell had been assembled, it was placed into the gas separation testing apparatus. Single gases were passed individually into the dead end cell at a gauge pressure of 29 psi and the system was held at this pressure for 2 hours in order to allow the flux to reach steady state. For a solution diffusion membrane, gas transport across the membrane occurs in three steps. First, the gas dissolves into the outer surface of the dense separating layer of the membrane, with its solubility coefficient reflecting on how readily it interacts with the polymer. Next, the gas diffuses

across the dense separating layer of the membrane, driven by a concentration gradient. The diffusion coefficient of the gas in the membrane is affected by multiple properties of the material, including the fractional free volume and crystallinity of the polymer, as well as the interaction between the polymer chains and the gas molecules. Lastly, the gas desorbs from the dense separating layer and flows freely through the porous support layer and out of the membrane holder, where the flowrate was measured by the soap film flowmeter. The volumetric flux, permeance, and ideal selectivity of the various gas pairs were then calculated using the equations presented in the previous section.

2.4.3 PDMS Caulking

In order to ensure that the polymeric membranes were defect free and showed solution diffusion (rather than Knudsen diffusion) separation characteristics, pinhole defects in the flat sheet membranes need to be repaired. It is very common in the membrane literature to repair these defects by "caulking" them with a high permeability/low selectivity polymer, such as polydimethylsiloxane (PDMS)[14-16]. In this work, the PDMS used was Sylgard-184, which was produced by Dow Corning and purchased from Galco Industrial Electronics.

The procedure for caulking the flat sheet and hollow fiber membranes was as follows. First, the curing agent was added to the Sylgard-184 silicone elastomer in a ratio of 1:10, per the manufacturer's recommendation. Hexane was then added to the PDMS mixture in order to dilute the solution to 3 wt.% PDMS and stirred using a magnetic stirrer. After the solution became completely homogeneous, the beaker was

covered with aluminum foil and the temperature of the solution was raised to 75°C in order to increase branching and chain extension of the polymer solution. After the solution had been held at 75 °C for 1 hour, a flat sheet membrane disc was immersed in the PDMS solution. For hollow fiber membranes, the solution was poured into a PVC tube with one end plugged, which contained the bundle of hollow fiber membranes, as shown in Figure 2.6. The membrane (or HFM bundle) was allowed to soak for 30 minutes at 75 °C, and was then removed from the solution and placed in a vacuum oven at 75 °C for 2 hours to complete PDMS curing.

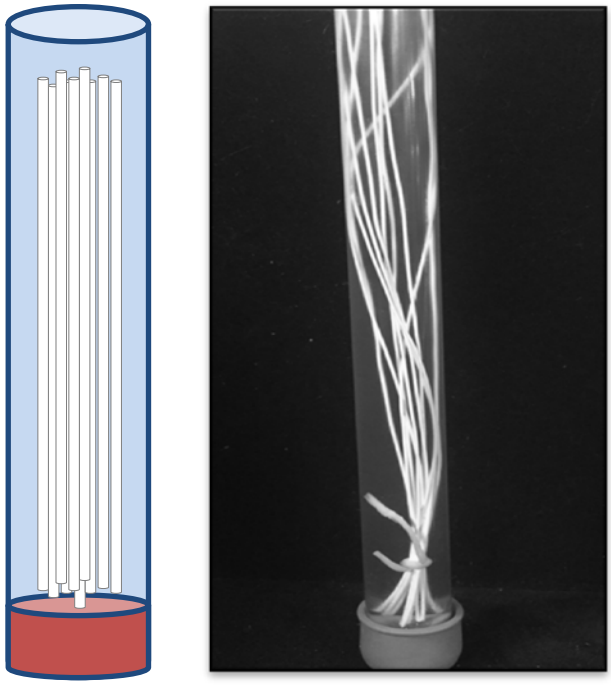

Figure 2.6: Schematic diagram of HFM PDMS caulking soak (left) and photograph of HFM PDMS caulking soak (right).

2.4.4 Hollow Fiber Membrane Testing

2.4.4.1 Hollow Fiber Membrane Module Construction

A schematic configuration of a hollow fiber membrane test module is shown in Figure 2.7a. As shown in the figure, the module is composed of an outer shell of PVC, with a hollow fiber bundle potted into each end with epoxy, and one end of the epoxy cut to expose the hollow core of the fibers. The outer shell consists of two tee fittings, with one connected to the gas inlet and the other connected to a pressure safety valve.

Poly(vinylchloride) (PVC) was the chosen material for the shell of the module. PVC pipe was cut into three 4 cm sections and glued into 0.5" tee fittings using PVC cement. A completed module shell is shown in Figure 2.7b. Hollow fibers were then tied together into a bundle using PTFE tape and paraffin wax was used to plug the ends of the fibers to prevent epoxy from entering the hollow bore during potting. A HFM bundle is shown in Figure 2.7c. The HFM bundle was then threaded through the module shell and Tygon tubing was fed up the bottom of the module and out through the bottom tee fitting. The thumb of a small, nitrile glove was used to cover the bottom of the module, as shown in Figure 2.7d. The epoxy mixture, consisting of a 10:1 ratio of resin to hardener, was then thoroughly mixed and pumped into the bottom of the module shell through the tubing with a syringe. The membrane module was then placed in convection oven at 50 °C for 2 hours to allow the epoxy to cure. After the epoxy was fully cured, the module was turned over and excess fiber was cut from the top of the module. The previous procedure was then repeated on the other side of the module.

Once the epoxy on both sides of the module was cured, one end of the HFM module was cut off with a saw, leaving the hollow core of the fibers open and embedded in an epoxy matrix. The cut end of the membrane module was immediately placed in a DI water sonication bath and allowed to sonicate for 45 minutes to remove any particulate epoxy that may be blocking the exit of the hollow fibers. A razor blade was then used to cut open any fibers that remain blocked after sonication. An end-on view of the potted, open hollow fibers is shown in Figure 2.7e. Since it was not possible to ensure that all fibers were unblocked, the total number of unblocked fibers was recorded. Vacuum grease was then applied to the PVC on the open end of the module and the brass outlet fitting was fixed in place with electrical tape. The final HFM gas separation testing module is shown in Figure 2.7f.

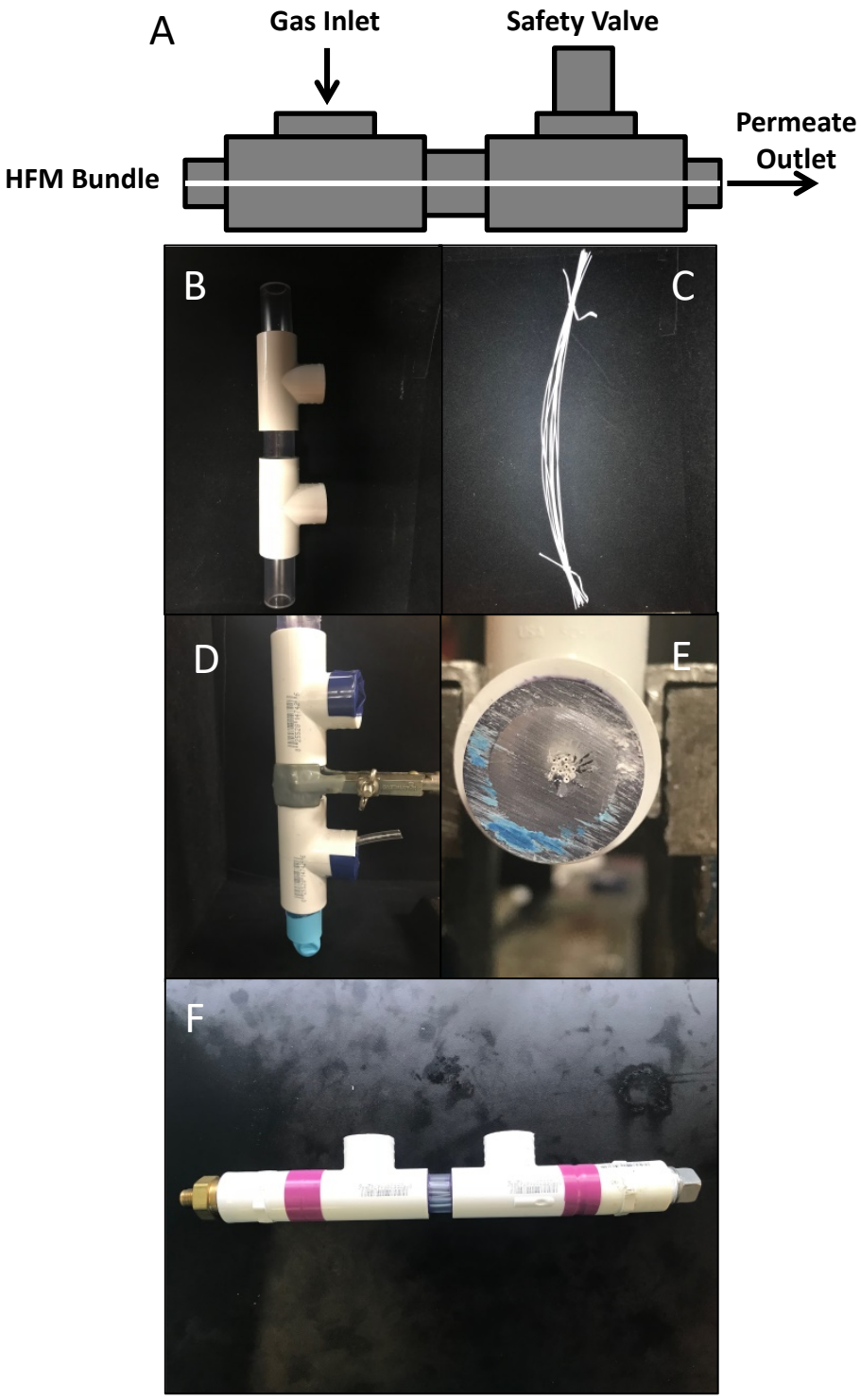

Figure 2.7: Hollow fiber membrane module (A) Schematic diagram of HFM module, (B) Empty module shell, (C) HFM bundle, (D) Module prepared for epoxy injection, (E) End view of potted, open fibers, (F) Completed module.

2.4.4.2 Hollow Fiber Membrane Module Testing

After construction of the HFM module, the permeance testing procedure for HFM membranes was very similar to that for the flat sheet membranes. The selected gas (N_2, He, CO_2, or O_2) was passed into the module in order to pressurize it to 29 psi. The membrane module was then held at this pressure for two hours in order to allow the flux to reach steady state. After this two hour conditioning period, the flowrate of the permeate stream was measured using the soap film flowmeter and recorded. The permeance of the membrane was then calculated accordingly.

2.5 Characterization Methods

2.5.1 Parallel Plate Rheometry

Polymer dope viscosity at various compositions, shear rates, and temperatures was determined using a TA instruments AR G2 parallel plate rheometer. All measurements were conducted using a 40 mm plate-plate geometry and a Peltier plate temperature controller. A 500 µm gap spacing was employed, with paraffin oil introduced at the edge to prevent solvent evaporation. Prior to measurement, each sample was conditioned by bringing the temperature to 25°C. Sample viscosity was then measured using steady state flow, with shear rates ranging from 0.01 – 10 s^{-1}. After completion of steady state flow measurements, the sample was conditioned at 25°C and 1 s^{-1} for 30 s. Oscillatory measurements were then conducted with an angular frequency range of 0.1 – 500 rad/s.

2.5.2 Scanning Electron Microscopy (SEM)

Qualitative observations of the morphology and surface topography of films and fibers were made using a Hitachi S-4800 scanning electron microscope. Membrane samples were first submerged in liquid nitrogen and then fractured using tweezers. All fracture surfaces were sputter coated with gold prior to imaging in the SEM to create a conductive surface and prevent sample surface charging. The SEM was primarily operated with an accelerating voltage (V_{acc}) of 15 kV and an emission current (I_e) of 10 μA.

2.5.3 Porometer

Liquid-liquid porometry is a characterization method that is designed to analyze the pore structure of membranes and other materials of low porosity, such as ceramics and textiles. It offers the ability to measure the pore diameter, pore size distribution and liquid flowrate through porous low permeability materials. In this technique, two immiscible liquids with differing surface tensions are employed. The liquid with the lower surface tension (A) is used to fill the pores of the sample. The liquid with the higher surface tension (B) is then added to the top of the sample and pressurized in order to displace liquid A and generate flow through the pores. Additionally, the flowrate of liquid B is measured without the pre-wetting of the sample by liquid A. The permeability of the membrane is calculated using the measured flowrates, while the pore diameter is calculated from the measured surface tension of the two liquids, using the equation:

$$D = 4\gamma cos\theta / \Delta P \qquad [2.6]$$

where D is the pore diameter, γ is the interfacial surface tension of the two liquids, θ is the contact angle of liquid A on the surface of the pore, and ΔP is the differential pressure applied to the sample by liquid B.

The pore size distribution of selected polymeric and mixed matrix membranes was characterized using a Porous Materials, Inc. liquid-liquid porometer. In this instrument, the liquid A (with lower surface tension) was Silwick™ liquid and liquid B (with higher surface tension) was isopropyl alcohol (IPA). Since the two liquids both have low surface tension, the contact angles are taken to be zero. Therefore, the pore diameter calculation is simplified to

$$D = 4\gamma/\Delta P \qquad [2.7]$$

The operating pressure range of the porometer used was 1 to 500 psi and it had a detectable pore size range of 0.001 – 0.5 µm. The membranes that were analyzed were all circular flat sheet asymmetric membranes with a diameter of 2.54 cm.

2.6 References

1. Baker, R.W., Beckman, I. N., Cussler, E. L., Doshi, K, Henis, J. M. S., Koros, W. J., Nakagawa, T., Paul, D. R., Petropoulos, J. H., Pinnau, I., Pixton, M. R., Plate, N, Prasad, R., Shaner, R. L., Wijmans, J. G., Yampolskii, Y. P., *Polymeric Gas Separation Membranes*. 1994: CRC Press Inc.
2. Hinds, B.J., Chopra, N., Rantell, T., Andrews, R., Gavalas, V., Bachas, L. G., *Aligned multiwalled carbon nanotube membranes.* Science, 2004. **303**(5654): p. 62-65.
3. Majumder, M., Chopra, N., Hinds, B. J., *Effect of tip functionalization on transport through vertically oriented carbon nanotube membranes.* Journal of the American Chemical Society, 2005. **127**(25): p. 9062-9070.
4. Majumder, M., Chopra, N., Hinds, B. J., *Mass transport through carbon nanotube membranes in three different regimes: ionic diffusion and gas and liquid flow.* ACS Nano, 2011. **5**(5): p. 3867-3877.
5. Ismail, A.F., Rahim N.H., Mustafa, A, Matsuura, T, Ng, B.C., Abdullah, S., Hashemifard, S.A., *Gas separation performance of polyethersulfone/multi-walled carbon nanotubes mixed matrix membranes.* Separation and Purification Reviews, 2011. **80**: p. 20-31.
6. Aroon, M.A., Ismail, A. F., Matsuura, T., Montazer-Rahmati, M. M., *Performance studies of mixed matrix membranes for gas separation: A review.* Separation and Purification Technology, 2010. **75**(3): p. 229-242.
7. Goh, P.S., Ismail, A. F., Sanip, S. M., Ng, B. C., Aziz, M., *Recent advances of inorganic fillers in mixed matrix membrane for gas separation.* Separation and Purification Technology, 2011. **81**(3): p. 243-264.
8. Goh, P.S., Ng, B. C., Ismail, A. F., Sanip, S. M., Aziz, M., Kassim, M. A., *Effect of dispersed multi-walled carbon nanotubes on mixed matrix membrane for O_2/N_2 separation.* Separation Science and Technology, 2011. **46**(8): p. 1250-1261.
9. Ismail, A.F., Goh, P. S., Sanip, S. M., Aziz, M., *Transport and separation properties of carbon nanotube-mixed matrix membrane.* Separation and Purification Technology, 2009. **70**(1): p. 12-26.
10. Moore, T.T., Koros, W. J., *Gas sorption in polymers, molecular sieves, and mixed matrix membranes.* Journal of Applied Polymer Science, 2007. **104**(6): p. 4053-4059.
11. S. Zeinali, M.A., *Improving O_2/N_2 Selective filtration using carbon nanotube-modified mixed-matrix membranes.* Chemical Engineering and Technology, 2015. **38**(11): p. 2079-2086.
12. Andrews, R., Jacques, D., Qian, D. L., Rantell, T., *Multiwall carbon nanotubes: Synthesis and application.* Accounts of Chemical Research, 2002. **35**(12): p. 1008-1017.
13. Loeb, S., Sourirajan, S., *Sea water demineralization bymeans of a semipermeable membrane.* Advances in Chemistry, 1962. **38**: p. 117-132.
14. Jomekian, A., Mansoori, S. A. A., Monirimanesh, N., Shafiee, A., *Gas transport behavior of DMDCS modified MCM-48/polysulfone mixed matrix membrane coated by PDMS.* Korean Journal of Chemical Engineering, 2011. **28**(10): p. 2069-2075.
15. Li, P., H.Z. Chen, and T.S. Chung, *The effects of substrate characteristics and pre-wetting agents on PAN-PDMS composite hollow fiber membranes for CO_2/N_2 and O_2/N_2 separation.* Journal of Membrane Science, 2013. **434**: p. 18-25.
16. Singh, A., Freeman, B. D., Pinnau, I., *Pure and mixed gas acetone/nitrogen permeation properties of polydimethylsiloxane PDMS.* Journal of Polymer Science Part B-Polymer Physics, 1998. **36**(2): p. 289-301.

Chapter 3: Development of PES-MWCNT Flat Sheet Membranes

3.1 Introduction

3.1.1 Asymmetric Flat Sheet Membranes

When first invented by Loeb and Sourirajan in the 1960s [1], asymmetric flat sheet membranes composed of cellulose acetate were an enormous technological breakthrough for membrane-based separations. They allowed for membranes to be fabricated in such a way as to increase the flux across the membrane to a practical level while maintaining structural integrity. This was achieved by producing a single membrane that was composed of a thin (0.1 – 1 μm) dense layer on top of a porous support of the same material. In this type of asymmetric structure, the dense top layer acts as a thin membrane through which separation occurs, while the porous sub-structure provides mechanical support to withstand the applied pressure differential.

In order to fabricate an asymmetric flat sheet gas separation membrane, a thin film of polymer solution (dope) is cast onto an appropriate substrate. This cast thin film is then immersed in a coagulation bath of nonsolvent or a solvent/nonsolvent mixture [2-6], which causes the dope to separate into two phases, one polymer-rich and the other polymer-lean. The polymer-rich phase solidifies during this process and forms the membrane, including the dense separating layer and the walls of the porous support. The polymer-lean phase forms the open pores in the membrane sub-structure. The final morphology and performance of the membrane are heavily influenced by the composition of both the dope and the coagulation medium [7]. For example, a dope without a sufficient weight fraction of polymer will form nodules of polymer-rich phase

suspended within a continuous matrix of polymer-lean phase, which is not conducive to membrane formation. Only if the polymer composition of the dope is sufficiently high will an asymmetric membrane form, leading to a continuous matrix of polymer-rich phase with droplets of polymer-lean phase forming the porous support structure. The composition of the coagulation medium is also vital to the structure and performance of the membrane by influencing the rate and type of demixing that occurs during coagulation. When the coagulation bath is composed of pure nonsolvent (or a high concentration of nonsolvent), instantaneous demixing occurs, which results in the formation of a dense separating layer at the dope-coagulant interface and the emergence of a porous sub-structure. Instantaneous demixing is often accompanied by the formation of finger-like macrovoids just below the dense layer which are created by the intrusion of non-solvent into the membrane during solidification. If the membrane is immersed in a coagulation bath that is solvent-rich, delayed demixing occurs, resulting in the suppression of macrovoids, but also a membrane that consists only of an open, homogeneous porous structure with no dense separating layer. The balance necessary to minimize the formation of macrovoids, which act as mechanical weak points in the membrane structure, while maintaining the integrity of the dense separating layer, is critical to the formation of a viable flat sheet membrane for gas separation.

The next major advance in the preparation of asymmetric gas separation membranes came in the late 1960s, when Loeb and Sourirajan developed a solvent exchange and drying procedure that prevented the collapse of the membrane pore structure upon drying [4]. This development expanded the applications for these

membranes from wet processes, such as reverse osmosis (RO) and ultrafiltration (UF), to dry processes, such as gas separation. In the solvent exchange procedure, the as-cast membrane is allowed to soak in water to extract residual solvent from within the pore structure. The membrane is then immersed in a lower boiling point water-miscible solvent (i.e. methanol) in order to extract the water within the membrane, and finally is immersed in a third low boiling point solvent that is miscible with the second solvent but is immiscible with water (i.e. hexane or pentane). The final solvent is then allowed to evaporate, resulting in a dried membrane without compromising the integrity of the pore structure.

For most industrial applications, flat sheet membranes are cast as long continuous sheets that are sealed and spiral wound around a central perforated tube. The membrane module is then pressurized with the gas mixture to be separated, which forces the gas that is more permeable in the membrane material to permeate across the membrane and exit out through the perforated tube in a more concentrated stream. The retentate gas then exits the module and is generally diverted back into the original feed stream to improve separation efficiency.

Flat sheet asymmetric membranes were an enormous improvement in the field of membrane-based gas separation technology. Prior to their invention, membranes that were thin enough (< 1 μm) to provide commercially-viable fluxes were not durable enough to remain intact in a high pressure (> 200 psi) environment. Asymmetric

membranes were able to deliver the high flux associated with ultrathin membranes as well as the structural durability of a much thicker membrane.

3.1.2 Material Systems of Interest

3.1.2.1 Membrane Polymer

Polyethersulfone (PES) has been one of the most commonly used polymers in the field of membrane separation for several decades. It is frequently used as both the separating element itself as well as the porous substrate upon which thin film composite membranes are cast. PES is a relatively high T_g glassy thermoplastic, with a rigid repeat unit structure which imparts good thermal, chemical, and mechanical properties. It also readily forms asymmetric membranes via phase inversion in aqueous media due to its strong hydrophobicity. Additionally, it is commercially available and is fairly low cost compared to other polymeric membrane materials. Therefore, it has been the focus of much membrane-related research in the area of liquid phase separation (reverse osmosis, micro/ultra/nanofiltration, etc.) as well as gas separation. Polysulfone (PSf) is a similar polymer to PES, but with an additional bisphenol moiety in the polymer repeat unit. It is more commonly used in industrial gas separations, such as the Air Products PRISM membrane system, because it shows comparable ideal selectivities and higher permeability than PES.

Research conducted on the gas transport properties of PES asymmetric membranes typically involves the characterization of membranes coated with a very thin layer of polydimethylsiloxane (PDMS), which is required to repair or “caulk” the microscopic pinhole defects that form in the dense selective layer during phase

inversion [8-10]. As discussed in Section 1.1.2.3, PDMS is used because its high permeability and low selectivity minimally impact membrane performance by shifting the dominant gas diffusion mechanism from non-selective Knudsen diffusion through the pinholes to solution diffusion across the membrane polymer [11, 12]. Accordingly, PES-PDMS asymmetric membranes have been reported to provide O_2/N_2 pure-gas ideal selectivities in the range of 5.6 [13] - 6.0 [9]. The O_2 permeance values for these types of membranes are reported to be in the range of 1.0 GPU [10] to 30 GPU [9].

3.1.2.2 Mixed Matrix Membranes

Due to their superior performance over wholly-polymeric membranes, much research in recent decades has been focused on the development of mixed matrix membranes [14-19]. Mixed matrix membranes are typically comprised of a porous inorganic filler material dispersed within a polymer matrix. Mixed matrix membranes (MMMs) often exhibit improved separation performance over traditional polymeric membranes through the addition of a molecular sieving component to the diffusion mechanism. As illustrated schematically in Figure 3.1, MMMs improve the size separation by forcing large molecules to take a more tortuous path through the membrane dense separating layer, while allowing small molecules to flow through the pores of the inorganic filler. Early versions of these membranes involved zeolites as the inorganic filler material, due to their low cost, commercial availability and narrow pore size distributions [20-23]. The major drawback of using zeolites is that, owing to their inorganic nature, they tend to exhibit poor adhesion to the polymer matrix, which results in a decrease in membrane selectivity by creating non-selective channels at the

interfaces between the zeolite filler and the polymer matrix. Voids that form at the interface between the inorganic filler material and the polymer matrix are a common issue that arises during the formation of mixed matrix membranes. If the adhesion of the inorganic filler material is not sufficient, the voids can connect together to form continuous channels through the membrane at high filler loadings [24].

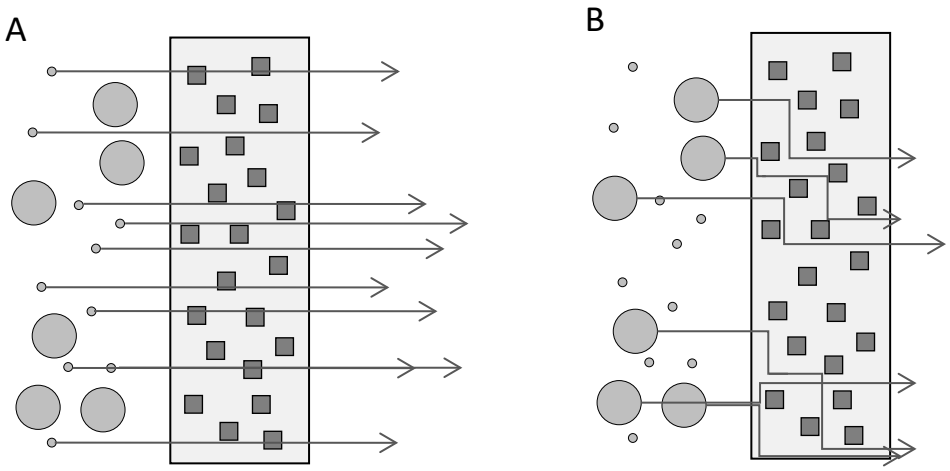

Figure 3.1: Schematic diagram demonstrating the mechanism by which selectivity is improved in a mixed matrix membrane. (A) Smaller gas molecules flow freely due to the porous nature of the filler material; (B) larger gas molecules (rejected from the filler via size discrimination) are forced to take a more tortuous path through the dense separating layer of the membrane, decreasing their permeability.

One approach to overcome the interfacial issues encountered in zeolite MMMs is the use of metal organic frameworks (MOFs) as the inorganic filler material [25-28]. MOFs are made of transition metals or transition metal oxides that are connected by organic linkers to create a microporous structure. MOFs provide many of the same positive qualities as zeolites, as they can be commercially synthesized relatively easily and at a fairly low cost. They also have very high surface area and, due to the organic

linkers, can be produced with tunable pore sizes and small pore size distributions. MOFs offer improvement over zeolites as the filler material in MMMs because the organic linker molecules can be selected to ensure good adhesion with the polymer matrix.

Since their first discovery and major reports in the early 1990s by Ijima et al., carbon nanotubes (CNTs) have been extensively studied for their mechanical, electrical and thermal properties, and more recently have begun to be incorporated into membrane materials[29]. For example, aligned carbon nanotubes have been used for the fabrication of highly-controlled nanoporous water filtration membranes [30-33]. Additionally, CNTs have been incorporated as the inorganic filler material in gas separation MMMs; multiwall carbon nanotubes (MWCNTs) have been thought to act as molecular sieves due to their intrinsic interlayer spacing [34]. Since carbon nanotubes have a strong tendency to agglomerate, much of the research surrounding their use in MMMs centers on CNTs that have been oxidized and/or functionalized in order to improve their adhesion to the polymer matrix [16, 19, 34-39]. In these studies, the oxidized and functionalized CNTs typically show better dispersion within the polymer matrix (usually PES or PSf) and a large improvement in both O_2/N_2 and CO_2/CH_4 selectivity as compared with the inclusion of pristine CNTs. The researchers attribute the selectivity difference to the poor dispersion of the pristine CNTs, resulting in agglomeration of the tubes. This agglomeration of CNTs leads to an increase in non-selective interface defects in the separating layer of the membrane.

Previous work by Weisenberger et al. has demonstrated the ability to achieve a uniform dispersion of MWCNTs in polyacrylonitrile (PAN) solution spinning dopes for the production of PAN-based carbon fiber precursor [40]. The dispersion was achieved without oxidation or functionalization of the MWCNTs, using a combination of wand ultrasonication and subsequent centrifugation to sediment agglomerated MWCNTs. Only the homogeneous MWCNT dispersion, decanted from the supernatant after centrifuging, was used. This result is important to the work reported herein because it suggested that a viable CNT-based polymeric mixed matrix membrane could be produced without the need for surface modification of the MWCNTs.

3.2 Results and Discussion

3.2.1 Rheology of Membrane Casting Dopes

3.2.1.1 Polyethersulfone Viscosity Measurements

One of the most important processing factors for both the casting of flat sheet membranes and the spinning of hollow fiber membranes is the viscosity of the polymer dope. In the sections that follow, the morphologies of flat sheet phase inversion-derived membranes, based on PES and PSf, are examined as a function of dope composition and coagulation conditions. A key consideration in establishing the dope composition (i.e. dissolved polymer content) is the corresponding solution viscosity of the dope. Prior work has suggested a target viscosity in the range of 100 to 200 Pa.s for dry-jet spinning of solid fiber under comparable operating conditions [41]. Since the flat sheet membrane experiments were conducted with an objective to extend the results to hollow fiber spinning, this target range was the basis by which initial dope compositions were established for studies of flat sheet membrane casting.

A TA instruments AR G2 parallel plate rheometer was used to determine the steady-shear viscosity of polymer dope solutions of varying composition with both N,N-dimethylacetimide (DMAc) and N-methylpyrrolidone (NMP) as solvents. Plots of the viscosity (at 25°C and 1 s^{-1}) versus polymer content for PES (M_W = 55,000) in DMAc and NMP, as well as PSf (M_W = 60,000) in NMP, are shown in Figure 3.2. For PES, the solution viscosity ranged from 1 to 500 Pa.s over the range of 20 to 40 wt.% polymer content, with similar results obtained for both solvents; PSf showed comparable viscosities for solutions prepared in NMP. In each case, an exponential relationship was obtained for viscosity as a function of concentration, leading to a linear result when plotted on a semi-log basis.

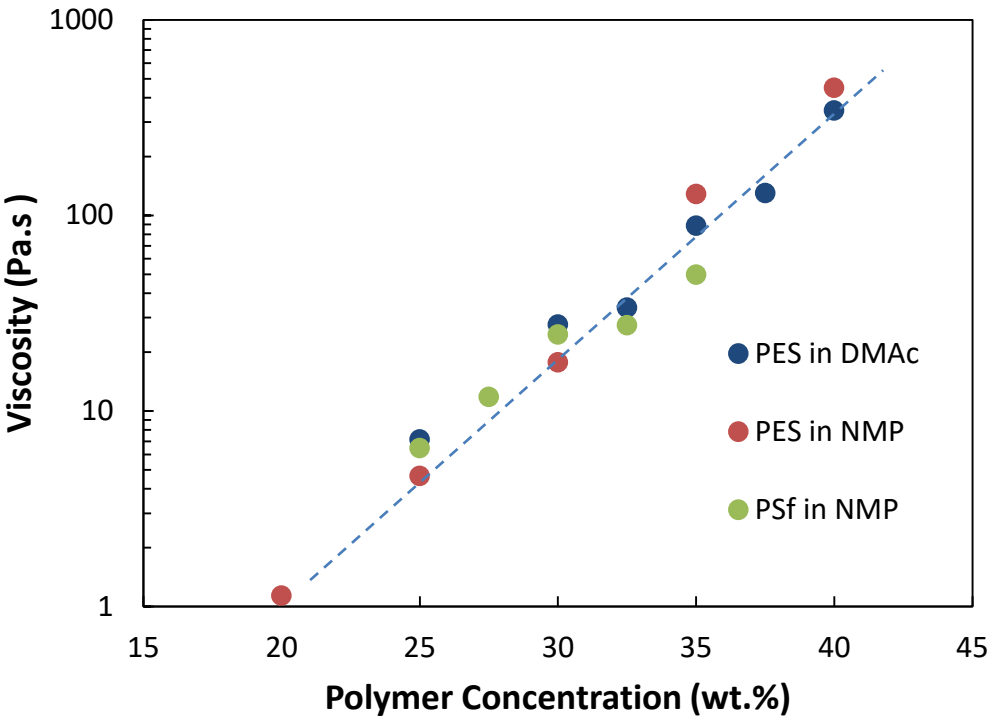

Figure 3.2: Relationship between the polymer dope viscosity at 25 °C and 1 s^{-1} and polymer concentration for PES in NMP and DMAc, as well as PSf in NMP.

3.2.1.2 Mixed Matrix Dope Viscosity Measurements

The viscosity of PES-MWCNT and PES-carbon black mixed matrix dopes was measured at various filler loading levels in order to determine the influence of filler loading on the rheological properties. Plots of the complex viscosity (η*) against angular frequency for a series of dopes composed of various loadings of MWCNT in NMP are presented in Figure 3.3.

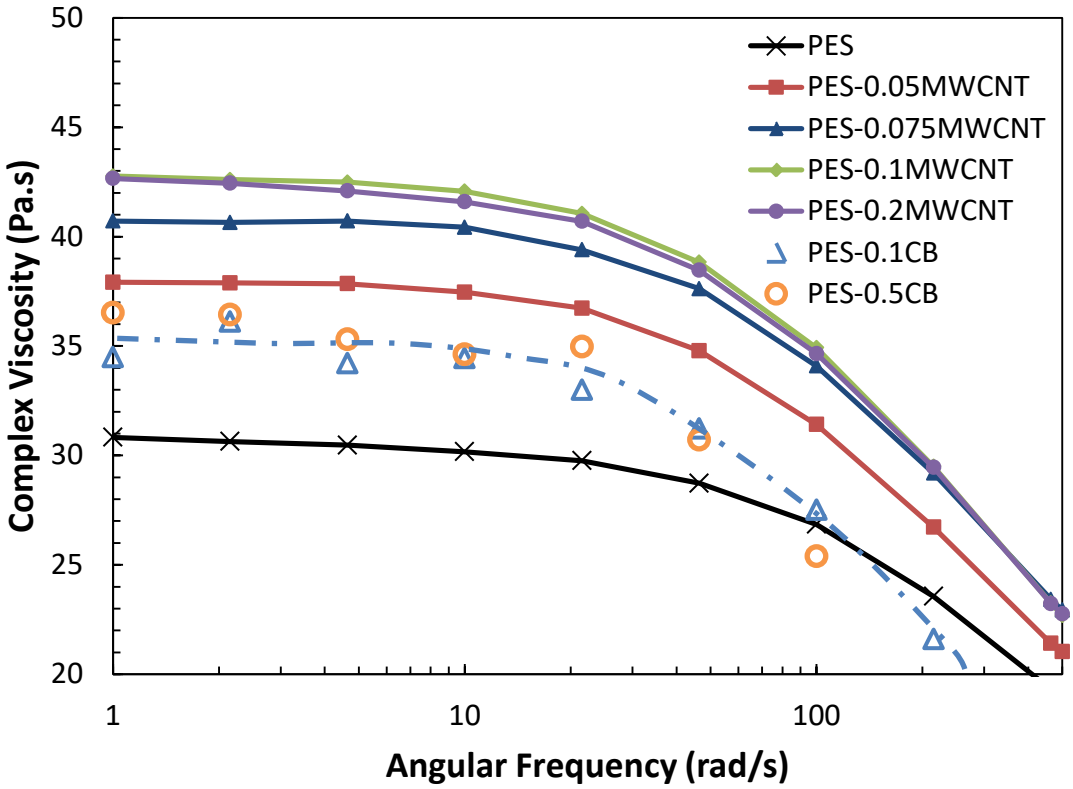

Figure 3.3: Complex viscosity vs. angular frequency for PES-MWCNT and PES-carbon black dopes with varying filler loadings at 25°C. PES-XXMWCNT corresponds to dope composed of 30 wt.% PES in NMP with XX wt.% MWCNT (or CB) relative to the polymer.

Increasing MWCNT concentration increased the complex viscosity of the dope until the loading reached 0.1 wt.% MWCNT relative to the polymer. At 0.2 wt.%, the complex viscosity did not appear to increase any further. As will be discussed later in Section 3.2.4.1, 0.1 wt.% MWCNT was coincident with a large increase in the ideal selectivity of membranes that were cast using this dope. In addition, the figure demonstrates that the carbon black filler resulted in a significantly smaller increase in the complex viscosity, compared to the MWCNT filler, even up to 0.5 wt.% carbon black. One of the primary differences between the two filler materials is the large aspect ratio of the MWCNTs compared to the (nominally-spherical) carbon black particles. After 20 minutes of similar sonication, the average length of MWCNTs in dispersion was elsewhere reported to be approximately 5 – 10 μm [42]. Since the MWCNTs are approximately 40 nm in outer diameter, this corresponds to an aspect ratio of 125 to 250. The large aspect ratio inherent to the nanotubes has been shown to foster entanglement with the polymer chains at relatively low MWCNT loadings, resulting in an increase in dope viscosity [43].

3.2.2 Flat Sheet Membrane Morphology

3.2.2.1 Effect of Coagulation Bath Composition on Membrane Morphology

Polyethersulfone (PES) asymmetric membranes were phase-inverted in coagulation baths of pure deionized water, and 50, 60, and 70 wt.% DMAc in deionized water. The initial target viscosity value of 200 Pa.s corresponded to a polymer content of approximately 38.5 wt.% PES in solution, which was selected at the outset for the flat sheet membrane casting studies. These studies were conducted in order to examine the phase inversion characteristics of the resulting flat sheet membranes, and to establish

the corresponding parameters for flat sheet membrane casting and hollow fiber membrane spinning in future experiments. SEM micrographs of each cryogenically fractured membrane surface are shown in Figure 3.4; the membrane surface exposed to the coagulation bath is indicated by an arrow in each case. For the membrane prepared via coagulation in deionized water, a dense top layer was observed, with finger-like macrovoids extending into the porous sub-structure to a depth equivalent to about one-half of the membrane thickness. It was clear from the micrographs that an increase in the solvent content of the coagulation bath resulted in a decrease in the relative penetration depth (i.e. length) of macrovoids extending from the film surface that was exposed to the coagulant. The membrane cross sections that are presented in Figures 3.4c-d showed a morphological transition between a coagulation composition of 60 wt.% DMAc, where relatively short finger-like macrovoids were observed, and 70 wt.% DMAc, where the thin films were virtually macrovoid free. The overall trend reflected the instantaneous demixing of the polymer solution that occurs when exposed to pure non-solvent, which creates a dense outer skin and finger-like macrovoids just below the surface. An increase in solvent content within the coagulation bath led increasingly to delayed demixing, resulting in a more uniform sponge-like substructure and the appearance of distinct pores on the surface of the membrane. These large surface pores were distinct from pinhole defects that can be repaired through PDMS caulking (as described in Section 1.1.2.3), as the former are formed when the porous substructure breaks through the top surface during phase inversion.

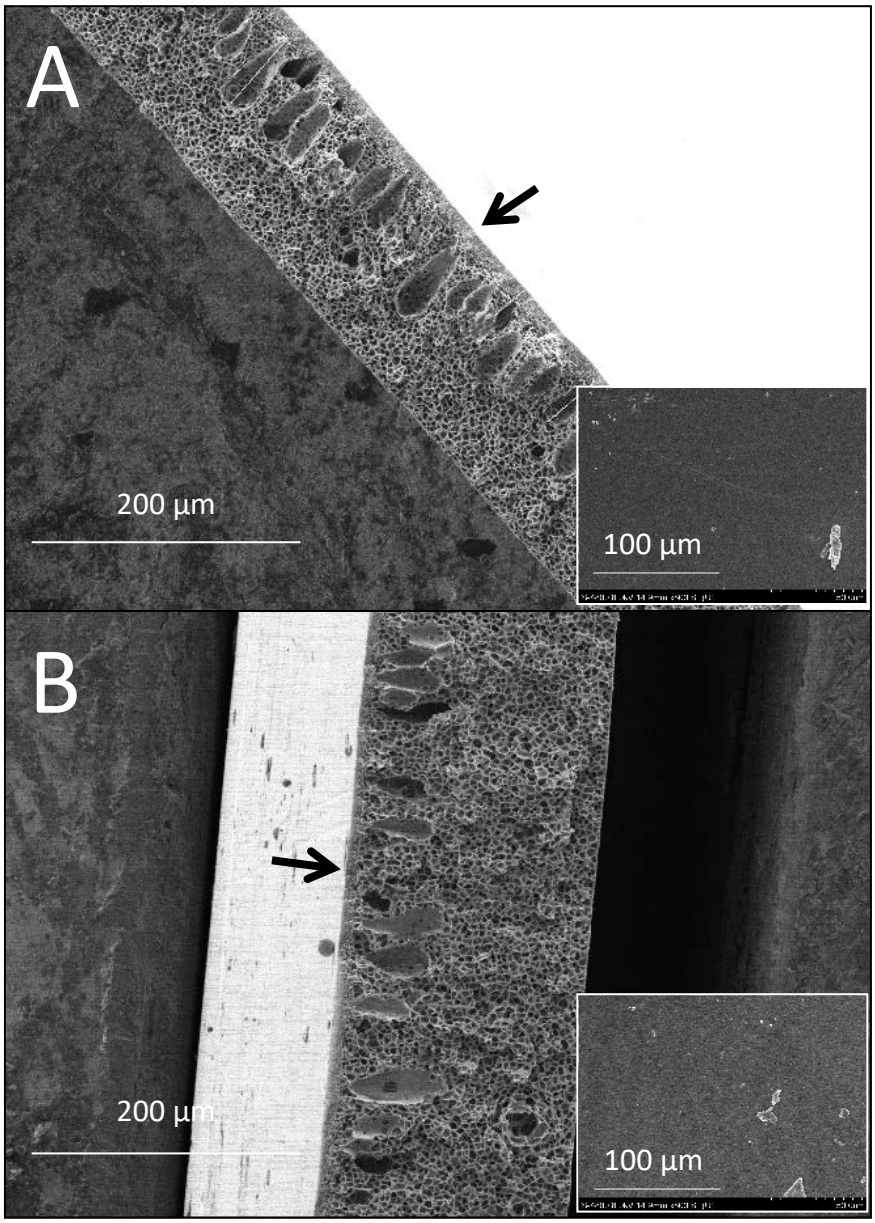

Figure 3.4a-b: SEM micrographs of PES thin films coagulated from 38.5 wt.% PES-DMAc dope in bath composed of (A) 0 wt.%, (B) 50 wt.% DMAc/water mixture. Arrows indicate surface that was exposed to coagulation bath. Inset: top surface of thin films at 800x magnification.

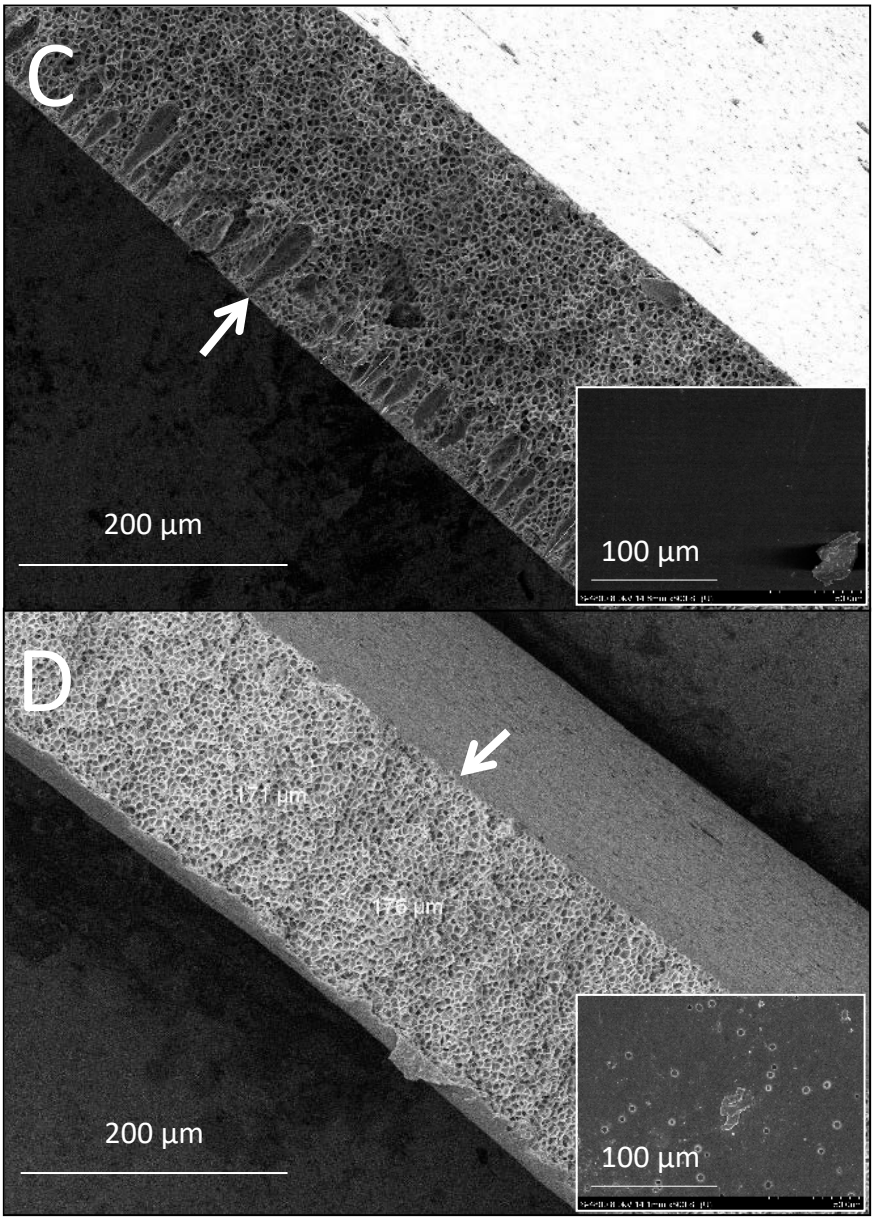

Figure 3.4c-d: SEM micrographs of PES thin films coagulated from 38.5 wt.% PES-DMAc dope in bath composed of (C) 60 wt.%, (D) 70 wt.% DMAc/water mixture. Arrow indicates exposure face. Inset: top surface of thin films at 800x magnification.

For gas separations, it is vitally important to have a thin, dense, defect-free separating layer on the outer surface of the membrane to maintain selectivity. For this reason, deionized water was used as the phase-inversion medium for all asymmetric flat sheet membranes that were prepared for the gas separation experiments reported in this work.

Similar experiments were conducted using dopes composed of 35 wt.% polysulfone (PSf) in N-methylpyrrolidone (NMP). Consistent with the PES flat-sheet membranes, low concentrations of NMP in the coagulation bath led to PSf membrane structures that exhibited a dense separating layer on top of a porous sub-structure with large finger-like macrovoids propagating downward through the cross-section of the membrane; see Figure 3.5. As the coagulation bath became more solvent-rich, the relative penetration depth of the finger-like voids decreased. In contrast to the PES casting system, when the coagulation bath composition was 70 wt.% solvent, a dense separating layer and sparse macrovoids were still evident.

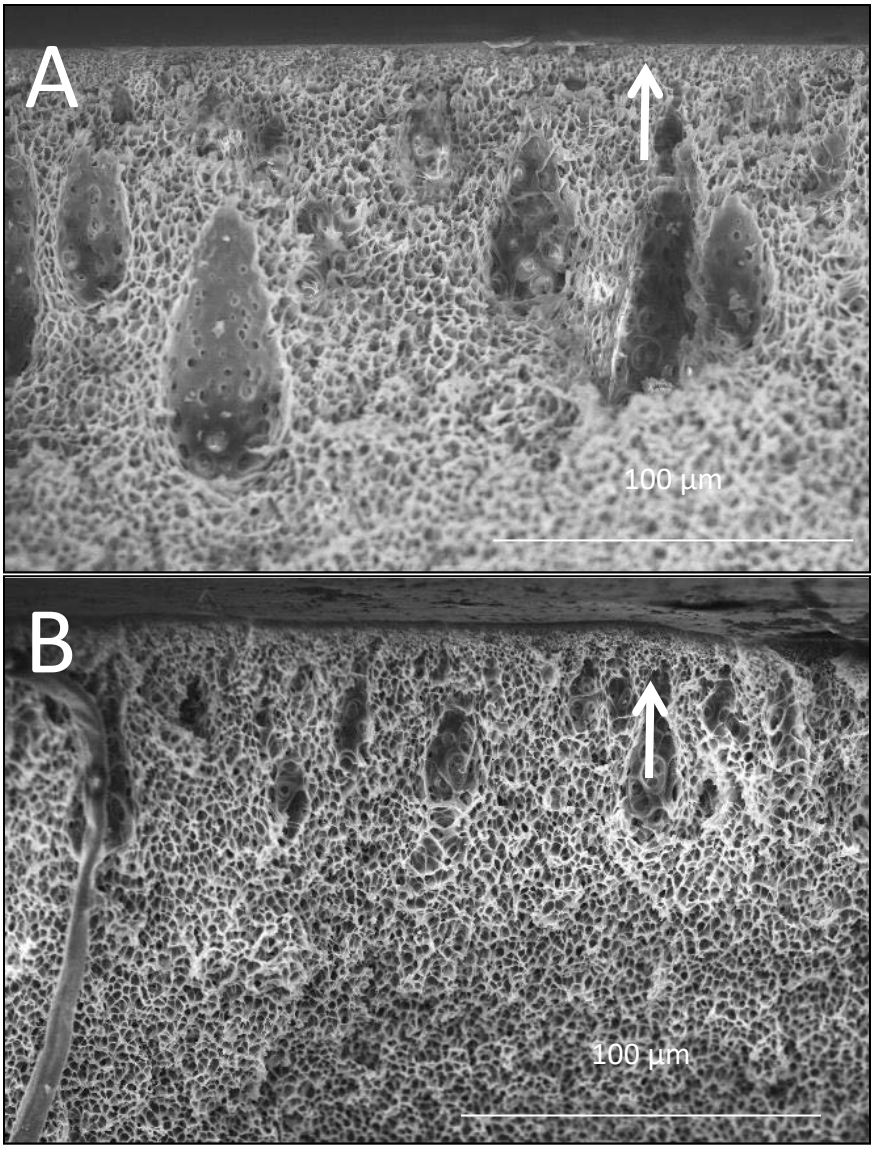

Figure 3.5a-b: SEM micrographs of PSf thin films coagulated from 35 wt.% PES-NMP dope in bath composed of (A) 0 wt.%, (B) 50 wt.% NMP/water mixture. Arrow indicates exposure face.

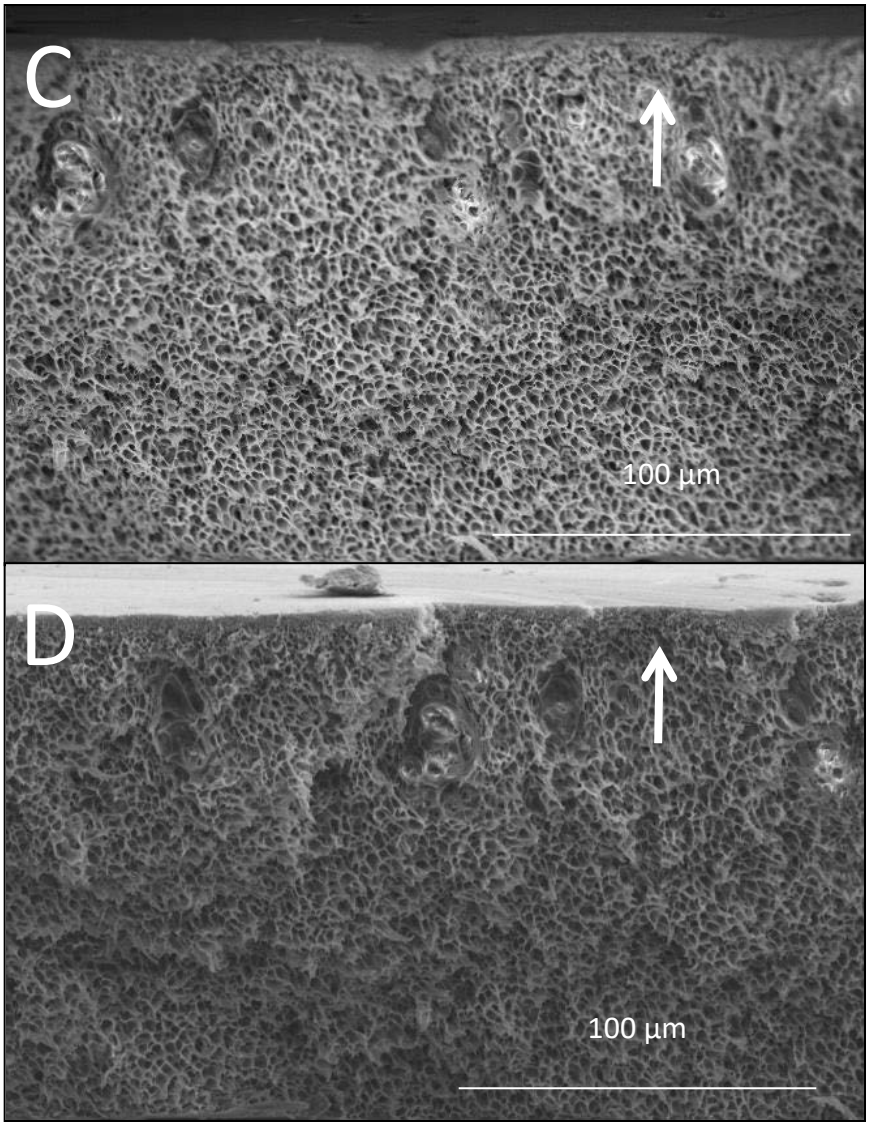

Figure 3.5c-d: SEM micrographs of PSf thin films coagulated from 35 wt.% PSf-NMP dope in bath composed of (A) 60 wt.%, (B) 70 wt.% NMP/water mixture. Arrow indicates exposure face.

3.2.2.2 Effect of Polymer Concentration on Membrane Morphology

The relationship between polymer concentration in the dope solution and asymmetric membrane morphology was examined by casting flat sheet membranes from dopes composed of varying concentrations of polymer. Dope preparation and casting were carried out using the methods detailed in section 2.3.1. The films were cast using solutions composed of 15, 20, 25, 30, and 35 wt.% PES in DMAc. For PSf, flat sheet membranes were cast from dopes of 25, 27.5, 30, 32.5, and 35 wt.% PSf in NMP.

Representative SEM micrographs for the PES flat sheet samples are shown in Figure 3.6. These samples were cast in a coagulation medium of deionized water. Cross sections of films cast from dopes with low concentrations of PES (< 25 wt.%) showed morphologies with large voids and comparatively little of the desired porous substructure. The PES dope composed of 30 wt.% PES in DMAc was found to produce an acceptable morphology that was virtually the same as that produced from 38.5 wt.% PES in DMAc. Additionally, as shown in Section 3.2.1.1, 30 wt.% PES in DMAc had a significantly lower viscosity than that of 38.5 wt.% PES, which allowed a much lower pressure drop during filtering (in later hollow fiber work). Since its coagulation resulted in comparable thin film membrane morphologies without the practical processing limitations of the higher viscosity formulation, 30 wt.% PES dope was chosen for all subsequent flat sheet PES membrane experiments.

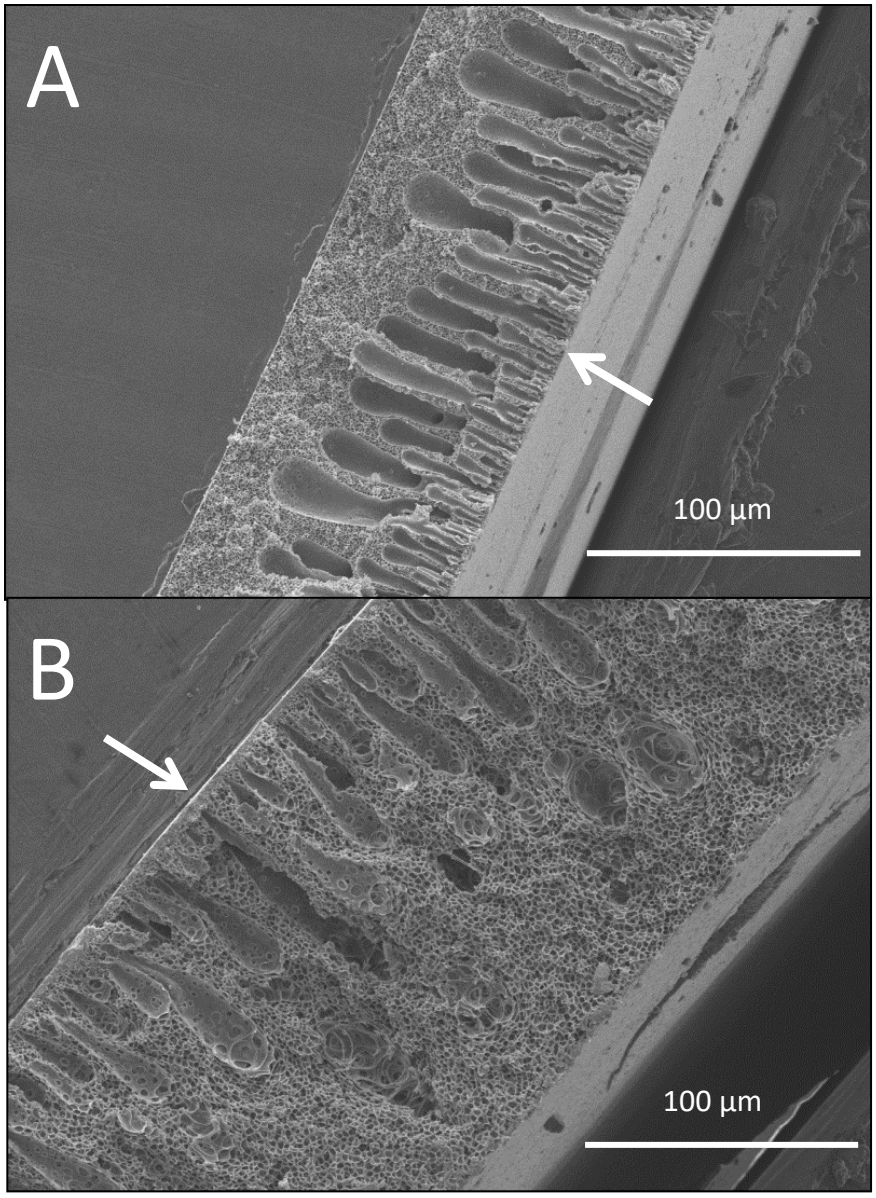

Figure 3.6a-b: SEM micrographs of PES thin films cast using dope composed of (A) 15 wt.% and (B) 20 wt.% PES in DMAc with deionized water as the coagulation medium. Arrow indicates exposure face.

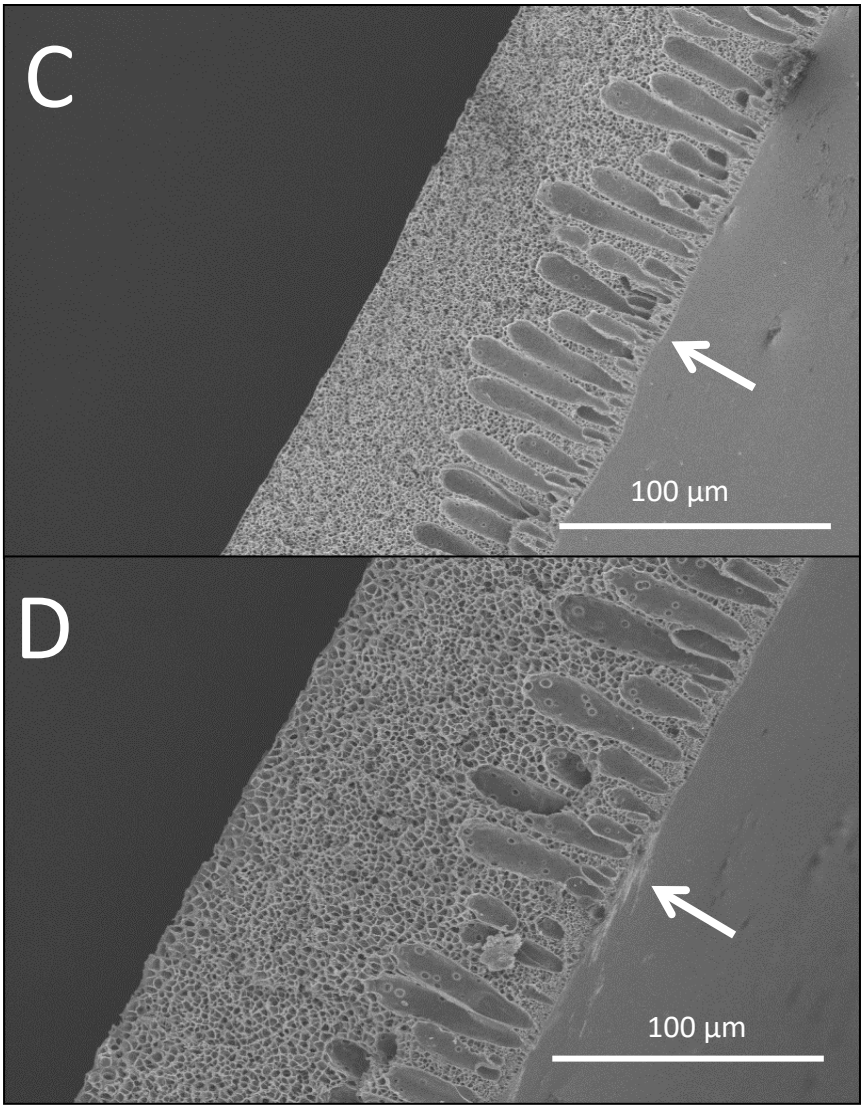

Figure 3.6c-d: SEM micrographs of PES thin films cast using dope composed of (C) 25 wt.% and (D) 30 wt.% PES in DMAc with deionized water as the coagulation medium. Arrow indicates exposure face.

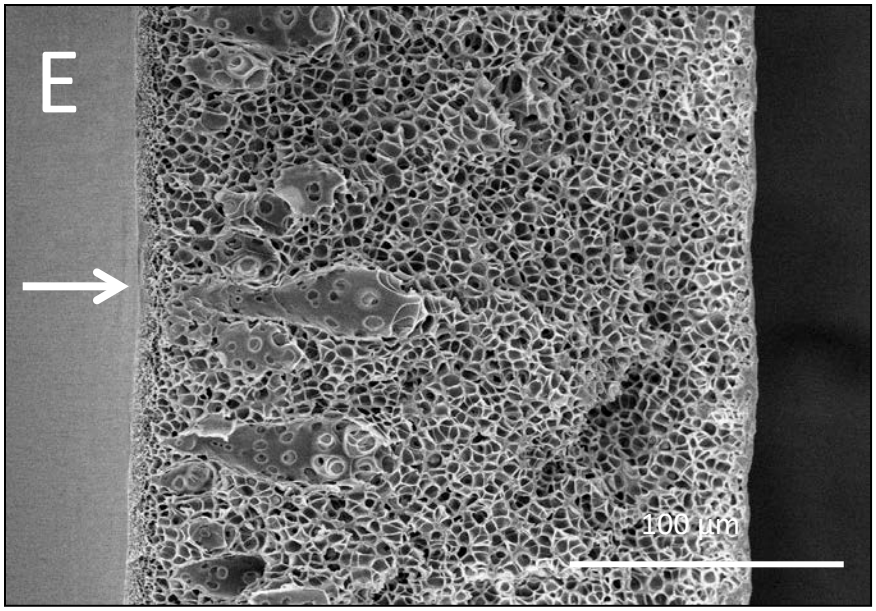

Figure 3.6e: SEM micrographs of PES thin films cast using dope composed of (E) 35 wt.% PES in DMAc with deionized water as the coagulation medium. Arrow indicates exposure face.

A similar result was obtained for PSf flat sheet specimens, which is shown in Figure 3.7. When concentrations of PSf below 30 wt.% were used to cast the films, very little of the desired sponge-like morphology was formed in the porous support layer, which was instead composed mostly of long, finger-like macrovoids. As the PSf concentration of the dope was increased to above 30 wt.%, a more consistent porous support region emerged, with a dense separating layer evident near the coagulation bath interface. Based on these results (as well as the viscosity data for the PSf dopes), 35 wt.% PSf in NMP was chosen as the preferred dope for flat sheet casting of polysulfone membranes. It should be noted that, when all other casting parameters were held equal, PSf flat sheet membranes showed both higher occurrence and longer macrovoids than the corresponding PES membranes.

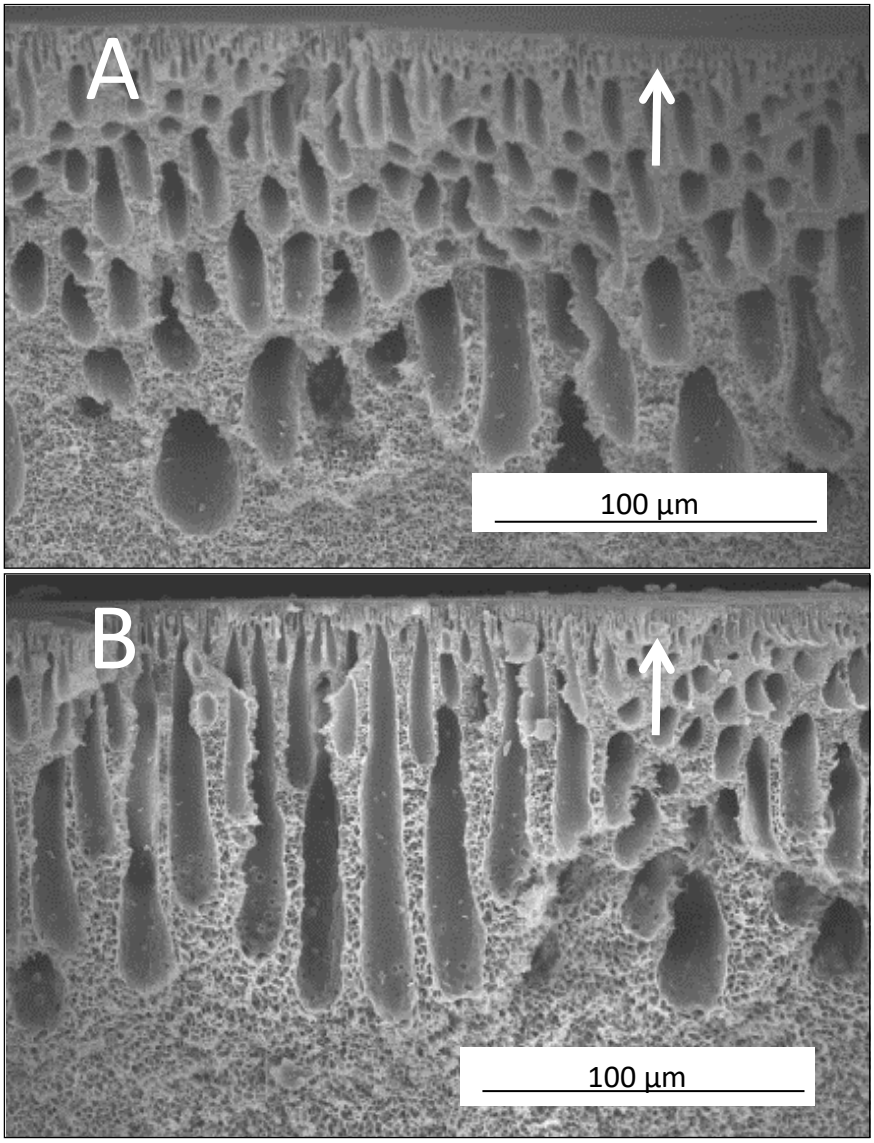

Figure 3.7a-b: SEM micrographs of PSf thin films cast using dope composed of (A) 25 wt.% and (B) 27.5 wt.% PSf in NMP with deionized water as the coagulation medium. Arrow indicates exposure face.

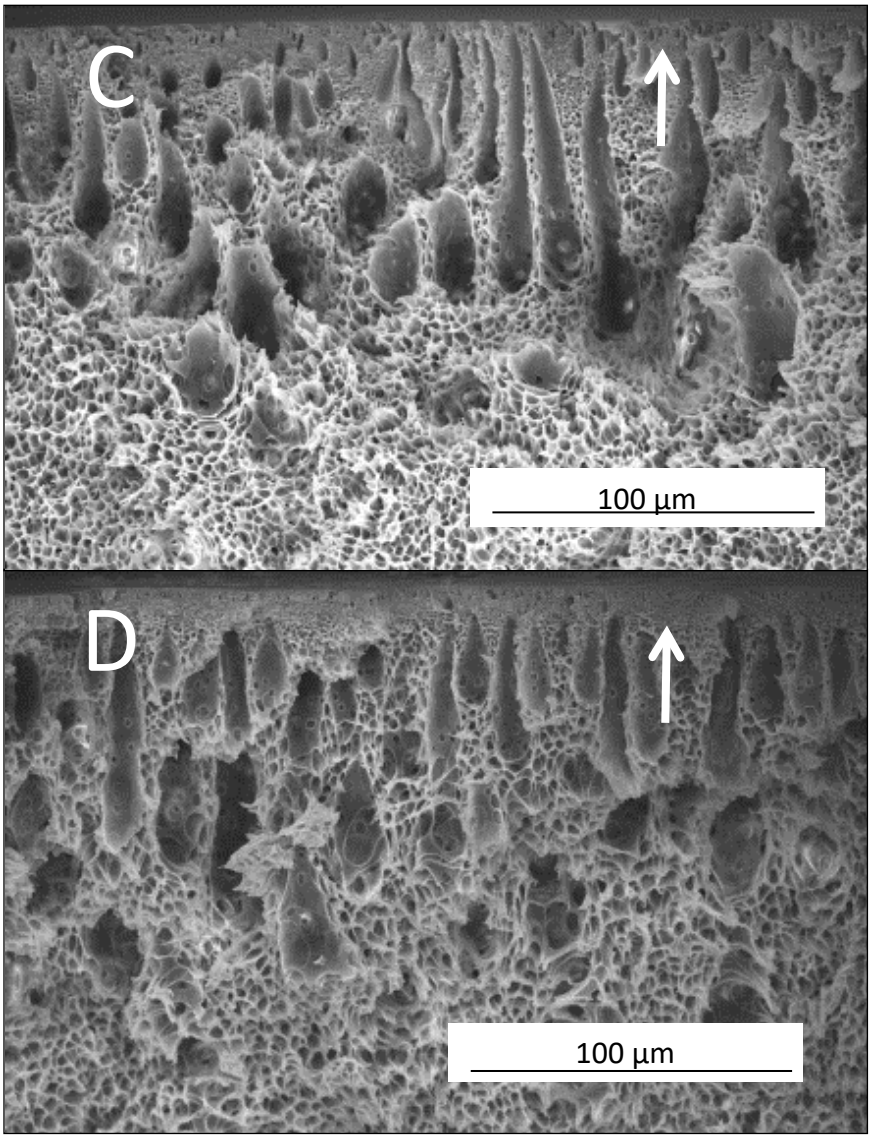

Figure 3.7c-d: SEM micrographs of PSf thin films cast using dope composed of (C) 30 wt.% and (D) 32.5 wt.% PSf in NMP with deionized water as the coagulation medium. Arrow indicates exposure face.

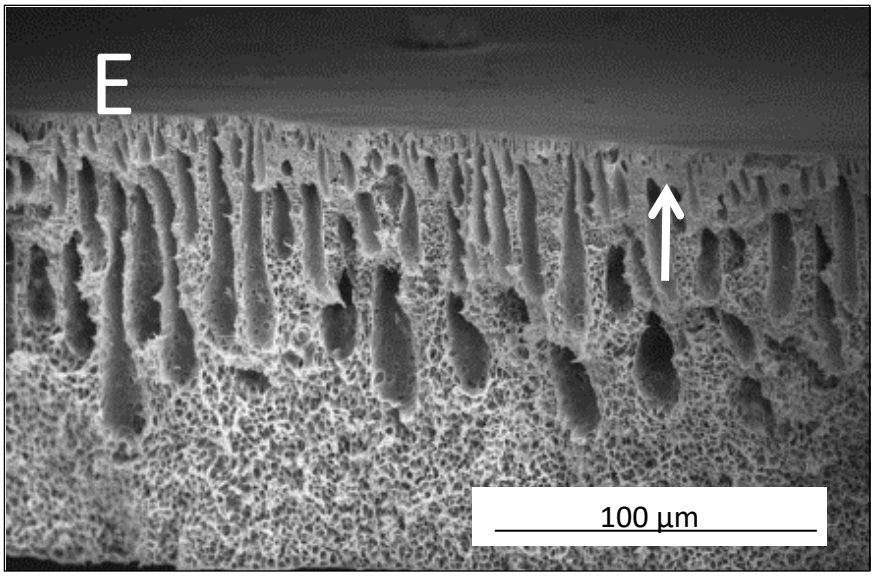

Figure 3.7e: SEM micrographs of PSf thin films cast using dope composed of 35 wt.% PSf in NMP with deionized water as the coagulation medium. Arrow indicates exposure face.

3.2.2.3 Effect of Solvent on Membrane Morphology

After performing several flat sheet membrane experiments using DMAc as the PES solvent, it was determined that N-Methylpyrrolidone (NMP) could easily replace DMAc as a less hazardous alternative without significantly altering membrane preparation. In order to assess the impact of the solvent change on membrane morphology, a series of PES membranes were cast from NMP dope solution with varying coagulant composition. A casting composition of 30 wt.% PES in NMP was selected for the dope, consistent with the discussion presented above; membranes were quenched in 0, 50, 60, and 70 wt.% NMP in water. SEM micrographs of these membranes are shown in Figure 3.8.

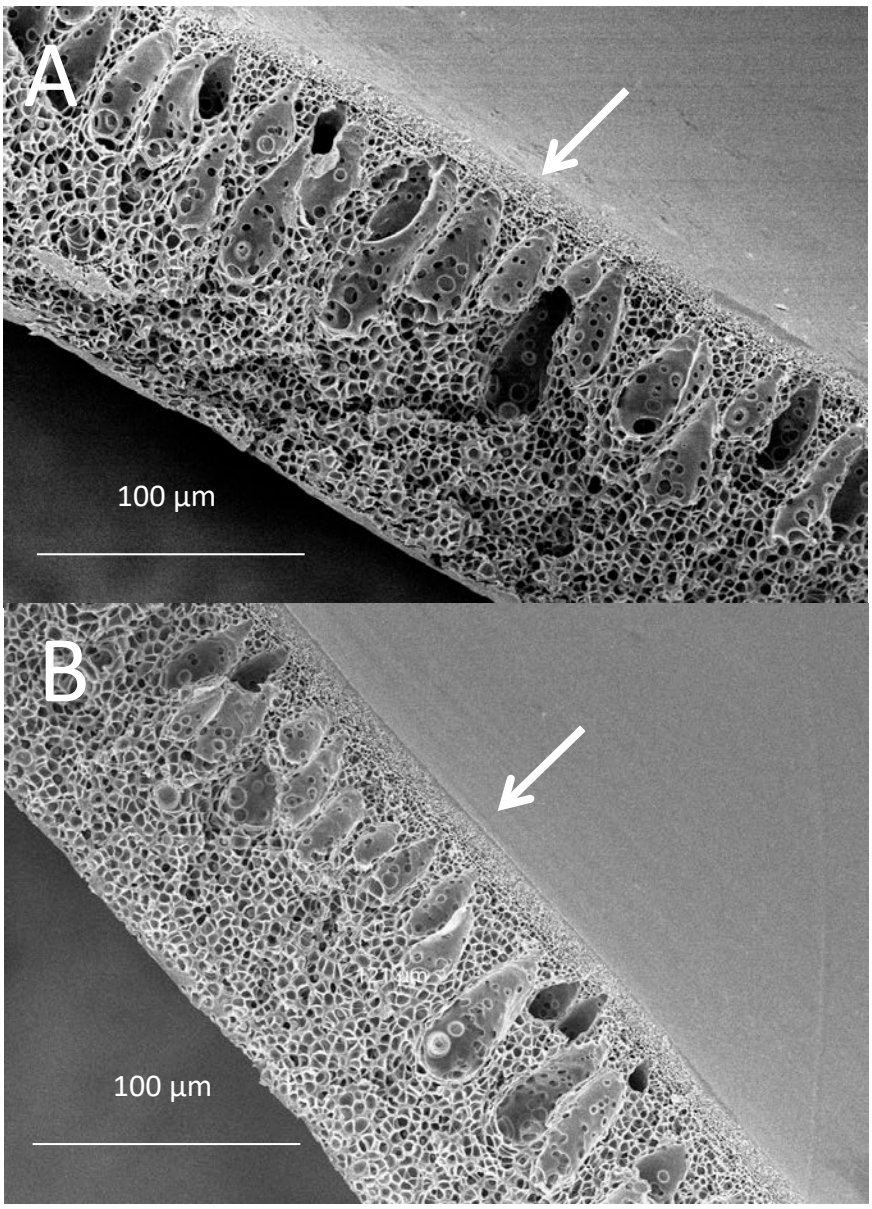

Figure 3.8a-b: SEM micrographs of PES thin films coagulated from 30 wt.% PES-NMP dope in bath composed of (A) 0 wt.%, (B) 50 wt.% NMP/water mixture. Arrow indicates exposure face.

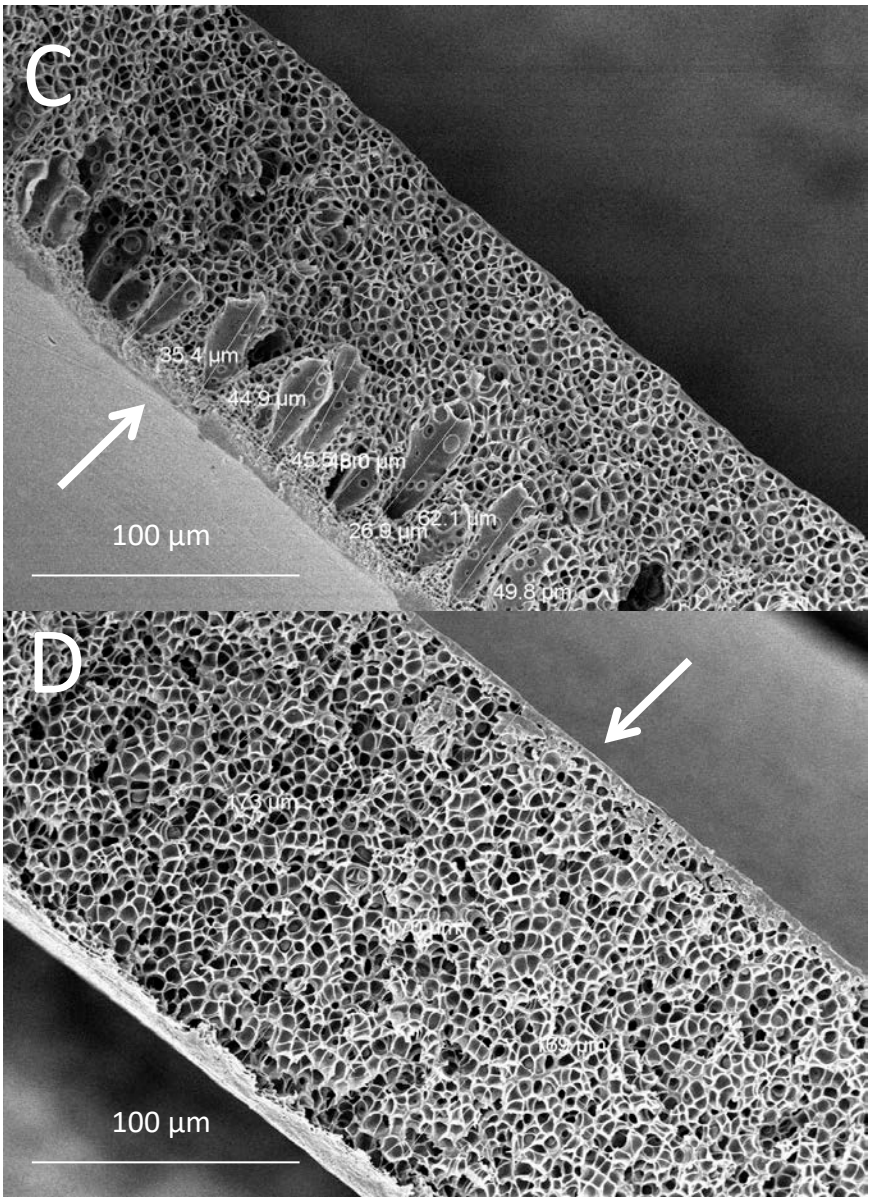

Figure 3.8c-d: SEM micrographs of PES thin films coagulated from 30 wt.% PES-NMP dope in bath composed of (C) 60 wt.%, (D) 70 wt.% NMP/water mixture. Arrow indicates exposure face.

When the coagulation medium was composed of pure deionized water, a dense separating layer was formed at the dope-coagulant interface, with finger-like macrovoids that extended approximately halfway across the membrane cross section. The remaining cross section was composed of sponge-like substructure, with a porous topology observed at the membrane-substrate interface. As the concentration of NMP in the coagulation bath was increased, the relative penetration depth of the voids decreased, and they were virtually eliminated when the coagulation bath concentration reached 70 wt.% NMP. A direct comparison of the thin film cross sections obtained using the two different solvents (and corresponding coagulation mixtures) is shown in Figure 3.9. Based on these micrographs, it was determined that thin films that were cast from these two solvents produced sufficiently similar morphologies. Therefore, it was deemed appropriate to use less hazardous NMP as the solvent for all subsequent flat sheet and hollow fiber membrane experiments.

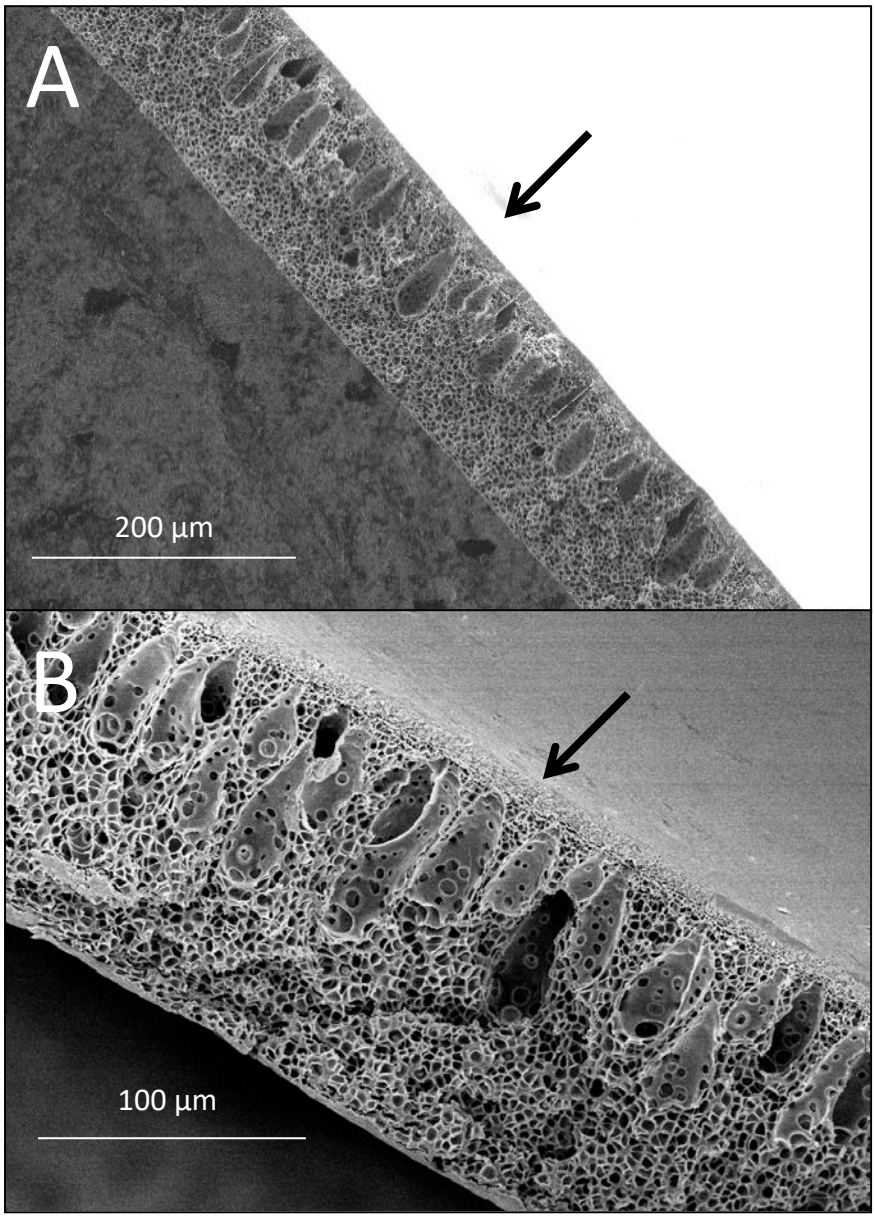

Figure 3.9a-b: Comparison of SEM micrographs of 30 wt.% PES thin films cast from (A) DMAc and (B) NMP using deionized water as the coagulation medium. Arrow indicates surface that was exposed to coagulation bath.

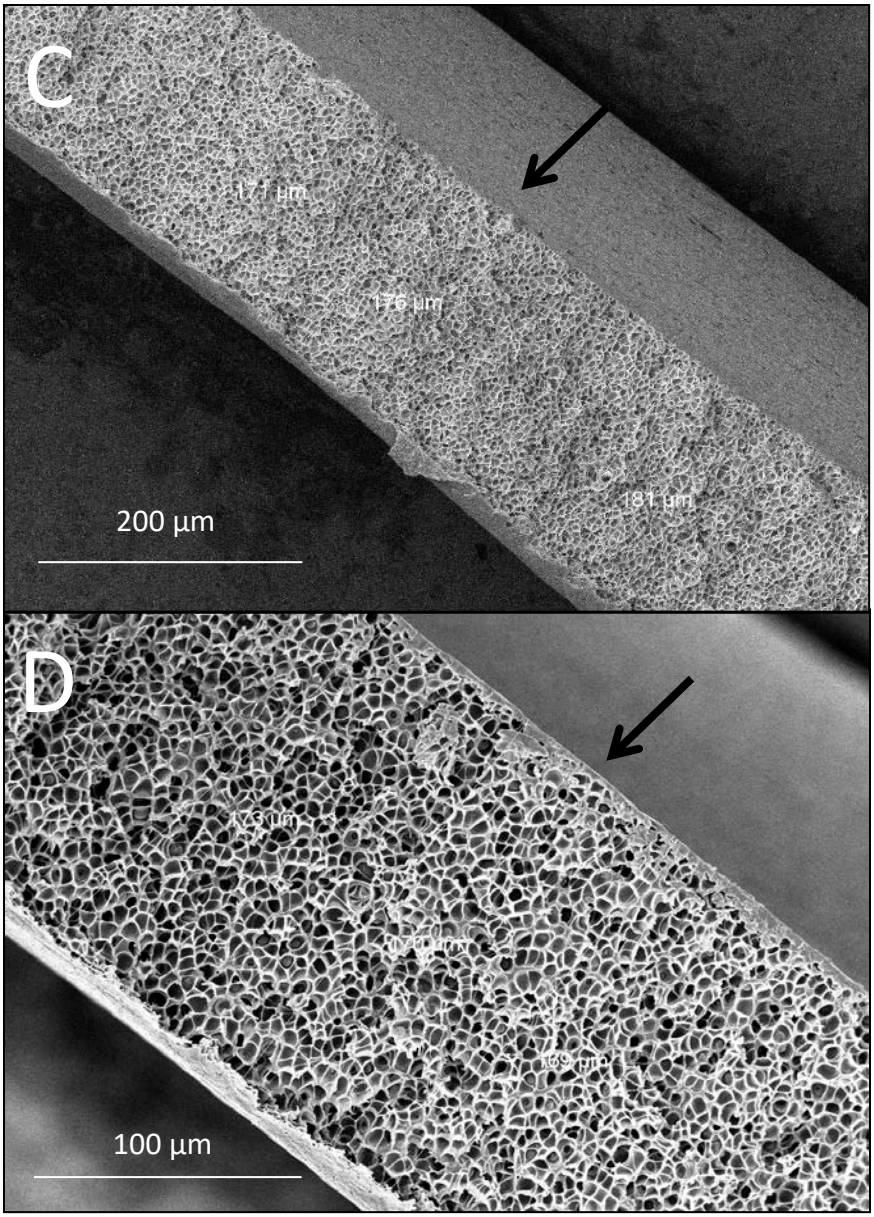

Figure 3.9c-d: Comparison of SEM micrographs of 30 wt.% PES thin films cast from (C) DMAc and (D) NMP using 70 wt.% solvent in water as the coagulation medium. Arrow indicates surface that was exposed to coagulation bath.

3.2.2.4 Effect of MWCNT Loading on PES Membrane Morphology

Experiments were conducted to examine the effects of incorporating multiple carbon-based filler materials into the polymeric membrane matrix. Previous studies by Ismail [34] and Zeinali [35] indicated that modest enhancements in O_2/N_2 selectivity could be achieved upon the incorporation of low levels of well-dispersed carbon nanotubes within flat-sheet PES membranes. In the current work, the impact of MWCNT incorporation on the morphology and transport properties of PES flat sheet membranes was assessed both for as-cast membranes and membranes subject to post-processing via coating with PDMS. In addition to evaluating the efficacy of nanotube inclusion for improving the performance of the flat sheet membranes, the extension of this approach to hollow fiber membranes is reported here for the first time, as discussed in Chapter 4.

Flat sheet membranes were cast from dopes of 30 wt.% PES in NMP, with a nominal dispersion of 0.05 to 0.5 wt.% MWCNT, relative to the polymer, using the MWCNT dope preparation and flat sheet membrane casting procedures described in Sections 2.3.1.1.2 and 2.3.1.2, respectively. Transmitted light optical microscope images of a series of PES-MWCNT casting dope samples are shown in Figure 3.10. An interesting contrast was observed in the MWCNT dispersion as the filler loading was increased. Up until a moderate loading (i.e. 0.1 wt.%), the MWCNTs appeared to be well dispersed within the polymer dope, while at 0.5 wt.% loading, the MWCNTs showed evidence of segregation into MWCNT-rich and MWCNT-lean regions. The MWCNT-rich regions appeared to be comprised of loosely-associated, segregated regions of MWCNTs. This

segregation was distinct from the formation of tightly-associated macro-scale MWCNT agglomerates, which would generally be removed during the centrifugation process.

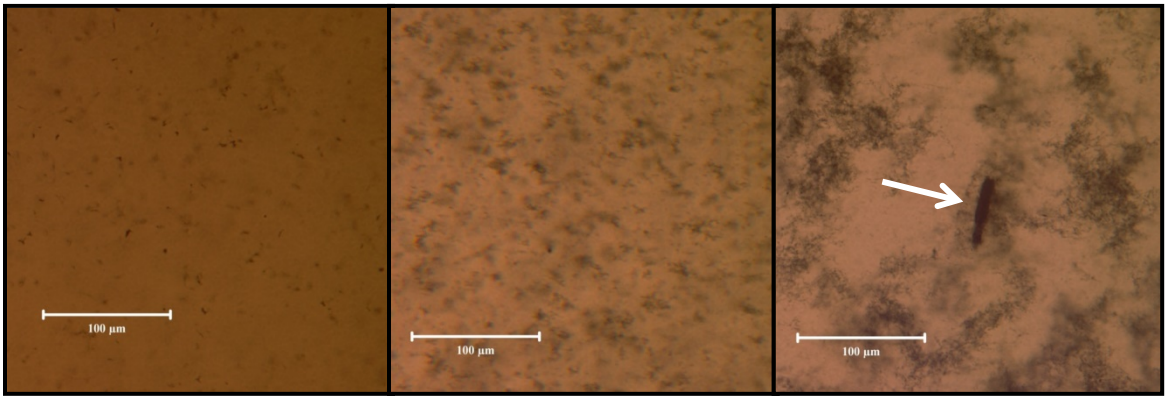

Figure 3.10: Optical microscope images of 30 wt.% PES in NMP dopes with (A) 0.05, (B) 0.1, and (C) 0.5 wt.% MWCNT dispersions (Arrow indicates MWCNT agglomerate that was not removed during centrifugation). Nominal magnification is 50x.

Membranes were cast from dopes containing 0.1 wt.% MWCNT relative to the polymer with coagulation baths of deionized water and 70 wt.% NMP/water. Figure 3.11 shows a comparison of the neat PES membrane and the PES-MWCNT flat sheet membrane (0.1 wt% MWCNT) that were phase-inverted in pure water. SEM micrographs of both samples showed a dense separating layer with large, finger-like macrovoids extending approximately halfway across the thickness of the membrane. Below the macrovoids, each membrane showed the desired sponge-like morphology for the porous support structure. The addition of the well-dispersed MWCNTs appeared to have a moderate impact on the characteristics of the porous substructure, which included longer, more slender finger-like macrovoids when quenched in deionized water. This change in the morphology is most likely due to an increase in the solution

viscosity slowing down the phase inversion dynamics, leading to longer macrovoid formation.

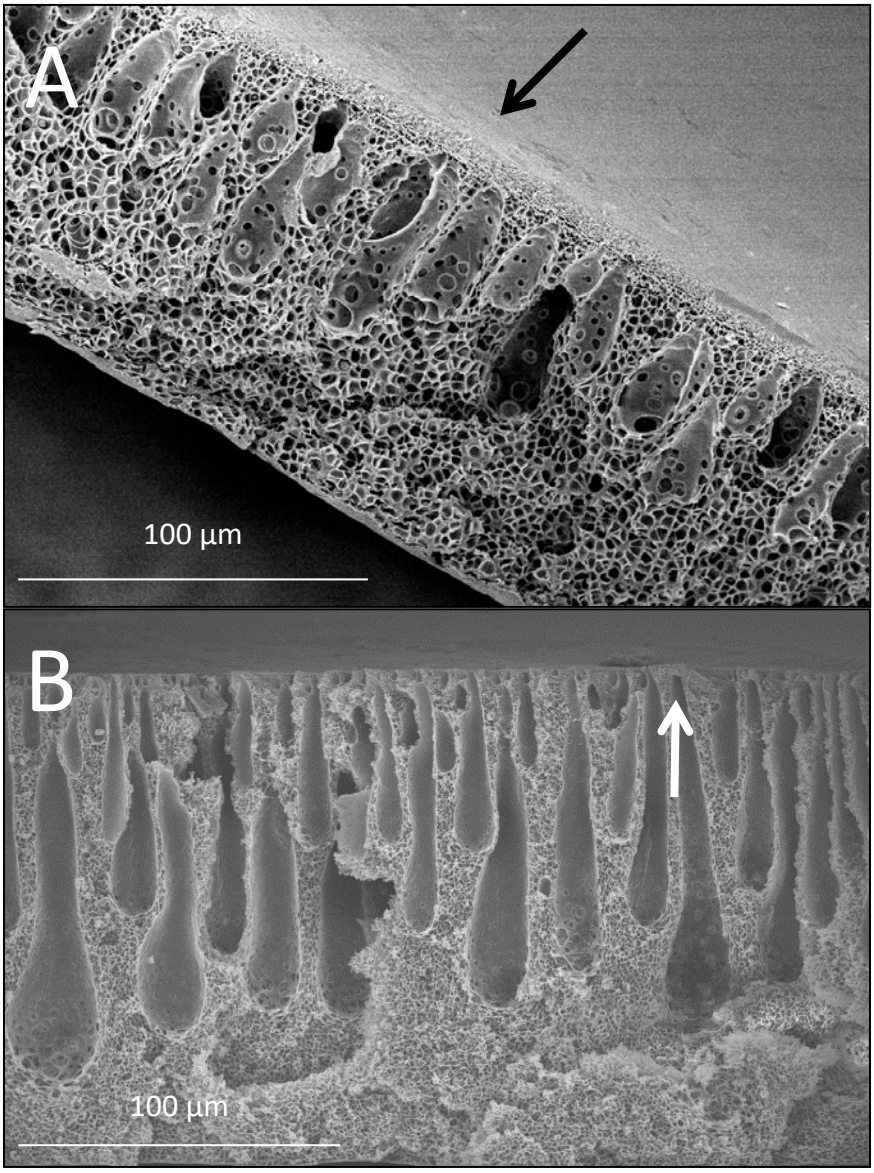

Figure 3.11: Comparison of SEM micrographs of (A) unfilled PES flat sheet membrane and (B) PES flat sheet membrane loaded with 0.1 wt.% MWCNT. Dopes contain 30 wt.% PES in NMP and deionized water was used as the coagulation medium. Arrow indicates exposure face.

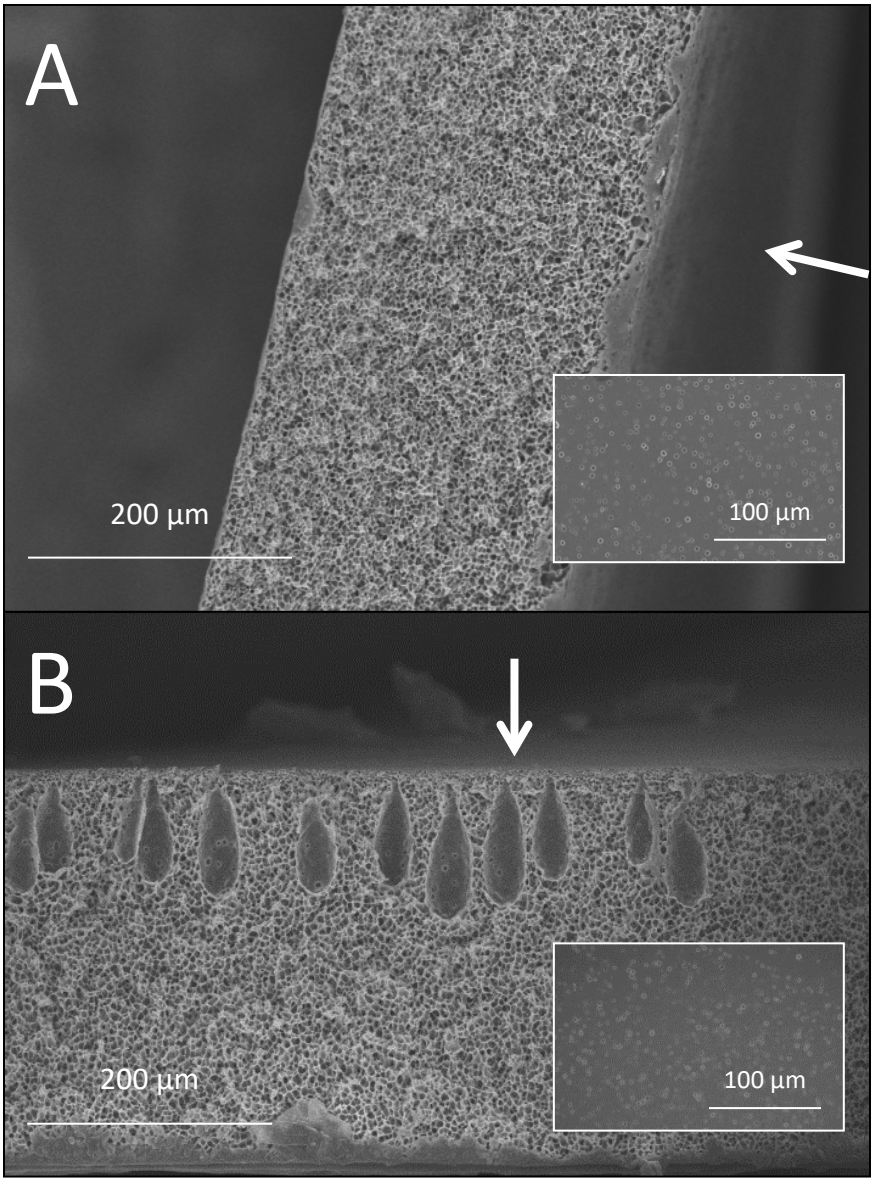

Figure 3.12: Comparison of SEM micrographs of (A) unfilled 30 wt.% PES-NMP flat sheet membrane and (B) 30 wt.% PES-NMP flat sheet membrane loaded with 0.1 wt.% MWCNT. 70 wt.% NMP/water was used as the coagulation medium. Arrow indicates exposure face. Inset: Membrane surface that was exposed to coagulation bath.

A small difference in morphology was also observed in the membranes that were cast in a coagulation bath of 70 wt.% NMP/water, as shown in Figure 3.12. For the unfilled PES membrane, this coagulation bath concentration resulted in a morphology that was entirely composed of sponge-like porous support structure, whereas in the PES-MWCNT membrane, small tear-drop shaped macrovoids persisted just below the exposed top layer. When looking at the top surface of the membrane, however, large pores, stemming from the break-through of the porous substructure, were still evident in the SEM micrographs, consistent with a phase inversion process dominated by delayed demixing (also observed in Figure 3.4d). Detection of the MWCNTs in an asymmetric membrane cross section using SEM was difficult at such low loadings, but they were observed in SEM images of PES dense films (Figure 3.13). Figure 3.13 also shows the macroscopic color change that provides additional evidence that the MWCNTs were fully incorporated in the final membrane coupons.

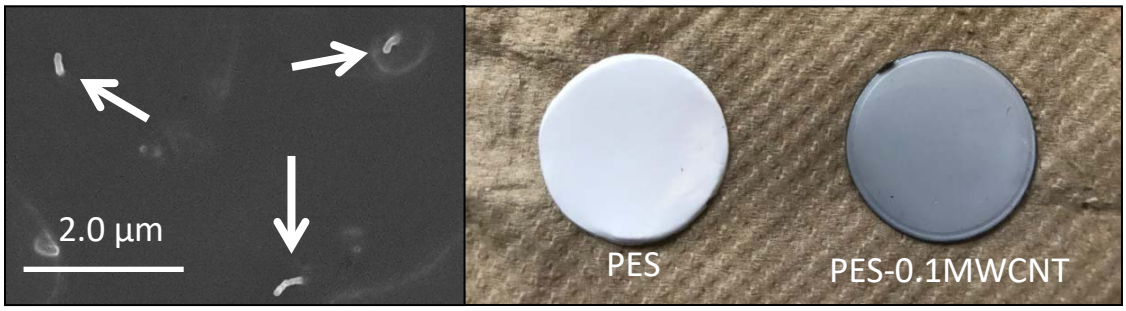

Figure 3.13: (Left) SEM image of PES-0.1MWCNT dense film cross-section. Arrows indicate MWCNTs. (Right) photograph of PES and PES-0.1MWCNT membrane coupons, showing macroscopic color change that accompanies MWCNT dispersion.

3.2.3 Gas Permeance and Selectivity for Flat Sheet Membranes

3.2.3.1 Permeance and Selectivity of PES and PSf Membranes

The gas permeance and selectivity of the flat sheet membrane coupons were measured using the procedure described in Section 2.4.2. The casting parameters for the flat sheet membranes that were tested for gas permeation properties were chosen based on the experimental results that were presented in Section 3.2.2. These parameters, which are summarized in Table 3.1, were specifically selected with consideration of future objectives related to the preparation of analogous hollow fiber membranes.

Table 3.1: Membrane casting parameters and test conditions for single gas permeance studies.

Process Parameters:	**Value:**
Polymer	PES, PSf
Solvent	NMP
Filler Materials	MWCNT, Carbon Black
Polymer Concentration (wt.%)	30 (PES), 35 (PSf)
Coagulation Bath	Deionized water
Casting Blade Height	250 μm
PDMS Caulk (where applicable)	3 wt.% PDMS in hexanes
Membrane Coupon Diameter (cm)	2.54
Pressure Differential (ΔP, psi)	29
Membrane Conditioning Period (hr)	2.0

The permeance of N_2 and O_2, as well as the O_2/N_2 pure-gas selectivity, are summarized for unfilled PES and PSf membranes in Table 3.2. While there were a total of three gas pairs that were examined in this work, the primary focus of these experiments was O_2/N_2 selectivity, due to the fact that air separation is the most industrially relevant process for the application of PES and PSf membranes in this context. As reported in the table, both PES and PSf as-cast membranes showed O_2/N_2 selectivities on the order of 0.90, which is characteristic of Knudsen diffusion for this gas pair[4]. Since Knudsen selectivity was observed in these membranes, it was concluded that the dense separating layer contained microscopic pinhole defects, and further post-treatments would be required to achieve the characteristic (i.e., dense film) selectivity inherent to the membrane polymers [13]. In fact, the presence of pinhole surface defects in polymer membranes, typically too small to clearly image with SEM, is a very common issue for the preparation of gas separation membranes, and is most often addressed by PDMS caulking. As discussed in Section 1.1.2.3, PDMS caulking is a method used to mitigate the negative effects of pinhole defects. By coating the membrane with the high permeability, low selectivity PDMS polymer, the properties of the bulk membrane are minimally affected, but the diffusion mechanism in the pinhole defects is changed from Knudsen diffusion to solution diffusion through PDMS, which largely eliminates the high gas flux and minimal selectivity inherent to the pinhole defects.

Table 3.2: Permeance and ideal selectivity of N_2 and O_2 for unfilled PES and PSf membranes in the as-cast and PDMS-caulked states.

Material	P/l (N_2) (GPU)	P/l (O_2) (GPU)	α(O_2/N_2)
PES-Flat Sheet	23.4 ± 0.5	20.8 ± 0.7	0.89 ± 0.05
PSf-Flat Sheet	31.9 ± 0.01	29.9 ± 0.5	0.94 ± 0.04
PES-PDMS-Flat Sheet	0.07 ± 0.01	0.41 ± 0.03	5.51 ± 0.03
PSf-PDMS-Flat Sheet	0.16 ± 0.02	0.82 ± 0.07	5.12 ± 0.03

Table 3.2 reports the N_2 and O_2 permeance as well as the O_2/N_2 selectivity of the unfilled PES and PSf membranes that were caulked with PDMS. The PDMS caulking was performed by soaking the membrane coupon for 30 minutes in a solution of 3 wt.% PDMS in hexanes. It is relevant to note at this point that relatively little effort was directed towards minimizing or otherwise optimizing the thickness of the PDMS coating that was applied to the membranes. Both membranes showed a large decrease in the permeance of O_2, along with a proportionally larger decrease in N_2 permeance with PDMS coating. The difference in the magnitude of the permeance reduction for the two gases resulted in an increase in the O_2/N_2 pure-gas selectivity for both the PES and PSf membranes. The O_2/N_2 ideal selectivity of PES increased from 0.89 to 5.5, and the O_2/N_2 ideal selectivity of PSf increased from 0.94 to 5.1. The previously reported literature values for the dense film O_2/N_2 ideal selectivity for PES and PSf are 5.6 and 5.2, respectively [13]. The observed increase in the selectivity of the membranes from Knudsen levels to the reference values reported for PES and PSf is consistent with the presence of pinhole defects in the membranes that were successfully caulked via the application of PDMS to the membrane surface.

3.2.3.2 Effect of MWCNT Loading on PES Membrane Permselectivity

In order to investigate the effect of MWCNT content on the permeance and selectivity of PES-MWCNT mixed matrix membranes, membranes were fabricated with nominal MWCNT loadings ranging from 0.05 to 0.5 wt.% relative to the polymer, with NMP as the solvent and deionized water as the coagulation medium (no solvent added) – see Table 3.1. The actual (retained) filler concentration was determined using the method described in Section 2.3.1.1.2.

Figure 3.14a shows plots of N_2, O_2, He and CO_2 permeance as related to MWCNT loading (expressed as wt.% relative to polymer) for as-cast membrane samples. At very low loading, nominally 0.05 wt.% MWCNT, the presence of the nanotubes appeared to have very little effect on the permeance of the membrane and Knudsen selectivity was observed. However, at a nominal loading of 0.1 wt.% MWCNT, O_2, He, and CO_2 permeance decreased by an order of magnitude, while the permeance of N_2 decreased by two orders of magnitude. This was a striking and unexpected observation, which resulted in an increase in ideal selectivity for all gas pairs relative to N_2, with O_2/N_2 peaking at an ideal selectivity very close to the inherent selectivity of unfilled PES, as shown in Figure 3.14b. This result suggested a change in the diffusion mechanism from Knudsen diffusion to solution diffusion transport. It is particularly noteworthy that this effect was observed prior to the use of any post-treatment, such as PDMS caulking.

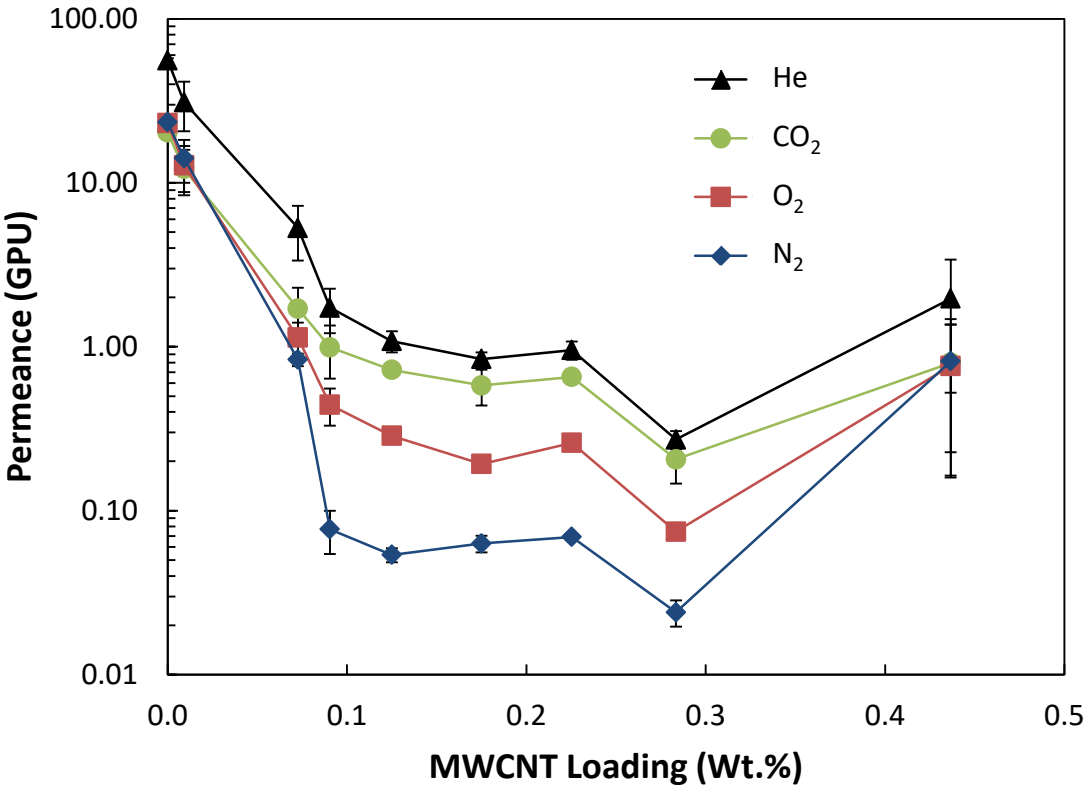

Figure 3.14a: Average He, CO_2, O_2, and N_2 permeance (GPU) of PES-MWCNT mixed matrix membranes, plotted against MWCNT loading. Each data point was measured in triplicate and error bars represent standard deviation of the three measurements.

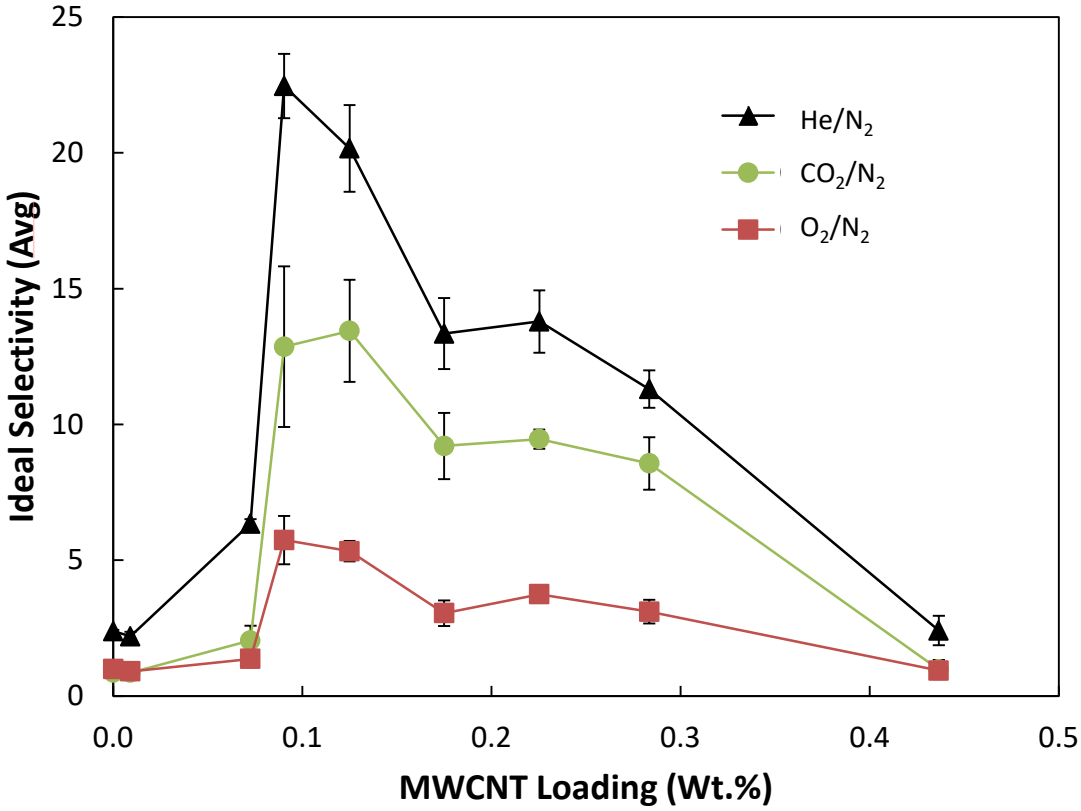

Figure 3.14b: Average He/N_2, CO_2/N_2, and O_2/N_2 ideal selectivity of PES-MWCNT mixed matrix membranes, plotted against MWCNT loading. Each data point was measured in triplicate and error bars represent standard deviation of the three measurements.

As the weight fraction of MWCNTs in the membranes was increased beyond 0.1 wt.%, the permeance of the membrane was maintained at relatively low levels until the loading reached a nominal level of 0.3 wt.%. The observed lower plateau in permeance was accompanied by a decrease in selectivity, which still remained well above the levels encountered with Knudsen diffusion. When the nominal weight fraction of MWCNTs reached 0.5 wt.% relative to the polymer, the permeance increased and the selectivity of the membrane was reduced back to Knudsen levels (re: Figure 3.14).

The large decrease in the observed permeance of the as-cast membranes and their enhanced pure gas selectivity with low levels of MWCNT incorporation was consistent with the outcomes achieved via PDMS caulking of the unfilled membranes, suggesting that the MWCNTs were in some way acting to suppress the formation of pinhole defects and thereby shifting the transport from Knudsen diffusion to a solution-diffusion mechanism. In order to further explore this phenomenon, the porosity of the membranes was analyzed using a Porous Materials Inc. automated liquid-liquid porometer. The results of this test showed that for neat PES membranes with no PDMS caulking, surface pores in the range of 1.1 to 2.7 nm were detected, providing confirmation that the observed high gas permeance as well as the Knudsen selectivity was due to the presence of pinhole defects in the dense separating layer of the membrane. For the PES-0.1 wt.% MWCNT membrane, the analyzer detected no surface porosity. Since this latter result was achieved without using any PDMS caulking, it indicated that the MWCNTs were somehow suppressing either the formation of pinhole defects or were fully obstructing flow in the pinhole defects, resulting in a large

decrease in the permeance and driving the transport to a solution-diffusion mechanism with gas pair selectivity reflecting the inherent separation properties of the polymer. The optical microscope images (Figure 3.10) of the PES-MWCNT casting dopes also provided some insight as to the observed trends in permeance and gas-pair selectivity as influenced by MWCNT loading. The images showed that when the loading was very low (i.e. 0.05 wt.%), the MWCNTs were well dispersed within the polymer solution. At a MWCNT loading of 0.1 wt.% relative to the polymer, the MWCNTs were still relatively evenly dispersed, but there was much less space between them, suggesting the potential formation of a physical network of polymer chains entangled with the MWCNTs upon phase inversion; this entanglement may play an important role in suppressing the formation of pinhole surface defects during the final stages of membrane solidification. As the MWCNT loading increased beyond this apparently optimum level, the nanotube filler began to loosely aggregate. This uneven dispersion likely resulted in local MWCNT-rich and MWCNT-lean areas in the incipient membrane, possibly leading to a reduction in the cohesion of the MWCNT-polymer entangled network. For regions that were relatively depleted in MWCNTs, the formation of pinhole defects (as in the neat polymer) may be more probable, eventually resulting in transport characteristics consistent with the (non-selective) Knudsen mechanism at higher MWCNT loadings. Table 3.3 reports the gas transport properties for both the PES and PSf filled membranes with a nominal loading of 0.1 wt.% MWCNT. The effect of adding the MWCNTs to the membrane formulation was almost identical to that of caulking the surface of the unfilled membranes with PDMS (re: Table 3.2); each

membrane pair (caulked PES vs. filled PES; caulked PSf vs. filled PSf) showed remarkable similarity in terms of both overall gas permeance and resulting O_2/N_2 selectivity. These results strongly support the hypothesis that the inclusion of relatively low levels of MWCNTs prevents the formation of pinhole surface defects during the casting of these membranes. In addition, the data presented in the tables indicate that this approach can be generalized to different membrane polymers, since both PES and PSf showed very similar results. As with the unfilled membranes, PSf showed higher permeance in both the caulked state as well as the mixed matrix state, but also displayed lower O_2/N_2 selectivity in both, as compared to PES. This was consistent with the literature, as it is well documented that PSf tends to have a higher permeance and lower ideal selectivity for most gas pairs due to the higher fractional free volume inherent to the polymer[13]. In sum, this is the first report clearly indicating the role of MWCNTs in suppressing pinhole defect formation during the phase inversion casting of asymmetric gas separation membranes.

Table 3.3: Summary of the permeance of N_2 and O_2 as well as the O_2/N_2 ideal selectivity for selected mixed matrix flat sheet membranes.

Material	P/l (N_2) (GPU)	P/l (O_2) (GPU)	$\alpha(O_2/N_2)$
PES-0.1 wt.% MWCNT-FS*	0.08 ± 0.03	0.44 ± 0.11	5.73 ± 0.89
PSf-0.1 wt.% MWCNT-FS†	0.21 ± 0.07	1.04 ± 0.13	4.89 ± 0.74
PES-0.1 wt.% MWCNT-PDMS-FS*	0.03 ± 0.01	0.20 ± 0.06	7.11 ± 0.28
PSf-0.1 wt.% MWCNT-PDMS-FS†	0.07 ± 0.03	0.39 ± 0.11	5.58 ± 0.20
PES-0.1Carbon Black-FS‡	0.66 ± 0.12	0.52 ± 0.07	0.80 ± 0.02
PES-PDMS-0.1 wt.% Carbon Black‡	0.02 ± 0.01	0.09 ± 0.03	4.5 ± 0.21

***Actual composition is 0.091 wt.%**
†Actual composition is 0.089 wt.%
‡Actual composition is 0.091 wt.%

3.2.3.3 Effect of Carbon Black Loading on PES Membrane Permselectivity

Further experiments were conducted to understand the mechanism by which the MWCNTs affected the permselectivity of the membrane; the approach was to replace MWCNTs with carbon black (average particle size = 42 nm) as the filler material. These membranes were prepared using the same casting conditions as were employed for PES-MWCNT flat sheet membranes, per Table 3.1. The compositions of the membranes examined in this section were derived from 30 wt.% PES in NMP, with dispersions of 0.075, 0.1, 0.2, 0.3, and 0.5 wt.% carbon black relative to the polymer.

Plots of the permeance and selectivity for the PES-carbon black mixed matrix membranes are presented in Figure 3.15. As shown, the addition of ~ 0.1 wt.% carbon black into the PES matrix led to a marked decrease in the permeance of all four gases tested by nearly two orders of magnitude. At higher loadings, very little additional reduction in permeance was evident. Across the entire range of carbon black

compositions, the pure gas selectivity was characteristic of Knudsen diffusion, presumably through pinhole surface defects.

It is proposed that the presence of MWCNTs prevented the creation of pinhole defects during polymer phase inversion by entangling with the polymer chains and forming a physical network that suppressed the formation of openings on the membrane surface during polymer solidification from solution. This hypothesis was further supported by the carbon black results, where this effect was largely absent. Owing to their lower aspect ratio, the carbon black particles are less likely to effectively entangle with the polymer chains during phase inversion, thus limiting the ability of the filler to physically inhibit the opening of pinhole gaps on the membrane surface as the polymer solidifies. Rather, the data suggest that the large decrease in the gas permeance of these membranes is due to the carbon black particles physically obstructing at least some fraction of the pinhole defects. Since the particles do not fully block all of the pinholes, Knudsen diffusion is still the predominant diffusion mechanism in the membrane, such that no improvement in ideal selectivity was observed as compared to an unfilled membrane.

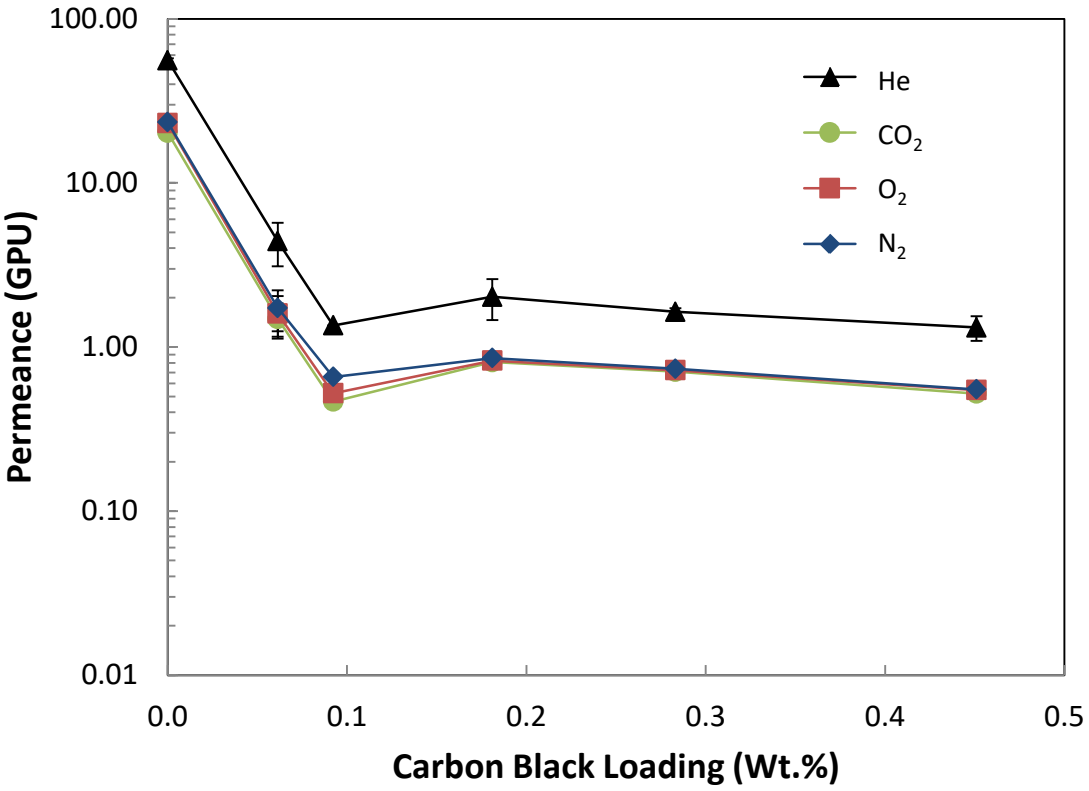

Figure 3.15a: Average He, CO_2, O_2, and N_2 permeance (GPU) of PES-carbon black mixed matrix membranes, plotted against carbon black loading. Each data point was measured in triplicate and error bars represent standard deviation of the three measurements.

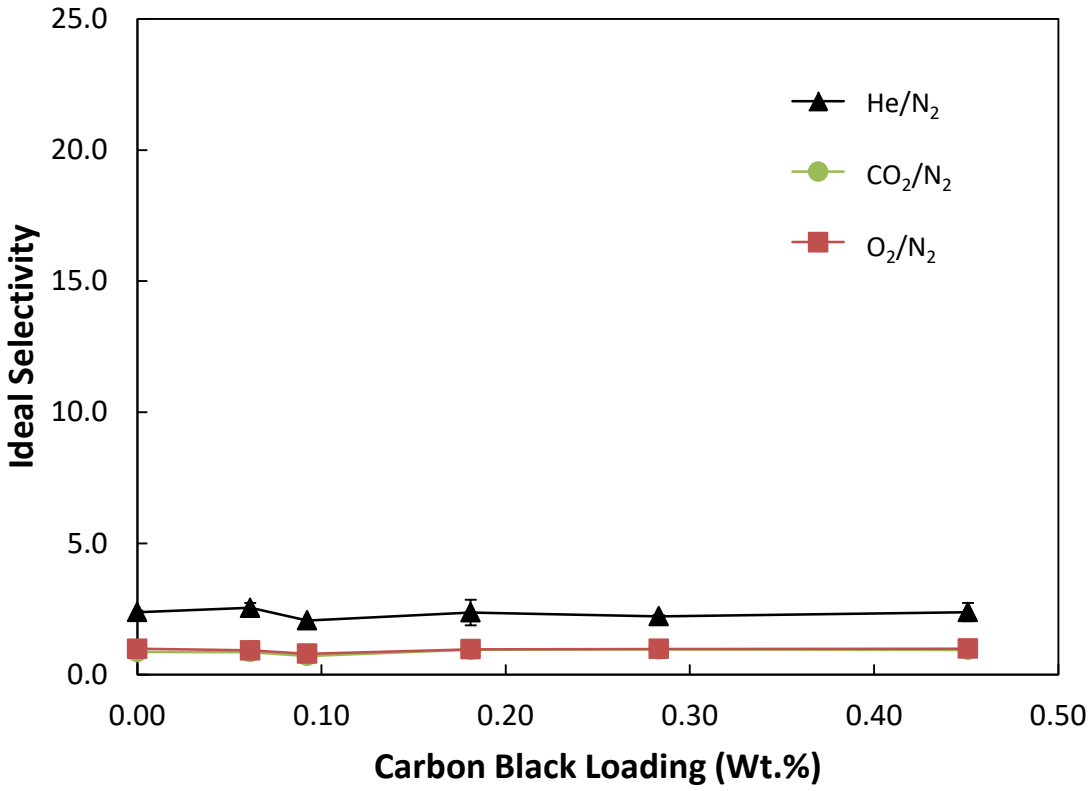

Figure 3.15b: Average He/N_2, CO_2/N_2, and O_2/N_2 ideal selectivity of PES-carbon black mixed matrix membranes, plotted against carbon black loading. Each data point was measured in triplicate and error bars represent standard deviation of three points.

3.2.3.4 Effect of MWCNT Loading on PES-PDMS Membrane Permselectivity

In addition to observing the effects of adding MWCNT and carbon black filler material to the as-cast PES membranes, the permeance and selectivity of the filled membranes were measured after the application of PDMS. Figure 3.16a shows the permeance of the four gases tested as they relate to MWCNT loading for membranes that were subsequently subjected to PDMS caulking. For all membrane compositions, the permeance and selectivity values were consistent with gas transport via solution-diffusion, as discussed above, with the PDMS coating eliminating potential Knudsen diffusion through pinhole surface defects. In addition, across the range of relatively low filler loadings investigated, increasing MWCNT content had little influence on the permeance of the caulked membranes. Plots of ideal selectivity vs. MWCNT loading for the PDMS-coated PES membranes are shown in Figure 3.16b. PDMS caulking increased the selectivity of the neat PES membrane from a level that was characteristic of Knudsen diffusion to a level that was consistent with solution-diffusion transport. A local maximum in ideal selectivity was evident at a nominal loading of 0.1 wt.% MWCNT, but was much less pronounced as compared to the uncaulked membrane series. Across this range of filler loading, it appeared that the primary benefit of PDMS coating was to repair any residual pinholes that may have been present on the surface of the MWCNT-filled membranes. The fact that there was a small further improvement in selectivity with the application of the PDMS surface layer could reflect the influence of an additional separation mechanism attributable to the presence of the MWCNTs, such as molecular sieving. Previous work performed by Ismail et al. on PES-MWCNT membranes

with PDMS caulking showed an increase in O_2/N_2 ideal selectivity from 5.52 to 10.65 at a loading of 0.5 wt.% when the nanotube dispersion was improved through chemical functionalization of the nanotubes. In their work, molecular sieving through the MWCNT interlayer spacing was cited as the primary mechanism for the observed improvement in ideal selectivity [34].

Parallel experiments were conducted for PSf membranes loaded with 0.1 wt.% MWCNT and subject to PDMS coating. The results for these membranes, as well as comparable PES specimens, are summarized in Table 3.3. For both polymers, the coated mixed-matrix membranes showed a slight decrease in permeance (owing to the added transport resistance of the PDMS toplayer), as well as an increase in the ideal selectivity of the membrane. As was the case in all of the previous experiments, PSf membranes showed a higher permeance as well as a lower ideal O_2/N_2 selectivity as compared to PES, owing to either the larger fractional free volume inherent to the PSf polymer or possibly a thinner dense separating layer in these membranes.

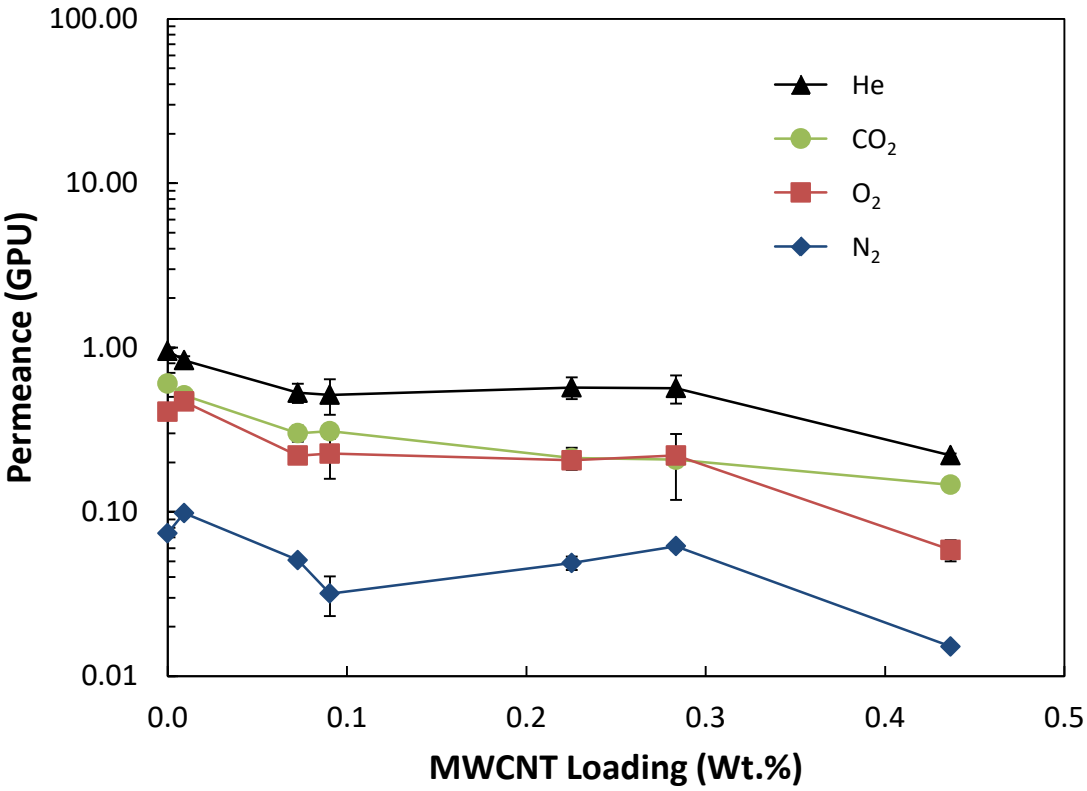

Figure 3.16a: Average He, CO_2, O_2, and N_2 permeance (GPU) of PDMS-caulked PES-MWCNT mixed matrix membranes, plotted against MWCNT loading. Each data point was measured in triplicate and error bars represent standard deviation of the three measurements.

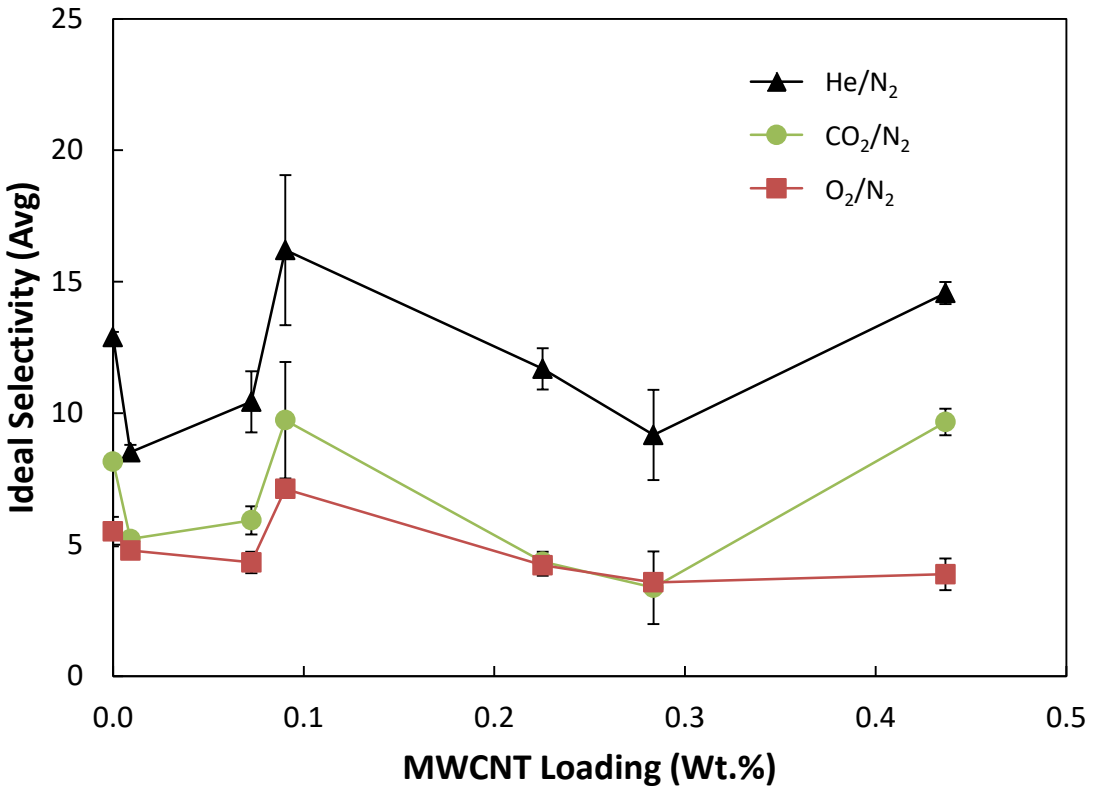

Figure 3.16b: Average He/N_2, CO_2/N_2, and O_2/N_2 ideal selectivity of PDMS-caulked PES-MWCNT mixed matrix membranes, plotted against MWCNT loading. Each data point was measured in triplicate and error bars represent standard deviation of the three measurements.

3.2.3.5 Effect of Carbon Black Loading on PES-PDMS Membrane Permselectivity

The effect of PDMS caulking on PES membranes loaded with carbon black particles was also examined. Plots of the permeance and selectivity as a function of carbon black loading are shown in Figure 3.17. As can be seen in Figure 3.17a, when PDMS caulking was applied after membrane casting, only a modest additional reduction in permeance was observed with increasing carbon black loading. This is consistent with the carbon black particles acting to substantially obstruct the surface defects; the subsequent PDMS coating, while producing only a small additional reduction in permeance with the sealing of surface gaps, effectively shifts the permeation mechanism to solution-diffusion transport for all membrane compositions. Examination of Figure 3.17b shows selectivity values largely independent of carbon black loading, and consistent with as-cast, caulked PES membranes; see also Table 3.3.

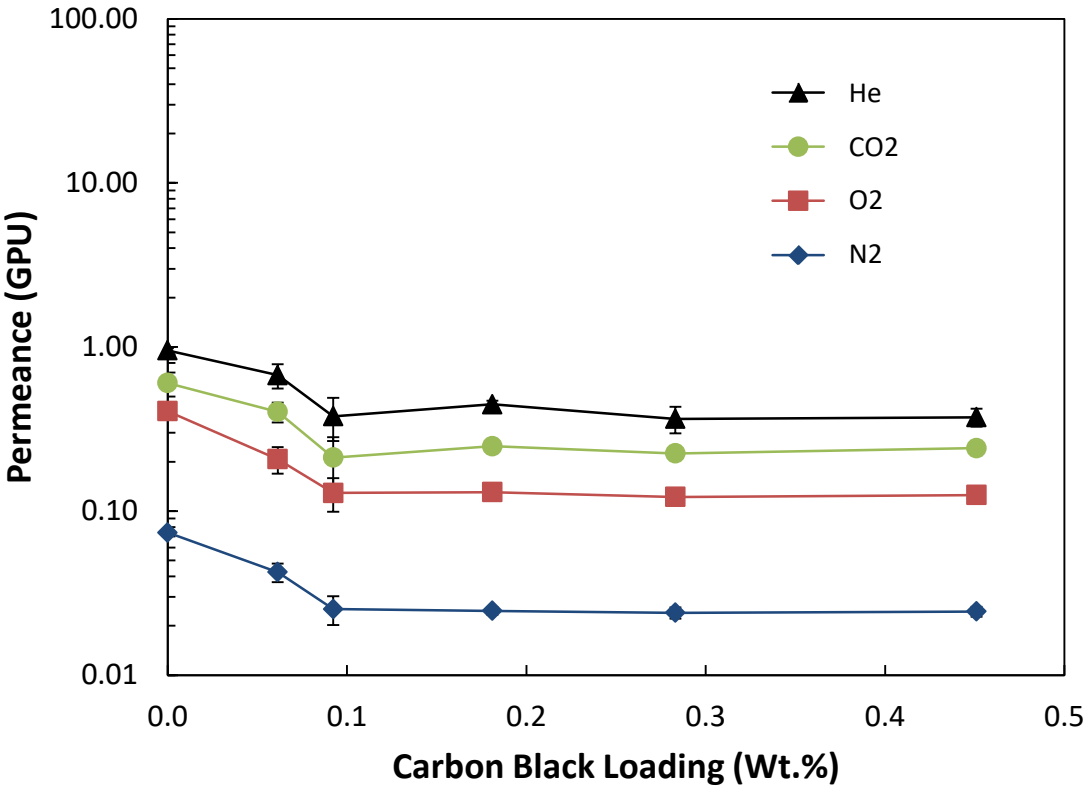

Figure 3.17a: Average He, CO_2, O_2, and N_2 permeance (GPU) of PDMS-caulked PES-carbon black mixed matrix membranes, plotted against carbon black loading. Each data point was measured in triplicate and error bars represent standard deviation of three points.

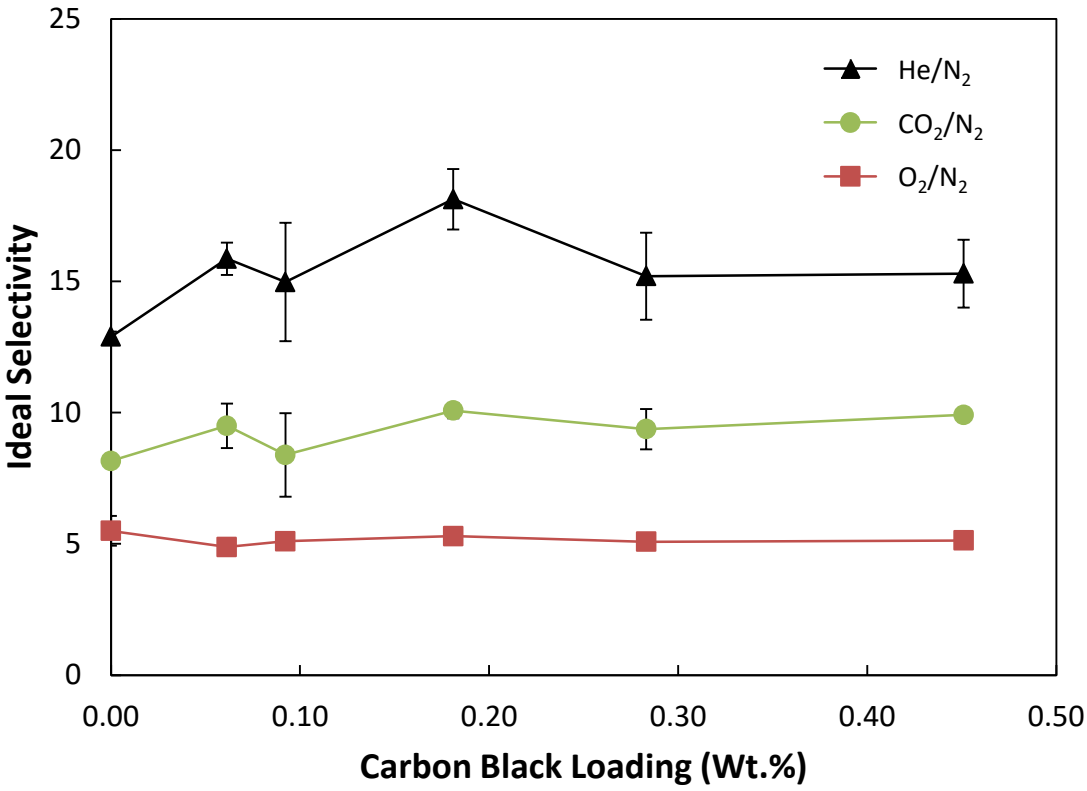

Figure 3.17b: Average He/N_2, CO_2/N_2, and O_2/N_2 ideal selectivity of PDMS-caulked PES-carbon black mixed matrix membranes, plotted against carbon black loading. Each data point was measured in triplicate and error bars represent standard deviation of three points.

3.3 Conclusions

In this chapter, multiple aspects of the preparation of polyethersulfone (PES) flat sheet phase inversion membranes were studied in order to establish appropriate conditions for flat sheet casting and (later) hollow fiber spinning of PES and PSf asymmetric membranes. Based on the solution viscosity and morphology of membranes that were cast from various dope compositions, it was determined to employ a dope solution of 30 wt.% PES in NMP for the preparation of gas separation membranes. This provided a dope viscosity low enough to avoid unsustainably high filtering pressures anticipated during hollow fiber spinning, while maintaining PES content sufficient to produce a suitable membrane morphology when cast as an asymmetric thin film. Experiments using various coagulation bath compositions were conducted to determine the effect of coagulation conditions on membrane morphology, and to guide the selection of the coagulation bath and bore fluid compositions for hollow fiber membrane spinning. Based on the morphologies of the flat sheet membranes that were produced, it was determined that the bore fluid should be composed of 70 wt.% NMP in water for PES hollow fiber membrane spinning and 75 wt.% NMP in water for PSf hollow fiber membrane spinning. When phase inversion was accomplished under these coagulation conditions, the membranes showed no macrovoid formation, and both the top and bottom surfaces of the membrane were porous, which is the ideal morphology for the inner wall of a hollow fiber membrane.

Multiwall carbon nanotubes and carbon black particles were dispersed in the polymer casting dopes in order to assess the influence of relatively low levels of these

fillers on the morphology and gas transport properties of the resulting asymmetric mixed-matrix membranes. At loadings up to 0.5 wt.% filler, the presence of the filler had minimal discernable impact on the membrane morphologies obtained under the various membrane casting conditions. Consideration of the gas separation performance indicated that the addition of pristine MWCNTs had a marked impact at a loading of approximately 0.1 wt.% relative to the polymer. At this loading, the as-cast PES-MWCNT mixed matrix membrane exhibited a large reduction in permeance and an increase in selectivity to a level comparable to that of unfilled PES membranes coated with polydimethylsiloxane (PDMS). The results the MWCNTs functioned to suppress the formation of microscopic pinhole defects on the surface of the polymer membrane. This is the first report clearly indicating the role of MWCNTs in eliminating pinhole defect formation during the phase inversion casting of asymmetric gas separation membranes. It was hypothesized that the observed improvement in the ideal selectivity of the mixed matrix membranes was the result of polymer chains entangling with the high aspect ratio MWCNTs during membrane formation, creating a physical network of polymer-MWCNT interphase which prevented the emergence of pinhole defects. As the loading of the MWCNTs was further increased, segregation of the tubes into MWCNT-rich and MWCNT-lean regions correlated with a progressive decrease in membrane selectivity. The MWCNT-lean regions were likely more susceptible to pinhole defect formation, as observed for the neat membranes. This corresponded to a strong increase in the permeance of the membranes and a return to selectivity levels consistent with Knudsen diffusion when the MWCNT loading was approximately 0.5 wt.% relative to the polymer.

The observed suppression of pinhole defect formation with the introduction of very low levels of MWCNTs in the membrane casting dope offers a range of potential technological benefits, including the possible elimination of a separate PDMS coating step as required to repair the membrane surface for acceptable gas separation performance. This could be especially important in the context of industrial processing requiring caulking of each gas separation module separately. In an effort to assess the generality of this outcome, similar membranes were prepared with low levels of carbon black particles as the filler. In the case of the carbon-black filled membranes, a decrease in permeance was encountered that suggested the partial blocking of pinhole surface defects with the presence of the particles, but the poor selectivity inherent to Knudsen diffusion persisted at all loading levels. It was conclusively shown that that the incorporation of MWCNTs suppressed the formation of pinhole defects and it was further hypothesized that filler (i.e. nanotube) aspect ratio was a key factor in establishing entanglement of the filler elements with the polymer chains during membrane coagulation. This entanglement may reinforce the emerging membrane top layer thereby suppressing pinhole formation.

3.4 References

1. Loeb, S., Sourirajan, S., *Sea water demineralization bymeans of a semipermeable membrane.* Advances in Chemistry, 1962. **38**: p. 117-132.
2. Kurdi, J., Tremblay, A. Y., *Preparation of defect-free asymmetric membranes for gas separations.* Journal of Applied Polymer Science, 1999. **73**(8): p. 1471-1482.
3. Kulprathipanja, S., Neuzil, R.W., Norman, N. L., *Separation of fluids by means of mixed matrix membranes*. 1989, Honeywell International Inc: USA, US5127925A.
4. Koros, W.J., Fleming, G. K., *Membrane-based gas separation.* Journal of Membrane Science, 1993. **83**(1): p. 1-80.
5. Khulbe, K.C., Feng, C., Matsuura, T., *The Art of Surface Modification of Synthetic Polymeric Membranes.* Journal of Applied Polymer Science, 2010. **115**(2): p. 855-895.
6. Kesting, R.E., *Synthetic Polymeric Membranes: A Structural Perspective*. Second ed. Vol. 1. 1985: John Wiley & Sons, Inc. 348.
7. Peng, N., Widjojo, N., Sukitpaneenit, P., Teoh, M. M., Lipscomb, G. G., Chung, T. S., Lai, J. Y., *Evolution of polymeric hollow fibers as sustainable technologies: Past, present, and future.* Progress in Polymer Science, 2012. **37**(10): p. 1401-1424.
8. Madaeni, S.S., Hoseini, S., *Fabrication and characterization of PDMS coated PES membranes for separation of ethylene from nitrogen.* Journal of Polymer Research, 2009. **16**(5): p. 591-599.
9. Sadrzadeh, M., Amirilargani, M., Shahidi, K., Mohammadi, T., *Gas permeation through a synthesized composite PDMS/PES membrane.* Journal of Membrane Science, 2009. **342**(1-2): p. 236-250.
10. Wang, D.L., Li, K., Teo, W. K., *Gas permselection properties in silicone-coated asymmetric polyethersulfone membranes.* Journal of Applied Polymer Science, 1997. **66**(5): p. 837-846.
11. Merkel, T.C., Bondar, V. I., Nagai, K., Freeman, B. D., Pinnau, I., *Gas sorption, diffusion, and permeation in poly(dimethylsiloxane).* Journal of Polymer Science Part B-Polymer Physics, 2000. **38**(3): p. 415-434.
12. Henis, J.M.S., Tripodi, M. K., *Composite hollow fiber membranes for gas separation - the resistance model approach.* Journal of Membrane Science, 1981. **8**(3): p. 233-246.
13. Baker, R.W., Beckman, I. N., Cussler, E. L., Doshi, K, Henis, J. M. S., Koros, W. J., Nakagawa, T., Paul, D. R., Petropoulos, J. H., Pinnau, I., Pixton, M. R., Plate, N, Prasad, R., Shaner, R. L., Wijmans, J. G., Yampolskii, Y. P., *Polymeric Gas Separation Membranes*. 1994: CRC Press Inc.
14. Galizia, M., Chi, W. S., Smith, Z. P., Merkel, T. C., Baker, R. W., Freeman, B. D., *50th Anniversary Perspective: Polymers and Mixed Matrix Membranes for Gas and Vapor Separation: A Review and Prospective Opportunities.* Macromolecules, 2017. **50**(20): p. 7809-7843.

15. Kemp, D.R., Paul, D. R., *Gas sorption in polymer membranes containing adsorptive fillers.* Journal of Polymer Science Part B-Polymer Physics, 1974. **12**(3): p. 485-500.
16. Moore, T.T., Koros, W. J., *Gas sorption in polymers, molecular sieves, and mixed matrix membranes.* Journal of Applied Polymer Science, 2007. **104**(6): p. 4053-4059.
17. Mahajan, R., Koros, W. J., *Mixed matrix membrane materials with glassy polymers. Part 2.* Polymer Engineering and Science, 2002. **42**(7): p. 1432-1441.
18. Chung, T.S., Jiang, L. Y., Li, Y., Kulprathipanja, S., *Mixed matrix membranes (MMMs) comprising organic polymers with dispersed inorganic fillers for gas separation.* Progress in Polymer Science, 2007. **32**(4): p. 483-507.
19. Goh, P.S., Ismail, A. F., Sanip, S. M., Ng, B. C., Aziz, M., *Recent advances of inorganic fillers in mixed matrix membrane for gas separation.* Separation and Purification Technology, 2011. **81**(3): p. 243-264.
20. Ahn, J., Chung, Wook-Jin, Pinnau, Ingo, Guiver, Michael D., *Poly sulfone/silica nanoparticle mixed-matrix membranes for gas separation.* Journal of Membrane Science, 2008. **314**(1-2): p. 123-133.
21. Husain, S. and W.J. Koros, *Mixed matrix hollow fiber membranes made with modified HSSZ-13 zeolite in polyetherimide polymer matrix for gas separation.* Journal of Membrane Science, 2007. **288**(1-2): p. 195-207.
22. Boroglu, M.S., Gurkaynak, Mehmet Ali, *Fabrication and characterization of silica modified polyimide-zeolite mixed matrix membranes for gas separation properties.* Polymer Bulletin, 2011. **66**(4): p. 463-478.
23. Li, Y., Chung, T. S., Cao, C., Kulprathipanja, S., *The effects of polymer chain rigidification, zeolite pore size and pore blockage on polyethersulfone (PES)-zeolite A mixed matrix membranes.* Journal of Membrane Science, 2005. **260**(1-2): p. 45-55.
24. Wang, M., Z. Wang, N. Li, J.Y. Liao, S. Zhao, J.X. Wang, and S.C. Wang, *Relationship between polymer-filler interfaces in separation layers and gas transport properties of mixed matrix composite membranes.* Journal of Membrane Science, 2015. **495**: p. 252-268.
25. Dai, Y., Johnson, J. R., Karvan, O., Sholl, D. S., Koros, W. J., *Ultem®/ZIF-8 mixed matrix hollow fiber membranes for CO_2/N_2 separations.* Journal of Membrane Science, 2012. **401-402**: p. 76-82.
26. Perez, E.V., Balkus, K. J., Ferraris, J. P., Musselman, I. H., *Mixed-matrix membranes containing MOF-5 for gas separations.* Journal of Membrane Science, 2009. **328**(1-2): p. 165-173.
27. Adams, R., Carson, Cantwell, Ward, Jason, Tannenbaum, Rina, Koros, William, *Metal organic framework mixed matrix membranes for gas separations.* Microporous and Mesoporous Materials, 2010. **131**(1-3): p. 13-20.
28. Jomekian, A., Mansoori, S. A. A., Monirimanesh, N., Shafiee, A., *Gas transport behavior of DMDCS modified MCM-48/polysulfone mixed matrix membrane coated by PDMS.* Korean Journal of Chemical Engineering, 2011. **28**(10): p. 2069-2075.

29. Iijima, S., *Helical microtubules of graphitic carbon.* Nature, 1991. **354**(6348): p. 56-58.
30. Majumder, M., Chopra, N., Hinds, B. J., *Mass transport through carbon nanotube membranes in three different regimes: ionic diffusion and gas and liquid f+low.* ACS Nano, 2011. **5**(5): p. 3867-3877.
31. Majumder, M., Chopra, N., Hinds, B. J., *Effect of tip functionalization on transport through vertically oriented carbon nanotube membranes.* Journal of the American Chemical Society, 2005. **127**(25): p. 9062-9070.
32. Majumder, M., Chopra, N., Andrews, R., Hinds, B. J., *Nanoscale hydrodynamics - Enhanced flow in carbon nanotubes.* Nature, 2005. **438**(7064): p. 44-44.
33. Hinds, B.J., Chopra, N., Rantell, T., Andrews, R., Gavalas, V., Bachas, L. G., *Aligned multiwalled carbon nanotube membranes.* Science, 2004. **303**(5654): p. 62-65.
34. Ismail, A.F., Rahim N.H., Mustafa, A, Matsuura, T, Ng, B.C., Abdullah, S., Hashemifard, S.A., *Gas separation performance of polyethersulfone/multi-walled carbon nanotubes mixed matrix membranes.* Separation and Purification Reviews, 2011. **80**: p. 20-31.
35. S. Zeinali, M.A., *Improving O_2/N_2 Selective filtration using carbon nanotube-modified mixed-matrix membranes.* Chemical Engineering and Technology, 2015. **38**(11): p. 2079-2086.
36. Kim, S., Chen, L., Johnson, J. K., Marand, E., *Polysulfone and functionalized carbon nanotube mixed matrix membranes for gas separation: Theory and experiment.* Journal of Membrane Science, 2007. **294**(1-2): p. 147-158.
37. Ismail, A.F., Rahim, N. H., Mustafa, A., Matsuura, T., Ng, B. C., Abdullah, S., Hashemifard, S. A., *Gas separation performance of polyethersulfone/multi-walled carbon nanotubes mixed matrix membranes.* Separation and Purification Technology, 2011. **80**(1): p. 20-31.
38. Goh, P.S., Ng, B. C., Ismail, A. F., Sanip, S. M., Aziz, M., Kassim, M. A., *Effect of dispersed multi-walled carbon nanotubes on mixed matrix membrane for O_2/N_2 separation.* Separation Science and Technology, 2011. **46**(8): p. 1250-1261.
39. Aroon, M.A., Ismail, A. F., Matsuura, T., Montazer-Rahmati, M. M., *Performance studies of mixed matrix membranes for gas separation: A review.* Separation and Purification Technology, 2010. **75**(3): p. 229-242.
40. Weisenberger, M.C., *Application of multiwall carbon nanotubes: mechanical, electrical and thermal properties*. 2007, University of Kentucky.
41. Morris, E.A., Weisenberger, M. C., Bradley, S. B., Abdallah, M. G., Mecham, S. J., Pisipati, P., McGrath, J. E., *Synthesis, spinning, and properties of very high molecular weight poly(acrylonitrile-co-methyl acrylate) for high performance precursors for carbon fiber.* Polymer, 2014. **55**(25): p. 6471-6482.
42. Hilding, J., Grulke, E. A., Zhang, Z. G., Lockwood, F., *Dispersion of carbon nanotubes in liquids.* Journal of Dispersion Science and Technology, 2003. **24**(1): p. 1-41.

43. Ghomshani, A.D., Ghaee, A., Mansourpour, Z., Esmaili, M., Sadatnia, B., *Improvement of H_2/CH_4 separation performance of PES hollow fiber membranes by addition of MWCNTs into polymeric matrix.* Polymer-Plastics Technology and Engineering, 2016. **55**(11): p. 1155-1166.

Chapter 4: Hollow Fiber Membrane Spinning and PES-MWCNT Hollow Fiber Membranes

4.1 Introduction

Asymmetric polymeric hollow fiber membranes (HFM) have existed since the mid-1960's and are often preferable to flat sheet membranes owing to their high surface area to volume ratio, as well as being more mechanically robust and easier to handle due to their self-supporting structure [1]. One major area of focus in the membrane literature and in industry is the extension of well understood dense film and asymmetric flat sheet membrane processing methods to the hollow fiber membrane geometry. There are multiple factors that present a challenge to making this conversion. One is that, generally speaking, dense film membranes are cast from dopes with a much lower polymer concentration than is required for the formation of hollow fiber membranes [2]. In the case of asymmetric flat sheet membranes, the phase-inversion process starts from the top surface when the cast film is immersed in the coagulation bath, while hollow fiber membrane spinning involves multiple coagulation fronts, which leads to differences in morphology that must be taken into account. Because of this, not only is the formulation of the dope critical, but so are the specific compositions of both the inner and outer coagulation fluids. Additionally, other processing parameters, such as the spinneret design, relative flow rates, air gap distance, and dope elongation (i.e. take-up) rate are critical to the final morphology and performance of the hollow fiber membrane [3-6].

The typical hollow fiber spinning process was discussed in Section 2.3.2.2, and illustrated in Figure 2.2. This figure shows a schematic diagram and photograph of the HFM spinning line (Figure 2.2a) as well as a diagram and photograph of the region that is near the annulus of the spinneret (Figure 2.2b). In this region, there are multiple processing parameters that influence the dimensions, morphology and ultimate transport performance properties of the hollow fiber membrane. The processing variables that are operative in this region include (a) the respective flowrates and compositions of the polymer solution (dope) and the internal coagulant (bore fluid), (b) the geometry of the spinneret, (c) the length and relative humidity of the air gap, (d) the elongation of the dope by both gravity and the draw that is imposed during take-up (i.e. draw down ratio), and (e) the properties of the coagulation bath, where the phase-inversion process is completed [7].

This chapter will be divided into two main sections. The first section will be a discussion of the development of the hollow fiber membrane spinning process. Included in this discussion is an examination of the relationships between multiple hollow fiber spinning parameters and the dimensions and morphology of PES hollow fibers. The second section of this chapter will focus on the gas permeation properties of the produced hollow fiber membranes. Extending flat sheet membrane performance reported in Chapter 3, the baseline separation characteristics of PES and PSf hollow fiber membranes were established and compared to their flat sheet counterparts, both before and after caulking with PDMS to repair pinhole surface defects. In addition, a study of the effects of incorporating multiwall carbon nanotubes (MWNCT) into a matrix

of PES and PSf at various loading levels was conducted. In Chapter 3 of this work, it was concluded that incorporating MWCNTs into the polymeric membrane matrix at low loadings acted to suppress the formation of pinhole defects during phase inversion. In this chapter, gas transport experiments were conducted using hollow fiber membranes to determine if the pinhole defect suppression effect could be extended from the flat sheet to the hollow fiber membrane geometry. As with the baseline separation studies, the properties of the mixed matrix hollow fiber membranes were compared to the flat sheet membranes that were investigated in Chapter 3.

4.2 Materials and Methods

All materials and methods that were employed for this work were described in detail in Chapter 2. This includes the polymers and solvents that were used to make hollow fiber membranes and the presentation of detailed procedures related to the operation of the hollow fiber membrane spinning system, PDMS caulking, hollow fiber membrane module construction, and gas permeation testing.

4.3 Results and Discussion

4.3.1 Effects of Varying Processing Parameters on Hollow Fiber Membrane Characteristics

The influence of various key processing parameters on the morphology and dimensions of the hollow fibers was investigated in detail. Through the studies presented in Chapter 3, the dope and bore fluid concentrations used for hollow fiber spinning were determined by casting flat sheet membranes and systematically varying the polymer concentration in the dope and the solvent concentration in the coagulation

bath. The results of these studies were used to establish a set of hollow fiber spinning conditions to produce fibers with a dense separating layer around the outer surface of the membrane, a porous support structure, and a porous wall on the lumen side of the fiber. A summary of the hollow fiber processing parameters are shown in Table 4.1. Although there are numerous processing conditions that can potentially have an effect on the final properties of the membrane, this work focused primarily on three: the ratio of the bore fluid velocity to the polymer dope velocity (V_b/V_d), the vertical length of the air gap between the spinneret and the surface of the coagulation bath, and the ratio of the take-up velocity to the dope velocity, which establishes the amount of draw that is applied to the nascent hollow fiber.

Table 4.1: Summary of hollow fiber membrane spinning conditions used in flowrate, air gap, and draw down ratio studies.

Process Parameters	**Value**
Spinning Solution	PES/DMAc
Polymer Concentration (by weight)	30%
Bore Fluid (by weight)	70/30 (Solvent:H_2O)
Coagulation Bath	Deionized water
Dope Annulus Diameter (D)	1.0 mm
Bore Needle Dimensions (d_o, d_i)	0.508, 0.254 mm
Dope Flowrate (cm^3/min)	1.36 – 3.40
Bore Flowrate (cm^3/min)	0.38 – 3.0
V_b/V_d	0.5 – 4.0
Draw Down Ratio	1.0 – 2.5
Air Gap (cm)	2 - 7

Figure 4.1 shows an example of typical phase-inversion morphology across the wall of a hollow fiber membrane, as well as a diagram defining the dimensions that were measured for each fiber. The dimensions that were of interest in this work were the outer diameter (OD), inner diameter (ID), and wall thickness (WT) of the fiber. Additionally, the morphology of the fiber wall was examined, with the primary focus being the influence of the various processing parameters on the formation of finger-like macrovoids and the sponge-like porous substructure. In a hollow fiber membrane (for shell-side separations), a thin, integral dense separating layer is established at the outer surface of the fiber, the presence of finger-like macrovoids is typically minimized, and most of the fiber wall is composed of sponge-like porous substructure. The lumen side of the hollow fiber membrane should also be porous, in order to maximize the permeance of the membrane.

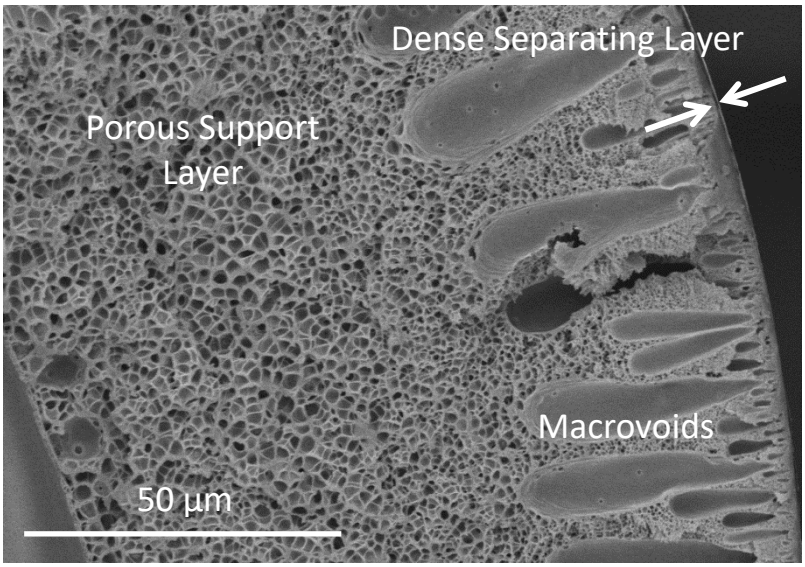

Figure 4.1a: SEM micrograph showing typical hollow fiber membrane wall morphology, with the dense separating layer, porous support layer, and macrovoids indicated.

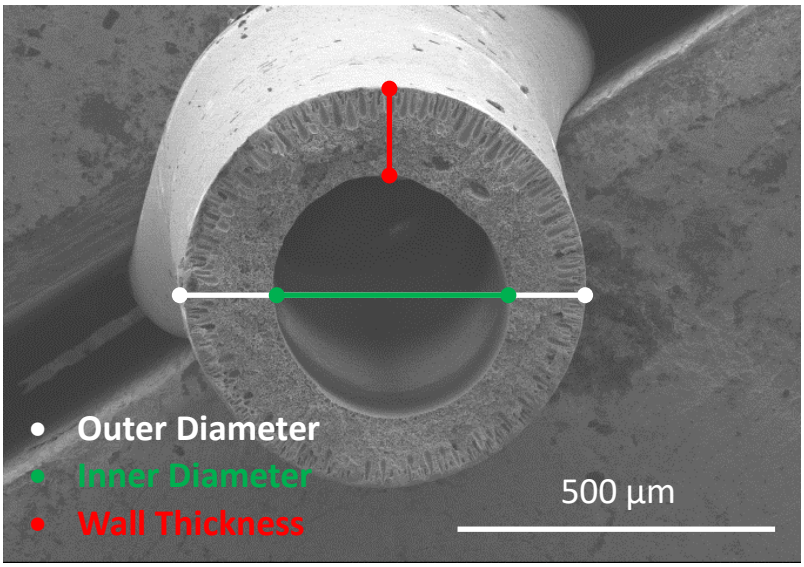

Figure 4.1b: SEM micrograph showing typical hollow fiber membrane cross section, with outer diameter (OD), inner diameter (ID), and wall thickness (WT) indicated.

4.3.1.1 Ratio of Bore Velocity to Dope Velocity (V_b/V_d)

Flowrates of the dope and bore fluids were easily controlled using independent syringe pumps, allowing for direct investigation of the relationships between the relative flowrates of these fluids and fiber dimensions and morphology. Although most of the literature on PES spinning involves a ratio of bore flowrate to dope flowrate of approximately 0.5 [3, 5, 6, 8-12], no study fully explains the relationship between the two flowrates and the resulting fiber properties. The design of the spinning apparatus allowed for relatively easy mid-run changes to processing parameters and the collection of several distinct fiber specimens over the course of a single spin run. Fluid velocity was calculated simply by dividing flowrate (cm^3/min) by cross sectional area of the die opening for each fluid (cm^2):

$$V_b = \frac{Q_b}{0.25\pi {d_i}^2} \quad [4.1]$$

$$V_d = \frac{Q_d}{0.25\pi(D^2 - {d_o}^2)} \quad [4.2]$$

where Q_b, Q_d, V_b and V_d are the flowrates and velocities of the bore fluid and the dope fluid, respectively. D is the outer diameter of the spinneret capillary, while d_o and d_i are the outer and inner diameters of the microtubing through which the bore fluid flows, as shown in Figure 2.3. The processing parameters for these studies are reported in Table 4.2, with the dope flowrate fixed at 3.4 cm^3/min. The ratio of flowrates (bore flowrate to dope flowrate) used for these experiments ranged from 0.11 to 0.88, which is consistent with the ratio value of approximately 0.5 that is commonly encountered in the literature.

Table 4.2: Processing parameters for V_b/V_d, air gap, and draw down ratio experiments.

Process Parameters			
Experiment	V_b/V_d	Air Gap	Draw Down Ratio
Spinning Solution	PES/DMAc	PES/DMAc	PES/DMAc
Polymer Concentration	30 wt.%	30 wt.%	30 wt.%
Bore Fluid	70 wt.% DMAc	70 wt.% DMAc	70 wt.% DMAc
Coagulation Bath	Deionized water	Deionized water	Deionized water
Dope Flowrate (cm^3/min)	3.40	2.70	1.36 – 3.40
Bore Flowrate (cm^3/min)	0.38 – 3.0	1.50	0.75 – 1.90
V_b/V_d	0.5 – 5.0	2.5	2.5
Air Gap (cm)	2	2 – 7	4
Draw Down Ratio	1.0	1.0	1.0 – 2.5

Dopes composed of 30 wt.% PES in DMAc were prepared employing the procedure described in Section 2.3.2.1 and subsequently used to produce the hollow fibers studied in this experiment. PES hollow fibers were spun, solvent exchanged, and dried using the methods described in Section 2.3.2.2. Ten short lengths of fiber were cut from various parts of the fiber spool and the outer and inner diameters were measured using calipers and an optical microscope, respectively. One additional fiber sample was immersed in liquid nitrogen and fractured using tweezers for SEM imaging.

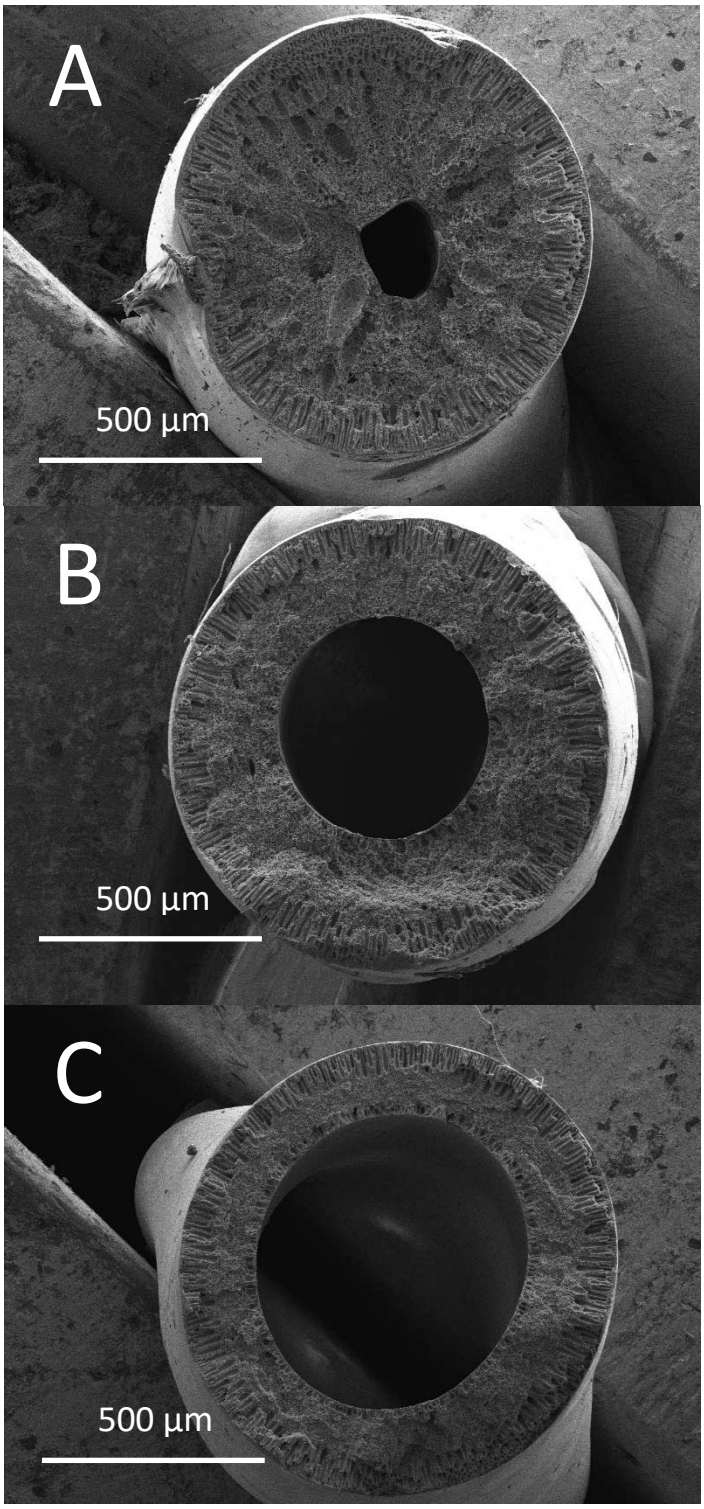

Figure 4.2: SEM micrographs of PES hollow fiber membranes spun from 30 wt% PES/DMAc dope with V_b/V_d = (A) 0.5, (B) 2.5, and (C) 4.0.

Figure 4.2 presents a series of cross sections for hollow fibers that were spun with various bore flowrates (i.e. various V_b/V_d ratios). An examination of the SEM micrographs showed a direct relationship between the outer and inner diameters of the hollow fibers with varying V_b/V_d ratio, and a decrease in the wall thickness as the V_b/V_d ratio was increased. A plot of outer and inner diameters and membrane wall thickness versus V_b/V_d is shown in Figure 4.3. The data indicated an increase in the outer diameter of the hollow fiber with increasing velocity ratio (i.e. increasing bore flowrate). The inner bore diameter of the hollow fiber also increased with V_b/V_d, with a higher slope. The difference in the slope of the trend lines resulted in a steady decrease in wall thickness as it related to V_b/V_d. The increased flow inside the bore with increasing V_b expanded the inner dope surface, and the free outer surface of the fiber expanded across the air gap in response, thereby increasing the outer diameter of the fiber while simultaneously reducing the wall thickness. The observed decrease in the wall thickness of the hollow fiber reflects the material balance of the flowing system (i.e. moving reference frame). As the inner and outer diameters of the fiber are increased (and assuming the pore structure remains consistent), the wall thickness of the membrane must necessarily decrease in order to satisfy the material balance.

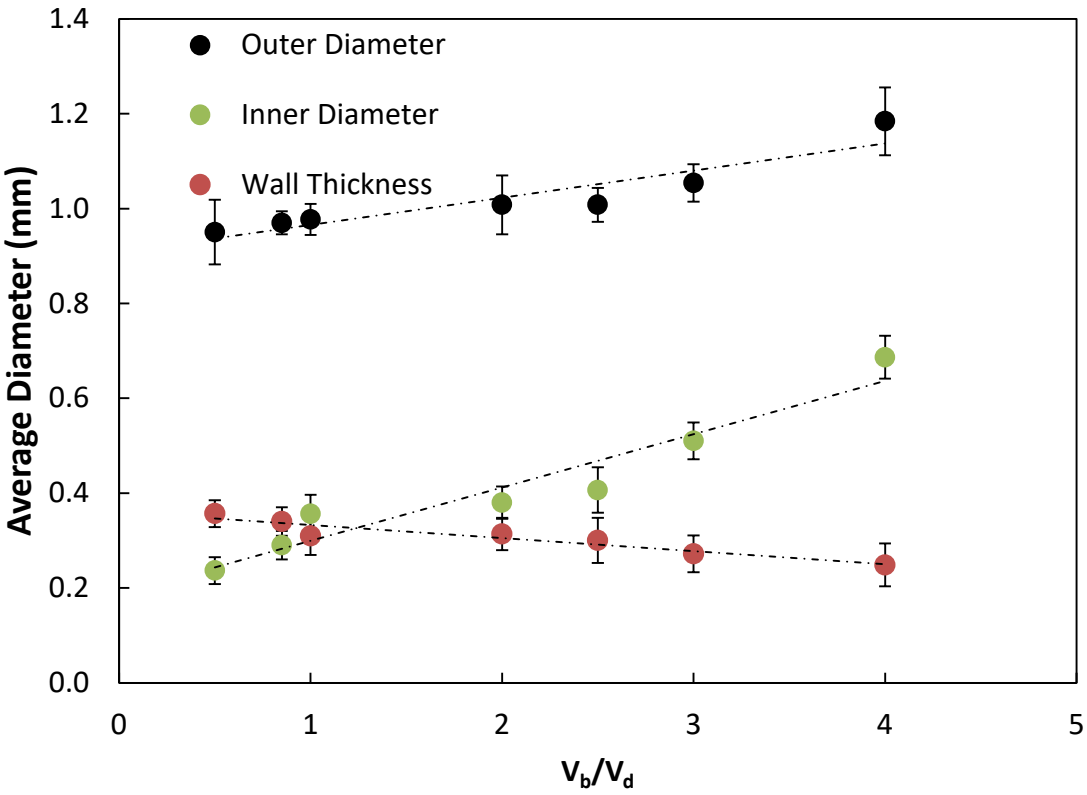

Figure 4.3: Relationship between fiber dimensions and V_b/V_d for hollow fibers spun from 30 wt% PES/DMAc dope using a 70 wt% DMAc/water bore fluid and a pure water coagulation bath (n = 10 for each fiber sample).

4.3.1.2 Air Gap Distance

The spinline design also allowed for the study of the effect of the vertical gap distance between the extrusion die and the surface of the coagulation bath (i.e. the air gap) and its influence on fiber dimensions and morphology. Direct changes to the air gap were enabled by mounting the spinneret on a lab-jack; this allowed for several data points to be collected over the course of a single spin run. The processing parameters that were controlled to examine the effect of the air gap on the fiber dimensions and morphology are presented in Table 4.2. For this experiment, V_b/V_d was held constant at 2.5 and draw down ratio (i.e the ratio of take-up velocity to the dope velocity at the die)

was held at 1.0. Again, ten fiber samples were cut from various parts of the hollow fiber spool and measured for their OD and ID. One fiber sample was also immersed in liquid nitrogen and fractured for SEM imaging of the cross-section. No significant changes were expected to be observed in the dimensions of the final hollow fibers, since the flowrates of the two fluids, geometry of the die, and the draw down ratio were all held constant. Additionally, there was sufficient draw on the fiber that, even at the largest air gaps, the influence of gravity was negligible compared to the drawing force imposed by the take-up godet. The primary expectation of this experiment was to observe the effect of varying the air gap residence time that the nascent fiber spent in contact solely with the solvent-rich bore fluid prior to being immersed in the deionized water coagulation bath.

The relationships between the fiber dimensions and the air gap, while holding all other processing parameters constant, are shown in Figure 4.4. It is clear from these data that changing the air gap length in the range tested did not appreciably change the measured dimensions of the hollow fiber. The effect of changing the air gap appeared to be primarily morphological for this process, with the SEM micrographs indicating a substantially larger pore size across the membrane substructure for the 7 cm air gap as compared to the 3 cm air gap, as shown in Figure 4.5. This result can be attributed to the longer time that the nascent fiber spends in contact with only the solvent-rich bore fluid for the 7 cm air gap. The longer residence time in the air gap allowed more time for phase inversion to progress at the inner surface owing to ingress of the solvent-rich bore fluid.

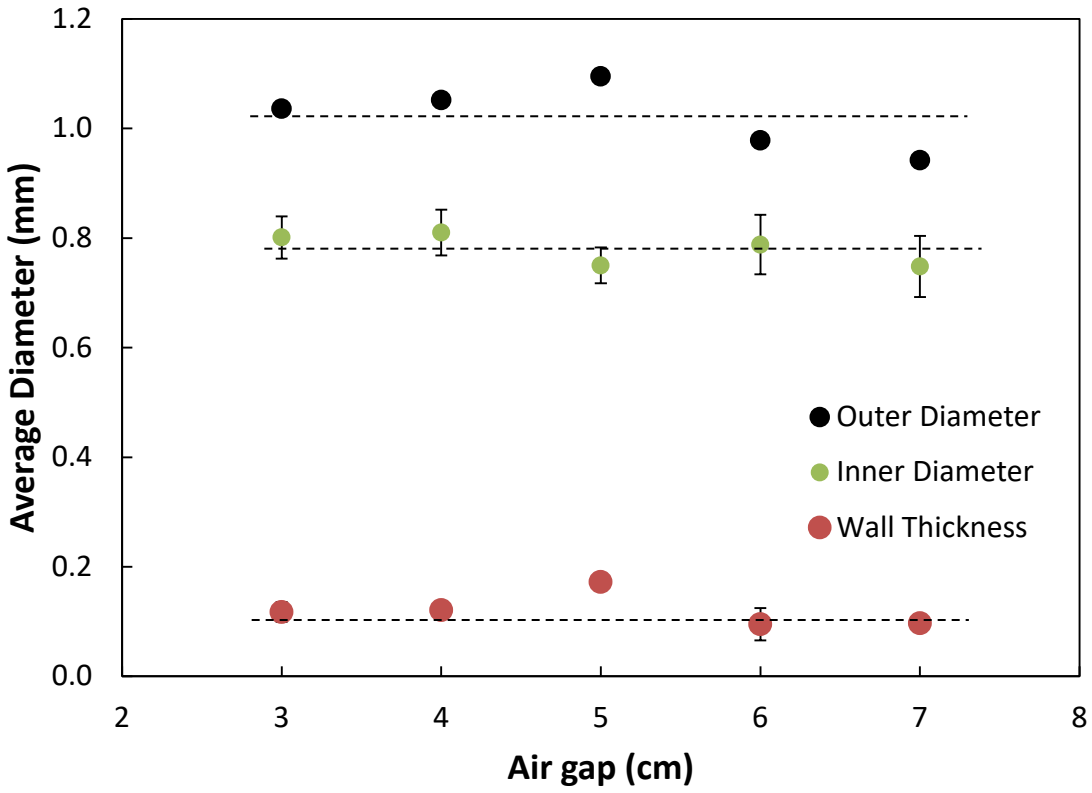

Figure 4.4: Relationship between fiber dimensions and air gap distance for hollow fibers spun from 30 wt% PES/DMAc dope using a 70 wt% DMAc/water bore fluid and a pure water coagulation bath (n = 10 for each fiber sample).

This led to extended delayed demixing, which resulted in the emergence of larger polymer-lean droplets in the substructure before the morphology was fully solidified when the fiber entered the coagulation bath. With everything else being held equal, an increase in the air gap distance from 3 cm to 7 cm more than doubled the residence time (from 0.39 s to 0.81 s) during which delayed demixing occurred, which resulted in a significant change in fiber morphology. The observed result is consistent with prior work by Chung et al., who reported a comparable change in morphology for air gap spun PES hollow fibers compared to fibers spun with no air gap exposure (i.e. wet spun fibers) [5].

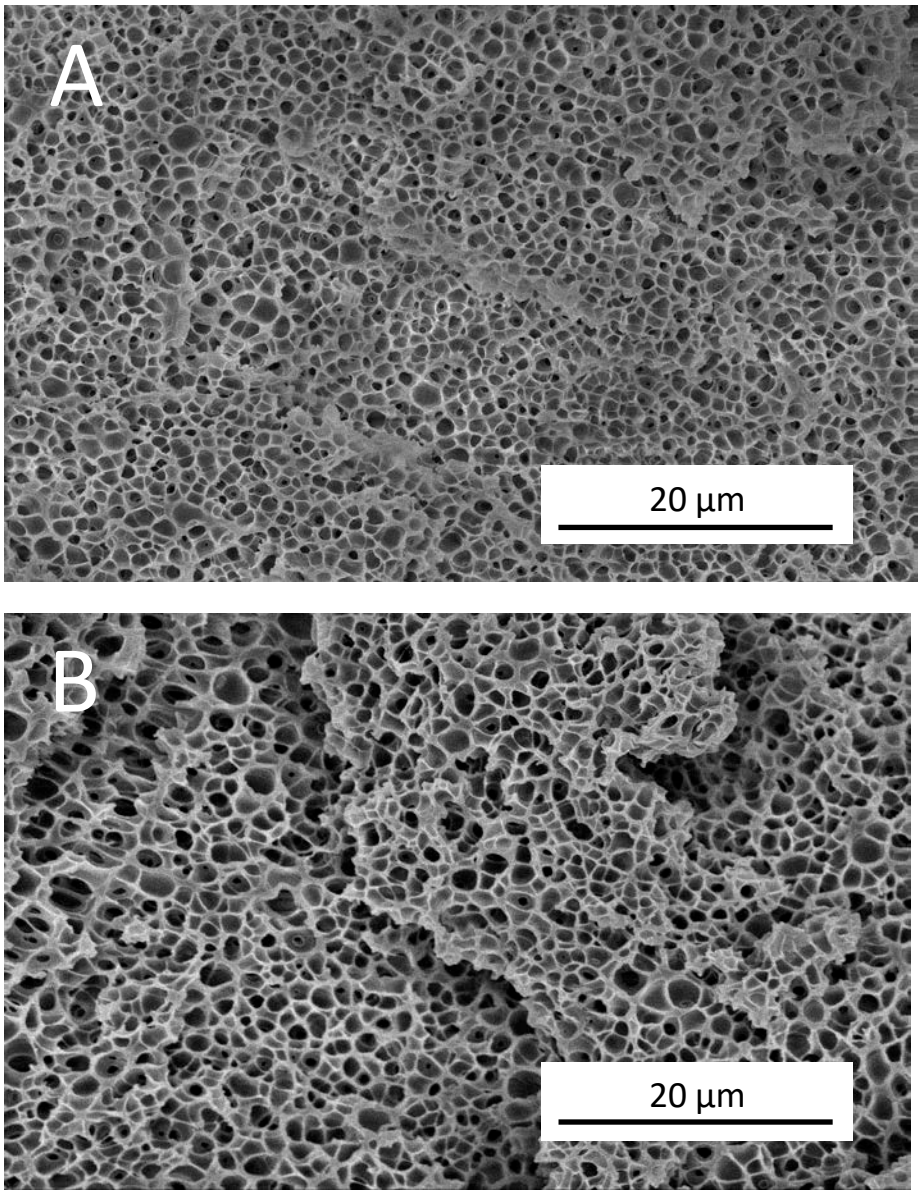

Figure 4.5: SEM micrographs of the porous support layer of hollow fiber membranes spun from 30 wt% PES/DMAc dope with (A) 3 cm air gap distance and (B) 7 cm air gap distance.

4.3.1.3 Ratio of Take-up Velocity to Dope Velocity (Draw Down Ratio)

The draw down ratio (DDR) was examined to determine its effect on PES hollow fiber properties. The DDR was defined in this work as the ratio of the take up velocity at the godet (V_g) to the velocity of the dope as it exits the die (V_d). Two different methods for adjusting DDR during the spinning process were possible using the hollow fiber spinning system. DDR could be changed either by increasing the take-up speed on the godet rollers or by holding the take-up speed constant and adjusting the dope/bore flowrates at the spinneret. For the purposes of these experiments, the draw down ratio was adjusted solely by changing the flowrates of the two fluids (at fixed V_b/V_d), while the take-up speed on the godet and the air gap distance were held constant. Additionally, the rotational velocity of the winder was calibrated to be exactly the same as that of the take-up godet. This was done to ensure that no further draw was imposed on the fiber between the godet and the winder.

When melt spinning solid fiber, conservation of volume dictates that, if all other processing parameters are held constant, the final fiber diameter will be inversely proportional to the square root of the draw down ratio. Despite the increase in complexity that comes from the multi-front phase-inversion solution process as compared to melt spinning solid fiber, it was hypothesized that a similar trend might be expected for the production of hollow fibers. The processing parameters for this experiment are shown in Table 4.2. All of the parameters that were held constant in this study were chosen based on the prior experiments detailed above.

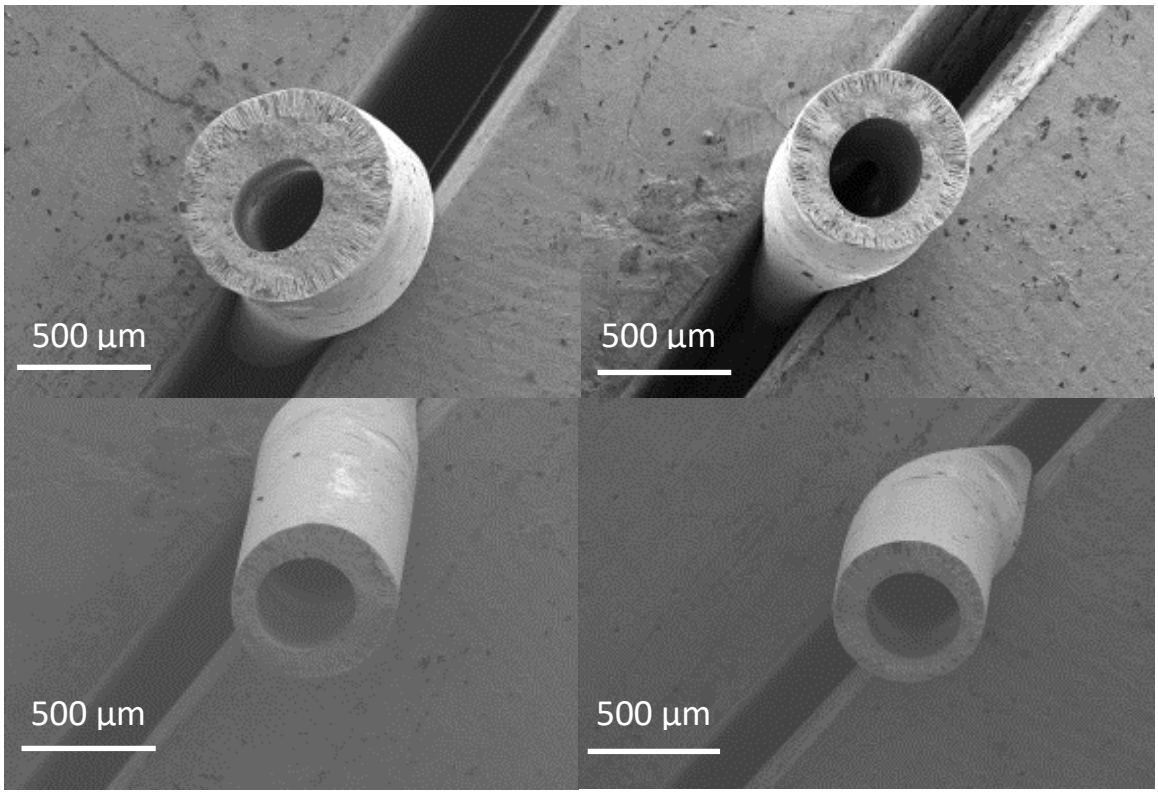

Figure 4.6: SEM micrographs of PES hollow fiber membranes spun from 30 wt% PES/DMAc dope with DDR = (A) 1.0, (B) 1.5, (C) 2.0, and (D) 2.5.

SEM micrographs of the cross sections of hollow fiber membranes that were spun with varying draw down ratios are shown in Figure 4.6. As expected, the images display a progressive decrease in fiber dimensions with increasing draw down ratio. A plot of the relationship between the hollow fiber diameter and the square root of the draw down ratio is shown in Figure 4.7. As suggested above, the outer diameter of the fibers was inversely proportional to $(DDR)^{1/2}$. The wall thickness of the hollow fibers also appeared to follow this relationship. An examination of the micrographs of these fibers also indicated a qualitative correlation between the pore size of the fiber substructure and the applied draw, as shown in Figure 4.8.

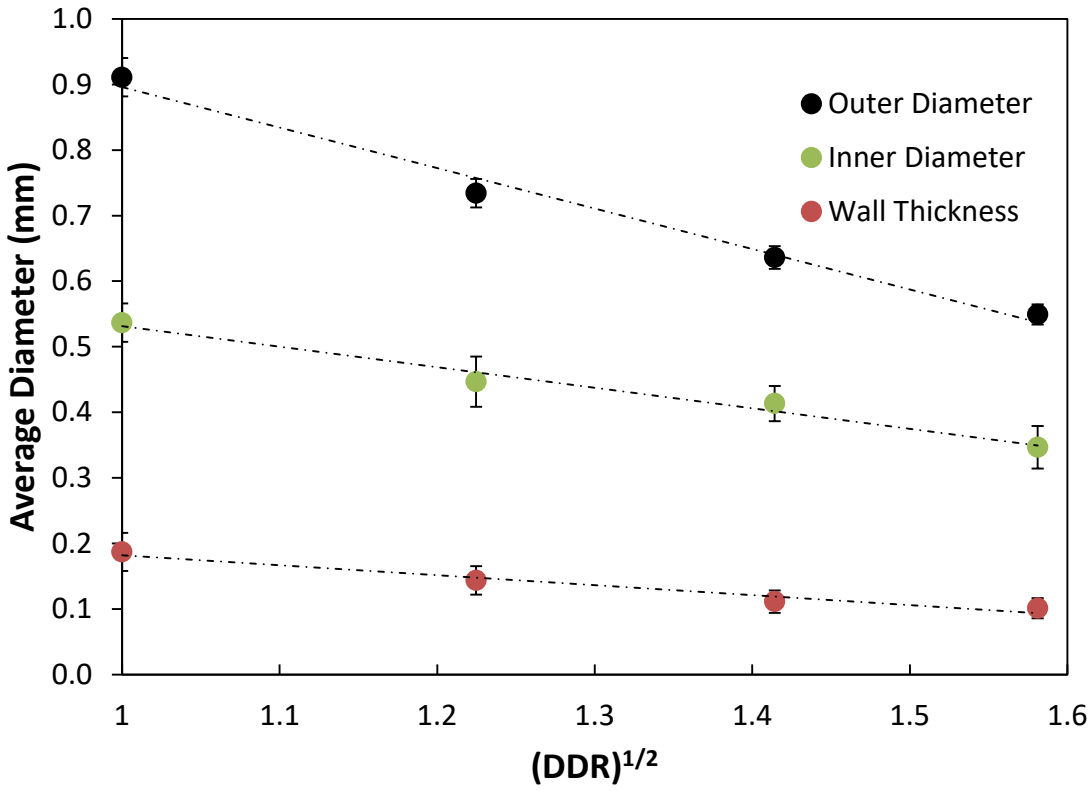

Figure 4.7: Relationship between fiber dimensions and the square root of draw down ratio for hollow fiber membranes spun from 30 wt% PES/DMAc dope, with 70 wt% DMAc/water bore fluid and deionized water coagulation bath (n = 10 for each fiber sample).

Similar to the effect of decreasing the air gap, a decrease in pore size was observed with increasing draw ratio. It is an interesting trend, as intuition would suggest that higher draw could compact or extend pores by deforming them via mechanical means after coagulation. However, the shape of the pores did not change in any meaningful way with higher draw, only the size, suggesting that the observed variation in pore size was established before the pore structure was set by coagulation and the pores were not mechanically stretched or altered after this point. A higher draw has a similar effect on the pore structure as a decrease in the air gap distance, as it shortens the relative air

gap residence time between the die exit and coagulation. This reduces the time available for coarsening of the polymer lean droplets (from 0.41 s to 0.59 s), resulting in a tighter pore structure at higher draw down rates.

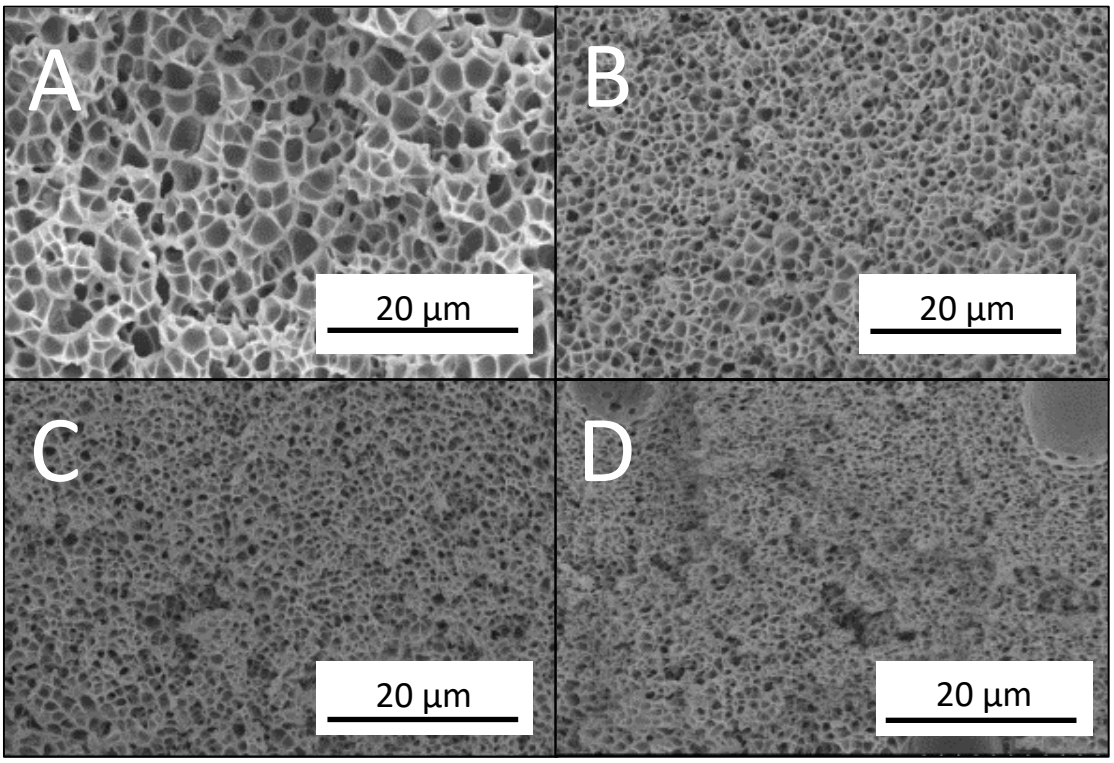

Figure 4.8: SEM micrographs of porous substructure of PES hollow fiber membranes spun from 30 wt% PES/DMAc dope with DDR = (A) 1.0, (B) 1.5, (C) 2.0, and (D) 2.5.

4.3.2 Gas Separation Properties of Hollow Fiber Membranes

4.3.2.1 Baseline Permeance and Selectivity of Hollow Fiber Membranes

The results of the experiments described in the previous sections were used to choose a set of hollow fiber processing conditions for the production of membranes suitable for gas transport studies. The spinning parameters that were employed to produce the hollow fiber membranes for gas separation experiments are shown in Table 4.3. These parameters were found to produce hollow fibers with a dense separating layer, relatively low occurrence of macrovoids, a sponge-like porous substructure, and a porous inner wall of the hollow fiber. The solvent that was used for hollow fiber spinning was NMP, which was determined through flat sheet studies in Chapter 3 to have no significant impact on either the viscosity of the dope or the morphology of the resulting polymeric membranes as compared to DMAc.

Table 4.3: Processing parameters used for the production of hollow fiber membranes for gas separation testing.

Process Parameters	Value
Spinning Solution	PES/NMP, PES/NMP/MWCNT, PES/NMP/Carbon Black
Polymer Concentration (by weight in solvent)	30 wt.%
Filler Concentration (by weight in polymer)	0 – 0.5 wt.%
Bore Fluid (wt.%)	70/30 (Solvent:H_2O)
Coagulation Bath	Deionized water
Spinneret Annulus Diameter (mm)	1.0
Bore Needle Dimensions (d_o, d_i)	0.508, 0.254 mm
Dope Flowrate (cm^3/min)	2.5
Bore Flowrate (cm^3/min)	0.75 – 1.90
V_b/V_d	2.5
Air Gap (cm)	4
Draw Down Ratio	2.0
Number of Fibers in HFM Module	10
Applied pressure difference (ΔP; psi)	29

The baseline gas separation performance of PES and PSf hollow fiber membranes was measured and compared to that of the flat sheet membranes, both with and without PDMS caulking. All fibers were spun using the parameters presented in Table 4.3 and were then subjected to solvent exchange and drying per the procedures described in Section 2.3.2.2. The permeance and ideal selectivity of the unfilled PES and PSf fibers in both the neat and PDMS caulked states were measured at an applied pressure difference of 29 psi, using the hollow fiber membrane module preparation and testing methods described in Section 2.4.1.

The transport results for the as-spun and caulked PES and PSf hollow fibers are presented in Table 4.4. The as-spun hollow fiber membranes showed virtually the same O_2/N_2 selectivity as the flat sheet membranes, which was characteristic of Knudsen diffusion through pinhole defects. It is notable in these data that the permeance of the as-cast flat sheet membranes was larger than that of the hollow fiber membranes by about a factor of two. This result suggested a larger density of pinhole defects present in the dense separating layer of the flat sheet membranes as compared to the hollow fiber membranes, as Knudsen diffusion through pinhole defects is the dominant mechanism controlling transport for uncaulked membranes.

Table 4.4: Summary of the permeance of N_2 and O_2 as well as the selectivity of O_2/N_2 for the unfilled hollow fiber and flat sheet membranes.

Material	P/l (N_2) (GPU)	P/l (O_2) (GPU)	α(O_2/N_2)
PES-HFM	12.95 ± 2.0	11.67 ± 1.7	0.90 ± 0.05
PSf-HFM	15.97 ± 1.8	14.45 ± 1.9	0.90 ± 0.02
PES-PDMS-HFM	0.56 ± 0.02	2.73 ± 0.15	4.87 ± 0.40
PSf-PDMS-HFM	0.68 ± 0.05	3.01 ± 0.12	4.43 ± 0.21
PES-Flat Sheet	23.4 ± 0.5	20.8 ± 0.7	0.89 ± 0.05
PSf-Flat Sheet	31.9 ± 0.01	29.9 ± 0.5	0.94 ± 0.04
PES-PDMS-Flat Sheet	0.07 ± 0.01	0.41 ± 0.03	5.5 ± 0.03
PSf-PDMS-Flat Sheet	0.16 ± 0.02	0.82 ± 0.07	5.1 ± 0.03

Both the PES and the PSf membranes displayed an order of magnitude reduction in O_2 permeance when PDMS caulking was employed, while the O_2/N_2 ideal selectivity of the membranes increased to approach that of the literature values for dense polymer

film [13]. The large reduction in membrane permeance and increase in ideal selectivity was consistent with a change in the dominant diffusion mechanism across the membrane from Knudsen diffusion to solution diffusion. Therefore, it can be concluded from these data that the PDMS caulking procedure effectively repaired the pinhole defects in the hollow fiber membrane dense separating layer.

It is also notable in these membranes that, for both polymers that were examined, the hollow fiber membranes showed permeance that was nearly an order of magnitude higher than the flat sheet membranes when caulked with PDMS. The larger permeance that was observed in the hollow fiber membranes was accompanied by slightly lower O_2/N_2 ideal selectivity. The transport properties that were observed for these membranes were consistent with the solution diffusion mechanism, with the ideal selectivity approaching that of a dense film membrane owing to the caulking of the pinhole defects by application of PDMS. Contrary to Knudsen diffusion, wherein the dominant driver of permeance is the number density of channels (i.e. pinhole defects) through which the gas can flow, when solution diffusion dominates, the permeance is controlled by the thickness of the dense separating layer of the membrane, as well as the PDMS caulking layer. The permeation resistance due to the PDMS coating is minimal compared to that of the dense separating layer, since PDMS is well known to be one of the most permeable polymers in existence [14]. Therefore, the generally higher permeance that was observed for the hollow fiber membranes prepared in this study is likely the result of a reduction in the thickness of the dense separating layer in the hollow fiber membranes as compared to their flat sheet analogs.

PSf hollow fiber membranes showed a higher permeance as compared to PES in both the as-spun and PDMS caulked state. This effect was also observed previously in the flat sheet membrane transport studies. The larger permeance across the as-spun PSf hollow fiber (as compared to PES) was most probably the result of a larger areal density of pinhole defects being formed in the dense separating layer of the membrane, a result that was previously observed for the analogous flat sheet membranes. Upon caulking, the PSf fibers showed gas selectivities consistent with successful repair of the pinhole defects. The higher permeance observed for caulked PSf compared to PES is consistent with the higher fractional free volume inherent to the dense separating layer of the PSf polymer [13]. However, it could also be a result of differences in the thickness of the dense separating layer in these membranes, which could result from differences in the dynamics of the phase inversion process. In order to deconvolute these contributions, further experiments would be necessary to fully characterize the thickness of the dense separating layer in the fibers, and its relation to spinning conditions and measured gas transport.

Overall, the hollow fiber membrane spinning conditions could be further optimized to render hollow fiber transport performance competitive with that reported in literature and achieved with commercial hollow fiber membranes. Both the ideal gas selectivity as well as the membrane permeance can be improved by optimizing various processing parameters. For example, the selectivity of the as-spun membrane can be improved by tailoring the dope and bore fluid compositions in order to produce a defect-free dense separating layer. In an ideal hollow fiber membrane, the dense

separating layer would be formed with no pinhole defects. This is an incredibly challenging goal to reach, but there are methods that can produce membranes with a defect-free dense separating layer. One strategy to prevent or minimize the formation of pinhole defects in polymeric membranes is through the introduction of volatile non-solvent additives, such as methanol or ethanol, into the polymer dope solution [15]. The addition of these additives leads to local phase inversion at the membrane surface due to solvent evaporation in the air gap (i.e. prior to bulk coagulation), which aids in the formation of a dense separating layer that is both thin and free of pinhole defects.

The improvements that can be made in the ideal selectivity of the membrane are generally less significant, however, than the improvements that can be achieved in the membrane permeance. In the membrane community, much focused research is conducted in order to increase the permeance of gas separation membranes while maintaining selectivity at an acceptable level [11, 16, 17]. There are multiple methods that are generally employed to achieve this result. The most common approach is the optimization of dope formulation and processing conditions in order to form the thinnest dense separating layer possible. Studies by Chung et al. have demonstrated the ability to produce PES hollow fiber membranes with dense separating layers as thin as 474 Å by incorporating non-solvent additives into the polymer spinning dope [18]. Hollow fiber membranes produced in Chung's work were able to achieve permeance values of 9.6 GPU while maintaining an O_2/N_2 ideal selectivity of 5.8. These values approach a common industry standard for hollow fiber permeance of >10 GPU [19], while maintaining an ideal selectivity of the PES dense film.

4.3.3 Effect of Multiwall Carbon Nanotubes (MWCNT) Addition

In Chapter 3 of this work, it was reported that the incorporation of MWCNTs decreased the permeance and increased the ideal selectivity of flat sheet membrane coupons by suppressing the formation of pinhole defects in the dense separating layer of the membrane during phase inversion. The studies presented in this chapter extend those results by considering analogous MWCNT-loading experiments for hollow fiber membranes. The dopes that were used for these experiments were produced with the same formulation approach as the flat sheet membranes studied in Chapter 3; the specific spinning conditions for the hollow fibers are detailed in Table 4.3. The objective of these experiments was to determine whether or not the pinhole elimination observed with MWCNT incorporation translated from the flat sheet PES and PSf membrane coupons to hollow fiber membranes.

SEM micrographs of both the unfilled PES hollow fiber membrane as well as the PES membrane loaded with 0.1 wt.% MWCNT are shown in Figure 4.9a. Although they are not easily visible in the SEM micrographs, it is clear that the hollow fibers contain a dispersion of MWCNTs, due to the macroscopic change in color from white to gray (Figure 4.9b). An examination of the micrographs revealed only a minimal difference in morphology, as was the case with the flat sheet membranes.

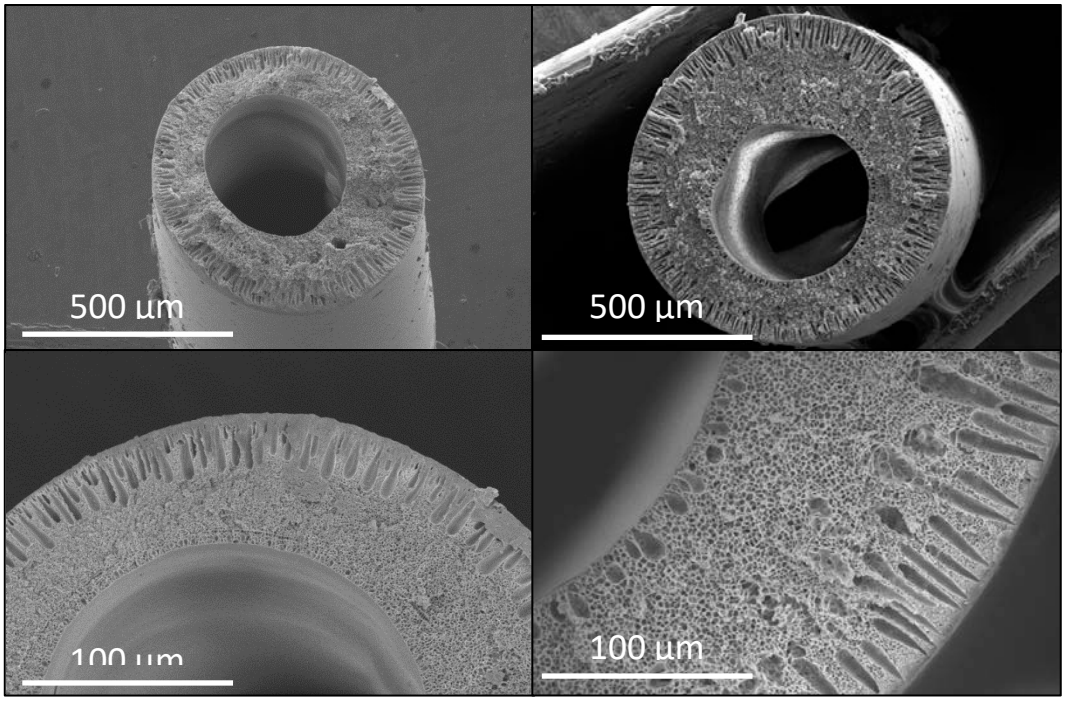

Figure 4.9a: SEM micrographs of hollow fiber membranes spun from dope composed of 30 wt.% PES in NMP (left) and dope composed of 30 wt.% PES in NMP with a MWCNT loading of 0.1 wt.% (right).

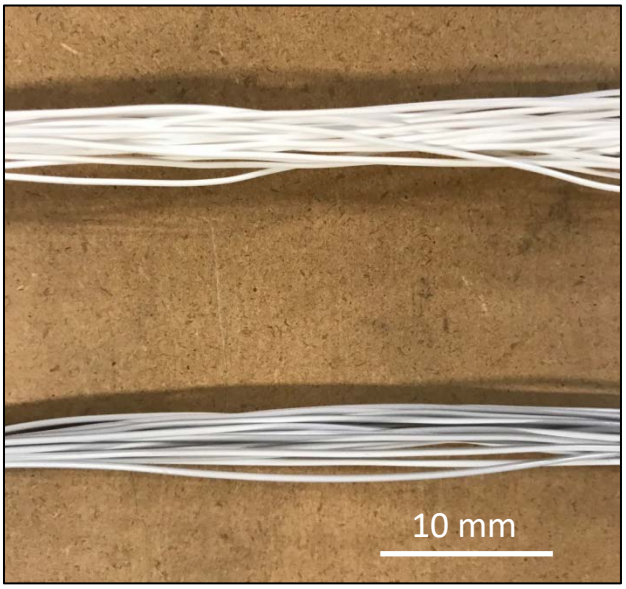

Figure 4.9b: Macroscopic comparison between neat PES HFM (top) and PES HFM loaded with 0.1 wt.% MWCNT (bottom)

The outer surfaces of the fibers, which were exposed to the deionized water coagulation bath, showed a well-defined dense separating later with finger-like macrovoids extending below the surface. The majority of the wall thickness for both hollow fiber membranes was composed of a sponge-like porous substructure. The main difference that was observed in the morphologies of the two fibers was at the inner wall of the fibers, which were phase-inverted in contact with the solvent-rich bore fluid. Similar to the flat sheet membrane results, the PES-0.1MWCNT hollow fiber membrane showed small teardrop-shaped macrovoids at the lumen surface, whereas no macrovoids were observed in the unfilled PES membrane. No changes to the hollow fiber processing were deemed necessary, because this difference in PES and PES-MWCNT membrane morphology was also observed in the flat sheet membranes that were phase-inverted in 70 wt.% NMP in deionized water. These (flat sheet) membranes retained a porous surface layer despite the small macrovoid formation, so the practical effect of the macrovoids on the membrane properties was considered to be negligible.

4.3.3.1 Effect of Filler Loading on PES-MWCNT Mixed Matrix HFM Permselectivity

In Chapter 3, the permeation properties of flat sheet PES-MWCNT mixed matrix membranes were examined at various MWCNT loadings. Through those experiments, it was concluded that the MWCNTs suppressed the formation of pinhole defects possibly by entangling with the polymer chains during phase inversion. Analogous transport experiments were conducted using hollow fiber membrane modules. Plots of the permeance and ideal selectivity of the hollow fiber membranes versus MWCNT loading for the as-spun PES-MWCNT hollow fibers are shown in Figures 4.10a and 4.10b,

respectively. The figures show the permeance values for He, CO_2, O_2, and N_2, as well as the ideal selectivity values for He/N_2, CO_2/N_2, and O_2/N_2 across hollow fiber membranes spun from dopes composed of 30 wt.% PES in NMP with nominal loadings of 0, 0.05, 0.075, 0.1, 0.2, 0.3, and 0.5 wt.% MWCNT relative to the polymer.

The addition of MWCNTs into PES hollow fiber membranes resulted in a reduction in permeance at very low MWCNT loadings. At a nominal loading of 0.1 wt.% MWCNT, the permeance of He, CO_2, and O_2 was reduced by an order of magnitude, while the permeance of N_2 saw a reduction of two orders of magnitude. This disproportionate decrease in permeance resulted in an increase in ideal selectivity that approached the literature value for PES dense film. The large reduction in permeance and accompanying increase in selectivity was consistent with a change in the dominant diffusion mechanism from Knudsen diffusion to solution diffusion; these results matched similar trends that were observed for the flat sheet PES-MWCNT membranes. As discussed in Chapter 3, the MWCNTs form an entangled network of polymer-MWCNT interphase that acts to suppress the formation of pinhole defects during phase inversion. As the MWCNT loading was increased beyond this level, poor dispersion led to the formation of MWCNT-rich and MWCNT-lean regions in the casting dope, which allowed for the reemergence of pinhole defects and the loss of dense film selectivity at higher nanotube loadings.

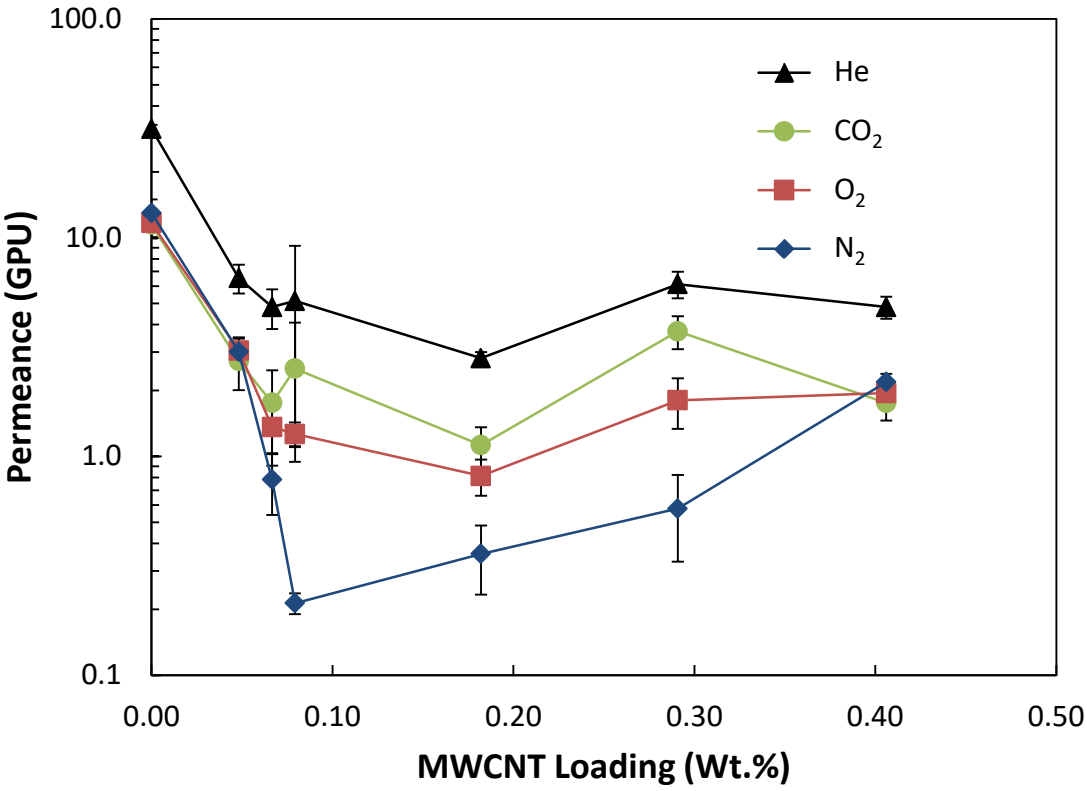

Figure 4.10a: Plot of He, CO_2, O_2, and N_2 permeance against MWCNT loading for PES-MWCNT mixed matrix hollow fiber membranes. Connecting lines provided as a guide for the eye (n = 3 for each composition).

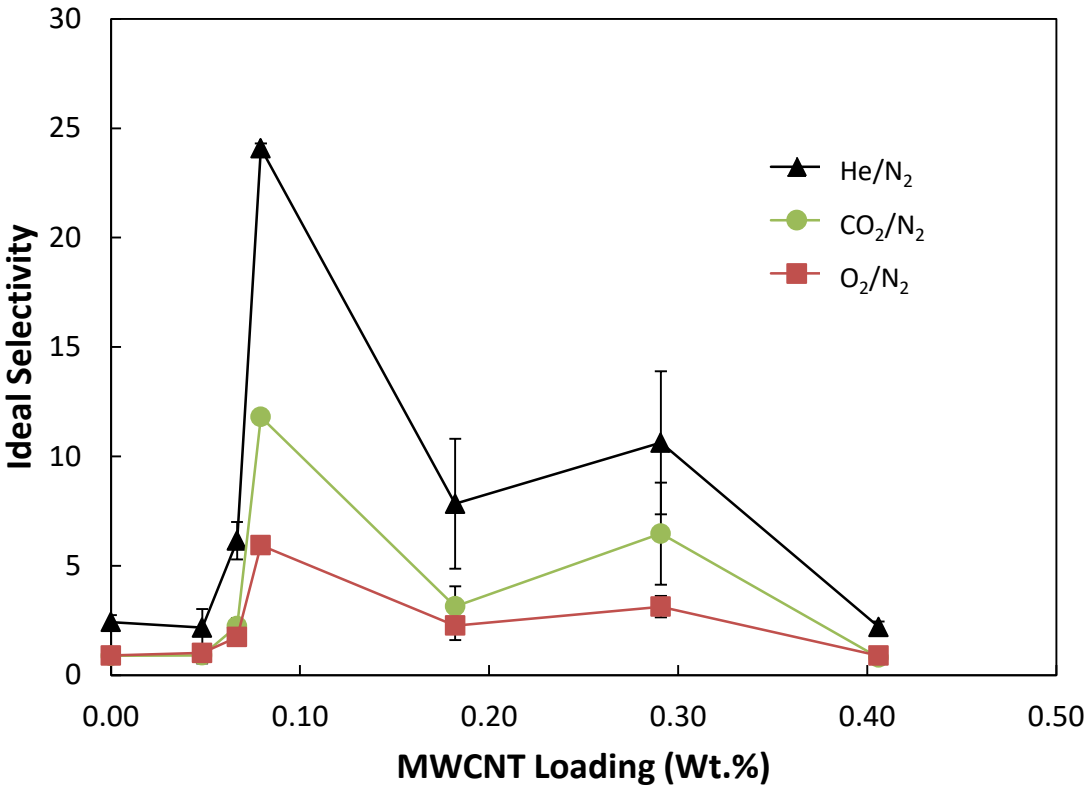

Figure 4.10b: Plot of ideal selectivity for He/N_2, CO_2/N_2, and O_2/N_2 against MWCNT loading of PES-MWCNT mixed matrix hollow fiber membranes. Connecting lines provided as a guide for the eye (n = 3 for each composition).

Table 4.5 shows a comparison of permeance results for unfilled PES (and PSf) membranes that were caulked with PDMS to PES-MWCNT mixed matrix membranes prepared at a nominal MWCNT loading of 0.1 wt.%. The table shows that PDMS caulking or adding MWCNTs at the optimum level (i.e. the loading level corresponding to the observed peak in selectivity) resulted in permeance values on the same order of magnitude. The membrane that had been prepared via PDMS caulking showed higher permeance, possibly due to the presence of a thinner dense separating layer, as well as the potential influence of tortuosity on diffusion in the mixed matrix membrane. More importantly, the O_2/N_2 ideal selectivity for both cases approached the literature value for dense film selectivity. The fact that both membrane preparations independently produced the same effects in terms of permeance and ideal selectivity of these membranes further supports the hypothesis that the MWCNTs improve the selectivity of the membranes by preventing the formation of pinhole defects in the dense separating layer.

Table 4.5: O_2/N_2 transport properties for MWCNT-loaded hollow fiber membranes as compared to unfilled caulked membranes.

Material	P/l (N_2) (GPU)	P/l (O_2) (GPU)	α(O_2/N_2)
PES-PDMS-HFM	0.56 ± 0.02	2.73 ± 0.15	4.87 ± 0.40
PSf-PDMS-HFM	0.68 ± 0.05	3.01 ± 0.12	4.43 ± 0.21
PES-0.1 wt.% MWCNT-HFM*	0.21 ± 0.12	1.27 ± 0.16	5.93 ± 0.24
PSf-0.1 wt.% MWCNT-HFM†	0.25 ± 0.08	1.24 ± 0.12	4.78 ± 0.22

***Actual composition is 0.079 wt.%**
†Actual composition is 0.085 wt%

Figures 4.11a and 4.11b show the permeance and ideal selectivity, respectively, versus MWCNT loading for PES-MWCNT hollow fiber membranes that were caulked with PDMS. Figure 4.11a showed a decrease in the permeance of all measured gases as MWCNT loading was increased. This decrease, however, was not accompanied by a net increase in the ideal selectivity, Figure 4.11b, of any of the measured gas pairs. Instead, as the MWCNT loading was increased, the ideal selectivity of the membrane stayed approximately constant near the dense film selectivity of the membrane. This lack of change in selectivity reaffirmed the hypothesis that the MWCNTs improved the selectivity of the as-spun membranes through the suppression of pinhole defects. At MWCNT loadings that were lower or higher than the "optimum" MWCNT loading that was observed at 0.1 wt.%, the PDMS caulk acted to repair the pinhole defects that formed in the MWCNT-lean regions of the dense separating layer. These MWCNT-lean regions were formed at low MWCNT loadings due to MWCNTs being spaced too far apart to form an entangled network, and at high MWCNT loadings due to inhomogeneous dispersion, as was previously discussed in Chapter 3. It is also notable that a local minimum in membrane permeance is evident at a nominal loading of 0.1 wt.% MWCNT. This is most likely caused by an increase in tortuosity in the membrane, which results from the homogeneous dispersion of MWCNTs at this loading.

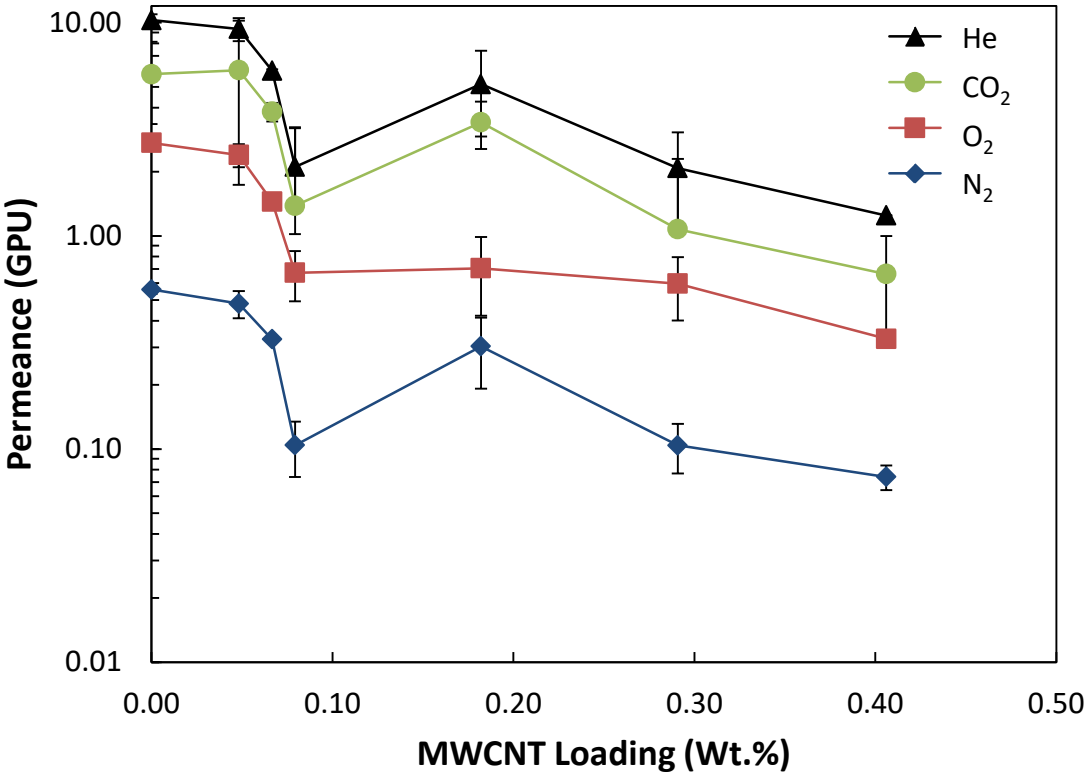

Figure 4.11a: Plot of He, CO_2, O_2, and N_2 permeance against MWCNT loading for PDMS caulked PES-MWCNT mixed matrix hollow fiber membranes. Connecting lines provided as a guide for the eye (n = 3 for each composition).

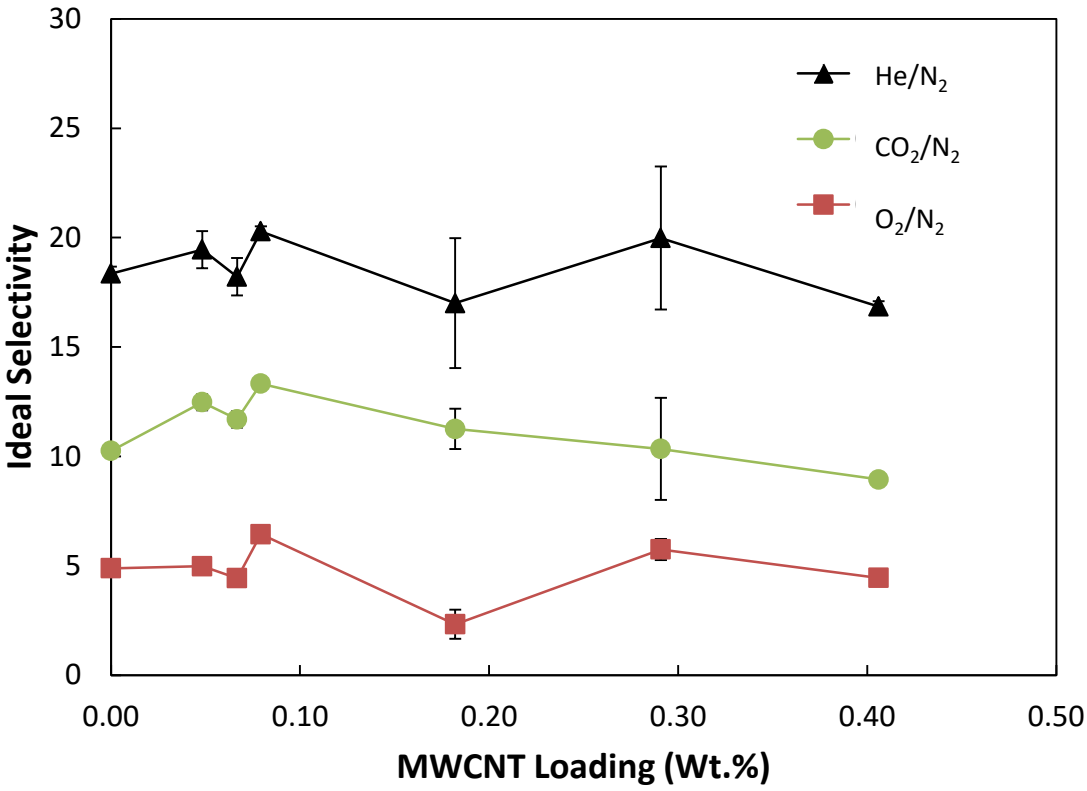

Figure 4.11b: Plot of He/N_2, CO_2/N_2, and O_2/N_2 ideal selectivity against MWCNT loading for PDMS caulked PES-MWCNT mixed matrix hollow fiber membranes. Connecting lines provided as a guide for the eye (n = 3 for each composition).

Table 4.6 shows a full comparison between flat sheet and hollow fiber membranes for MWCNT-loaded PES and PSf membranes, both with and without PDMS caulking. All samples showed very similar O_2/N_2 ideal selectivity values in both the flat sheet and hollow fiber geometries, and all approach the literature value for ideal selectivity of a dense film membrane. The measured gas permeance was found to be higher in hollow fiber membranes but on the same order of magnitude of the flat sheets, which was consistent with previous membranes that were discussed in this chapter. The small differences in the gas permeance of these membranes is most likely due to small differences in the thickness of the dense separating layer of the membrane, since the dominant diffusion mechanism in all of these membranes was solution-diffusion.

Table 4.6: O_2/N_2 transport properties for MWCNT-loaded flat sheet and hollow fiber membranes with and without PDMS caulking.

Material	P/l (N_2) (GPU)	P/l (O_2) (GPU)	α(O_2/N_2)
PES-0.1 wt.% MWCNT-HFM*	0.21 ± 0.12	1.27 ± 0.16	5.93 ± 0.24
PSf-0.1 wt.% MWCNT-HFM†	0.25 ± 0.08	1.24 ± 0.12	4.78 ± 0.22
PES-0.1 wt.% MWCNT-PDMS-HFM*	0.10 ± 0.04	0.67 ± 0.21	6.40 ± 0.23
PSf-0.1 wt.% MWCNT-PDMS-HFM†	0.17 ± 0.01	0.87 ± 0.23	5.11 ± 0.21
PES-0.1 wt.% MWCNT-FS‡	0.08 ± 0.03	0.44 ± 0.11	5.73 ± 0.89
PSf-0.1 wt.% MWCNT-FS•	0.21 ± 0.07	1.04 ± 0.13	4.89 ± 0.74
PES-0.1 wt.% MWCNT-PDMS-FS‡	0.03 ± 0.01	0.20 ± 0.06	6.72 ± 0.28
PSf-0.1 wt.% MWCNT-PDMS-FS•	0.07 ± 0.03	0.39 ± 0.11	5.58 ± 0.20

***Actual composition is 0.079 wt.%**
†Actual composition is 0.085 wt.%
‡Actual composition is 0.091 wt.%
•Actual composition is 0.089 wt.%

The measured similarities in permeance and ideal selectivity for the flat sheet and hollow fiber membrane preparations reflect the close correspondence in formulation and casting conditions that was maintained for both membrane geometries. The ability to directly translate the gas transport properties of flat sheet membrane coupons to hollow fiber membrane modules is very important to the development of future membrane-based gas separation systems. Flat sheet membrane coupons can be prepared more quickly and easily than hollow fiber membranes, so they allow efficient experimentation as a basis to identify membrane formulations and processing strategies that lead to useful gas separation properties, which can then be translated into the hollow fiber geometry.

4.3.3.2 Effect of Filler Loading on PES-Carbon Black Mixed Matrix HFM Permselectivity

The effect of using carbon black as the inorganic filler was also studied for the PES hollow fibers. This was done in order to compare and contrast its influence on the permeance and selectivity of the membranes with that of the MWCNTs. The hollow fibers that were tested in these experiments were spun from dopes that were prepared using the procedure described in Section 2.3.2.1, with the processing parameters shown in Table 4.3. A comparison of the permeance of N_2 and O_2 as well as the O_2/N_2 ideal selectivity for unfilled PES and PES with 0.1 wt.% carbon black in both flat sheet coupons and hollow fiber membranes is provided in Table 4.7.

Table 4.7: Comparison of the permeance of N_2 and O_2 and O_2/N_2 selectivity for PES filled with carbon black versus the unfilled PES membrane.

Material	P/l (N_2) (GPU)	P/l (O_2) (GPU)	$\alpha(O_2/N_2)$
PES-Flat Sheet	23.4 ± 0.21	20.8 ± 0.16	0.89 ± 0.04
PES-0.1Carbon Black-FS‡	0.66 ± 0.12	0.52 ± 0.07	0.80 ± 0.02
PES-HFM	12.95 ± 2.0	11.67 ± 1.7	0.90 ± 0.05
PES-Carbon Black-HFM*	1.51 ± 0.20	1.21 ± 0.11	0.80 ± 0.05

***Actual composition is 0.089 wt%**
‡Actual composition is 0.091 wt.%

As discussed previously, the flat sheet unfilled membrane showed a higher permeance compared to that of the hollow fiber membrane, although both membranes showed selectivity consistent with Knudsen diffusion dominating in the dense selective layer. As noted in Chapter 3, regarding PES and PSf flat sheet membranes loaded with carbon black, the large reduction in permeance that is observed with no improvement in ideal selectivity is likely a reflection of the low aspect ratio of the carbon black particles (average particle size = 45 nm). It is hypothesized that they did not effectively entangle with the polymer chains, and did not prevent the formation of pinhole defects, as was observed with PES-MWCNT mixed matrix membranes. The carbon black particles reduced the permeance of the membrane simply by obstructing the gas flow through the pinhole defects to some extent. Therefore, Knudsen diffusion still predominated through the pinhole defects that remained open or only partially obstructed, but overall flow was reduced, since the primary driver of permeance in Knudsen diffusion is the number density of channels available for diffusion.

A comparison of the permeance of N_2 and O_2 and the ideal selectivity of the gas pair between PES and PES filled with 0.1 wt.% carbon black after PDMS caulking is reported in Table 4.8. The membranes presented in this table were produced using the same dope preparation, spinning procedures, and PDMS caulking method as all previous hollow fiber membranes.

Table 4.8: Comparison of the permeance of N_2 and O_2 and O_2/N_2 selectivity of caulked PES hollow fibers filled with 0.1 wt.% carbon black to that of the unfilled membrane.

Material	P/l (N_2) (GPU)	P/l (O_2) (GPU)	α(O_2/N_2)
PES-HFM	12.95 ± 2.0	11.67 ± 1.7	0.90 ± 0.05
PES-PDMS-HFM	0.56 ± 0.02	2.73 ± 0.15	4.87 ± 0.40
PES-Carbon Black-HFM*	1.51 ± 0.20	1.21 ± 0.11	0.80 ± 0.05
PES-PDMS-Carbon Black-HFM*	0.081 ± 0.22	0.445 ± 0.38	5.50 ± 0.14

***Actual composition is 0.089 wt.%**

After PES carbon black hollow fibers were caulked with PDMS, a further substantial decrease in the permeance of both N_2 and O_2 was observed. This was accompanied by an increase in the ideal selectivity of the membranes from 0.80, which reflects Knudsen diffusion through pinhole defects, to 5.50, which approaches the dense film value for PES[13]. This is consistent with all previous results herein concerning PES-carbon black mixed matrix membranes. Since the reduction in permeance with the addition of carbon black was due to the partial obstruction of pinhole defects, rather than the prevention of their formation, Knudsen diffusion still predominated. However, after PDMS caulking was applied to these membranes, the pinhole defects were repaired, resulting in a shift

to solution-diffusion transport that produced both a further reduction in permeance and an increase in selectivity to inherent (dense film) levels.

4.4 Conclusions

A bench-scale, hollow fiber spinning system was designed, fabricated and commissioned at the University of Kentucky Center for Applied Energy Research. Through literature review and consideration of best practices, several processing parameters were identified as having key influence over the hollow fiber membrane dimensions and morphology. These processing parameters included the composition and relative flowrates of both the HFM spinning dope and the bore fluid, the vertical air gap distance between the spinneret and the coagulation bath, and the ratio of the take-up velocity to the dope extrusion velocity (i.e. draw down ratio).

Appropriate hollow fiber membrane spinning dope and bore fluid compositions were chosen based on flat sheet membrane morphology studies that were reported in Chapter 3 of this work. In the current chapter, experiments were conducted in order to further understand the influence of key processing parameters on the dimensions and morphology of the hollow fiber membranes. These experiments were used to develop a set of controlled processing parameters to consistently produce hollow fiber membranes with a dense outer separating layer, short macrovoids, a sponge-like porous substructure, and a porous wall on the lumen side of the fiber.

In addition to establishing key relationships between process parameters and the morphological character of the resulting hollow fibers, experiments were conducted to

measure the gas transport properties of these membranes in the hollow fiber geometry. These permeation experiments were conducted to first establish a baseline of gas separation performance for the unfilled membranes, and then to examine the influence of inorganic filler loading on the permeance and selectivity of the PES and PSf membranes. The primary objective of these studies was to determine if the effects that were observed in Chapter 3 for asymmetric flat sheet membrane coupons could be extended to the hollow fiber geometry.

The addition of MWCNTs into a polymeric matrix at low loading increased the ideal selectivity of the membrane to approach that of the literature value for a dense polymer film. Coincident with this increase in the ideal selectivity was a decrease in the gas permeance of the membrane. The increase in selectivity suggested that the MWCNTs acted to suppress the formation of pinhole defects in the membrane by entangling with the polymer chains to form a physical network of MWCNT-polymer interphase. In doing so, the MWCNTs produced the same essential effect as PDMS caulking. This outcome was also critical in the sense that it demonstrated the ability to directly translate the results that were observed for the flat sheet coupons in Chapter 3. This was enabled by the flat sheet membrane casting experiments being conducted specifically with an eye toward future hollow fiber membrane spinning. The relatively straightforward scale up to hollow fibers was critical not only for the results presented in this work, but also to the development of future gas separation membranes, since flat sheet membranes provide the possibility of more rapid investigation into potentially interesting membrane formulations.

The incorporation of carbon black into the PES membrane was also examined, in order to assess the generality of the outcomes observed with the introduction of low levels of MWCNTs. Once again, carbon black reduced the permeance of all gases, but did not result in an improvement in gas pair selectivity, apparently owing to the lower aspect ratio of the carbon black particles. It is likely that the lower aspect ratio of the carbon black particles (as compared to that of the carbon nanotubes) did not produce the requisite entanglement between the filler and the polymer chains needed for pinhole defect suppression during membrane casting. Instead, the carbon black particles apparently reduced the permeance of the membrane by obstructing the pinhole defects, rather than suppressing their formation.

The observation that a dispersion of multiwall carbon nanotubes in a polymeric membrane matrix suppressed the formation of pinhole defects is the first of its kind. It is also important to note that this effect was observed in both flat sheet membrane coupons as well as hollow fiber membrane modules. The membrane fabrication process still requires further optimization with regard to the thickness of the dense separating layer of the membrane, as the permeance of the membranes presented in this work was significantly lower than what is considered necessary for commercially viable membranes. However, the ability to achieve what is essentially the same state as is typically accomplished with PDMS caulking could lead to advancements in hollow fiber membrane processing. Currently, when polymeric hollow fiber membrane modules are manufactured, the PDMS caulking is conducted on each membrane module individually in a separate and time-intensive post-processing step. The suppression of pinhole

surface defect formation via the incorporation of low levels of MWCNT's offers a route by which to eliminate this separate caulking step, thereby rendering membrane module fabrication more efficient and less costly.

4.5 References

1. Peng, N., Widjojo, N., Sukitpaneenit, P., Teoh, M. M., Lipscomb, G. G., Chung, T. S., Lai, J. Y., *Evolution of polymeric hollow fibers as sustainable technologies: Past, present, and future.* Progress in Polymer Science, 2012. **37**(10): p. 1401-1424.
2. Chen, C.-C., W. Qiu, S.J. Miller, and W.J. Koros, *Plasticization-resistant hollow fiber membranes for CO_2/CH_4 separation based on a thermally crosslinkable polyimide.* Journal of Membrane Science, 2011. **382**(1-2): p. 212-221.
3. Chung, T.S., Hu, X. D., *Effect of air-gap distance on the morphology and thermal properties of polyethersulfone hollow fibers.* Journal of Applied Polymer Science, 1997. **66**(6): p. 1067-1077.
4. Chung, T.S., Kafchinski, E. R., *The effects of spinning conditions on asymmetric 6FDA/6FDAM polyimide hollow fibers for air separation.* Journal of Applied Polymer Science, 1997. **65**(8): p. 1555-1569.
5. Chung, T.S., Z.L. Xu, and W.H. Lin, *Fundamental understanding of the effect of air-gap distance on the fabrication of hollow fiber membranes.* Journal of Applied Polymer Science, 1999. **72**(3): p. 379-395.
6. Peng, N., Chung, T. S., *The effects of spinneret dimension and hollow fiber dimension on gas separation performance of ultra-thin defect-free Torlon® hollow fiber membranes.* Journal of Membrane Science, 2008. **310**(1-2): p. 455-465.
7. Chung, T.S., E.R. Kafchinski, and P. Foley, *Development of asymmetric hollow fibers from polyimides for air separation.* Journal of Membrane Science, 1992. **75**(1-2): p. 181-195.
8. Cao, C., Chung, Tai-Shung, Chen, Shing Bor, Dong, ZhengJun, *The study of elongation and shear rates in spinning process and its effect on gas separation performance of Poly(ether sulfone) (PES) hollow fiber membranes.* Chemical Engineering Science, 2004. **59**(5): p. 1053-1062.
9. Chung, T.S. and S.K. Teoh, *The ageing phenomenon of polyethersulphone hollow fibre membranes for gas separation and their characteristics.* Journal of Membrane Science, 1999. **152**(2): p. 175-188.
10. Chung, T.S., S.K. Teoh, and X.D. Hu, *Formation of ultrathin high-performance polyethersulfone hollow-fiber membranes.* Journal of Membrane Science, 1997. **133**(2): p. 161-175.
11. Li, Y., C. Cao, T.-S. Chung, and K.P. Pramoda, *Fabrication of dual-layer polyethersulfone (PES) hollow fiber membranes with an ultrathin dense-selective layer for gas separation.* Journal of Membrane Science, 2004. **245**(1-2): p. 53-60.
12. Qin, J.J., Gu, J., Chung, T. S., *Effect of wet and dry-jet wet spinning on the sheer-induced orientation during the formation of ultrafiltration hollow fiber membranes.* Journal of Membrane Science, 2001. **182**(1-2): p. 57-75.

13. Baker, R.W., Beckman, I. N., Cussler, E. L., Doshi, K, Henis, J. M. S., Koros, W. J., Nakagawa, T., Paul, D. R., Petropoulos, J. H., Pinnau, I., Pixton, M. R., Plate, N, Prasad, R., Shaner, R. L., Wijmans, J. G., Yampolskii, Y. P., *Polymeric Gas Separation Membranes*. 1994: CRC Press Inc.
14. Singh, A., Freeman, B. D., Pinnau, I., *Pure and mixed gas acetone/nitrogen permeation properties of polydimethylsiloxane PDMS.* Journal of Polymer Science Part B-Polymer Physics, 1998. **36**(2): p. 289-301.
15. Clausi, D.T. and W.J. Koros, *Formation of defect-free polyimide hollow fiber membranes for gas separations.* Journal of Membrane Science, 2000. **167**(1): p. 79-89.
16. Li, F.Y., Y. Li, T.-S. Chung, H. Chen, Y.C. Jean, and S. Kawi, *Development and positron annihilation spectroscopy (PAS) characterization of polyamide imide (PAI)–polyethersulfone (PES) based defect-free dual-layer hollow fiber membranes with an ultrathin dense-selective layer for gas separation.* Journal of Membrane Science, 2011. **378**(1-2): p. 541-550.
17. Li, Y., Chung, T. S., Xiao, Y., *Superior gas separation performance of dual-layer hollow fiber membranes with an ultrathin dense-selective layer.* Journal of Membrane Science, 2008. **325**(1): p. 23-27.
18. Chung, T., Teoh, S. K., Hu, X. D., *Formation of ultrathin high-performance polyethersulfone hollow-fiber membranes.* Journal of Membrane Science, 1997. **133**: p. 161-175.
19. Lipscomb, G.G.L., Personal Communication, 2018.

Chapter 5: Conclusions and Future Work

5.1 Conclusions

Over the course of the work presented in this dissertation, the four primary objectives that were described in Section 1.4 were executed. These four objectives consisted of (i) the design, fabrication, and commissioning of a hollow fiber membrane spinning line, (ii) the use of flat sheet membrane experiments to determine appropriate dope and bore fluid compositions for hollow fiber spinning, (iii) the variation of HFM processing parameters in order to examine their influence on the dimensions and morphology of the produced fibers and to establish a set of standard operating conditions, and (iv) the investigation of nanoscale filler incorporation on membrane permeance and selectivity in both the flat sheet and hollow fiber geometries. The conclusions that emerged from these experiments are summarized in the following section. In addition, the experimental results led to a number of interesting research questions for further investigation; these questions are discussed below.

5.1.1 Flat Sheet Membranes

Asymmetric flat sheet membranes were cast using non-solvent induced phase inversion in order to study the influence of dope composition and coagulation medium on the membrane morphology. These experiments were conducted to assess the phase-inversion dynamics and establish appropriate conditions for flat sheet casting and hollow fiber spinning. It was determined that dope solution compositions of 30 wt.% polyethersulfone (PES) and 35 wt.% polysulfone (PSf) in N-methylpyrrolidone (NMP) were appropriate for flat sheet and hollow fiber membrane fabrication, based on the

relatively low viscosity of the casting dope and the characteristics of the membrane morphology that was produced. Additionally, experiments were conducted using various coagulation bath formulations in order to determine appropriate compositions for the internal and external coagulants employed during hollow fiber membrane spinning. It was established that deionized water would be used for all flat sheet membrane preparations (re: mixed-matrix membranes and gas permeation studies), and as the external coagulant for hollow fiber membrane spinning. This selection was based on both the membrane morphology that was obtained, as well as the practical considerations of maintaining a large external coagulation bath for hollow fiber spinning. The flat sheet experiments also informed the determination of the bore fluid composition used for hollow fiber membrane spinning. Specifically, solvent-rich bore fluid compositions were identified as needed to achieve the desired morphological properties in the resulting hollow fiber membranes: 70 wt.% NMP in water for PES, and 75 wt.% NMP in water for PSf. These bore fluid compositions resulted in flat sheet membranes that contained no macrovoids and displayed large surface pores at the coagulation interface that were caused by the breakthrough of the porous support layer of the membrane during phase inversion. In most cases, this is the desired topology for the lumen surface of a hollow fiber membrane.

Multiwall carbon nanotubes (MWCNTs) were dispersed in PES and PSf casting dopes at low loadings in order to examine their influence on the morphology and gas permeation properties of the resulting phase inversion membranes. Low loadings of MWCNTs were found to induce relatively little change in the morphology of the

membranes as compared to the unfilled casting system, with the presence of the tubes leading to slightly longer and more pronounced macrovoids. A nominal loading of 0.1 wt.% MWCNT relative to the polymer resulted in a marked decrease in the permeance of the resulting membrane and an O_2/N_2 selectivity that approached the literature value for a dense polymer film. These two effects suggested that the presence of the MWCNTs suppressed the formation of pinhole defects in the dense separating layer of the membrane during phase inversion. This is a phenomenon that has not previously been reported in the membrane literature. Further experiments were conducted with PES membranes containing a dispersion of nanoscale carbon black as the filler. The inclusion of carbon black resulted in a similarly large decrease in the permeance of the membrane, but with no observed increase in ideal selectivity across the same range of loading levels. It was hypothesized that the large aspect ratio of the MWCNTs caused them to entangle with the polymer chains, forming a network of polymer-MWCNT interphase which suppressed the formation of pinhole defects during membrane solidification.

The observed effect, that a low loading of well-dispersed MWCNTs suppresses the formation of pinhole defects in asymmetric gas separation membranes, is the first of its kind. This discovery is important in the context of industrial gas separation membrane fabrication, as the ability to form a defect-free asymmetric membrane could result in the elimination of the PDMS caulking step typically required during the preparation of membrane modules. This is notable because during commercial membrane manufacturing, PDMS caulking is necessarily performed on individual

modules. The ability to directly produce defect-free asymmetric membranes has the potential to significantly simplify the module manufacturing process by eliminating this time-consuming step.

5.1.2 Hollow Fiber Membranes

A bench-scale, hollow fiber membrane spinning system was designed, fabricated and commissioned at the University of Kentucky. A set of key processing parameters were identified as having primary influence over the dimensions and morphology of the hollow fiber membranes. These processing parameters included the relative flowrates of the dope and bore fluid, the vertical air gap distance between the spinneret and the coagulation bath, and the ratio of the take-up velocity to the dope velocity at the die (i.e. draw down ratio). The hollow fiber spinning system was designed to allow systematic and controlled variation of these processing parameters in order to assess their impact on the resulting fiber dimensions and morphology. The results of the flat sheet membrane studies were used to determine the dope composition, external coagulation bath and bore fluid formulations that were used in the hollow fiber membrane spinning experiments.

The effect of adding a dispersion of MWCNTs into the fiber spinning dope was examined in order to determine if the pinhole suppression that was encountered in the flat sheet experiments would also be observed in the hollow fiber membrane geometry. This was accomplished by first establishing baseline permeation properties for unfilled PES and PSf hollow fiber membranes, each with and without PDMS caulking. Both the PES and PSf hollow fiber membranes showed high permeance and gas pair selectivities

that reflected Knudsen diffusion through pinhole defects prior to PDMS caulking. The introduction of the PDMS coating led to a strong decrease in permeance (consistent with filling of the pinholes), and the recovery of ideal selectivity values approaching those of the dense polymer.

The transport properties of the unfilled membranes were compared to membranes with a range of MWCNT loadings. The addition of MWCNTs at a nominal loading of 0.1 wt.% showed a large decrease in permeance, coincident with a restoration of the dense film selectivity, similar to the results that were obtained with flat sheet membranes. This effect was not observed when incorporating a dispersion of carbon black into the membrane matrix. Here again, these results suggested that the MWCNTs suppressed the emergence of pinhole defects by entangling with the polymer chains, thereby constraining the opening of surface gaps as the membrane solidified from solution.

The observation that low level incorporation of MWCNTs can suppress the formation of pinhole surface defects in hollow fiber membranes has not previously been reported. In terms of the hollow fiber membranes produced in this study, the spinning process requires further optimization in order to fully exploit this outcome. In particular, it would be necessary to refine the spinning conditions to reduce the thickness of the dense separating layer, as both the flat sheet and hollow fiber membranes produced in this work showed permeance values that were significantly lower than what is required for viable commercial use. As noted above, the introduction

of MWCNTs to directly suppress the formation of pinhole defects and achieve dense film selectivity could lead to important efficiencies in hollow fiber membrane manufacture by eliminating the time-consuming process of (PDMS) membrane caulking during module fabrication.

5.2 Future Work

The observation that multiwall carbon nanotubes suppress the formation of pinhole defects may be novel, but further research will be required to develop the membranes that were produced in this work into viable commercial membranes. Some of this future work involves the optimization of the processing parameters employed during hollow fiber membrane spinning to enable the formation of a thinner dense separating layer while maintaining overall membrane integrity. There is also the potential research that can be conducted using the processing and testing apparatus that were constructed in this work. Research possibilities include the study of a wider range of matrix polymers and nanoscale filler elements than those that were discussed here.

Additionally, the observation that MWCNTs suppress the formation of pinhole defects in PES and PSf has prompted several other questions surrounding the exact mechanism responsible for this effect as well as the enhancement of gas selectivity that is achievable via the inclusion of MWCNTs. Future experiments should be conducted in order to further probe the influence of aspect ratio and chemical compatibility of the filler in an attempt to validate the hypothesis that was proposed herein with respect to the mechanism by which MWCNTs suppress the formation of pinhole defects. One

approach that could be used to probe the influence of the filler aspect ratio would be to progressively decrease the aspect ratio of the MWCNTs in the dispersion using shatter milling. With this technique, one may render the MWCNT aspect ratio to near that of carbon black (using sufficiently energetic and long milling). This method would provide a CNT analogue comparable to carbon black, but with physical and chemical surface characteristics consistent with the MWCNTs.

Another potential experiment would be to investigate a mixed matrix membrane system based on a different inorganic filler material (with a similar aspect ratio to the MWCNTs), in order to explore the influence of chemical compatibility between the inorganic filler and the polymeric matrix on membrane performance. A potential filler candidate that could be used to probe the influence of chemical compatibility in these membranes is TiO_2 nanotubes. TiO_2 nanotubes have a similar shape to carbon nanotubes as well as a comparable aspect ratio, but are different in terms of chemical composition. For example, TiO_2 nanotubes tend to be hydrophilic, and would require surface treatment to make them compatible with a hydrophobic polymer such as PES. If the aspect ratio is a key to suppressing pinholes, the incorporation of TiO_2 nanotubes with similar aspect ratios should yield similar results. It is also possible that the suppression of pinhole defects was not the only mechanism at play in producing enhanced selectivity. Specifically, in the PES/MWCNT membranes that were caulked with PDMS (0.1 wt.% MWCNT), O_2/N_2 selectivities were achieved that were approximately 25% higher as compared to the dense film selectivity of the polymer.

This suggests that the MWCNTs serve an added separation function, beyond the suppression of pinhole defects.

An additional mechanism that could be operative in the mixed matrix membranes is molecular sieving through the interlayer spacing of the MWCNTs. This mechanism has been suggested as a means by which MWCNTs can improve the selectivity of PES mixed matrix membranes. The addition of MWCNTs into a flat sheet PES matrix that had been caulked with PDMS has been previously demonstrated by other investigators to result in an O_2/N_2 ideal selectivity of approximately 10, as discussed in Chapter 3. One key difference in these earlier studies was the use of acid purification and functionalization of the nanotubes prior to membrane casting in order to better facilitate their adhesion into the PES matrix, while the experiments conducted in this dissertation employed pristine nanotubes. Using surface-modified MWCNTs could allow for better dispersion at higher loadings, potentially extending the pinhole suppression effect while simultaneously introducing a greater contribution from molecular sieving through the interlayer spacing of the MWCNTs.

One final research question that remains after the completion of this work is whether or not the pinhole defect suppression observed with MWCNTs extends to polymers beyond the polysulfone family. The research reported here definitively showed that the formation of pinhole defects could be suppressed during polyethersulfone phase inversion by adding a dispersion of multiwall carbon nanotubes at low loading. These results were found to apply to polysulfone as well. It remains to be

seen if this effect extends to polymers that are not a part of the polysulfone family. A key consideration in this context is the chemical compatibility of the dispersed nanotubes with the surrounding polymer matrix. Since MWCNTs are hydrophobic, using a hydrophobic polymer (e.g. PES or PSf) may also be necessary; this includes common membrane polymers such as polyetherimide (PEI) and Matrimid®. Such a requirement would presumably eliminate hydrophilic membrane polymers as candidates, for example polyvinyl alcohol (PVA) or blends containing polyvinylpyrrolidone (PVP). Additionally, polymers such as thermally rearranged polybenzoxazole (PBO) and polymers of intrinsic microporosity could be examined, but may not benefit from incorporation of MWCNTs, because their effectiveness as membranes is dependent upon a particular structure within the dense separating layer. This structure could potentially be disrupted by the inclusion of MWCNTs. The ability to generalize the benefit of incorporating a dispersion of MWCNTs to a wide range of polymeric materials is crucial to its future application in both industrial and academic membrane research.

Bibliography

Adams, R., Carson, Cantwell, Ward, Jason, Tannenbaum, Rina, Koros, William, *Metal organic framework mixed matrix membranes for gas separations.* Microporous and Mesoporous Materials, 2010. **131**(1-3): p. 13-20.

Ahn, J., Chung, Wook-Jin, Pinnau, Ingo, Guiver, Michael D., *Poly sulfone/silica nanoparticle mixed-matrix membranes for gas separation.* Journal of Membrane Science, 2008. **314**(1-2): p. 123-133.

Andrews, R., Jacques, D., Qian, D. L., Rantell, T., *Multiwall carbon nanotubes: Synthesis and application.* Accounts of Chemical Research, 2002. **35**(12): p. 1008-1017.

Aroon, M.A., Ismail, A. F., Matsuura, T., Montazer-Rahmati, M. M., *Performance studies of mixed matrix membranes for gas separation: A review.* Separation and Purification Technology, 2010. **75**(3): p. 229-242.

Baker, R.W., Beckman, I. N., Cussler, E. L., Doshi, K, Henis, J. M. S., Koros, W. J., Nakagawa, T., Paul, D. R., Petropoulos, J. H., Pinnau, I., Pixton, M. R., Plate, N, Prasad, R., Shaner, R. L., Wijmans, J. G., Yampolskii, Y. P., *Polymeric Gas Separation Membranes*. 1994: CRC Press Inc.

Bindal, R.C., Hanra, M. S., Misra, B. M., *Novel solvent exchange cum immersion precipitation technique for the preparation of asymmetric polymeric membrane.* Journal of Membrane Science, 1996. **118**(1): p. 23-29.

Boroglu, M.S., Gurkaynak, Mehmet Ali, *Fabrication and characterization of silica modified polyimide-zeolite mixed matrix membranes for gas separation properties.* Polymer Bulletin, 2011. **66**(4): p. 463-478.

Budd, P.M., Ghanem, B. S., Makhseed, S., McKeown, N. B., Msayib, K. J., Tattershall, C. E., *Polymers of intrinsic microporosity (PIMs): robust, solution-processable, organic nanoporous materials.* Chemical Communications, 2004(2): p. 230-231.

Budd, P.M., Elabas, E. S., Ghanem, B. S., Makhseed, S., McKeown, N. B., Msayib, K. J., Tattershall, C. E., Wang, D., *Solution-processed, organophilic membrane derived from a polymer of intrinsic microporosity.* Advanced Materials, 2004. **16**(5): p. 456-465.

Budd, P.M., Msayib, K. J., Tattershall, C. E., Ghanem, B. S., Reynolds, K. J., McKeown, N. B., Fritsch, D., *Gas separation membranes from polymers of intrinsic microporosity.* Journal of Membrane Science, 2005. **251**(1-2): p. 263-269.

Calle, M., Lee, Y. M., *Thermally Rearranged (TR) Poly(ether-benzoxazole) Membranes for Gas Separation.* Macromolecules, 2011. **44**(5): p. 1156-1165.

Cao, C., Chung, Tai-Shung, Chen, Shing Bor, Dong, ZhengJun, *The study of elongation and shear rates in spinning process and its effect on gas separation performance of Poly(ether sulfone) (PES) hollow fiber membranes.* Chemical Engineering Science, 2004. **59**(5): p. 1053-1062.

Caro, J., Noack, M., *Zeolite membranes - Recent developments and progress.* Microporous and Mesoporous Materials, 2008. **115**(3): p. 215-233.

Chen, C.C., Qiu, W. L., Miller, S. J., Koros, W. J., *Plasticization-resistant hollow fiber membranes for CO_2/CH_4 separation based on a thermally crosslinkable polyimide.* Journal of Membrane Science, 2011. **382**(1-2): p. 212-221.

Chung, T., Kafchinski, E. R., Foley, P., *Development of asymmetric hollow fibers from polyimides for air separation.* Journal of Membrane Science, 1992. **75**: p. 181-195.

Chung, T., Kafchinski, E. R., Vora, R., *Development of a defect-free 6FDA-durene asymmetric hollow fiber and its composite hollow fibers.* journal of Membrane Science, 1994. **88**: p. 21-36.

Chung, T., Kafchinski, E. R., *Aging Phenomenon of 6FDA-Polyimide/Polyacrylonitrile Composite Hollow Fibers.* Journal of Applied Polymer Science, 1996. **59**: p. 77-82.
Chung, T., Teo, S.K, Hu, X. D., *Formation of ultrathin high-performance polyethersulfone hollow-fiber membranes.* Journal of Membrane Science, 1997. **133**: p. 161-175.
Chung, T., Xu, Z. L., Lin, W. H., *Fundamental Understanding of the effect of air-gap distance on the fabrication of hollow fiber membranes.* Journal of Applied Polymer Science, 1998. **72**: p. 379-395.
Chung, T., Teoh, S. K., *The aging phenomenon of polyethersulphone hollow fibre membranes for gas separation and their characteristics.* Journal of Membrane Science, 1999. **152**: p. 175-188.
Chung, T.S., Kafchinski, E. R., *The effects of spinning conditions on asymmetric 6FDA/6FDAM polyimide hollow fibers for air separation.* Journal of Applied Polymer Science, 1997. **65**(8): p. 1555-1569.
Chung, T.S., Hu, X. D., *Effect of air-gap distance on the morphology and thermal properties of polyethersulfone hollow fibers.* Journal of Applied Polymer Science, 1997. **66**(6): p. 1067-1077.

Chung, T.S., Jiang, L. Y., Li, Y., Kulprathipanja, S., *Mixed matrix membranes (MMMs) comprising organic polymers with dispersed inorganic fillers for gas separation.* Progress in Polymer Science, 2007. **32**(4): p. 483-507.
Clausi, D.T., Koros, W. J., *Formation of defect-free polyimide hollow fiber membranes for gas separations.* Journal of Membrane Science, 2000. **167**(1): p. 79-89.
Dai, Y., Johnson, J. R., Karvan, O., Sholl, D. S., Koros, W. J., *Ultem®/ZIF-8 mixed matrix hollow fiber membranes for CO_2/N_2 separations.* Journal of Membrane Science, 2012. **401-402**: p. 76-82.
Echt, W., *Hybrid systems combining technologies leads to more efficient gas conditioning*, in *Laurance Reid Gas Conditioning Conference*. 2002: Norman, OK.
Ettouney, H., Majeed, U., *Permeability functions for pure and mixture gases in silicone rubber and polysulfone membranes: Dependence on pressure and composition.* Journal of Membrane Science, 1997. **135**(2): p. 251-261.
Galizia, M., Chi, W. S., Smith, Z. P., Merkel, T. C., Baker, R. W., Freeman, B. D., *50th Anniversary Perspective: Polymers and Mixed Matrix Membranes for Gas and Vapor Separation: A Review and Prospective Opportunities.* Macromolecules, 2017. **50**(20): p. 7809-7843.
Gantzel, P.K., Merten, U., *Gas Separations with High-Flux Cellulose Acetate Membranes.* Industrial & Engineering Chemistry Process Design and Development, 1970. **9**(2): p. 331-&.

Ghomshani, A.D., Ghaee, A., Mansourpour, Z., Esmaili, M., Sadatnia, B., *Improvement of H_2/CH_4 Separation Performance of PES Hollow Fiber Membranes by Addition of MWCNTs into Polymeric Matrix.* Polymer-Plastics Technology and Engineering, 2016. **55**(11): p. 1155-1166.

Goh, P.S., Ismail, A. F., Sanip, S. M., Ng, B. C., Aziz, M., *Recent advances of inorganic fillers in mixed matrix membrane for gas separation.* Separation and Purification Technology, 2011. **81**(3): p. 243-264.
Goh, P.S., Ng, B. C., Ismail, A. F., Sanip, S. M., Aziz, M., Kassim, M. A., *Effect of Dispersed Multi-Walled Carbon Nanotubes on Mixed Matrix Membrane for O_2/N_2 Separation.* Separation Science and Technology, 2011. **46**(8): p. 1250-1261.

Goh, P.S., Ng, B. C., Ismail, A. F., Aziz, M., Hayashi, Y., *Pre-treatment of multi-walled carbon nanotubes for polyetherimide mixed matrix hollow fiber membranes.* Journal of Colloid and Interface Science, 2012. **386**: p. 80-87.
Henis, J.M.S., Tripodi, M. K., *Composite hollow fiber membranes for gas separation - the resistance model approach.* Journal of Membrane Science, 1981. **8**(3): p. 233-246.
Hilding, J., Grulke, E. A., Zhang, Z. G., Lockwood, F., *Dispersion of carbon nanotubes in liquids.* Journal of Dispersion Science and Technology, 2003. **24**(1): p. 1-41.
Hinds, B.J., Chopra, N., Rantell, T., Andrews, R., Gavalas, V., Bachas, L. G., *Aligned multiwalled carbon nanotube membranes.* Science, 2004. **303**(5654): p. 62-65.
Husain, S., Koros, W. J., *Mixed matrix hollow fiber membranes made with modified HSSZ- 13 zeolite in polyetherimide polymer matrix for gas separation.* Journal of Membrane Science, 2007. **288**(1-2): p. 195-207.
Iijima, S., *Helical microtubules of graphitic carbon.* Nature, 1991. **354**(6348): p. 56-58.
Ismail, A.F., Goh, P. S., Sanip, S. M., Aziz, M., *Transport and separation properties of carbon nanotube-mixed matrix membrane.* Separation and Purification Technology, 2009. **70**(1): p. 12-26.
Ismail, A.F., Rahim N.H., Mustafa, A, Matsuura, T, Ng, B.C., Abdullah, S., Hashemifard, S.A., *Gas Separation Performance of Polyethersulfone/Multi-Walled Carbon Nanotubes Mixed Matrix Membranes.* Separation and Purification Reviews, 2011. **80**: p. 20-31.
Ismail, A.F., Rahim, N. H., Mustafa, A., Matsuura, T., Ng, B. C., Abdullah, S., Hashemifard, S. A., *Gas separation performance of polyethersulfone/multi-walled carbon nanotubes mixed matrix membranes.* Separation and Purification Technology, 2011. **80**(1): p. 20-31.
Jawad, Z.A., Ahmad, A. L., Low, S. C., Chew, T. L., Zein, S. H. S., *Influence of solvent exchange time on mixed matrix membrane separation performance for CO_2/N_2 and a kinetic sorption study.* Journal of Membrane Science, 2015. **476**: p. 590-601.
Jomekian, A., Mansoori, S. A. A., Monirimanesh, N., Shafiee, A., *Gas transport behavior of DMDCS modified MCM-48/polysulfone mixed matrix membrane coated by PDMS.* Korean Journal of Chemical Engineering, 2011. **28**(10): p. 2069-2075.
Kemp, D.R., Paul, D. R., *Gas sorption in polymer membranes containing adsorptive fillers.* Journal of Polymer Science Part B-Polymer Physics, 1974. **12**(3): p. 485-500.
Keskin, S., Liu, J., Rankin, R. B., *Progress, Opportunities, and Challenges for Applying Atomically Detailed Modeling to Molecular Adsorption and Transport in Metal-Organic Framework Materials.* Industrial & Engineering Chemistry Research, 2009. **48**: p. 2355-2371.
Kesting, R.E., *Synthetic Polymeric Membranes: A Structural Perspective*. Second ed. Vol. 1. 1985: John Wiley & Sons, Inc. 348.
Khulbe, K.C., Feng, C., Matsuura, T., *The Art of Surface Modification of Synthetic Polymeric Membranes.* Journal of Applied Polymer Science, 2010. **115**(2): p. 855-895.
Kim, H.W., Park, H. B., *Gas diffusivity, solubility and permeability in polysulfone-poly(ethylene oxide) random copolymer membranes.* Journal of Membrane Science, 2011. **372**(1-2): p. 116-124.
Kim, S., Chen, L., Johnson, J. K., Marand, E., *Polysulfone and functionalized carbon nanotube mixed matrix membranes for gas separation: Theory and experiment.* Journal of Membrane Science, 2007. **294**(1-2): p. 147-158.
Koros, W.J., Fleming, G. K., *Membrane-based gas separation.* Journal of Membrane Science, 1993. **83**(1): p. 1-80.
Kulprathipanja, S., Neuzil, R.W., Norman, N. L., *Separation of fluids by means of mixed matrix membranes*. 1989, Honeywell International Inc: USA, US5127925A.

Kurdi, J., Tremblay, A. Y., *Preparation of defect-free asymmetric membranes for gas separations.* Journal of Applied Polymer Science, 1999. **73**(8): p. 1471-1482.
Latimer, R.E., *Distillation of air.* Chemical Engineering Progress, 1967. **63**(2): p. 35-37.
Li, F.Y., et al., *Development and positron annihilation spectroscopy (PAS) characterization of polyamide imide (PAI)–polyethersulfone (PES) based defect-free dual-layer hollow fiber membranes with an ultrathin dense-selective layer for gas separation.* Journal of Membrane Science, 2011. **378**(1-2): p. 541-550.
Li, P., H.Z. Chen, and T.S. Chung, *The effects of substrate characteristics and pre-wetting agents on PAN-PDMS composite hollow fiber membranes for CO_2/N_2 and O_2/N_2 separation.* Journal of Membrane Science, 2013. **434**: p. 18-25.
Li, Y., Chung, T. S., Cao, C., Kulprathipanja, S., *The effects of polymer chain rigidification, zeolite pore size and pore blockage on polyethersulfone (PES)-zeolite A mixed matrix membranes.* Journal of Membrane Science, 2005. **260**(1-2): p. 45-55.
Li, Y., Chung, T. S., Xiao, Y., *Superior gas separation performance of dual-layer hollow fiber membranes with an ultrathin dense-selective layer.* Journal of Membrane Science, 2008. **325**(1): p. 23-27.
Li, Y., et al., *Fabrication of dual-layer polyethersulfone (PES) hollow fiber membranes with an ultrathin dense-selective layer for gas separation.* Journal of Membrane Science, 2004. **245**(1-2): p. 53-60.
Lipscomb, G.G.L., Personal Communication, 2018.
Loeb, S., Sourirajan, S., *Sea water demineralization bymeans of a semipermeable membrane.* Advances in Chemistry, 1962. **38**: p. 117-132.
Loeb, S., McCutcha J. W, *Electrolytic additives in casting solution for cellulose acetate desalination membranes.* Industrial & Engineering Chemistry Product Research and Development, 1965. **4**(2): p. 114-118.
Madaeni, S.S., Hoseini, S., *Fabrication and characterization of PDMS coated PES membranes for separation of ethylene from nitrogen.* Journal of Polymer Research, 2009. **16**(5): p. 591-599.
Mahajan, R., Koros, W. J., *Mixed matrix membrane materials with glassy polymers. Part 2.* Polymer Engineering and Science, 2002. **42**(7): p. 1432-1441.
Mahon, H., *Permeability separatory apparatus, permeability separatory membrane element, method of making the same and process utilizing the same*. 1966, Dow Chemical Co, US3228876: USA ,US3228876.
Majumder, M., Chopra, N., Andrews, R., Hinds, B. J., *Nanoscale hydrodynamics - Enhanced flow in carbon nanotubes.* Nature, 2005. **438**(7064): p. 44-44.
Majumder, M., Chopra, N., Hinds, B. J., *Effect of tip functionalization on transport through vertically oriented carbon nanotube membranes.* Journal of the American Chemical Society, 2005. **127**(25): p. 9062-9070.
Majumder, M., Chopra, N., Hinds, B. J., *Mass Transport through Carbon Nanotube Membranes in Three Different Regimes: Ionic Diffusion and Gas and Liquid Flow.* ACS Nano, 2011. **5**(5): p. 3867-3877.
Manos, P., *Solvent drying of cellulose ester membranes*, U. Patent, Editor. 1978, DuPont: USA, US4068387.
McKeown, N.B., Budd, P. M., *Polymers of intrinsic microporosity (PIMs): organic materials for membrane separations, heterogeneous catalysis and hydrogen storage.* Chemical Society Reviews, 2006. **35**(8): p. 675-683.

Merkel, T.C., Bondar, V. I., Nagai, K., Freeman, B. D., Pinnau, I., *Gas sorption, diffusion, and permeation in poly(dimethylsiloxane).* Journal of Polymer Science Part B-Polymer Physics, 2000. **38**(3): p. 415-434.
Mitchell, J.K., *On the penetrativeness of fluids.* The Journal of the Royal Institution of Great Britain, 1831. **4**: p. 101.
Moore, T.T., Koros, W. J., *Gas sorption in polymers, molecular sieves, and mixed matrix membranes.* Journal of Applied Polymer Science, 2007. **104**(6): p. 4053-4059.
Morris, E.A., Weisenberger, M. C., Bradley, S. B., Abdallah, M. G., Mecham, S. J., Pisipati, P., McGrath, J. E., *Synthesis, spinning, and properties of very high molecular weight poly(acrylonitrile-co-methyl acrylate) for high performance precursors for carbon fiber.* Polymer, 2014. **55**(25): p. 6471-6482.
Mosqueda-Jimenez, D.B., Narbaitz, R. M., Matsuura, T., Chowdhury, G., Pleizier, G., Santerre, J. P., *Influence of processing conditions on the properties of ultrafiltration membranes.* Journal of Membrane Science, 2004. **231**(1-2): p. 209-224.
Paul, D.R., Kemp, D. R., *Diffusion time lag in polymer membranes containing adsorptive fillers.* Journal of Polymer Science Part C-Polymer Symposium, 1973(41): p. 79-93.
Peng, N., Chung, T. S., Wang, K. Y., *Macrovoid evolution and critical factors to form macrovoid-free hollow fiber membranes.* Journal of Membrane Science, 2008. **318**(1-2): 36p.-372.
Peng, N., Chung, T. S., *The effects of spinneret dimension and hollow fiber dimension on gas separation performance of ultra-thin defect-free Torlon® hollow fiber membranes.* Journal of Membrane Science, 2008. **310**(1-2): p. 455-465.
Peng, N., Chung, T. S., Lai, J. Y., *The rheology of Torlon® solutions and its role in the formation of ultra-thin defect-free Torlon® hollow fiber membranes for gas separation.* Journal of Membrane Science, 2009. **326**(2): p. 608-617.
Peng, N., Widjojo, N., Sukitpaneenit, P., Teoh, M. M., Lipscomb, G. G., Chung, T. S., Lai, J. Y., *Evolution of polymeric hollow fibers as sustainable technologies: Past, present, and future.* Progress in Polymer Science, 2012. **37**(10): p. 1401-1424.
Perez, E.V., Balkus, K. J., Ferraris, J. P., Musselman, I. H., *Mixed-matrix membranes containing MOF-5 for gas separations.* Journal of Membrane Science, 2009. **328**(1-2): p. 165-173.
Pesek, S.C., Koros, W. J., *Aqueous quenched asymmetric polysulfone hollow fibers prepared by dry/wet phase separation.* Journal of Membrane Science, 1993. **88**: p. 1-19.
Qin, J., Wang, R., Chung, T., *Investigation of shear stress effect within a spinneret on flux, separation, and thermomechanical properties of hollow fiber ultrafiltration membranes.* Journal of Membrane Science, 2000. **175**: p. 197-213.
Qin, J.J., Gu, J., Chung, T. S., *Effect of wet and dry-jet wet spinning on the sheer-induced orientation during the formation of ultrafiltration hollow fiber membranes.* Journal of Membrane Science, 2001. **182**(1-2): p. 57-75.
R. Surya Murali, T.S., and S. Sridhar, *Air Separation by Polymer-based Membrane Technology.* Separation and Purification Reviews, 2013(42): p. 130-186.
Robeson, L.M., *Correlation of separation factor versus permeability for polymeric membranes.* Journal of Membrane Science, 1991. **62**(2): p. 165-185.
Robeson, L.M., *The upper bound revisited.* Journal of Membrane Science, 2008. **320**(1- 2): p. 390-400.
S. Zeinali, M.A., *Improving O_2/N_2 Selective Filtration Using Carbon Nanotube-Modified Mixed-Matrix Membranes.* Chemical Engineering and Technology, 2015. **38**(11): p. 2079-2086.

Sadrzadeh, M., Amirilargani, M., Shahidi, K., Mohammadi, T., *Gas permeation through a synthesized composite PDMS/PES membrane.* Journal of Membrane Science, 2009. **342**(1-2): p. 236-250.
Sanders, D.E., Smith, Z. P., Guo, R. Robeson, L. M., McGrath, J. E., Paul, D. R., Freeman, B. D., *Energy-efficient polymeric gas separation membranes for a sustainable future: A review.* Polymer, 2013. **54**(18): p. 4729-4761.
Sanders, D.F., Smith, Z. P., Ribeiro, C. P., Guo, R., McGrath, J. E., Paul, D. R., Freeman, B. D., *Gas permeability, diffusivity, and free volume of thermally rearranged polymers based on 3,3'-dihydroxy-4,4'-diamino-biphenyl (HAB) and 2,2'-bis-(3,4-dicarboxyphenyl) hexafluoropropane dianhydride (6FDA).* Journal of Membrane Science, 2012. **409-410**: p. 232-241.
Shieh, J.J., Chung, T. S., *Effect of liquid-liquid demixing on the membrane morphology, gas permeation, thermal and mechanical properties of cellulose acetate hollow fibers.* Journal of Membrane Science, 1998. **140**(1): p. 67-79.
Singh, A., Freeman, B. D., Pinnau, I., *Pure and mixed gas acetone/nitrogen permeation properties of polydimethylsiloxane PDMS.* Journal of Polymer Science Part B-Polymer Physics, 1998. **36**(2): p. 289-301.
Smith, Z.P., Hernandez, G., Gleason, K. L., Anand, A., Doherty, C. M., Konstas, K., Alvarez, C., Hill, A. J., Lozano, A. E., Paul, D. R., Freeman, B. D., *Effect of polymer structure on gas transport properties of selected aromatic polyimides, polyamides and TR polymers.* Journal of Membrane Science, 2015. **493**: p. 766-781.
Song, Q.L., Nataraj, S. K., Roussenova, M. V., Tan, J. C., Hughes, D. J., Li, W., Bourgoin, P., Alam, M. A., Cheetham, A. K., Al-Muhtaseb, S. A., Sivaniah, E., *Zeolitic imidazolate framework (ZIF-8) based polymer nanocomposite membranes for gas separation.* Energy & Environmental Science, 2012. **5**(8): p. 8359-8369.
Sridhar, S., Smitha, B., Aminabhavi, T. M., *Separation of carbon dioxide from natural gas mixtures through polymeric membranes - A review.* Separation and Purification Reviews, 2007. **36**(2): p. 113-174.
Strathmann, H., Koch, K., *The formation mechanism of phase inversion membranes.* Desalination, 1977. **21**: p. 241.
Strathmann, H., *Production of microporous media by phase inversion processes.* ACS Symposium Series, 1985. **269**: p. 165.
Su, J.C., Yang, Q., Teo, J. F., Chung, T. S., *Cellulose acetate nanofiltration hollow fiber membranes for forward osmosis processes.* Journal of Membrane Science, 2010. **355**(1- 2): p. 36-44.
Uhlhorn, R.J.R., Keizer, K., Burggraaf, A. J., *Gas and surface-diffusion in modified gamma-alumina systems.* Journal of Membrane Science, 1989. **46**(2-3): p. 225-241.
VandeWitte, P., Dijkstra, P. J., VandenBerg, J. W. A., Feijen, J., *Phase separation processes in polymer solutions in relation to membrane formation.* Journal of Membrane Science, 1996. **117**(1-2): p. 1-31.
Wang, D.L., Li, K., Teo, W. K., *Gas permselection properties in silicone-coated asymmetric polyethersulfone membranes.* Journal of Applied Polymer Science, 1997. **66**(5): p. 837-846.
Wang, K.Y., Matsuura, T., Chung, T. S., Guo, W. F., *The effects of flow angle and shear rate within the spinneret on the separation performance of poly (ethersulfone) (PES) ultrafiltration hollow fiber membranes.* Journal of Membrane Science, 2004. **240**(1-2): p. 67-79.

Wang, R., Chung, T., *Determination of pore sizes and surface porosity and the effect of shear stress within a spinneret on asymmetric hollow fiber membranes.* Journal of Membrane Science, 2001. **188**: p. 29-37.
Ward, T.L., Dao, T., *Model of hydrogen permeation behavior in palladium membranes.* Journal of Membrane Science, 1999. **153**(2): p. 211-231.
Weisenberger, M.C., *Application of Multiwall Carbon Nanotubes: Mechanical, Electrical and Thermal Properties*. 2007, University of Kentucky.
Widjojo, N., Chung, T., *Thickness and air gap dependence of macrovoid evolution in phase-inversion asymmetric hollow fiber membranes.* Industrial & Engineering Chemistry Product Research and Development, 2006. **45**: p. 7618-7626.
Widjojo, N., Chung, T. S., Arifin, D. Y., Weber, M., Warzelhan, V., *Elimination of die swell and instability in hollow fiber spinning process of hyperbranched polyethersulfone (HPES) via novel spinneret designs and precise spinning conditions.* Chemical Engineering Journal, 2010. **163**(1-2): p. 143-153.
Wienk, I.M., Boom, R. M., Beerlage, M. A. M., Bulte, A. M. W., Smolders, C. A., Strathmann, H., *Recent advances in the formation of phase inversion membranes made from amorphous or semi-crystalline polymers.* Journal of Membrane Science, 1996. **113**(2): p. 361-371.
Won, J., Kim, M. H., Kang, Y. S., Park, H. C., Kim, U. Y., Choi, S. C., Koh, S. K., *Surface modification of polyimide and polysulfone membranes by ion beam for gas separation.* Journal of Applied Polymer Science, 2000. **75**(12): p. 1554-1560.
Woo, K.T., Lee, J., Dong, G., Kim, J. S., Do, Y. S., Jo, H. J., Lee, Y. M., *Thermally rearranged poly(benzoxazole-co-imide) hollow fiber membranes for CO_2 capture.* Journal of Membrane Science, 2016. **498**: p. 125-134.
Woo, K.T., Dong, G., Lee, J., Kim, J. S., Do, Y. S., Lee, W. H., Lee, H. S., Lee, Y. M., *Ternary mixed-gas separation for flue gas CO_2 capture using high performance thermally rearranged (TR) hollow fiber membranes.* Journal of Membrane Science, 2016. **510**: p. 472-480.
Xu, L.R., Zhang, C., Rungta, M., Qiu, W. L., Liu, J. Q., Koros, W. J., *Formation of defect-free 6FDA-DAM asymmetric hollow fiber membranes for gas separations.* Journal of Membrane Science, 2014. **459**: p. 223-232.
Yang, Q., Chung, T. S., Chen, S. B., Weber, M., *Pioneering explorations of rooting causes for morphology and performance differences in hollow fiber kidney dialysis membranes spun from linear and hyperbranched polyethersulfone.* Journal of Membrane Science, 2008. **313**(1-2): p. 190-198.
Zeman, L., Fraser, T., *Formation of air-cast cellulose acetate membranes. Part I: Study of macrovoid formation.* Journal of Membrane Science, 1993. **84**: p. 93.
Zeman, L., Fraser, T., *Formation of air-cast cellulose acetate membranes. Part II: Kinetics of demixing and microvoid growth.* Journal of Membrane Science, 1994. **87**: p. 267.
Zhou, H., Su, Y., Chen, X. R., Luo, J. Q., Tan, S., Wan, Y. H., *Plasma modification of substrate with poly(methylhydrosiloxane) for enhancing the interfacial stability of PDMS/ PAN composite membrane.* Journal of Membrane Science, 2016. **520**: p. 779-789.

Vita

Nicholas William Linck was born on January 25th, 1989 in Arlington, TX, USA. He completed a Bachelor's degree in Chemistry at the Colorado School of Mines (CSM) in December 2011. He joined the University of Kentucky in August 2012 to pursue a PhD in Materials Science and Engineering, with Dr. Bruce J. Hinds as his advisor. In 2014, he completed a Masters' degree in Materials Science and Engineering at the University of Kentucky and began a new pursuit of a PhD in Materials Science and Engineering, with Dr. Matthew C. Weisenberger and Dr. Douglass S. Kalika as his advisors.

Publications:

- **Nicholas Linck**, Alex Peek, and Bruce J. Hinds, "Monolayer Growth Front of Precious Metals through Insulating Mesoporous Membranes", *ACS Appl. Mater. Interfaces* 2017, 9, 30964−30968

Presentations:

- **Nicholas W. Linck**, Matthew C. Weisenberger, and Douglass S. Kalika, (July 2018) "Effect of MWCNT Composition on the Permselectivity of PES-MWCNT Mixed Matrix Membranes for Gas Separation." Oral presentation at The World Conference on Carbon in Madrid, Spain.
- **Nicholas W. Linck**, Matthew C. Weisenberger, and Douglass S. Kalika, (June 2018) "Effect of MWCNT Loading on the Permselectivity of PES-MWCNT Mixed Matrix

Membranes for Gas Separation." Poster Session Presentation at the annual meeting of the North American Membrane Society (NAMS) in Lexington, KY.

- **Nicholas W. Linck**, Matthew C. Weisenberger, and Douglass S. Kalika, (May 2017) "Effects of Post-treatments on Permeance and Selectivity of Polyethersulfone and Polyacrylonitrile Hollow Fiber Membranes." Poster session presentation at the University of Kentucky Materials and Chemical Engineering GSA Spring Symposium.
- **Nicholas W. Linck**, Matthew C. Weisenberger, and Douglass S. Kalika, (May 2016) "Polymeric Hollow Fiber Processing for Development of New Membrane Material Platforms." Poster session presentation at the University of Kentucky Materials and Chemical Engineering GSA Spring Symposium
- **Nicholas W. Linck** and Bruce J. Hinds, (March 2013) "Monolayer Plating of Precious Metals on Insulating Mesoporous Supports." Poster session presentation at the 2013 Kentucky Workshop on Renewable Energy and Energy Efficiency (RE3).